CHAPTER 3: AERODYNAMIC AND THRUST FORCES AND MOMENTS

The purpose of this chapter is to present approaches to the modelling of aerodynamic and thrust forces and moments for the following two types of flight conditions:

1) Steady state: see Section 3.1 2) Perturbed state: see Section 3.2

Aerodynamic and thrust forces and moments can be determined in two ways:

* by experimental methods (flight test or tunnel test)
* by computational and/or empirical methods

Experimental methods have the great advantage of allowing rather accurate predictions of full scale airplane aerodynamic behavior over a wide range of flight conditions, including nonlinear effects. A disadvantage of experimental methods is that they tend to be very costly, both in calendar time and money. For these reasons, experimental methods are used primarily in research and in design verification prior to committing to building flying hardware. In most preliminary design and parametric design studies theoretical and/or empirical methods are used.

In this chapter, relatively simple mathematical models for aerodynamic and thrust forces and moments are developed by means of a combination of theoretical and empirical methods. The main emphasis is on the so–called component build–up method for modelling aerodynamic and thrust forces and moments. In this method the airplane is assumed to be built up from a number of components. The total forces and moments which act on the airplane are then assumed to follow from summing the forces and moments which act on these components. For example, in the case of the total aerodynamic force the following type of expression will be used:

$$F_{A_{airplane}} = F_{A_{wing}} + F_{A_{fuselage}} + F_{A_{hor.tail}} + F_{A_{vert.tail}} + \text{etc.} \qquad (3.1)$$

Interference effects are accounted for by using empiricism. The number of components which should be used depends on the airplane configuration and on the level of accuracy desired. In the presentations which follow, emphasis is placed on gaining a physical understanding of the fundamental mechanisms which cause forces and moments to act on airplanes.

The axis system used in modelling all forces and moments is a modification of the body–fixed axis system: XYZ (See Figure 1.1), called the stability axis system $X_S Y_S Z_S$. Figure 3.1 shows how the stability axis system is defined for an airplane in a steady state, wings level, straight line flight condition with NO initial sideslip. Figure 3.2 shows how the stability axis system is defined incase initial sideslip is not zero. Note that the stability X–axis in that case is defined along the projection of the total airplane velocity vector onto the airplane XZ–plane.

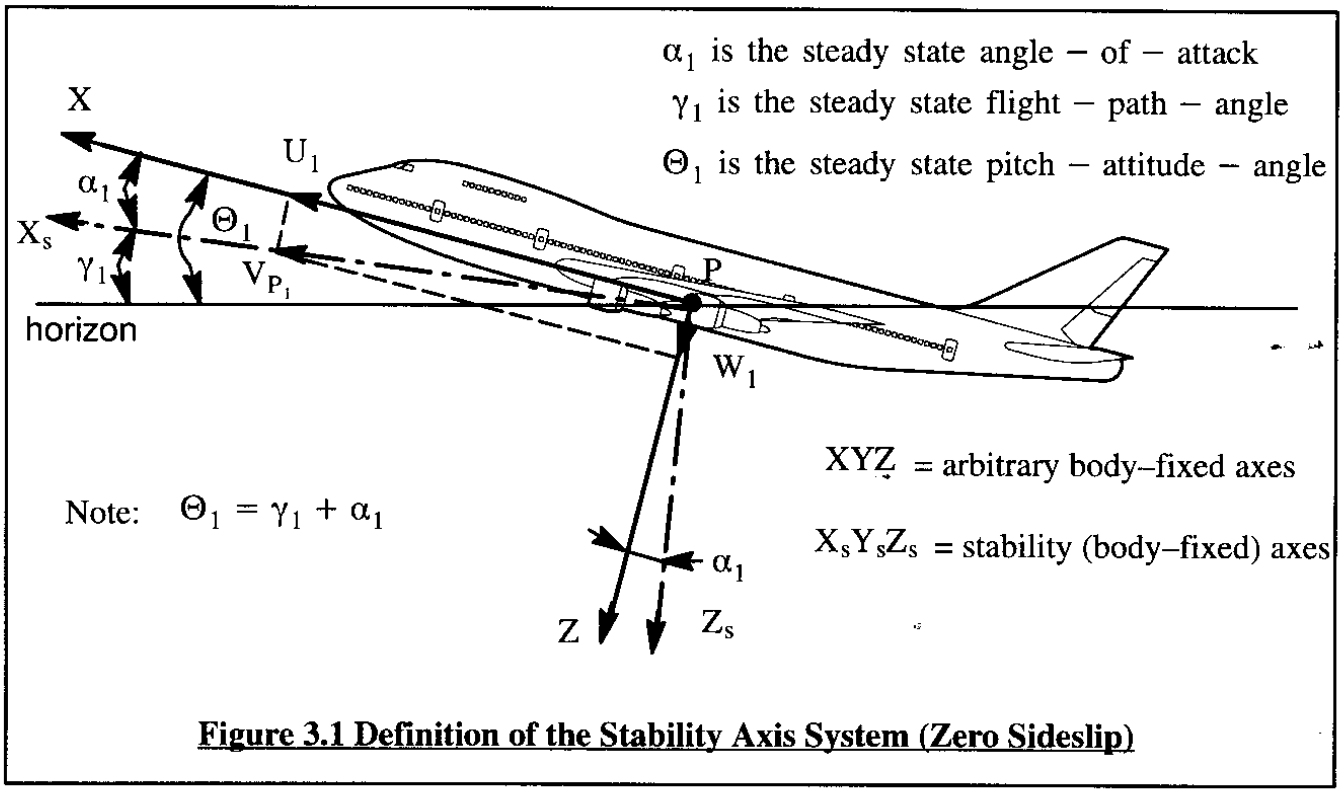

Figure 3.1 Definition of the Stability Axis System (Zero Sideslip)

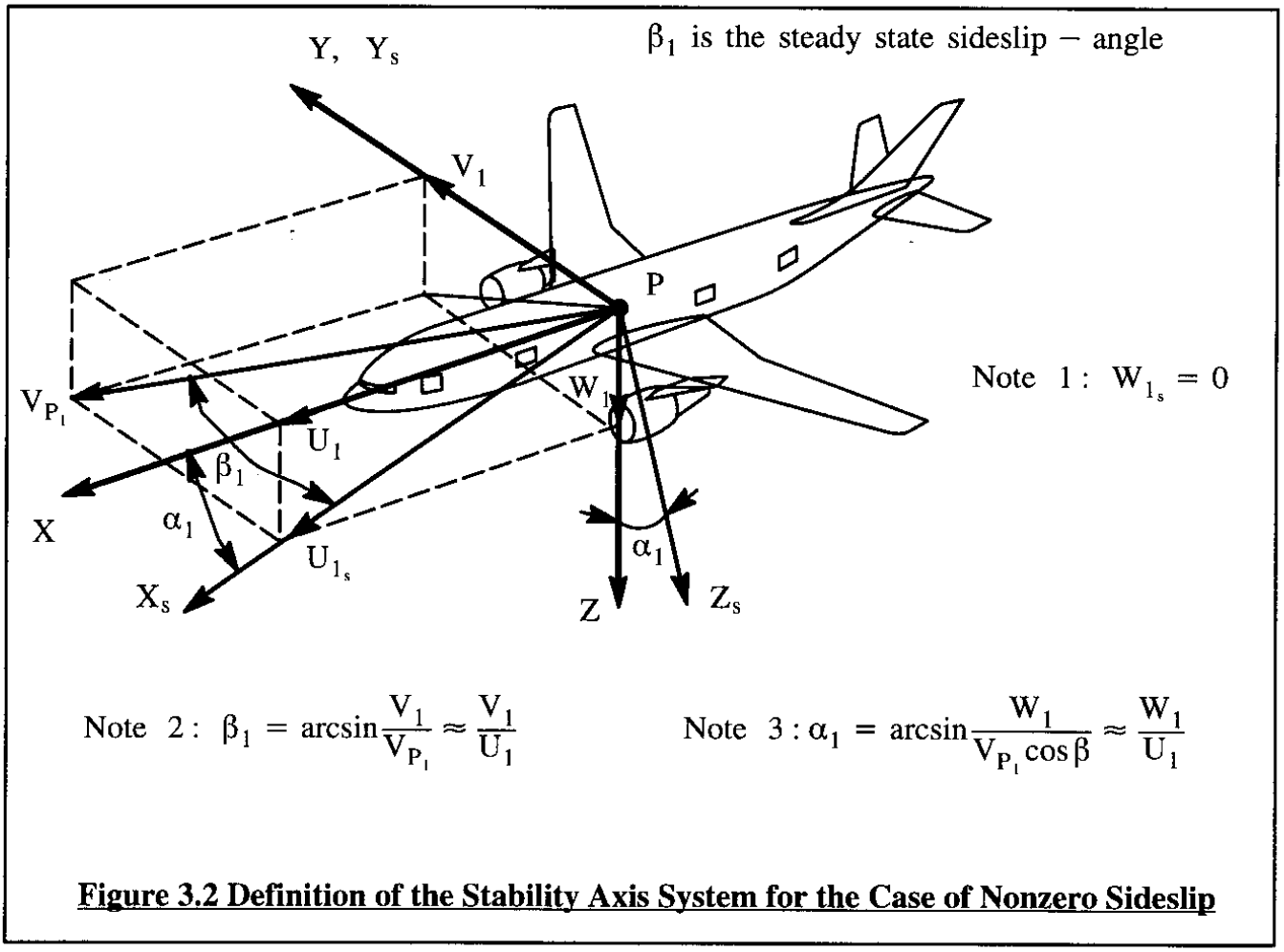

Figure 3.2 Definition of the Stability Axis System for the Case of Nonzero Sideslip

NOTE: the reader should not lose sight of the fact that the stability axis system still is a body-fixed axis system. Therefore, the equations of motion developed in Chapter 1 can be applied directly to the stability axis system. Note from Figures 3.1 and 3.2 that in the stability axis system:

$$V_{P_1} = U_{1_s} \qquad \text{and:} \qquad W_{1_s} = 0 \tag{3.2}$$

In developing the mathematical models for aerodynamic and thrust forces and moments, intensive use will be made of the idea of stability and control derivatives. Several of these were already encountered in Chapter 2: C_{L_α} and C_{L_δ} are typical examples. To illustrate typical magnitudes and trends for airplane stability and control derivatives, example plots of derivatives (and their variation with Mach number) are presented. Figures 3.3 through 3.6 show three-views of four airplanes for which data will be presented. These figures also present the reference geometries on which all derivatives are based.

3.1 STEADY STATE FORCES AND MOMENTS

Since airplanes differ from one another in configuration, shape and size, it should be expected that it is not feasible to develop a mathematical model for airplane steady state forces and moments which applies to all airplanes. The approach taken here is to first list the forces and moments to be modeled. Second, those variables of motion which experience shows to have a significant effect on the forces and moments, are also listed. For the aerodynamic forces and moments, this is done in the form of a table such as Table 3.1.

Table 3.1 Dependence of Steady State Aerodynamic Forces and Moments on Variables

Variable	all = 0	α	β	δ_a	δ_e	δ_r
$F_{A_{x_{1_s}}}$	drag at zero value for all variables	induced drag	negligible for small: β	negligible for small: δ_a	negligible for small: δ_e	negligible for small: δ_r
$F_{A_{y_{1_s}}}$	zero	negligible for small: α	side force due to: β	zero	zero	side force due to: δ_r
$F_{A_{z_{1_s}}}$	lift at zero value for all variables	lift due to: α	negligible for small: β	negligible	lift due to: δ_e	negligible
$L_{A_{1_s}}$	zero	rolling moment due to sideslip is affected by: α	rolling moment due to: β	rolling moment due to: δ_a	zero	rolling moment due to: δ_r
$M_{A_{1_s}}$	pitching moment at zero value for all variables	pitching moment due to: α	negligible for small: β	negligible	pitching moment due to: δ_e	negligible
$N_{A_{1_s}}$	zero	yawing moment due to sideslip is affected by: α	yawing moment due to: β	yawing moment due to: δ_a	zero	yawing moment due to: δ_r

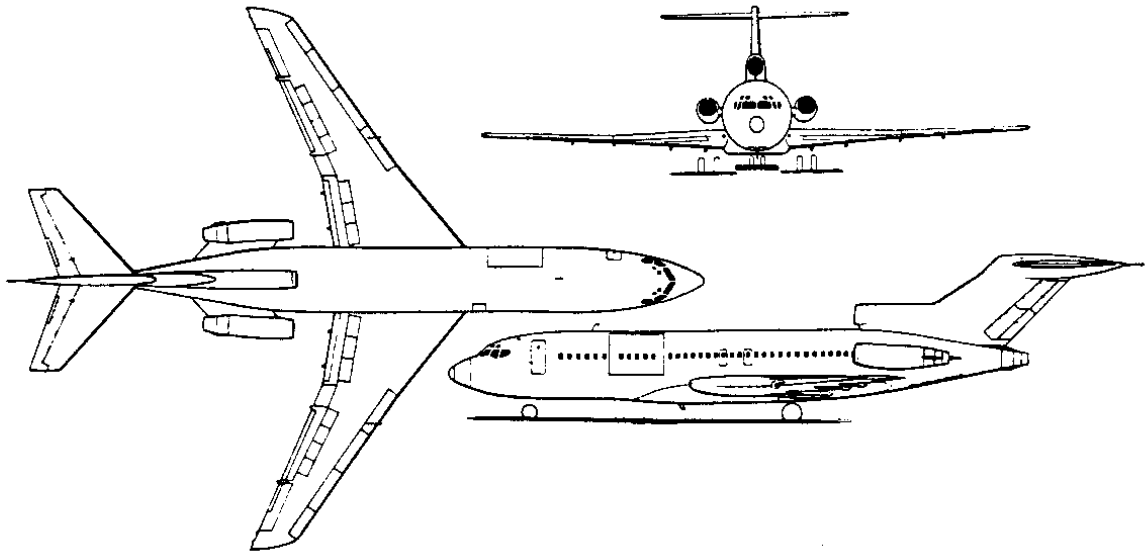

$S = 1,560 \text{ ft}^2$ $b = 106 \text{ ft}$ $\bar{c} = 15 \text{ ft}$

$S_h = 376 \text{ ft}^2$ $S_v = 356 \text{ ft}^2$

$W_{TO} = 152,000 \text{ lbs}$ $W_L = 135,000 \text{ lbs}$ $W_{OWE} = 88,000 \text{ lbs}$

Figure 3.3 Three–view and Reference Geometry for the Boeing 727–100

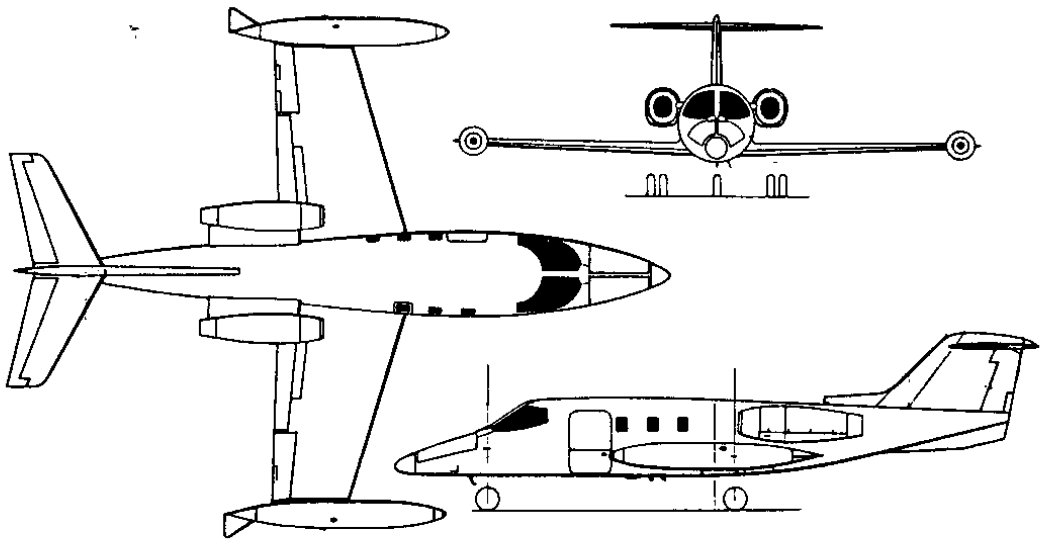

$S = 232 \text{ ft}^2$ $b = 34.2 \text{ ft}$ $\bar{c} = 7.04 \text{ ft}$

$S_h = 54.0 \text{ ft}^2$ $S_v = 37.4 \text{ ft}^2$

$W_{TO} = 13,500 \text{ lbs}$ $W_L = 11,880 \text{ lbs}$ $W_{OWE} = 7,252 \text{ lbs}$

Figure 3.4 Three–view and Reference Geometry for the Learjet 24B

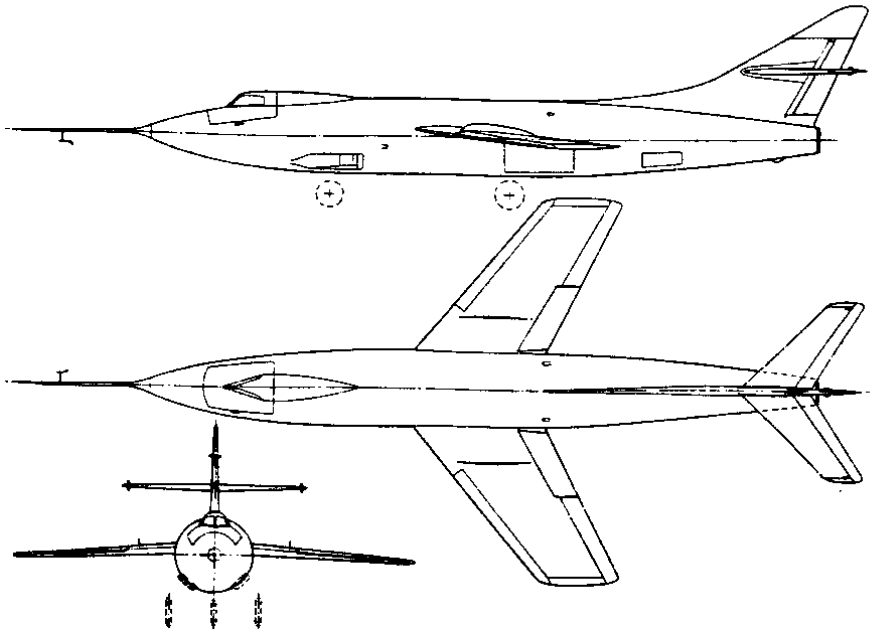

$S = 175.0\ ft^2$ $b = 25.0\ ft$ $\bar{c} = 7.27\ ft^2$

$S_h = 39.9\ ft^2$ $S_v = 36.0\ ft^2$

$W_{TO} = 10,000\ lbs$

Figure 3.5 Three–view and Reference Geometry for the Douglas D–558–II

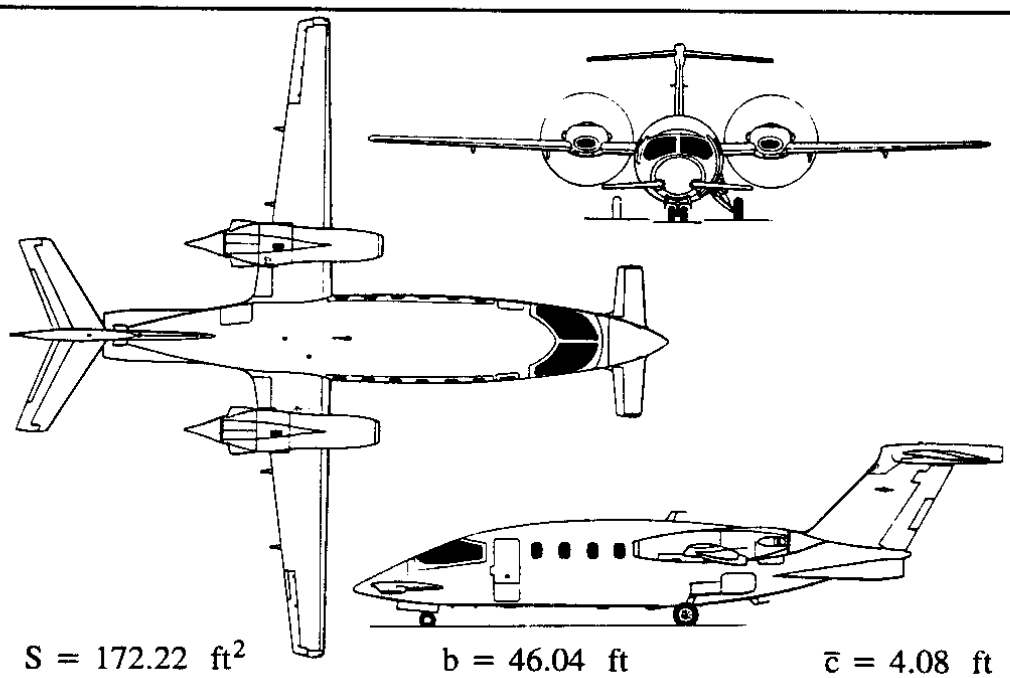

$S = 172.22\ ft^2$ $b = 46.04\ ft$ $\bar{c} = 4.08\ ft$

$S_h = 41.23\ ft^2$ $S_v = 50.91\ ft^2$ $S_c = 24.22\ ft^2$

$W_{TO} = 10,810\ lbs$ $W_L = 10,270\ lbs$ $W_{OWE} = 7,370\ lbs$

Figure 3.6 Three–view and Reference Geometry for the Piaggio P–180

Note: in the model of Table 3.1 it is assumed that all steady state angular rates, P_1, Q_1 and R_1 are zero: in other words, the steady state is a straight line flight condition. The effect of non–zero P_1, Q_1 and R_1 (i.e. curvilinear steady state flight) on aerodynamic forces and moments is discussed in Chapter 4.

Table 3.1 lists only the aerodynamic forces and moments. Also, Table 3.1 lists only three types of flight control surfaces: δ_a, δ_e and δ_r. Most airplanes have more than three types of flight control surfaces. Examples of other types of flight control surface are: flaps, spoilers, speed-brakes, drag–rudders (as on the Northrop B–2) etc. Table 3.1 should be adjusted/expanded to fit any particular airplane which is being analyzed or designed.

Each box in Table 3.1 represents a cause–and–effect statement. The cause–and–effect statements in Table 3.1 will apply to conventional airplanes most of the time. Such conventional airplanes are said not to have any significant coupling between lateral–directional variables and longitudinal forces and moments. The opposite also tends to be true for such airplanes. As is often the case in aeronautics: there are certainly exceptions. **Some examples:**

1) In fighter aircraft with very slender fuselages there may be significant side–forces, rolling moments and pitching moments due to sideslip as a result of asymmetric vortex shedding from the nose of the airplane. In fact, some configurations even have a side–force, rolling moment and yawing moment at zero sideslip!

2) If an airplane has a highly swept vertical tail and a highly swept rudder hinge line, there may be a significant pitching moment due to rudder deflection. Such a moment would also be nonlinear because it is independent of the sign of the rudder deflection!

3) If an airplane is not symmetrical about its XZ–plane, significant coupling effects may prevail. Figure 1.3 shows two example airplanes for which aerodynamic coupling effects are present.

In this text it will be assumed that the airplane aerodynamic force and moment models behave more or less as indicated by Table 3.1. In other words, in this text it will be generally assumed that no significant coupling exists between lateral–directional variables and longitudinal forces and moments. The opposite will also be assumed in most cases.

The thrust forces and moments which act on an airplane depend on the magnitude of the installed thrust, T_i, of each engine.. The installed thrust, T_i, is itself a function of:

* Altitude	* Mach number	* Temperature and humidity
* Thrust setting	* Mixture setting	* Propeller setting
* Inlet conditions	* Installation losses	* Angle of attack and sideslip

A detailed treatment of how to predict the magnitude of T_i as a function of all these variables is beyond the scope of this text. References 3.1, 3.2 and 3.3 may be consulted for such details. Part VI of Reference 3.1 contains step–by–step methods for estimating these effects in the preliminary

design stage. In this text it will be assumed that the magnitude of the installed thrust of each engine, T_i is known.

Depending on the placement of propellers and/or jet exhausts, there may be significant interference effects between aerodynamic and thrust forces and moments. These interference effects are also considered to be beyond the scope of this text. The reader may wish to consult References 3.4 and 3.5 for further study of such interference effects.

Because it is assumed that little coupling between the longitudinal variables and the lateral–directional variables exists, the modelling of forces and moments will be discussed in two independent sets in the following Sub–sections:

3.1.1 through 3.1.6 Longitudinal Forces and Moments

3.1.7 through 3.1.12 Lateral–Directional Forces and Moments

3.1.1 LONGITUDINAL AERODYNAMIC FORCES AND MOMENTS

Figure 3.7 illustrates the longitudinal aerodynamic forces and moments which act on an airplane in a steady state flight condition. In the stability axis system, these forces and moments are written as follows:

$$\begin{aligned} F_{A_{x_{1_s}}} &= -D \\ F_{A_{z_{1_s}}} &= -L \\ M_{A_{1_s}} &= M_A \end{aligned} \tag{3.3}$$

In the development of models for drag, lift and pitching moment, the subscripts 1 and s will be dropped for the remainder of this section. This can be done without ambiguity because it is understood that the material deals only with steady state effects in the stability axis system!

The modelling of drag, lift and pitching moment is discussed in Sub–sections 3.1.2 through 3.1.4 respectively.

3.1.2 AIRPLANE DRAG

Airplane drag, D, is non–dimensionalized as follows:

$$D = C_D \bar{q} S \tag{3.4}$$

where: C_D is the total airplane drag coefficient.

The steady state airplane drag coefficient depends on the following factors:

* airplane wetted area
* angle of attack, α
* dynamic pressure, $\bar{q}$
* airplane average skin friction coefficient
* control surface deflection(s), δ_e, i_h, etc.
* Mach number and Reynolds number

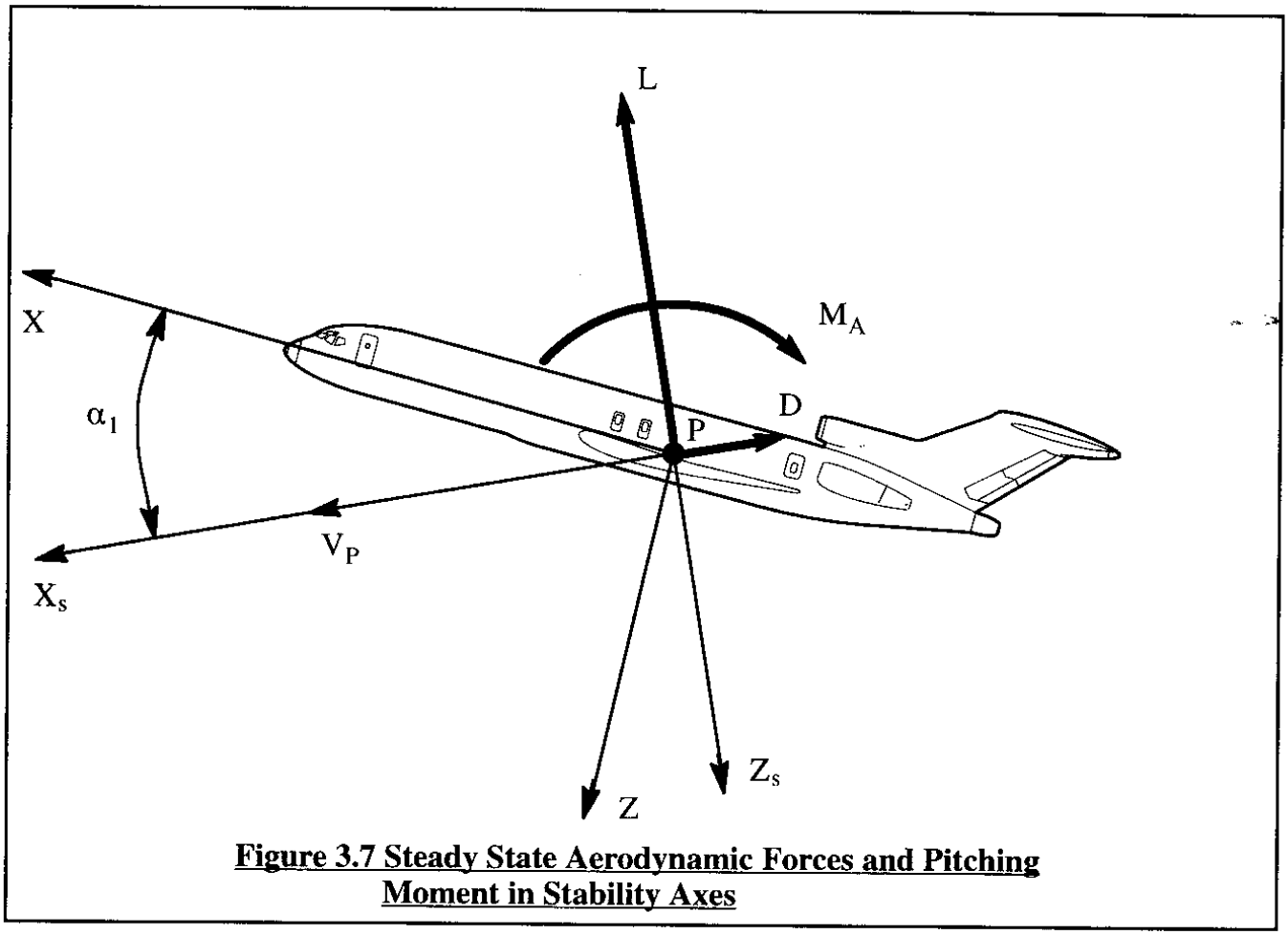

Figure 3.7 Steady State Aerodynamic Forces and Pitching Moment in Stability Axes

For an airplane equipped with an elevator and a variable incidence horizontal tail, the drag coefficient, C_D , is expressed with the help of a first order Taylor series:

$$C_D = C_{D_0} + C_{D_\alpha}\alpha + C_{D_{i_h}} i_h + C_{D_{\delta_e}}\delta_e \tag{3.5}$$

The coefficient and derivatives in Eqn (3.5) are to be evaluated at constant Mach number and Reynolds number. The terms in Eqn (3.5) have the following meanings:

C_{D_0}	is the value of C_D for: $\alpha = i_h = \delta_e = 0$
$C_{D_\alpha} = \partial C_D/\partial\alpha$	is the change in airplane drag due to a change in airplane angle of attack, α
$C_{D_{i_h}} = \partial C_D/\partial i_h$	is the change in airplane drag due to a change in stabilizer incidence angle, i_h , for: $\alpha = \delta_e = 0$
$C_{D_{\delta_e}} = \partial C_D/\partial\delta_e$	is the change in airplane drag due to a change in elevator angle, δ_e , for: $\alpha = i_h = 0$

Figure 3.8 shows a graphical interpretation of C_{D_0} and C_{D_α} . Note that the numerical values for C_{D_0} and C_{D_α} depend on the steady state itself! For most stability and control applications

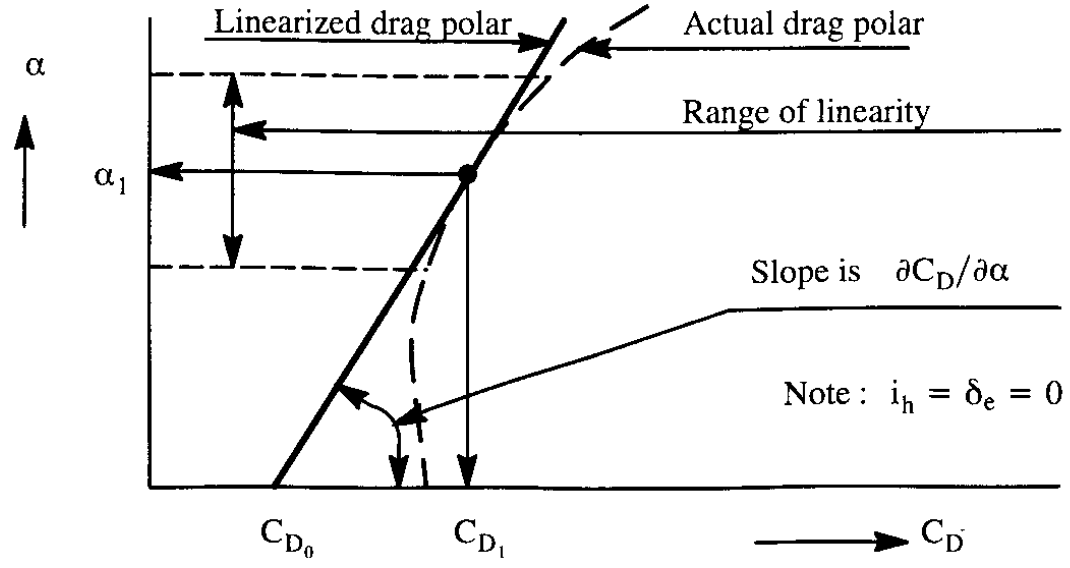

Figure 3.8 Graphical Interpretation of Terms in Eqn (3.5)

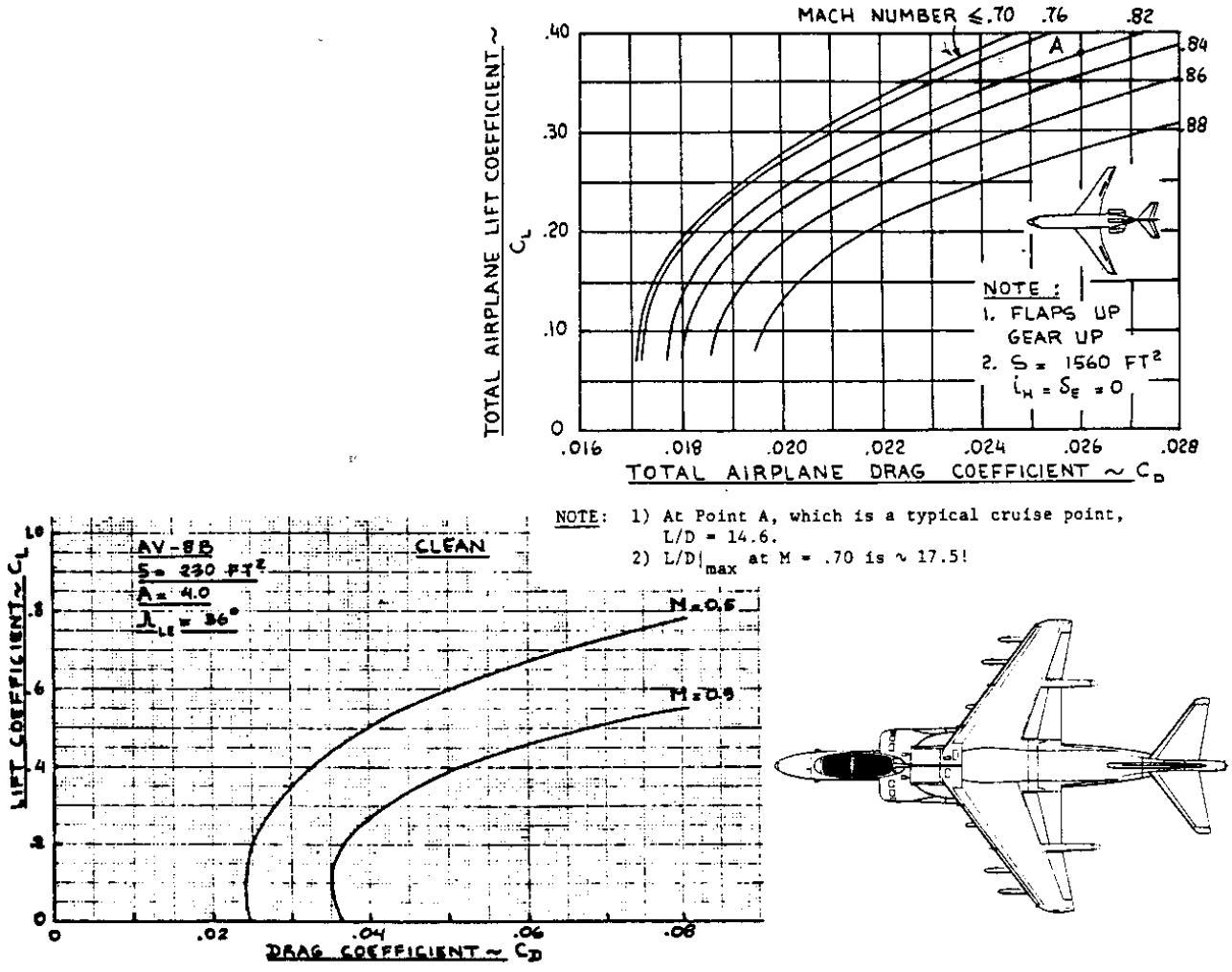

Figure 3.9 Example Drag Polars for a Jet Transport and for a Fighter

it has been found acceptable to neglect drag changes due to control surface deflections (one of several exceptions to this is the so–called minimum control speed problem to be discussed in Chapter 4). Therefore, usually:

$$C_{D_{i_h}} = C_{D_{\delta_e}} = 0 \tag{3.6}$$

In performance problems where trim drag is important, Eqn(3.6) should NOT be used!

There is a notational problem with C_{D_0} in Eqn (3.5): the symbol C_{D_0} as used here is the value of airplane drag coefficient for zero angle of attack, zero elevator deflection and zero stabilizer incidence angle. In performance applications, the symbol C_{D_0} stands for the value of airplane drag coefficient at zero lift coefficient, zero elevator deflection and zero stabilizer incidence deflection. To avoid confusion between these two physically different drag coefficients in this text, the notation $\overline{C}_{D_0}$ will be used for the zero–lift drag coefficient. Therefore, in this text the standard parabolic form of the airplane drag polar will be written as:

$$C_D = \overline{C}_{D_0} + \frac{C_L^2}{\pi A e} \tag{3.7}$$

where: $\overline{C}_{D_0}$ is the value of airplane drag coefficient at zero lift coefficient

A is the wing aspect ratio
e is Oswald's efficiency factor

Examples of typical drag polars for a jet transport and a fighter are given in Figure 3.9.

It is usually acceptable to write $\overline{C}_{D_0}$ as follows:

$$\overline{C}_{D_0} = f/S \tag{3.8}$$

where: f is the equivalent parasite area of the airplane, which in turn depends on total wetted area S_{wet}, and on the airplane equivalent skin friction coefficient, C_f . Methods for estimating equivalent parasite area, f, and wetted area, S_{wet} , for any type airplane are presented in Part I of Reference 3.1. With the help of those methods the value of $\overline{C}_{D_0}$ for any airplane can be obtained. An example of the typical relationship between f, S_{wet} and C_f for jet propelled airplanes is given in Figure 3.10.

The derivative C_{D_α} is most easily estimated by differentiation of Eqn (3.7):

$$C_{D_\alpha} = (2C_{L_1}C_{L_\alpha})/(\pi A e) \tag{3.9}$$

A method for estimating C_{L_α} is discussed in Sub–section 3.1.3. Figures 3.11 and 3.12 present graphical examples of the variation of C_D and C_{D_α} with Mach number for several example airplanes. The steady state model for the aerodynamic force in the stability X–axis direction is:

$$F_{A_{x_{1_s}}} = -D = -C_D\bar{q}S = -(C_{D_0} + C_{D_\alpha}\alpha + C_{D_{i_h}}i_h + C_{D_{\delta_e}}\delta_e)\bar{q}S \tag{3.10}$$

This figure was generated with the Advanced Aircraft Analysis (AAA) Program described in Appendix A

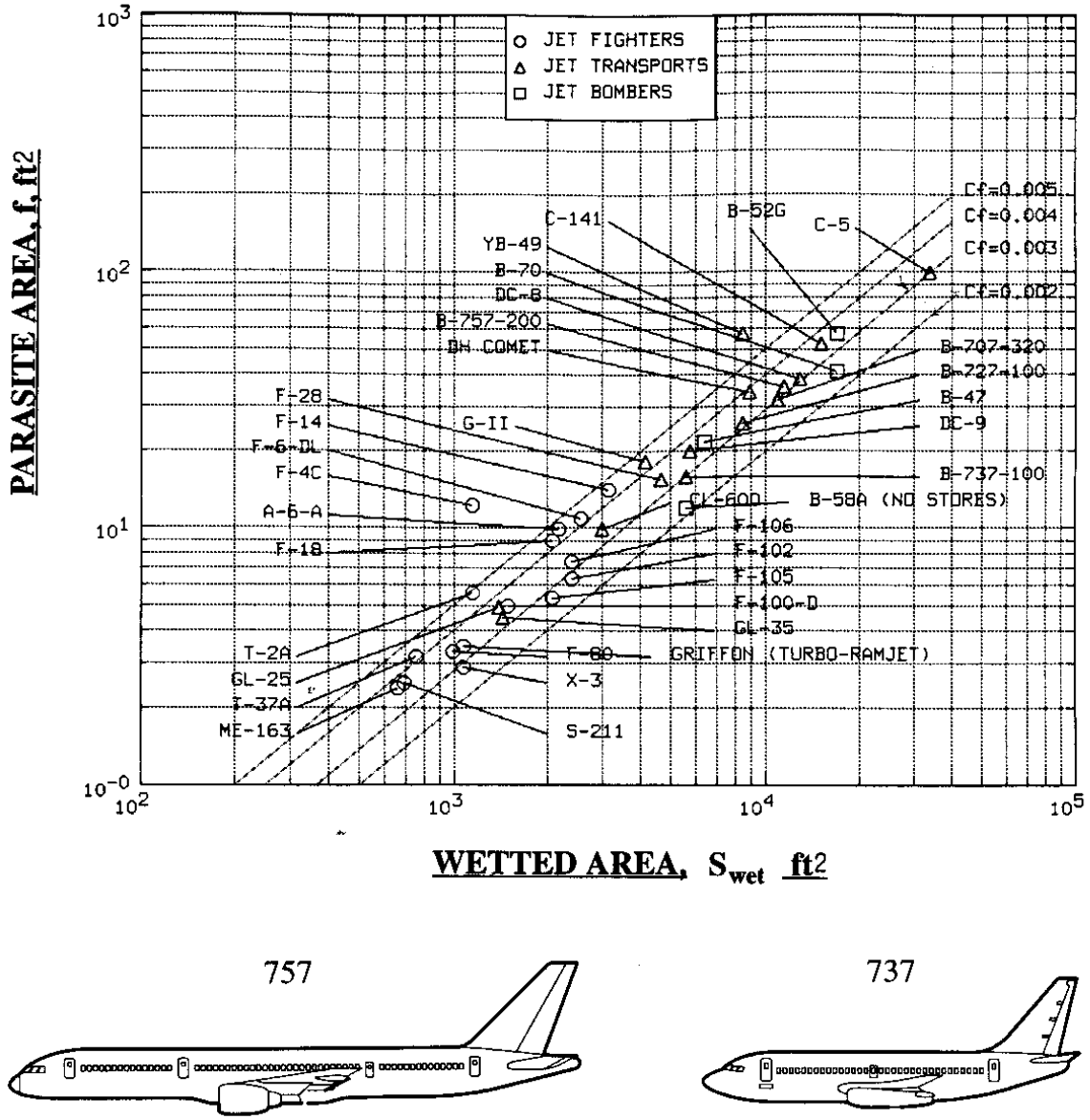

Figure 3.10 Effect of Wetted Area and Equivalent Skin Friction on Parasite Area of Jet Powered Airplanes

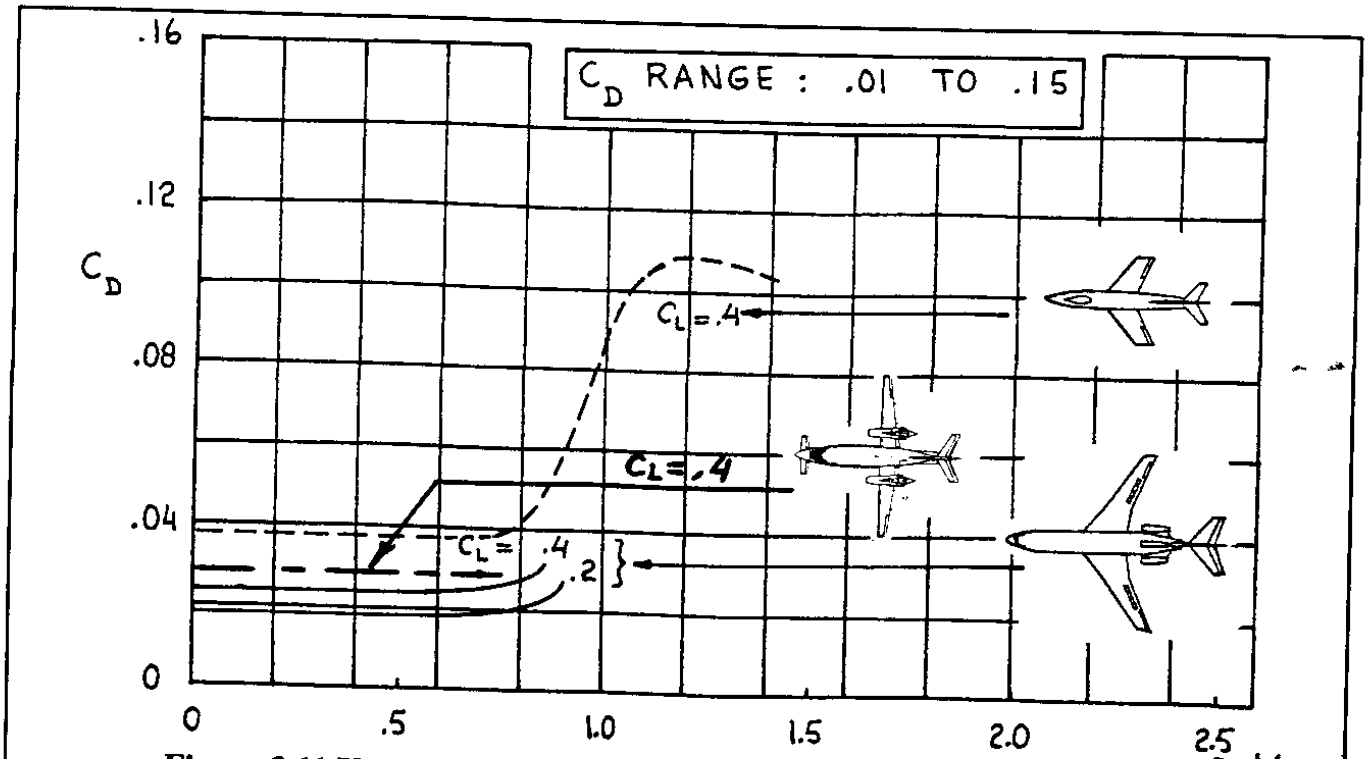

Figure 3.11 Variation of C_D with Mach Number for several Airplanes

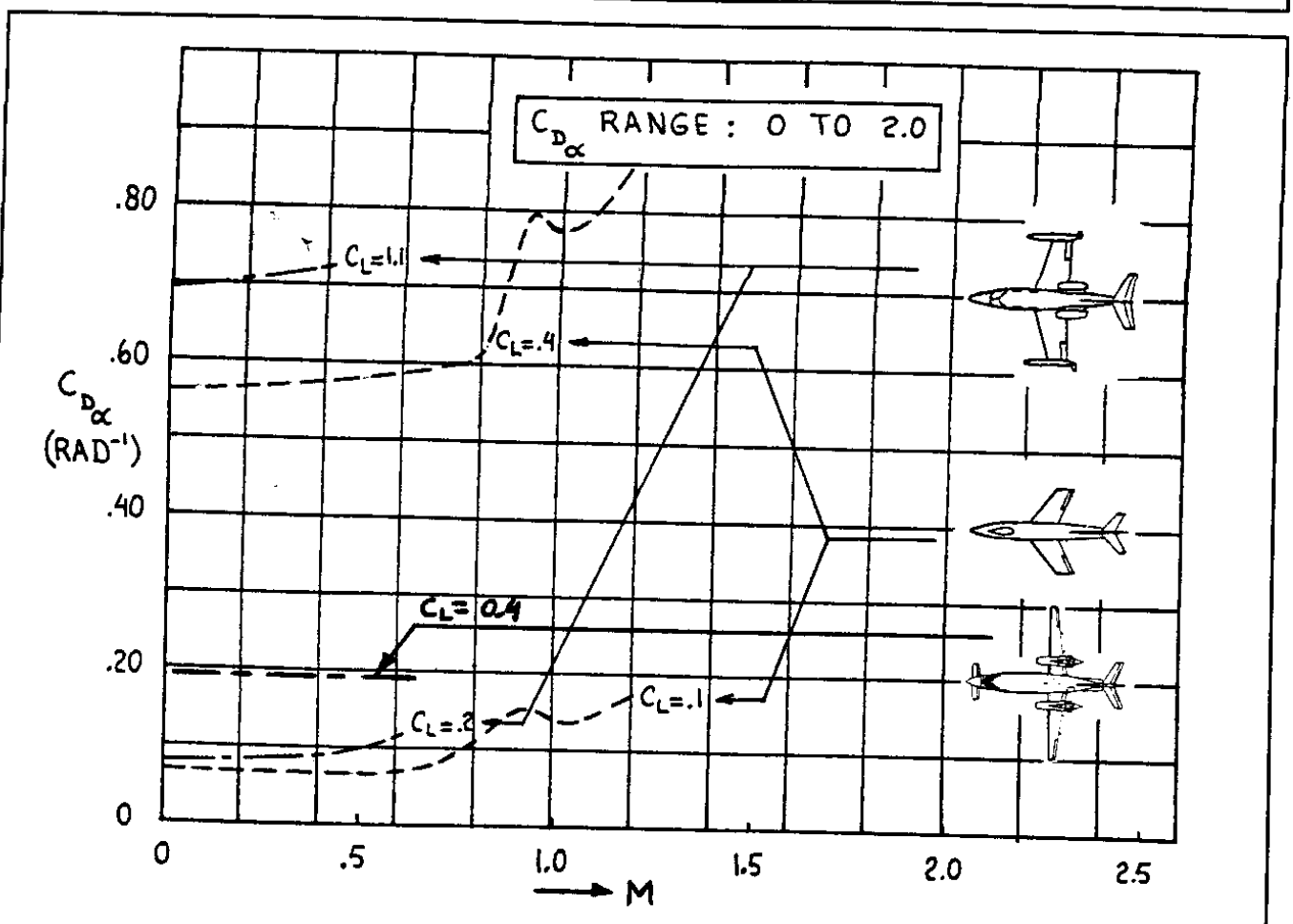

Figure 3.12 Variation of C_{D_α} with Mach Number for several Airplanes

3.1.3 AIRPLANE LIFT

Airplane lift is non–dimensionalized as follows:

$$L = C_L \bar{q} S \tag{3.11}$$

where: C_L is the total airplane lift coefficient.

The steady state airplane lift coefficient depends on the following factors:

* angle of attack, α
* control surface deflection(s), δ_e, i_h, etc.
* dynamic pressure, $\bar{q}$
* Mach number and Reynolds number

For an airplane equipped with an elevator and variable incidence horizontal tail (stabilizer) the lift coefficient, C_L, is expressed with the help of a first order Taylor series:

$$C_L = C_{L_0} + C_{L_\alpha}\alpha + C_{L_{i_h}} i_h + C_{L_{\delta_e}} \delta_e \tag{3.12}$$

The coefficient and derivatives in Eqn (3.12) are to be evaluated at constant Mach number and Reynolds number. The terms in Eqn (3.12) have the following meanings:

C_{L_0}	is the value of C_L for: $\alpha = i_h = \delta_e = 0$
$C_{L_\alpha} = \partial C_L / \partial \alpha$	is the change in airplane lift due to a change in airplane angle of attack, α
$C_{L_{i_h}} = \partial C_L / \partial i_h$	is the change in airplane lift due to a change in stabilizer incidence angle, i_h for: $\alpha = \delta_e = 0$
$C_{L_{\delta_e}} = \partial C_L / \partial \delta_e$	is the change in airplane lift due to a change in elevator angle, δ_e for: $\alpha = i_h = 0$

In the following, it will be shown how the coefficients and derivatives in Eqn (3.12) can be estimated using the airplane component build–up philosophy. To keep the development simple, a conventional (tail–aft) airplane will be used as an example. Figure 3.13 shows the definition of geometric parameters to be used.

It will be assumed that the drag forces acting on the wing–fuselage and the horizontal tail are negligible. The total lift which acts on the airplane is then found from:

$$L \approx L_{wf} + L_h \cos\varepsilon \approx L_{wf} + L_h \tag{3.13}$$

This can be written in coefficient form:

$$C_L \bar{q} S = C_{L_{wf}} \bar{q} S + C_{L_h} \bar{q}_h S_h \tag{3.14}$$

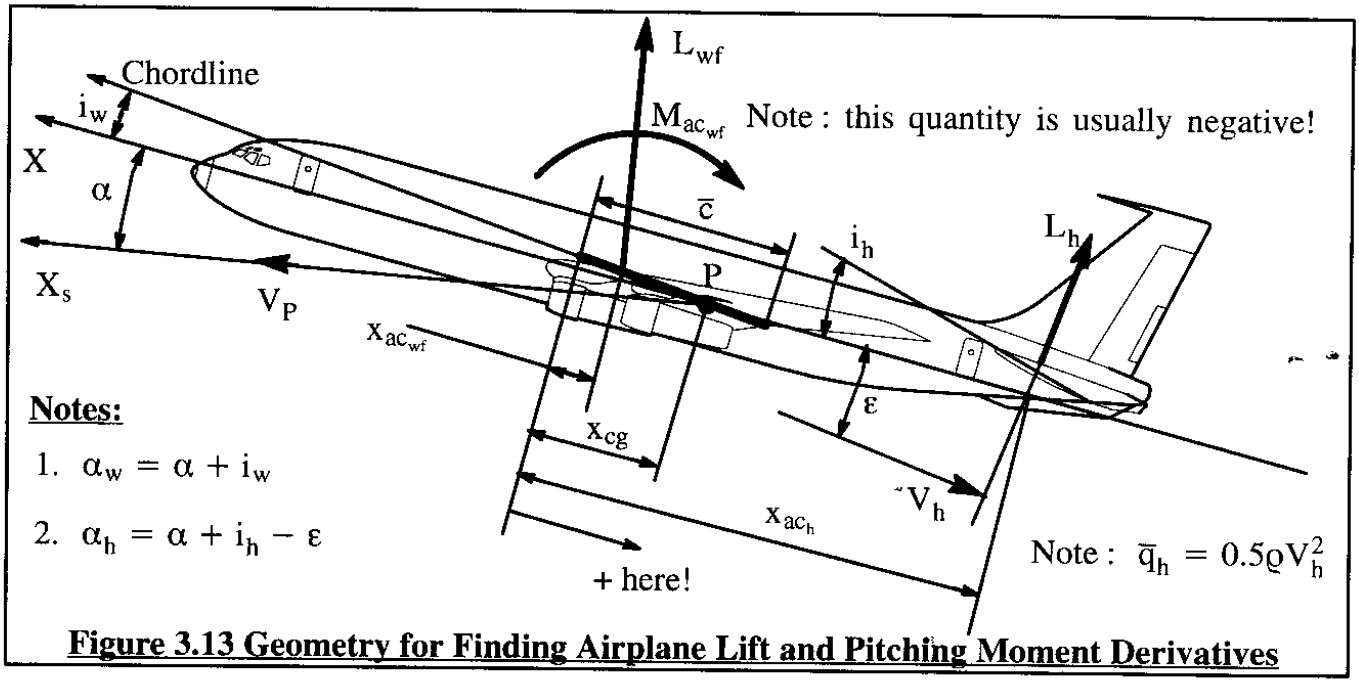

Figure 3.13 Geometry for Finding Airplane Lift and Pitching Moment Derivatives

Note that the dynamic pressure at the horizontal tail, $\bar{q}_h$ is potentially different from that at the wing–fuselage, $\bar{q}$. Reasons for this difference can be that the tail is affected by propeller slipstream, by jet exhaust effects and by fuselage boundary layer effects. The difference in dynamic pressure is accounted for by the introduction of the so–called dynamic pressure ratio, η_h :

$$\eta_h = \bar{q}_h/\bar{q} \qquad \text{Note : } \bar{q}_h = 0.5\varrho V_h^2 \tag{3.15}$$

Eqn (3.14) can be rewritten as:

$$C_L = C_{L_{wf}} + C_{L_h}\eta_h\frac{S_h}{S} \tag{3.16}$$

The wing–fuselage lift coefficient, $C_{L_{wf}}$ can be expressed as follows:

$$C_{L_{wf}} = C_{L_{\alpha_{wf}}} + C_{L_{\alpha_{wf}}}\alpha \tag{3.17}$$

The wing–fuselage lift–curve slope, $C_{L_{\alpha_{wf}}}$ differs from the wing lift–curve slope, $C_{L_{\alpha_w}}$ because of the wing–to–fuselage interference effect. Methods for accounting for this effect are presented in Part VI of Reference 3.1. For airplanes with a wing span to fuselage diameter ratio of six or higher it is usually acceptable to assume: $C_{L_{\alpha_{wf}}} \approx C_{L_{\alpha_w}}$.

Observe from Figure 3.13 that airplane angle of attack, α is not the same as wing angle of attack, α_w :

$$\alpha_w = \alpha + i_w \tag{3.18}$$

The wing incidence angle, i_w is determined by factors such as cruise drag, maintaining a

level cabin floor in cruise and/or visibility on approach to landing. Part III of Reference 3.1 contains more detailed discussions on this subject.

The horizontal tail lift coefficient, C_{L_h}, is determined from:

$$C_{L_h} = C_{L_{0_h}} + C_{L_{\alpha_h}}\alpha_h + C_{L_{\alpha_h}}\tau_e\delta_e \tag{3.19}$$

where: $C_{L_{0_h}}$ equals 0 for tails with symmetrical airfoils. It should be noted that many airplanes have negatively cambered tails. For such airplanes $C_{L_{0_h}}$ is negative!

α_h is the horizontal tail angle of attack:

$$\alpha_h = \alpha + i_h - \varepsilon \tag{3.20}$$

where: i_h is the horizontal tail incidence angle. In many high performance airplanes this angle is controllable from the cockpit. It is defined as positive, trailing edge down (=leading edge up!). In such an operating mode the surface is referred to as a stabilator or variable incidence stabilizer.

ε is the average downwash angle induced by the wing on the tail and often expressed as:

$$\varepsilon = \varepsilon_0 + \frac{d\varepsilon}{d\alpha}\alpha \tag{3.21}$$

where: ε_0 is the downwash angle at zero airplane angle of attack

τ_e is the elevator angle of attack effectiveness

δ_e is the elevator deflection angle, positive trailing edge down.

Methods for estimating the various quantities introduced here are found in Part VI of Reference 3.1. By substituting Eqns (3.17) through (3.21) into Eqn (3.16) and rearranging it follows:

$$C_L = C_{L_{0_{wf}}} + C_{L_{\alpha_{wf}}}\alpha + C_{L_{\alpha_h}}\eta_h\frac{S_h}{S}[\alpha - (\varepsilon_0 + \frac{d\varepsilon}{d\alpha}\alpha) + i_h + \tau_e\delta_e] + C_{L_{0_h}} \tag{3.22}$$

By comparing this equation with Eqn (3.12) the following equations for the airplane coefficient and derivatives are found by partial differentiation:

$$C_{L_0} = C_{L_{0_{wf}}} - C_{L_{\alpha_h}}\eta_h\frac{S_h}{S}\varepsilon_0 + C_{L_{0_h}} \approx C_{L_{0_{wf}}} \text{ in many airplanes} \tag{3.23}$$

$$C_{L_\alpha} = C_{L_{\alpha_{wf}}} + C_{L_{\alpha_h}}\eta_h\frac{S_h}{S}(1 - \frac{d\varepsilon}{d\alpha}) \tag{3.24}$$

$$C_{L_{i_h}} = C_{L_{\alpha_h}}\eta_h\frac{S_h}{S} \tag{3.25}$$

$$C_{L_{\delta_e}} = C_{L_{\alpha_h}}\eta_h\frac{S_h}{S}\tau_e \tag{3.26}$$

The derivative C_{L_α} is called the total airplane lift–curve slope. It is of major importance to stability, control and response to turbulence of airplanes.

Figure 3.14 shows how airplane lift coefficient is related to angle of attack and stabilizer incidence angle for a flaps up and flaps down case. Typical magnitudes of the coefficient and derivatives of Eqns (3.23) through (3.26) are presented in Figures 3.15 through 3.18. Observe that the only difference between $C_{L_{i_h}}$ and $C_{L_{\delta_e}}$ is the elevator angle of attack effectiveness parameter, τ_e . This parameter is called α_δ in Figure 2.23. For airplanes with roughly 30% chord elevators it is seen from Figure 2.23 that $C_{L_{i_h}}$ will therefore be about twice the value of $C_{L_{\delta_e}}$. Note from Equation (3.24) that the magnitude of airplane lift–curve slope can be significantly higher than the magnitude for wing–fuselage lift–curve slope for airplanes with a large horizontal tail.

The steady state model for the aerodynamic force in the stability Z–axis direction is:

$$F_{A_{z_s}} = -L = -C_L\bar{q}S = -(C_{L_0} + C_{L_\alpha}\alpha + C_{L_{i_h}} i_h + C_{L_{\delta_e}}\delta_e)\bar{q}S \tag{3.27}$$

3.1.4 AIRPLANE AERODYNAMIC PITCHING MOMENT

The airplane aerodynamic pitching moment, M_A, is non–dimensionalized as follows:

$$M_A = C_m\bar{q}S\bar{c} \tag{3.28}$$

where: C_m is the total airplane aerodynamic pitching moment coefficient.

The steady state airplane aerodynamic pitching moment coefficient depends on the following factors:

* angle of attack, α
* control surface deflection(s), δ_e, i_h, etc.
* dynamic pressure, $\bar{q}$
* Mach number and Reynolds number
* moment reference center (usually the center of gravity) location

For an airplane with an elevator and a variable incidence horizontal tail, the aerodynamic pitching moment coefficient C_m is expressed in the form of a first order Taylor series as:

$$C_m = C_{m_o} + C_{m_\alpha}\alpha + C_{m_{i_h}} i_h + C_{m_{\delta_e}}\delta_e \tag{3.29}$$

The coefficient and derivatives in Eqn (3.29) are to be evaluated at constant Mach number and Reynolds number. The terms in Eqn (3.29) have the following meanings:

C_{m_0} is the value of C_m for: $\alpha = i_h = \delta_e = 0$

$C_{m_\alpha} = \partial C_m/\partial\alpha$ is the change in airplane aerodynamic pitching moment coefficient due to a change in angle of attack

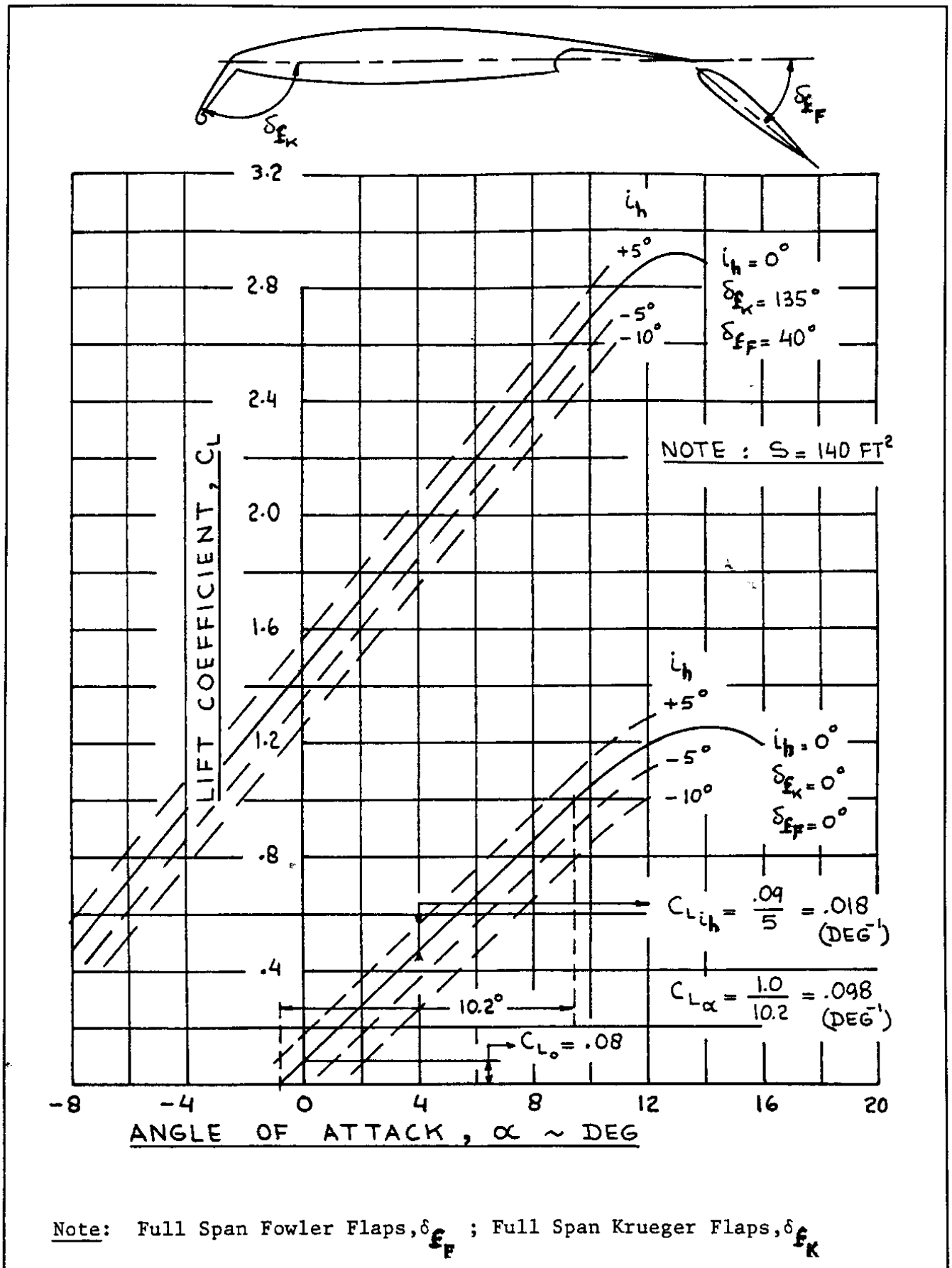

Note: Full Span Fowler Flaps, δ_{f_F} ; Full Span Krueger Flaps, δ_{f_K}

Figure 3.14 Effect of Stabilizer Incidence, Flaps and Angle of Attack on Lift Coefficient

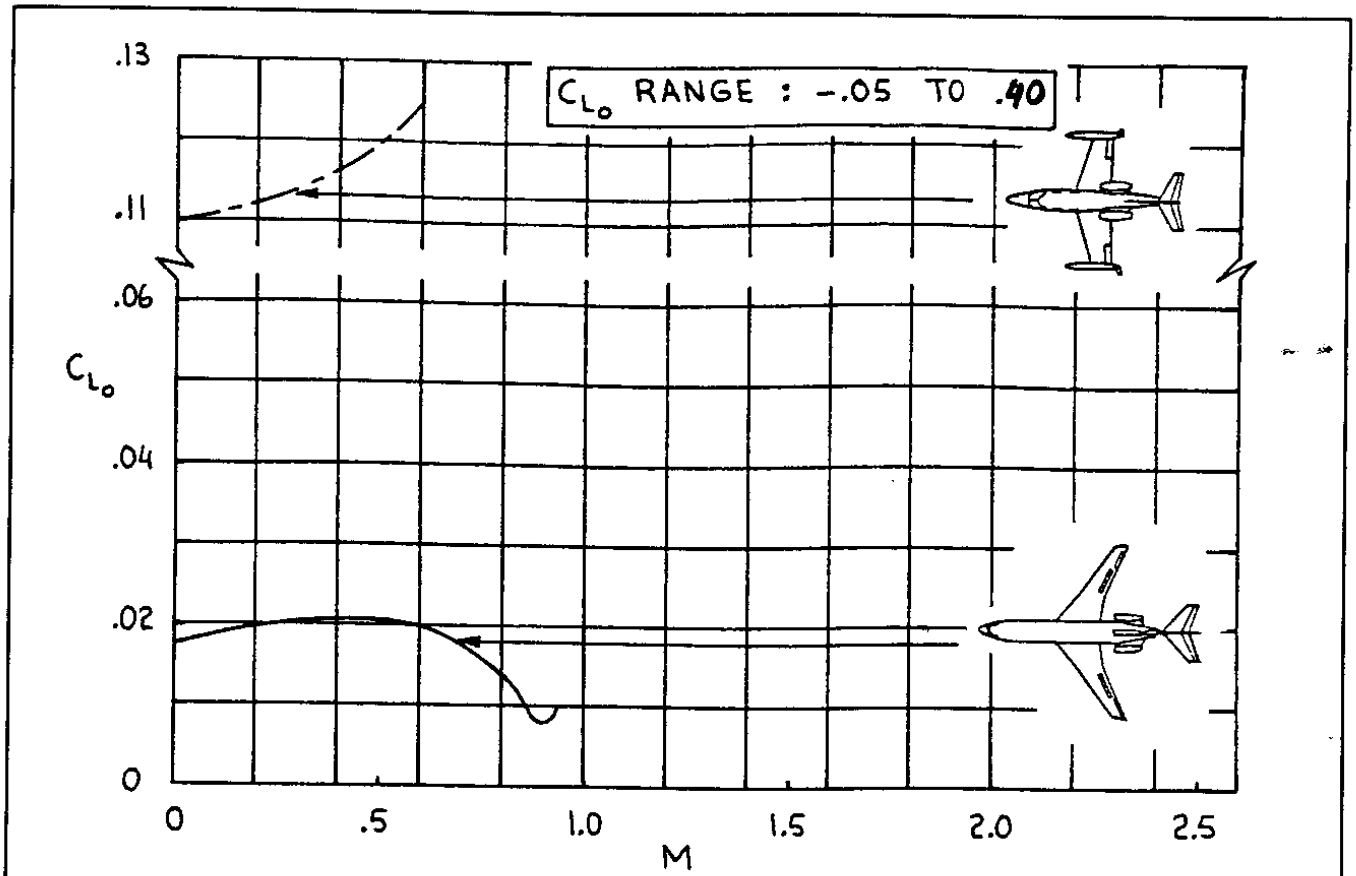

Figure 3.15 Effect of Mach Number on C_{L_0} for Several Airplanes

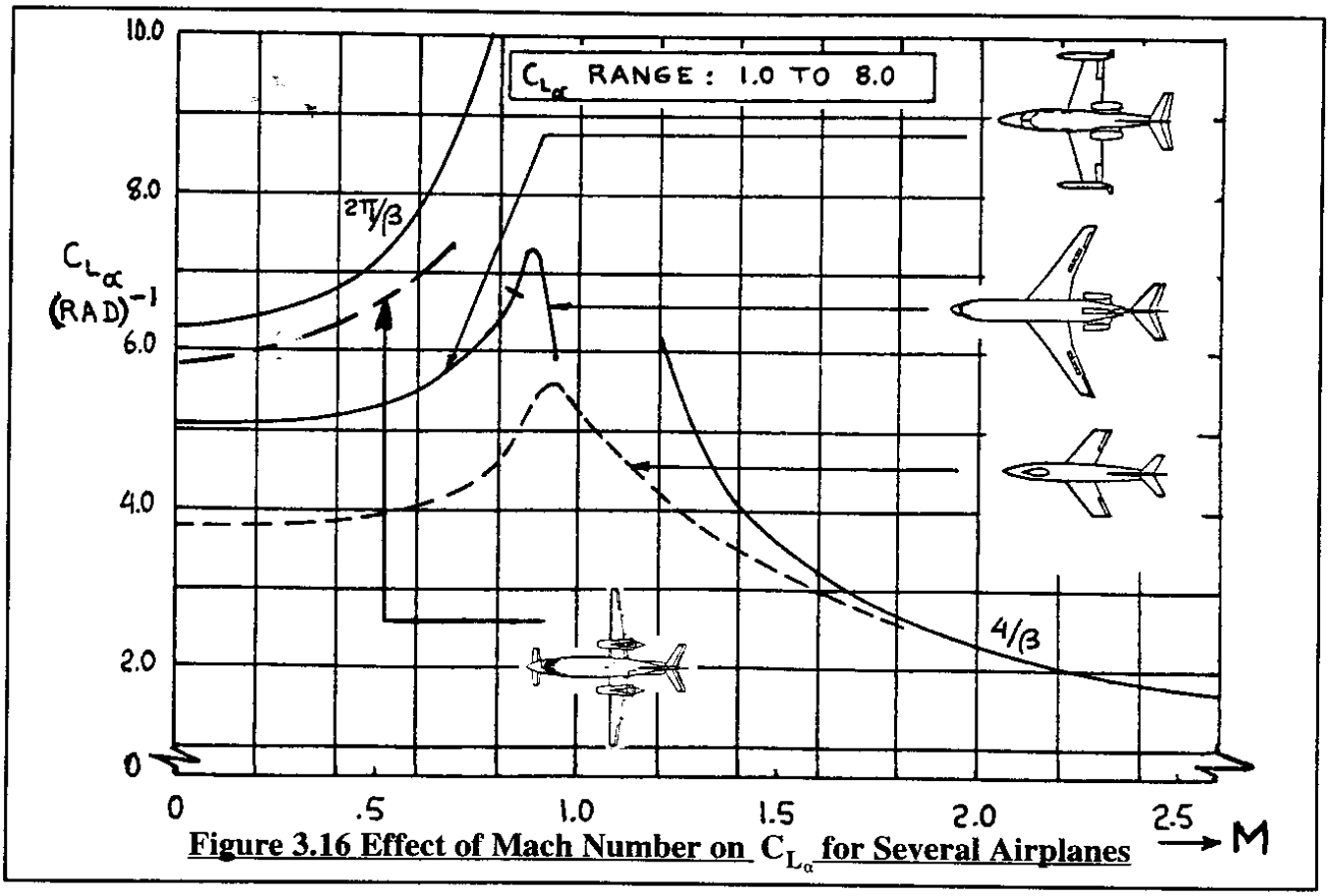

Figure 3.16 Effect of Mach Number on C_{L_α} for Several Airplanes

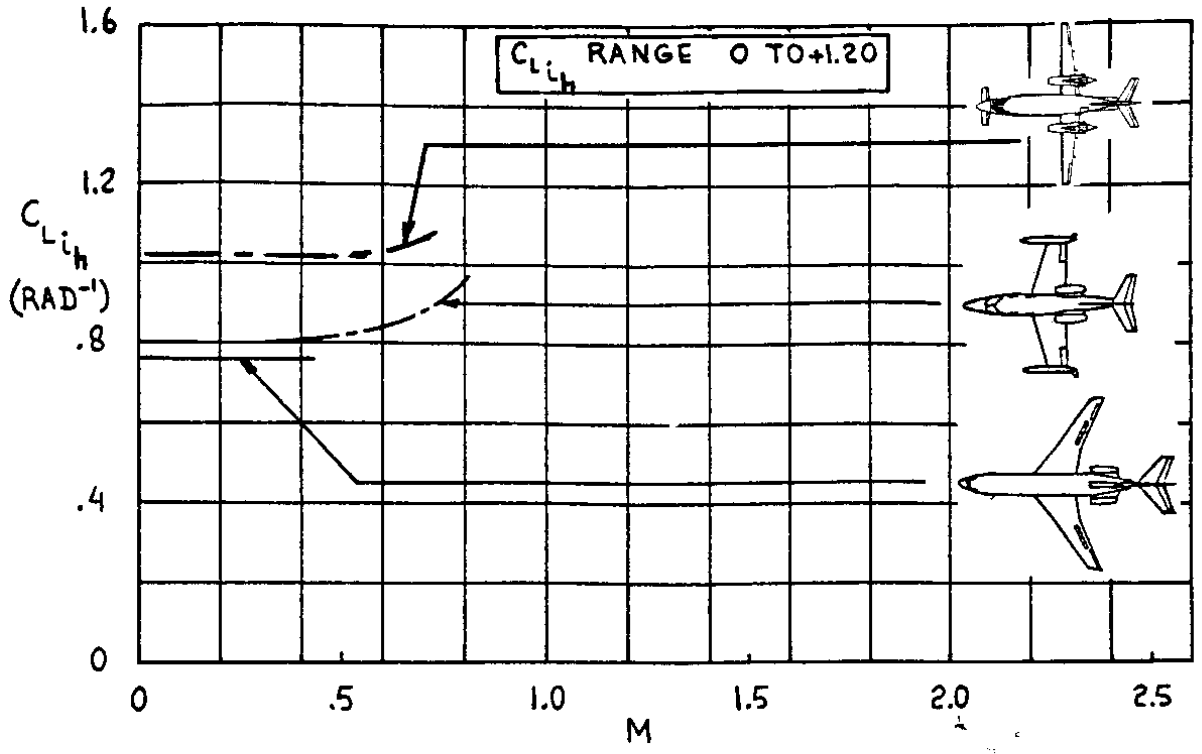

Figure 3.17 Effect of Mach Number on $C_{L_{i_h}}$ for Several Airplanes

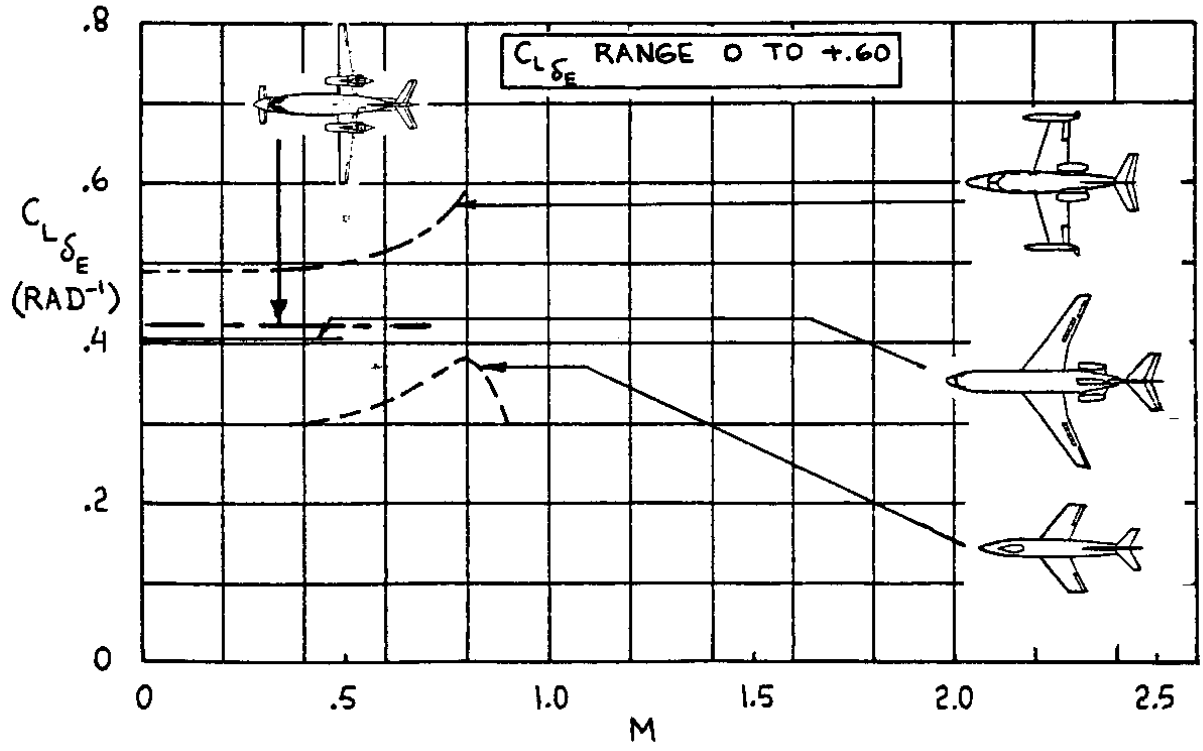

Figure 3.18 Effect of Mach Number on $C_{L_{\delta_e}}$ for Several Airplanes

$C_{m_{i_h}} = \partial C_m / \partial i_h$ is the change in airplane aerodynamic pitching moment coefficient due to a change in stabilizer incidence angle, i_h for: $\alpha = \delta_e = 0$

$C_{m_{\delta_e}} = \partial C_m / \partial \delta_e$ is the change in airplane aerodynamic pitching moment coefficient due to a change in elevator angle, δ_e for: $\alpha = i_h = 0$

In the following, it will be shown how the coefficient and derivatives in Eqn (3.29) can be estimated using the airplane component build-up idea. To keep the development simple, the tail-aft airplane geometry of Figure 3.13 will again be used. Point P in Figure 3.13 acts as the moment reference center (usually the center of gravity).

It will be assumed that the effect of wing-fuselage drag and tail drag on airplane pitching moment is negligible. Referring back to Figure 3.13, it is seen that the airplane aerodynamic pitching moment about point P can be expressed as:

$$M_A = M_{ac_{wf}} + L_{wf}(x_{cg} - x_{ac_{wf}})\cos(\alpha + i_w) - L_h(x_{ac_h} - x_{cg})\cos(\alpha + i_w - \epsilon) \qquad (3.30)$$

In most instances it is acceptable to set the cosines in Eqn (3.30) equal to 1.0. Doing that and non-dimensionalizing yields:

$$C_m = C_{m_{ac_{wf}}} + C_{L_{wf}}\frac{(x_{cg} - x_{ac_{wf}})}{\bar{c}} - C_{L_h}\eta_h\frac{S_h}{S}\frac{(x_{ac_h} - x_{cg})}{\bar{c}} \qquad (3.31)$$

At this point Equations (3.17), (3.19), (3.20) and (3.21) are substituted in Eqn (3.31) while at the same time introducing the 'bar' notation for the moment arms:

$$C_m = C_{m_{ac_{wf}}} + (C_{L_{0_{wf}}} + C_{L_{\alpha_{wf}}}\alpha)(\bar{x}_{cg} - \bar{x}_{ac_{wf}}) +$$

$$- C_{L_{\alpha_h}}\eta_h\frac{S_h}{S}(\bar{x}_{ac_h} - \bar{x}_{cg})[\alpha - (\epsilon_0 + \frac{d\epsilon}{d\alpha}\alpha) + i_h + \tau_e\delta_e] \qquad (3.32)$$

In this equation, the wing-fuselage aerodynamic center location, $\bar{x}_{ac_{wf}}$, is normally expressed as follows:

$$\bar{x}_{ac_{wf}} = \bar{x}_{ac_w} + \Delta\bar{x}_{ac_{fus}} \qquad (3.33)$$

where: $\Delta\bar{x}_{ac_{fus}}$ is the shift in wing+fuselage aerodynamic center from the wing aerodynamic center as caused by the so-called Munk effect discussed in Sub-section 2.5.6. Figure 2.19 gives examples of the magnitude of this shift for three airplanes. Methods for computing this shift for any configuration are given in Part VI of Reference 3.1.

By comparing Eqn (3.32) with Eqn (3.29) the following equations for the airplane aerodynamic pitching moment coefficient and derivatives are found by partial differentiation:

$$C_{m_0} = C_{m_{ac_{wf}}} + C_{L_{0_{wf}}}(\bar{x}_{cg} - \bar{x}_{ac_{wf}}) + C_{L_{\alpha_h}}\eta_h\frac{S_h}{S}(\bar{x}_{ac_h} - \bar{x}_{cg})\epsilon_0 \approx$$

$$\approx C_{m_{ac_{wf}}} + C_{L_{0_{wf}}}(\bar{x}_{cg} - \bar{x}_{ac_{wf}}) \text{ if } \epsilon_0 \text{ is negligible} \qquad (3.34)$$

$$C_{m_\alpha} = C_{L_{\alpha_{wf}}}(\bar{x}_{cg} - \bar{x}_{ac_{wf}}) - C_{L_{\alpha_h}}\eta_h\frac{S_h}{S}(\bar{x}_{ac_h} - \bar{x}_{cg})(1 - d\varepsilon/d\alpha) \tag{3.35}$$

$$C_{m_{i_h}} = -C_{L_{\alpha_h}}\eta_h\frac{S_h}{S}(\bar{x}_{ac_h} - \bar{x}_{cg}) = -C_{L_{\alpha_h}}\eta_h\bar{V}_h \tag{3.36}$$

$$\text{where : } \bar{V}_h = (S_h/S)(\bar{x}_{ac_h} - \bar{x}_{cg}) \tag{3.36a}$$

is the horizontal tail volume coefficient. This volume coefficient is useful in preliminary tail–sizing which is used in the early aircraft design process. A detailed explanation is found in Part II of Reference 3.1.

$$C_{m_{\delta_e}} = -C_{L_{\alpha_h}}\eta_h\bar{V}_h\tau_e \tag{3.37}$$

The derivatives $C_{m_{i_h}}$ and $C_{m_{\delta_e}}$ are referred to as longitudinal control power derivatives. They are of major importance in airplane controllability considerations as will become clear in Chapters 4 and 5.

Figure 3.19 shows how airplane aerodynamic pitching moment coefficient is related to angle of attack and stabilizer incidence angle. Figures 3.20 through 3.23 present typical magnitude of the coefficient and derivatives represented by Eqns (3.34) through (3.37). Several observations are in order:

1) Note that the only difference between $C_{m_{i_h}}$ and $C_{m_{\delta_e}}$ (Figures 3.22 and 3.23) is the angle of attack effectiveness of the elevator, τ_e . For airplanes with roughly 30% chord elevators it is seen from Figure 3.22 that $C_{m_{i_h}}$ will therefore be about twice the value of $C_{m_{\delta_e}}$.

2) Note from Figure 3.20 that the zero–angle–of–attack pitching moment coefficient, C_{m_0} can be negative as well a positive. From a trim point of view, a positive value is to be preferred.

3) Note from Figure 3.20 that C_{m_0} tends to change in the negative (i.e. nose–down) direction with increasing Mach number. This phenomenon is referred to as 'tuck'. It can lead to handling quality problems during recoveries from a high speed dive.

4) Note the 'stable' and 'unstable' breaks in the pitching moment coefficient at high angle of attack. Whether a stable or an unstable break occurs, depends on the detail design of the configuration. For a detailed discussion, see Part III of Reference 3.1.

The derivative C_{m_α} is called the static longitudinal stability derivative. It is of major importance to airplane stability and control as will become clear in Chapters 4 and 5. By introducing the idea of total airplane aerodynamic center it is possible to simplify Eqn (3.35).

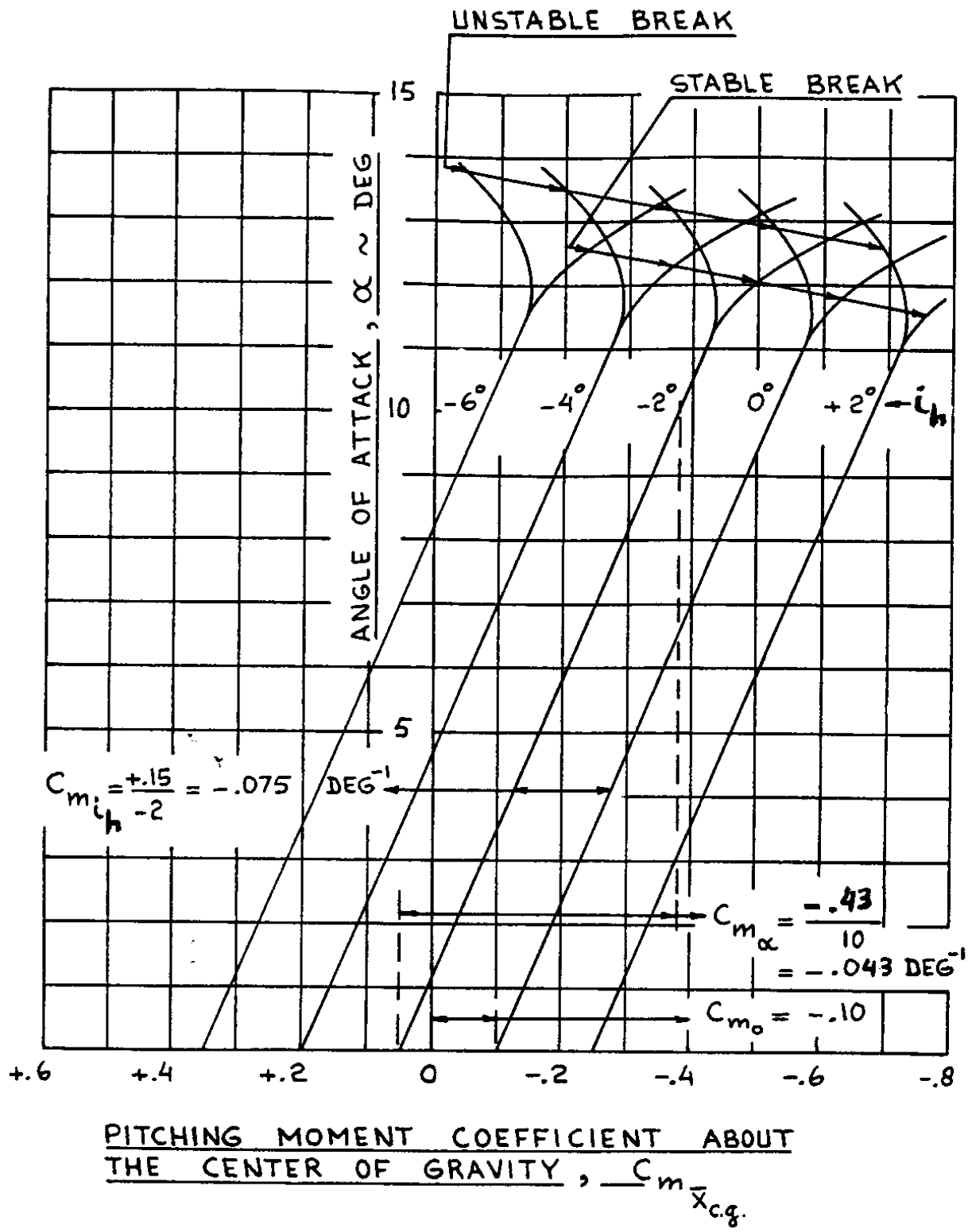

Figure 3.19 Effect of Angle of Attack and Stabilizer Incidence Angle on Aerodynamic Pitching Moment Coefficient

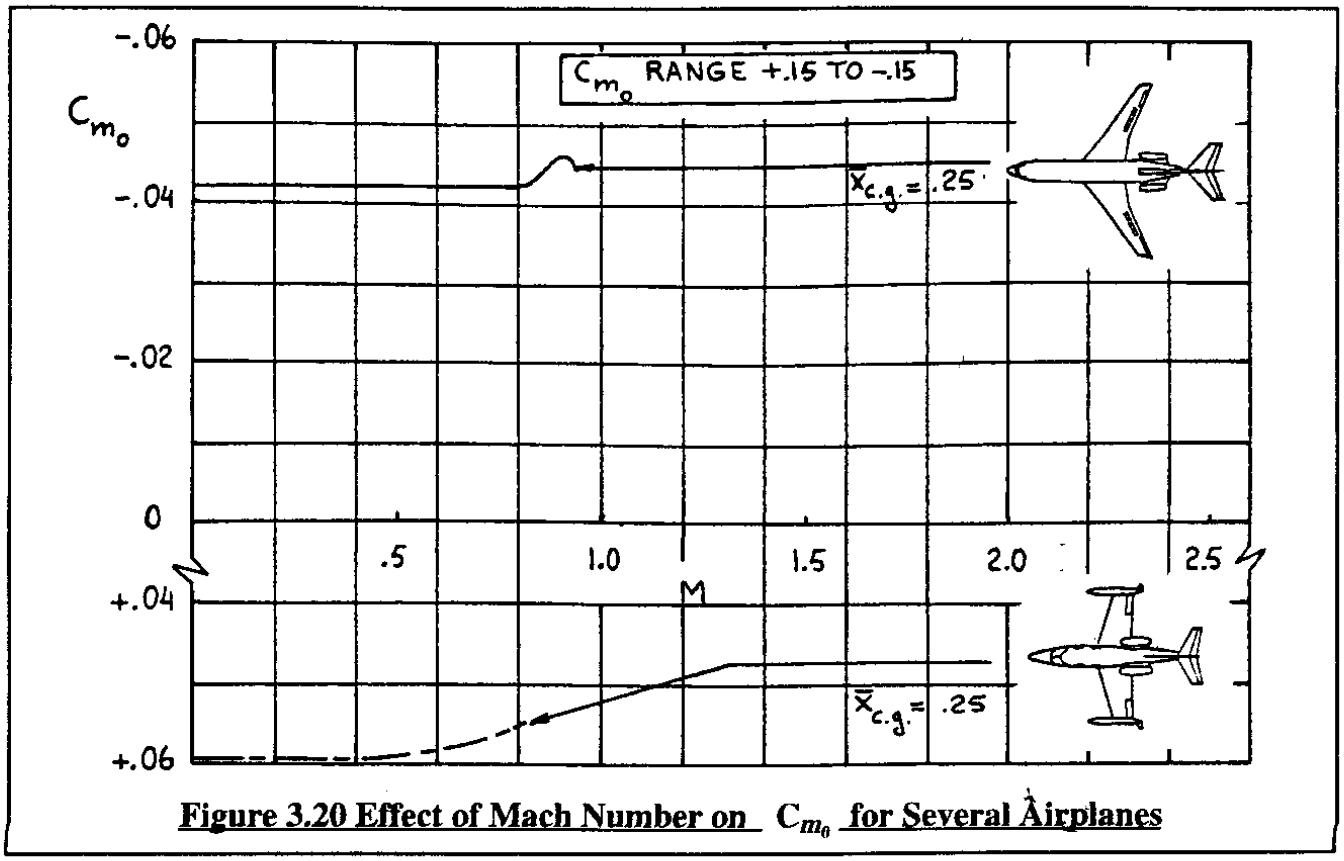

Figure 3.20 Effect of Mach Number on C_{m_0} for Several Airplanes

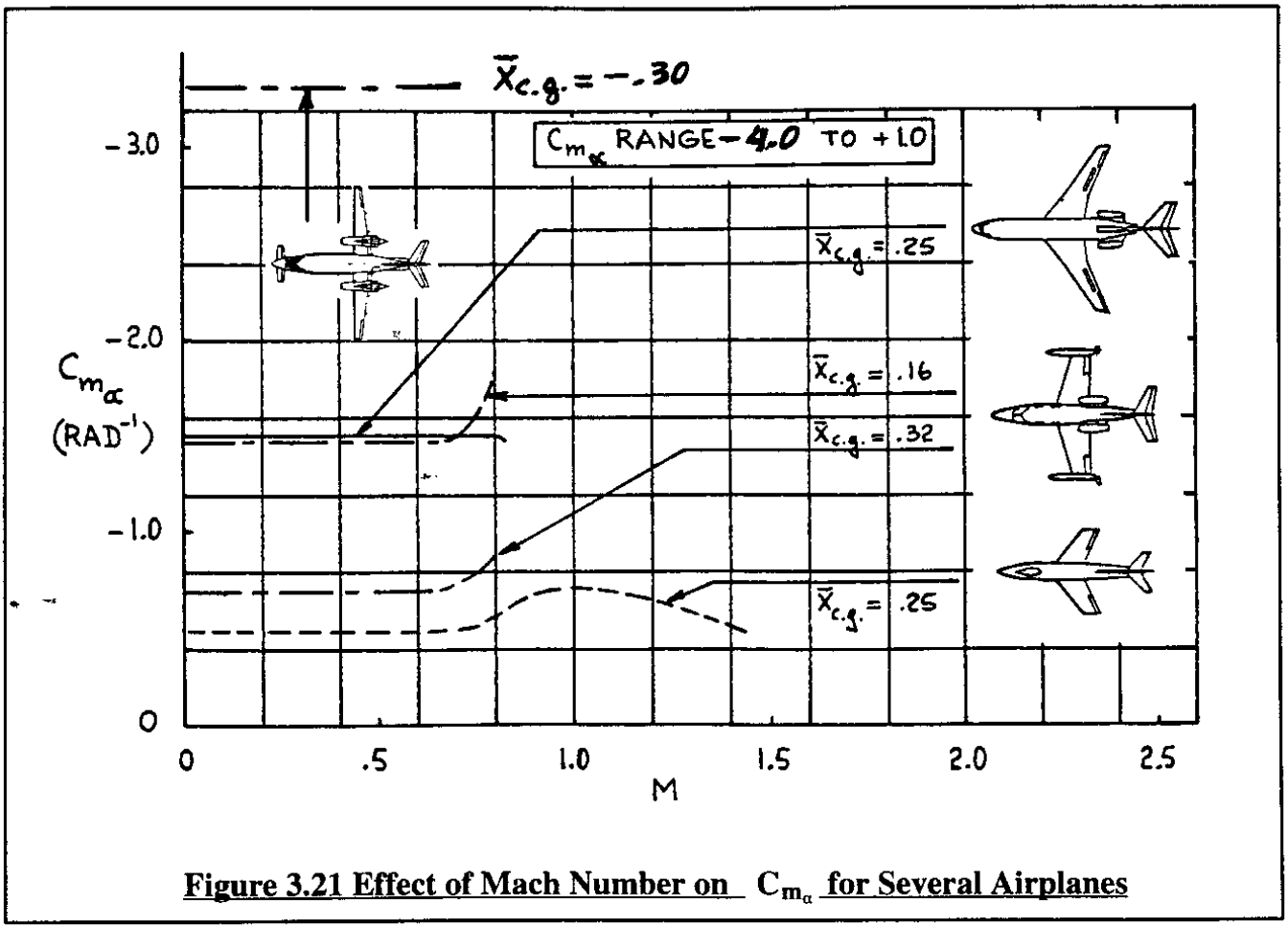

Figure 3.21 Effect of Mach Number on C_{m_α} for Several Airplanes

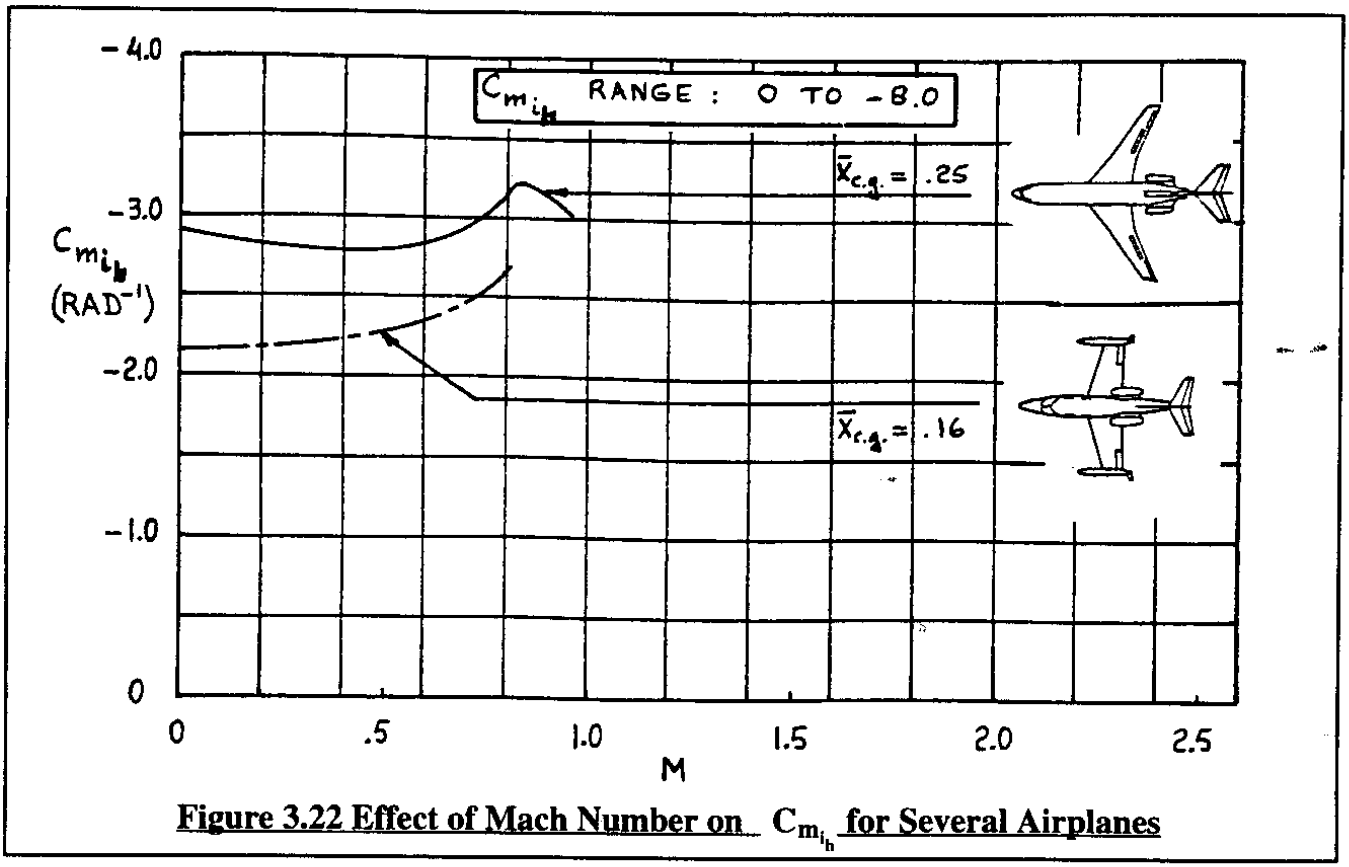

Figure 3.22 Effect of Mach Number on $C_{m_{i_h}}$ for Several Airplanes

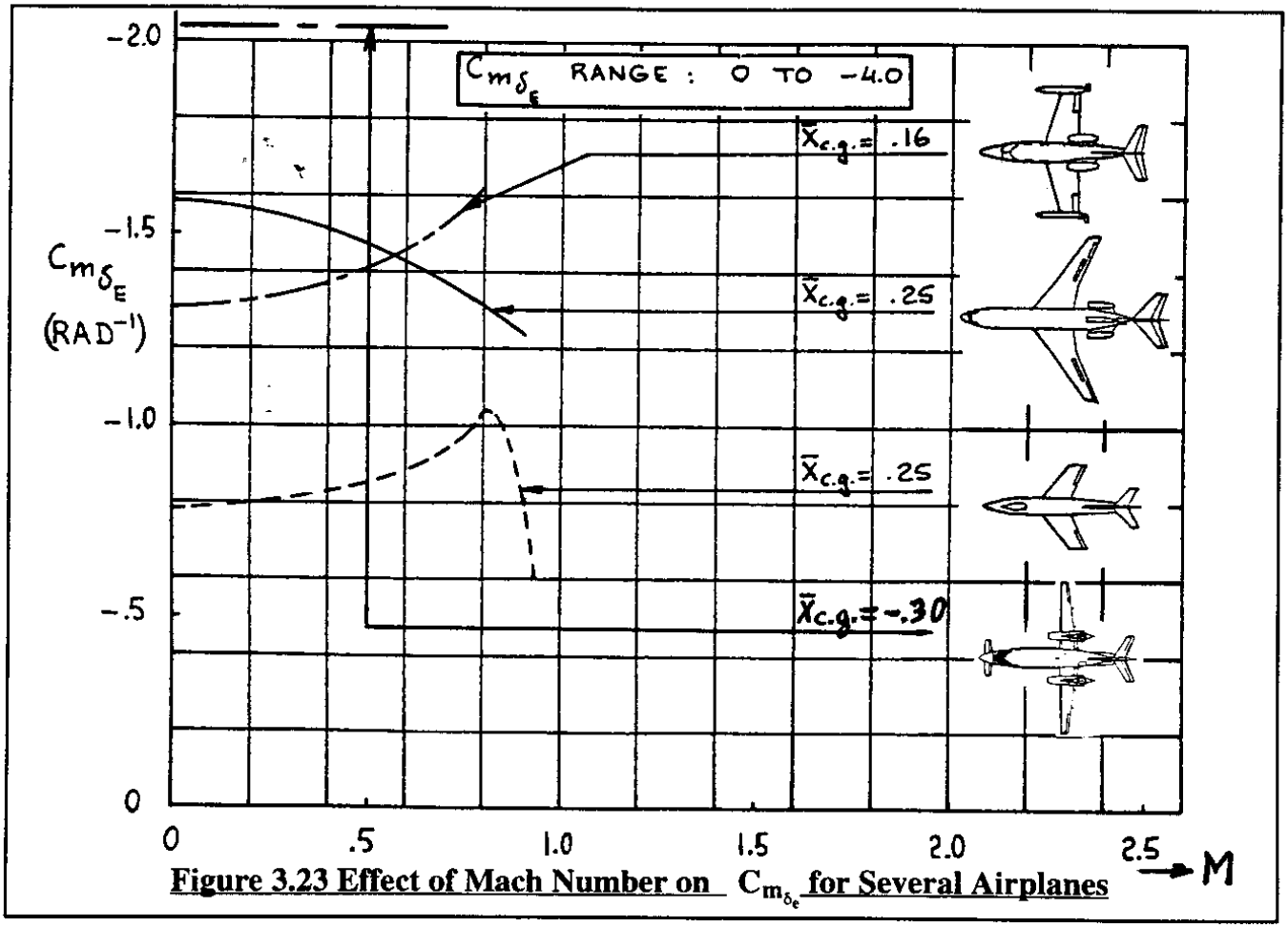

Figure 3.23 Effect of Mach Number on $C_{m_{\delta_e}}$ for Several Airplanes

Definition: The aerodynamic center of an airplane is defined as that point on the wing mean geometric chord about which the variation of pitching moment coefficient with angle of attack is zero.

The location of airplane aerodynamic center on the wing mean geometric chord is normally expressed as a fraction of the mgc, $\bar{x}_{ac_A}$, and is also referred to as the airplane (stick–fixed) neutral point. The significance of the 'stick–fixed' addition will be made clear in Chapter 4.

The definition of airplane aerodynamic center, when applied to Eqn (3.35), leads to the condition: $C_{m_\alpha} = 0$ and $\bar{x}_{cg} \mapsto \bar{x}_{ac_A}$ so that:

$$\bar{x}_{ac_A} = \frac{\bar{x}_{ac_{wf}} + \frac{C_{L_{\alpha_h}}}{C_{L_{\alpha_{wf}}}} \eta_h \frac{S_h}{S} \bar{x}_{ac_h} (1 - \frac{d\varepsilon}{d\alpha})}{1 + \frac{C_{L_{\alpha_h}}}{C_{L_{\alpha_{wf}}}} \eta_h \frac{S_h}{S} (1 - \frac{d\varepsilon}{d\alpha})} \tag{3.38}$$

The reader is asked to show that Equations (3.35) and (3.38) can be combined to yield:

$$C_{m_\alpha} = C_{L_\alpha} (\bar{x}_{cg} - \bar{x}_{ac_A}) \tag{3.39}$$

At this point the reader is reminded of two facts:

1) Equations (3.38) and (3.39) do not include the pitching moment contribution due to the propulsive installation. Particularly in propeller driven airplanes there can exist a significant shift in aerodynamic center due to the so–called propeller normal force as well as due to propeller tilt angle. See Part VI of Reference 3.1 for more details.

2) Equation (3.38) applies to tail–aft airplanes only. For canard and for three–surface airplanes (such as the Beech Starship I and the Piaggio P–180 Avanti) Eqn (3.38) must be modified. For airplanes where the canard does NOT SIGNIFICANTLY interfere with the wing (or tail) flow–field it is possible to show that Eqn (3.38) when applied to a three–surface airplane becomes:

$$\bar{x}_{ac_A} = \frac{\bar{x}_{ac_{wf}} - \frac{C_{L_{\alpha_c}}}{C_{L_{\alpha_{wf}}}} \eta_c \frac{S_c}{S} \bar{x}_{ac_c} (1 + \frac{d\varepsilon_c}{d\alpha}) + \frac{C_{L_{\alpha_h}}}{C_{L_{\alpha_{wf}}}} \eta_h \frac{S_h}{S} \bar{x}_{ac_h} (1 - \frac{d\varepsilon}{d\alpha})}{1 + \frac{C_{L_{\alpha_c}}}{C_{L_{\alpha_{wf}}}} \eta_c \frac{S_c}{S} (1 + \frac{d\varepsilon_c}{d\alpha}) + \frac{C_{L_{\alpha_h}}}{C_{L_{\alpha_{wf}}}} \eta_h \frac{S_h}{S} (1 - \frac{d\varepsilon}{d\alpha})} \tag{3.40}$$

For a pure canard airplane the horizontal tail term in Eqn (3.40) must be stricken. Figure 3.24 shows how $\bar{x}_{ac_c}$ is defined in relationship to $\bar{x}_{ac_h}$ for a three–surface airplane. The quantity η_c represents the dynamic pressure ratio, $\bar{q}_c/\bar{q}$, at the canard location. The angle ε_c is the up–wash angle caused by the wing at the canard location. Methods for determining the various quantities in Eqn (3.40) are contained in Part VI of Reference 3.1.

The steady state model for the aerodynamic pitching moment about the stability Y–axis (same as body–fixed Y–axis!) is:

$$M_{A_{1_s}} = M_A = C_m \bar{q} S \bar{c} = (C_{m_0} + C_{m_\alpha} \alpha + C_{m_{i_h}} i_h + C_{m_{\delta_e}} \delta_e) \bar{q} S \bar{c} \tag{3.41}$$

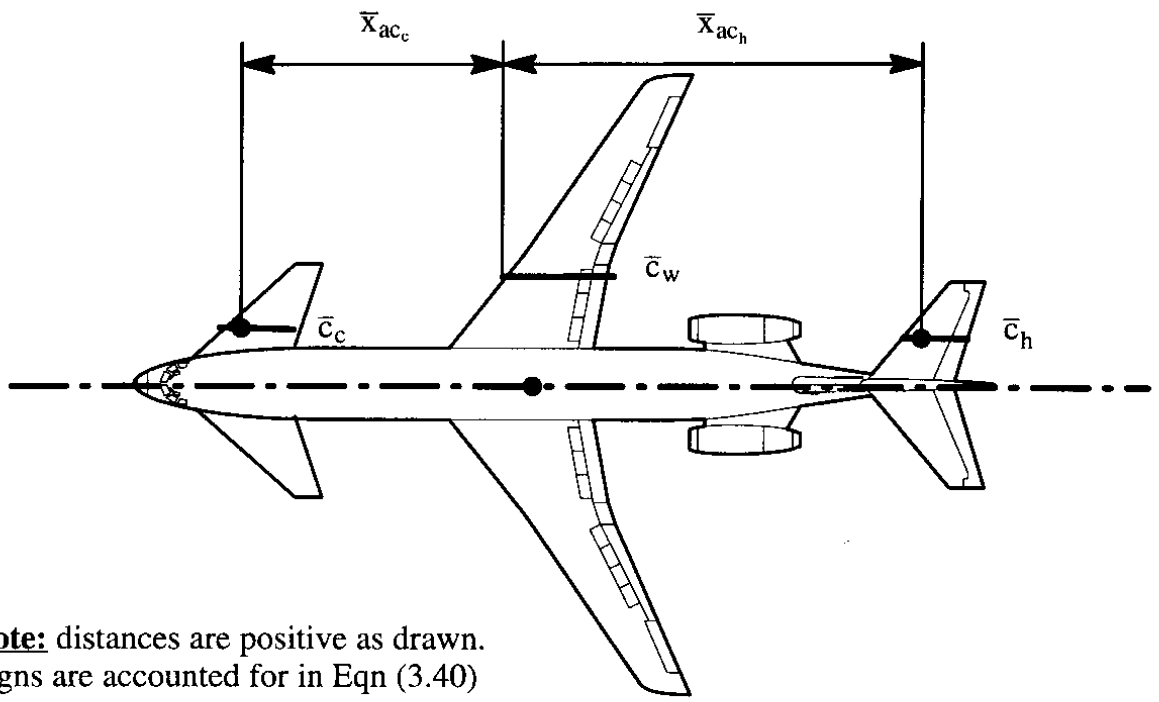

Note: distances are positive as drawn.
Signs are accounted for in Eqn (3.40)

Figure 3.24 Definition of Canard and Horizontal Tail Aerodynamic Center Geometry

3.1.5 LONGITUDINAL THRUST FORCES AND MOMENTS

Most airplanes are equipped with one or more engines. The number of engines and their disposition over the airplane depends on many mission and airworthiness related factors. For a discussion of these factors, the reader may consult Parts II and III of Reference 3.1. In this text it will be assumed that the number and disposition of the engines over the airplane is given.

The effect of thrust on the airplane forces and moments will be assumed to be comprised of:

1) Direct thrust effects 2) Indirect thrust effects

1) Direct thrust effects can be modeled in the body–fixed XYZ axis system as illustrated in Figure 3.25. The thrust output of each engine is referred to as the installed thrust. Installed thrust is computed from engine manufacturer's thrust data by accounting for various installation losses as described in Part VI of Reference 3.1. In this text it is assumed that the installed thrust for each engine is a given.

2) Indirect thrust effects occur when propeller flow fields or jet exhausts interfere with lifting surfaces, for example, by impinging on them. These effects will not be modelled in detail because they tend to be strongly configuration dependent which makes a generalized modelling approach of questionable value. Specific examples of indirect thrust effects are:

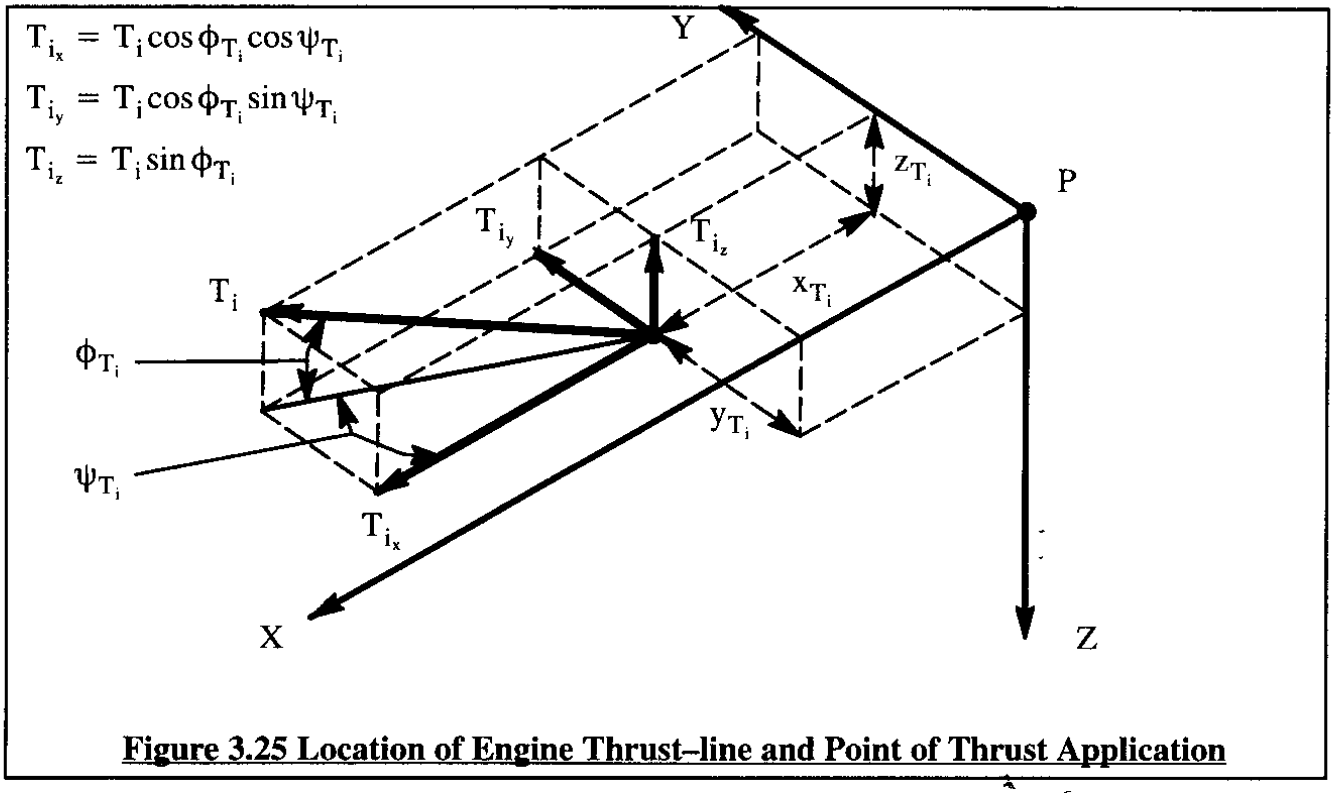

Figure 3.25 Location of Engine Thrust–line and Point of Thrust Application

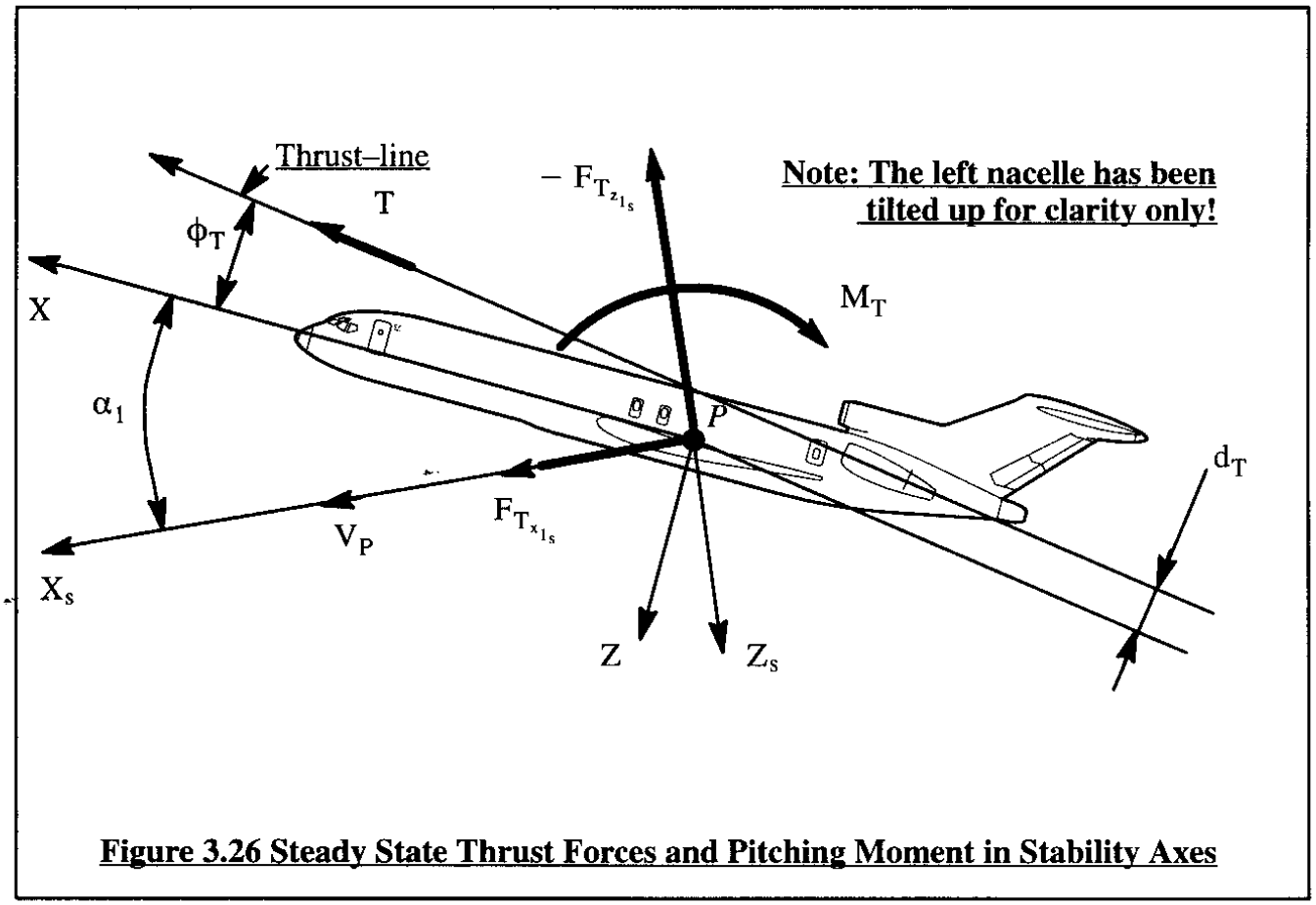

Figure 3.26 Steady State Thrust Forces and Pitching Moment in Stability Axes

a) propeller slipstream effect on a wing when the propeller is mounted in front of the wing

b) propeller slipstream effect on the downwash of a wing which in turn can affect the aerody–namics of the horizontal and/or vertical tail

Indirect thrust effects are frequently modelled by the use of thrust coefficient derivatives. The thrust coefficient of an airplane is defines as:

$$C_T = T/\bar{q}S \tag{3.42}$$

As was seen in Sub–section 3.1.1 the aerodynamic forces and moments are modelled using the idea of stability and control derivatives. One such derivative was the static longitudinal stability derivative, C_{m_α} : see Eqn (3.35). The indirect thrust effect on this derivative can be accounted for by using the following expression:

$$C_{m_\alpha} = C_{m_{\alpha_{C_T=0}}} + \frac{\partial C_{m_\alpha}}{\partial C_T} C_T \tag{3.43}$$

where: the derivative $C_{m_{\alpha_{C_T=0}}}$ is in fact the same as C_{m_α} of Eqn (3.35).

the derivative $\partial C_{m_\alpha}/\partial C_T$ can be most effectively evaluated using windtunnel data on powered models. A detailed treatment of these effects is beyond the scope of this text.

Part VI of Reference 3.1 (Sub–section 8.2.8) contains a more detailed discussion of several corrections which may have to be made to aerodynamic derivatives as a result of thrust induced effects caused by propeller installations.

Using the thrust line orientations of Figure 3.25 results in the following model for the longitudinal thrust forces and moments:

$$F_{T_{x_{1_s}}} = \left(\sum_{i=1}^{i=n} T_i \cos\phi_{T_i} \cos\psi_{T_i}\right) \cos\alpha_1 + \left(\sum_{i=1}^{i=n} T_i \sin\phi_{T_i}\right) \sin\alpha_1 \tag{3.44a}$$

$$F_{T_{z_{1_s}}} = \left(\sum_{i=1}^{i=n} T_i \sin\phi_{T_i}\right) \cos\alpha_1 - \left(\sum_{i=1}^{i=n} T_i \cos\phi_{T_i} \cos\psi_{T_i}\right) \sin\alpha_1 \tag{3.44b}$$

$$M_{T_{1_s}} = \sum_{i=1}^{i=n} T_i \cos\phi_{T_i} \cos\psi_{T_i} z_{T_i} + \sum_{i=1}^{i=n} T_i \sin\phi_{T_i} x_{T_i} \tag{3.44c}$$

Figure 3.26 shows the net thrust for the case where ψ_{T_i} is negligibly small for ALL i engines and where $\phi_{T_i} = \phi_T$ for all engines. The thrust, T, then is the vector sum of the thrust vectors of all i engines. This results in the following model for the longitudinal thrust forces and moment:

$$F_{T_{x_{1_s}}} = T\cos(\phi_T + \alpha_1) \tag{3.45a}$$

$$F_{T_{z_{1_s}}} = -T\sin(\phi_T + \alpha_1) \tag{3.45b}$$

$$M_{T_{1_s}} = M_{T_1} = -Td_T \tag{3.45c}$$

3.1.6 ASSEMBLING THE STEADY STATE LONGITUDINAL FORCES AND MOMENTS

It is now possible to assemble all expressions for the longitudinal steady state forces and moments in matrix format. This is done in Table 3.2. Note that the aerodynamic forces and moments are treated as linear. The thrust terms still contain transcendental terms. Later, in the discussion of the equations of motion in Chapter 4, it will be shown that by the introduction of iteration schemes or by using the small angle assumption this problem will fade away.

Table 3.2 Matrix Format for Steady State Longitudinal Forces and Moments

$$\begin{Bmatrix} F_{A_{x_{1_s}}} \\ F_{A_{z_{1_s}}} \\ M_{A_{1_s}} \end{Bmatrix} = \begin{Bmatrix} -D \\ -L \\ M_A \end{Bmatrix} = \begin{Bmatrix} -C_D\bar{q}S \\ -C_L\bar{q}S \\ C_m\bar{q}S\bar{c} \end{Bmatrix} \quad \textbf{with:}$$

$$\begin{Bmatrix} C_D \\ C_L \\ C_m \end{Bmatrix} = \begin{bmatrix} C_{D_0} & C_{D_\alpha} & C_{D_{i_h}} & C_{D_{\delta_e}} \\ \text{drag polar} & \text{drag polar} & \text{small} & \text{small} \\ C_{L_0} & C_{L_\alpha} & C_{L_{i_h}} & C_{L_{\delta_e}} \\ (3.23) & (3.24) & (3.25) & (3.26) \\ C_{m_0} & C_{m_\alpha} & C_{m_{i_h}} & C_{m_{\delta_e}} \\ (3.34) & (3.35) & (3.36) & (3.37) \end{bmatrix} \begin{Bmatrix} 1 \\ \alpha \\ i_h \\ \delta_e \end{Bmatrix} \tag{3.46a}$$

$$\begin{Bmatrix} F_{T_{x_{1_s}}} \\ F_{T_{z_{1_s}}} \\ M_{T_{1_s}} \end{Bmatrix} = \begin{Bmatrix} T\cos(\phi_T + \alpha) \\ -T\sin(\phi_T + \alpha) \\ -Td_T \end{Bmatrix} \tag{3.46b}$$

3.1.7 LATERAL–DIRECTIONAL AERODYNAMIC FORCES AND MOMENTS

When an airplane is in a steady state flight condition such that $V_1 \neq 0$, the airplane is said to be side–slipping. The sideslip angle, β_1 is defined in Figure 3.27. As seen in Table 3.1 this sideslip gives rise to an aerodynamic rolling moment, $L_{A_{1_s}}$, an aerodynamic side force, $F_{A_{y_{1_s}}}$, and an aerodynamic yawing moment, $N_{A_{1_s}}$. In addition (as also suggested by Table 3.1), any lateral–directional control surface deflections will contribute to this force and to these moments. Figure 3.27, where the subscript 1 has been deleted, shows how the side force, rolling and yawing moments are oriented relative to the airplane.

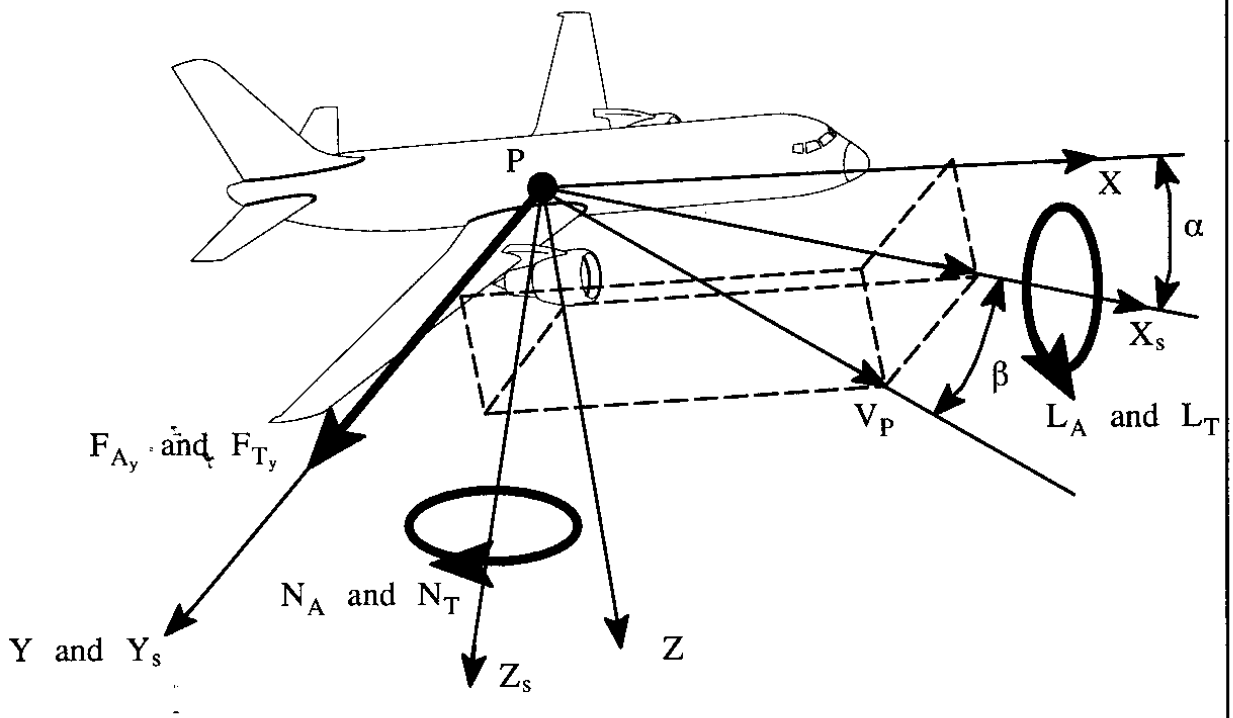

Figure 3.27 Lateral–Directional Force and Moments in Stability Axes

In the stability axis system they are written as follows:

$$L_{A_{1_s}} = L_A \tag{3.47}$$

$$F_{A_{y_{1_s}}} = F_{A_y} \tag{3.48}$$

$$N_{A_{1_s}} = N_A \tag{3.49}$$

As indicated before, the stability axis system will be used and all force and moment expressions are defined in the steady state and therefore, the subscripts 1 and s will be dropped without ambiguity.

3.1.8 AIRPLANE AERODYNAMIC ROLLING MOMENT

The steady state airplane aerodynamic rolling moment, L_A, is non–dimensionalized as:

$$L_A = C_l \bar{q} S b \tag{3.50}$$

where: C_l is the airplane aerodynamic rolling moment coefficient.

The steady state airplane aerodynamic rolling moment coefficient, C_l, depends on the following factors:

* angle of sideslip, β
* angle of attack, α
* dynamic pressure, $\bar{q}$ (see p.103)
* deflection of lateral control surface(s)
* deflection of directional control surface(s)
* Mach number and Reynolds number
* moment reference center (usually the center of gravity) location

For an airplane equipped with ailerons and rudder, the rolling moment coefficient is expressed in first order Taylor series form:

$$C_l = C_{l_0} + C_{l_\beta}\beta + C_{l_{\delta_a}}\delta_a + C_{l_{\delta_r}}\delta_r \tag{3.51}$$

The coefficient and derivatives in Eqn (3.51) are to be evaluated at constant Mach number and Reynolds number. The terms in Eqn (3.51) have the following meanings:

C_{l_0}	is the value of C_l for: $\beta = \delta_a = \delta_r = 0$
$C_{l_\beta} = \partial C_l / \partial \beta$	is the change in airplane rolling moment coefficient due to a change in airplane sideslip angle, β
$C_{l_{\delta_a}} = \partial C_l / \partial \delta_a$	is the change in airplane rolling moment coefficient due to a change in aileron deflection, δ_a
$C_{l_{\delta_r}} = \partial C_l / \partial \delta_r$	is the change in airplane rolling moment coefficient due to a change in rudder deflection, δ_r

The coefficient C_{l_0} tends to be equal to zero for symmetrical airplane configurations. Exceptions to this are found in airplanes (such as fighters) with very slender, long fore–bodies. In such cases it is possible that the flow–field around the nose becomes dominated by asymmetrically shed vortices which can cause C_{l_0} to have nonzero values. For asymmetrical airplanes such as those shown in Figure 1.3, the coefficient C_{l_0} also tends to have a non– zero value.

The derivative C_{l_β} is called the airplane dihedral effect. This derivative plays a major role

in determining airplane stability. The control power derivative $C_{l_{\delta_a}}$ is a dominant factor in the bank angle maneuverability of airplanes. The control power derivative $C_{l_{\delta_r}}$ is a so–called cross–control derivative. The magnitude of this derivative should preferably be close to zero.

In the following, it will be shown how the derivatives in Eqn (3.51) can be determined by using the component build–up philosophy.

Rolling Moment Coefficient Derivative Due to Sideslip, C_{l_β}

The rolling moment coefficient due to sideslip (dihedral effect) derivative, C_{l_β}, may be estimated by summing the individual dihedral effect of the airplane components. For a conventional airplane this yields:

$$C_{l_\beta} = C_{l_{\beta_{wf}}} + C_{l_{\beta_h}} + C_{l_{\beta_v}} \tag{3.52}$$

For non–conventional airplanes the reader should adjust this equation accordingly. A physical explanation for the dihedral effect of the wing–fuselage, the horizontal tail and the vertical tail will be given next.

Wing–fuselage Contribution, $C_{l_{\beta_{wf}}}$

The dihedral effect of the wing–fuselage combination is caused primarily by three factors:

1) Wing geometric dihedral effect
2) Effect of wing position on the fuselage (high or low)
3) Effect of wing sweep angle

1) Wing geometric dihedral effect

Figure 3.28 illustrates how the geometric dihedral angle, Γ, of a wing, can cause a rolling moment due to sideslip. Observe the right wing panel. As a result of the combination of angle of attack and sideslip, a normal velocity, V_n, is induced on that panel. This normal velocity is:

$$V_n = W\cos\Gamma + V\sin\Gamma \approx W + V\Gamma \tag{3.53}$$

If $\Gamma > 0$ (as shown in Figure 3.28) it is called positive. If $\Gamma < 0$, it is called negative. The latter is also referred to as 'anhedral'. As a result of a positive dihedral angle, the right wing sees a positive increase in angle of attack given by:

$$\Delta\alpha \approx \frac{V\Gamma}{U} \approx \frac{U\beta\Gamma}{U} \approx \beta\Gamma \tag{3.54}$$

It is this increment in angle of attack which produces a corresponding increment in lift. This in turn results in a negative rolling moment contribution. Note that the left wing panel experiences

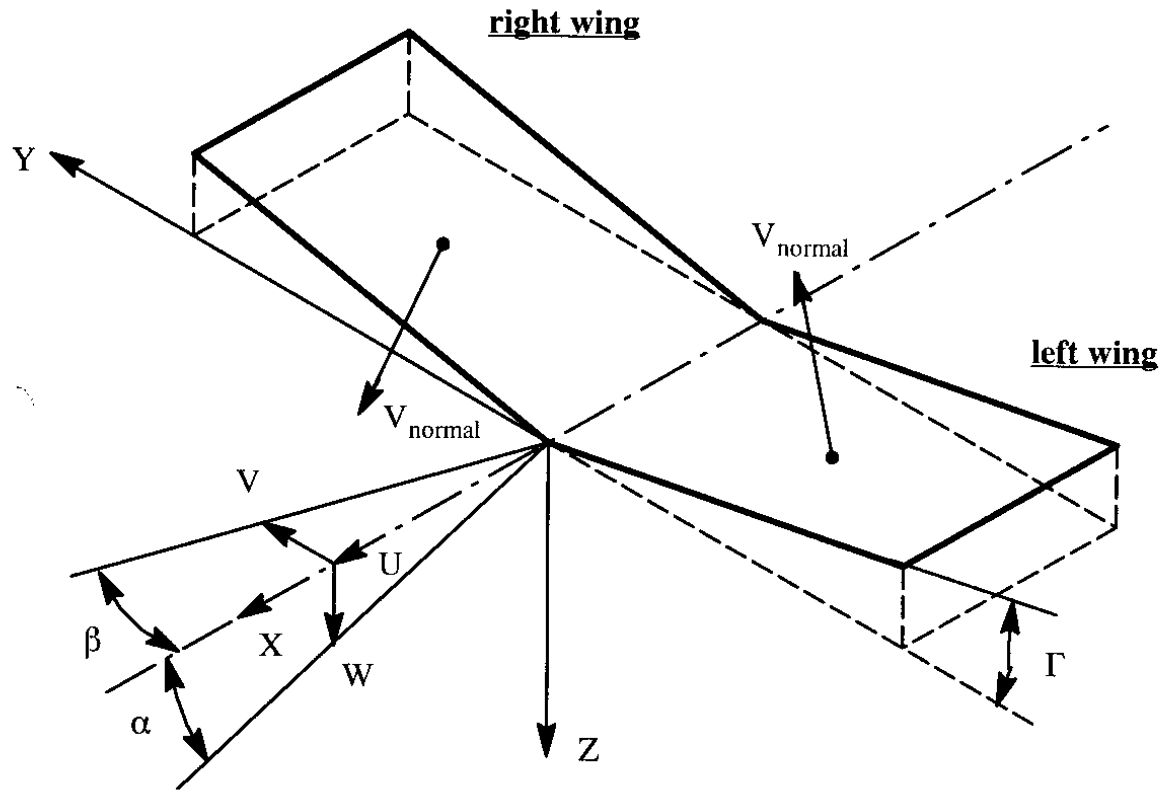

Figure 3.28 Normal Velocities Induced by Angle of Attack and Sideslip due to Geometric Dihedral on the Wing of an Airplane

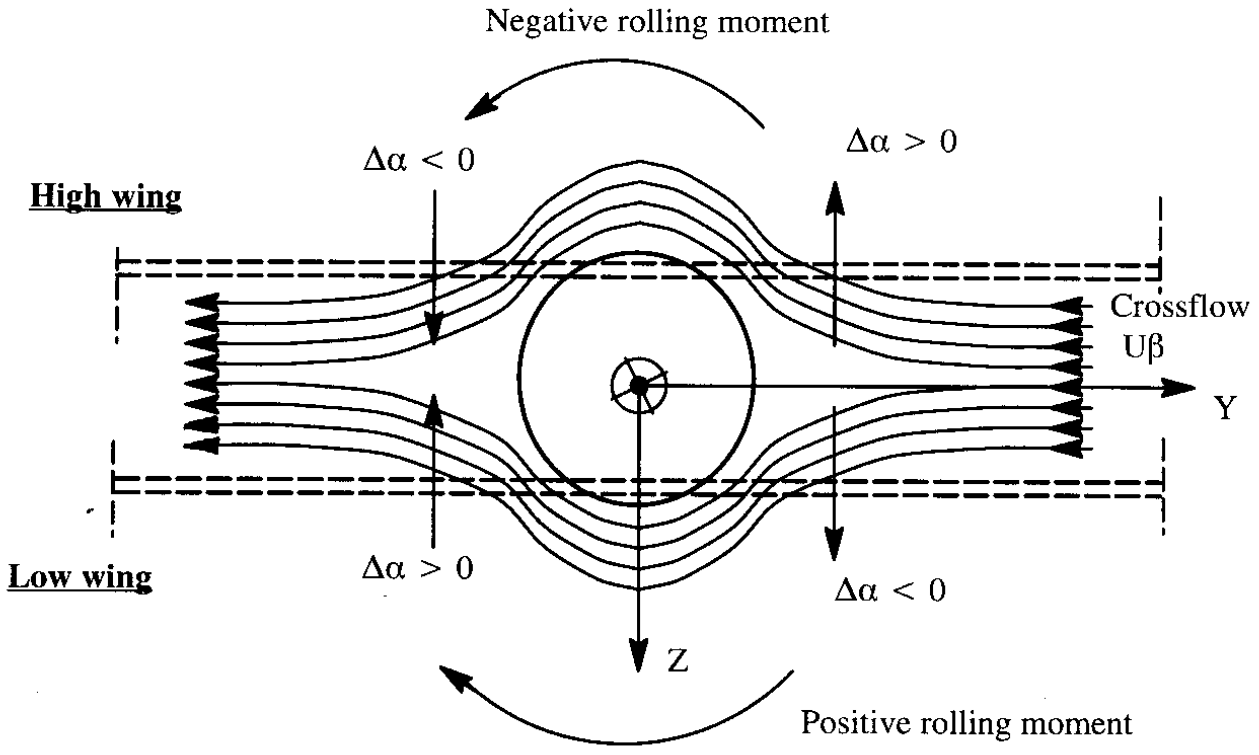

Figure 3.29 Explanation for Rolling Moment due to Sideslip as Affected by Wing Position on the Fuselage

exactly the opposite effect which also results in a negative rolling moment. The rolling moment due to sideslip due to geometric wing dihedral is therefore proportional to the geometric dihedral angle itself! Part VI of Reference 3.1 contains detailed methods for estimating this contribution.

2) Effect of wing position on the fuselage (high or low)

In Figure 3.29 the flow-field in sideslip is split into two components: a symmetrical flow-field along the X-axis (not shown) and a cross-flow field with velocity $U\beta$. This cross-flow is seen to produce incremental angles of attack near the wing-fuselage intersection. These incremental angles of attack produce ultimately incremental rolling moments which are negative for a high wing position and positive for a low wing position.

This is the reason why in high wing airplanes the wing has significantly less geometric dihedral than in low wing airplanes. This effect can be clearly seen by studying three-views of airplanes in Jane's All the World's Aircraft.

3) Effect of wing sweep angle

Figure 3.30 shows that aft (= positively) swept wings produce a negative rolling moment because of a difference in velocity components normal to the leading edge between the left and right wing panels. Consider two wing strips at distances +/- y_i from the centerline. The local lift on each strip may be approximated by:

$$\Delta L_i = C_{L_i} \bar{q}_i S_i \tag{3.55}$$

where:

$$\bar{q}_i = 0.5\rho V_{n_i}^2 \tag{3.56}$$

As shown in Figure 3.30, the velocity component normal to the leading edge is larger for the right wing strip than for the left wing strip:

$$[V_{n_{i_{l.h.s.}}} = V_P \cos(\Lambda_{LE} + \beta)] < [V_{n_{i_{r.h.s.}}} = V_P \cos(\Lambda_{LE} - \beta)] \tag{3.57}$$

The two wing strips together cause a negative rolling moment which is:

$$\Delta L_{A_{strips}} = - y_i C_{L_i} \frac{1}{2} \rho S_i V_P^2 [\cos^2(\Lambda_{LE} - \beta) - \cos^2(\Lambda_{LE} + \beta)] \tag{3.58}$$

This result, when expanded for small values of sideslip angle yields:

$$\Delta L_{A_{strips}} = - y_i C_{L_i} \bar{q} S_i (2\beta \sin 2\Lambda_{LE}) \tag{3.59}$$

The reader is asked to show that for forward swept wings the sign of Eqn (3.59) reverses! It is of interest to note from Eqn (3.59) that:

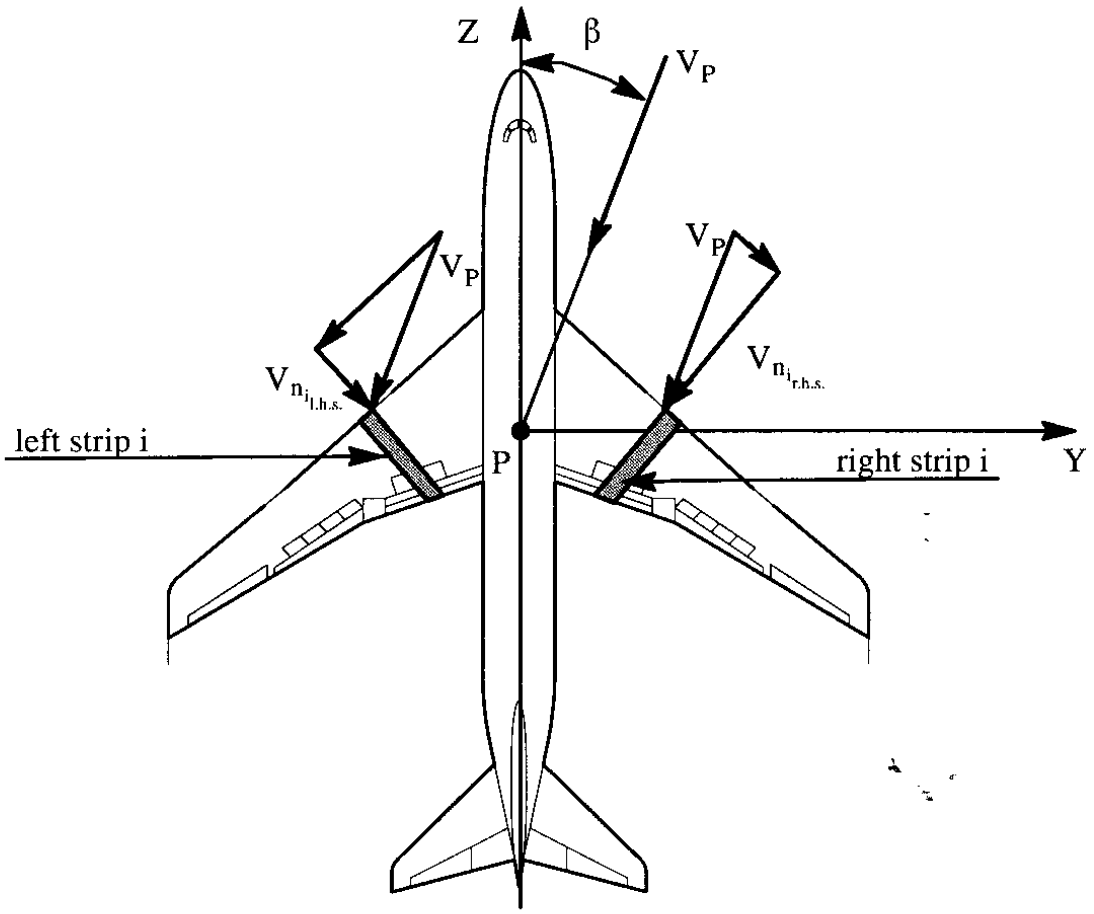

Figure 3.30 Differential Strip Velocities due to Sweep

a) rolling moment due to sideslip, due to sweep (aft) is negative

b) the rolling moment due to sideslip, due to sweep (aft) is proportional to lift coefficient

c) the rolling moment due to sideslip, due to sweep (aft) is proportional to the sine of twice the leading edge sweep angle

It will be shown later that the overall airplane dihedral effect, C_{l_β}, is of major significance to stability and controllability of airplanes. The fact that this important derivative itself, for swept wing airplanes is proportional to the lift coefficient (and therefore dependent on wing–loading and dynamic pressure) also has significant consequences to configuration design.

In Chapter 4, it will be shown that making the dihedral effect, C_{l_β}, more negative will make an airplane more spirally stable. At the same time, the dutch–roll damping ratio tends to decrease. This presents a design conflict which must be resolved through some compromise.

Methods for predicting numerical values of $C_{l_{\beta_w}}$ are found in Part VI of Reference 3.1.

Horizontal Tail Contribution, $C_{l_{\beta_h}}$

The explanations given for the various wing–fuselage contributions to C_{l_β} can be directly applied to the horizontal tail by merely considering the tail to be a lifting surface. Using the notation $\overline{C}_{l_{\beta_h}}$ for the horizontal tail dihedral effect based on its own reference geometry it is possible to write:

$$\Delta L_{A_{h_{sideslip}}} = \overline{C}_{l_{\beta_h}} \beta \bar{q}_h S_h b_h \tag{3.60}$$

From this it follows that:

$$C_{l_{\beta_h}} = \overline{C}_{l_{\beta_h}} \left(\frac{\bar{q}_h S_h b_h}{\bar{q} S b}\right) \tag{3.61}$$

The bracketed quantity in Eqn (3.61) tends to be small for most airplanes because the horizontal tail area and span are normally significantly smaller than the wing area and span. However, by endowing horizontal tail surfaces with large geometric dihedral angles it is possible to obtain relatively large values for $\overline{C}_{l_{\beta_h}}$ and thereby use the tail as a 'tailoring device' to achieve the desired level of overall airplane dihedral effect. This type of design philosophy was employed on the McDonnell F–4 and the British Aerospace Harrier.

Vertical Tail Contribution, $C_{l_{\beta_v}}$

Figure 3.31 shows that when an airplane is side–slipping, the vertical tail will 'see' a side–force which causes a rolling moment. The sign and magnitude of this rolling moment depends on the 'vertical' moment arm of the vertical tail.

First, consider the lift coefficient which acts on the vertical tail:

$$C_{L_v} = C_{L_{\alpha_v}}(\beta - \sigma) = C_{L_{\alpha_v}}\left(1 - \frac{d\sigma}{d\beta}\right)\beta \tag{3.62}$$

where: $C_{L_{\alpha_v}}$ is the lift–curve slope of the vertical tail, based on its own reference geometry

σ is the side–wash angle induced at the vertical tail by the fact that the wing–fuselage combination will itself be generating a side–force which creates side–wash. This effect is the aerodynamic equivalent of horizontal tail down–wash created by the wing.

The 'lift' on the vertical tail causes a negative rolling moment which can be expressed by:

$$\Delta L_{A_v} = - z_{v_s} C_{L_{\alpha_v}}(\beta - \sigma)\bar{q}_v S_v \tag{3.63}$$

By non–dimensionalizing and by using the notation of Eqn (3.62):

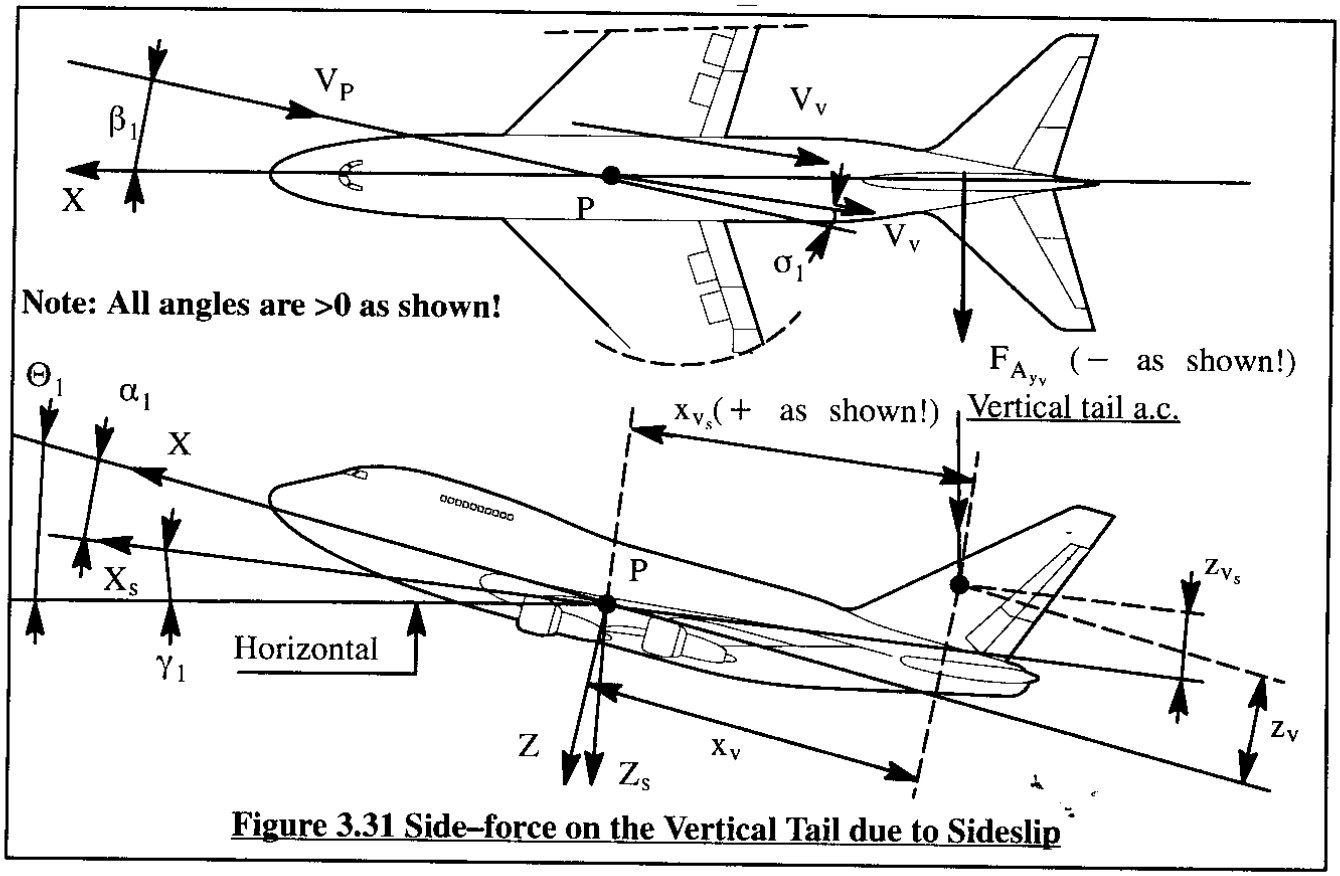

Figure 3.31 Side–force on the Vertical Tail due to Sideslip

$$C_{l_{\beta_v}}\beta\bar{q}Sb = -z_{v_s}C_{L_{\alpha_v}}\left(1-\frac{d\sigma}{d\beta}\right)\beta\bar{q}_vS_v \tag{3.64}$$

From this it follows for the vertical tail contribution to airplane dihedral effect:

$$C_{l_{\beta_v}} = -C_{L_{\alpha_v}}\left(1-\frac{d\sigma}{d\beta}\right)\eta_v\frac{S_vz_{v_s}}{Sb} \tag{3.65}$$

It is seen that the vertical tail contribution to the derivative C_{l_β} depends on five factors:

1) the geometry of the vertical tail: aspect ratio and sweep angle determine $C_{L_{\alpha_v}}$

2) the side–wash derivative $d\sigma/d\beta$ which is normally rather small

3) the dynamic pressure ratio at the vertical tail, η_v , which tends to have a value close to 1.0 except in the case of propeller driven airplanes with the vertical tail immersed in the propeller slipstream

4) the vertical tail moment arm, z_{v_s} . Note in Figure 3.31 that this moment arm depends on the steady state angle of attack! In extreme high angle of attack cases it is possible for this moment arm to reverse sign!

5) the size of the vertical tail in relation to the size of the wing: S_v/S . An example of an airplane with a large vertical tail relative to the wing is the Boeing 747–SP: see Figure 3.31.

Examples of numerical trends for the airplane dihedral effect derivative, C_{l_β} are given in Figure 3.32.

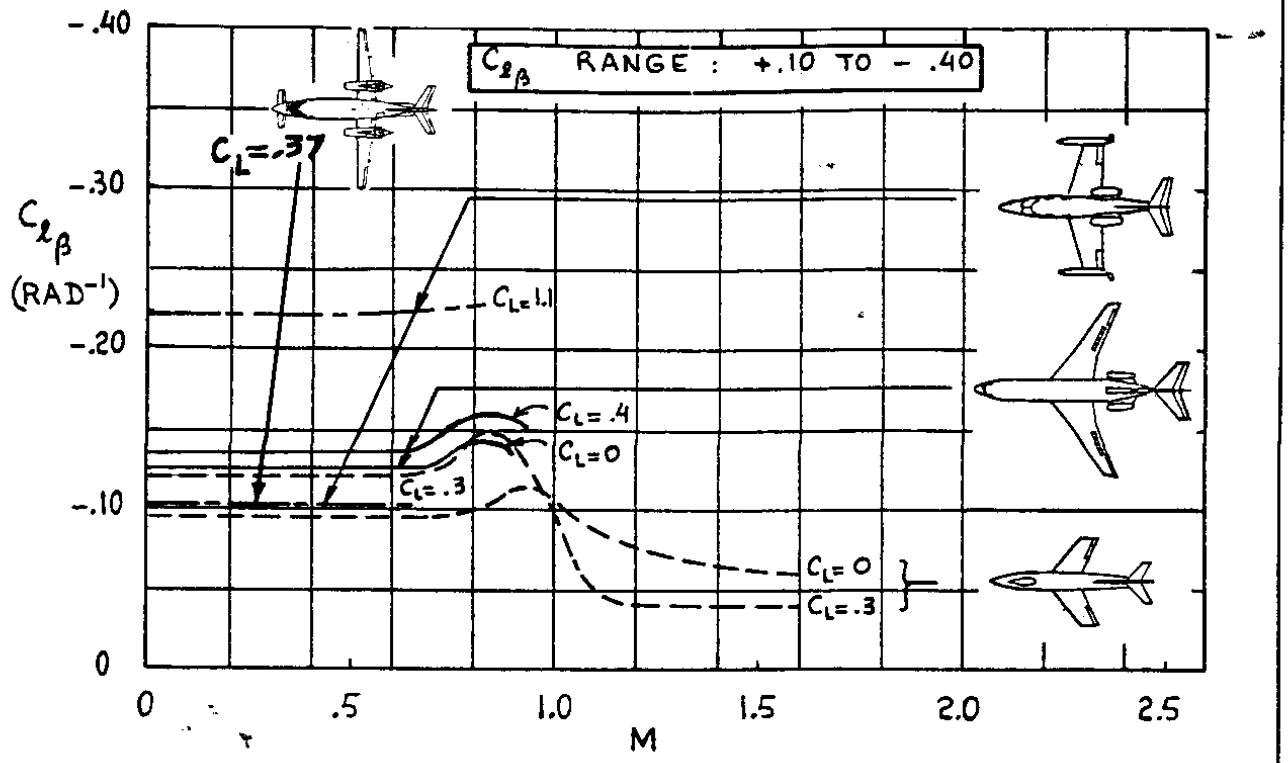

Figure 3.32 Effect of Mach Number on C_{l_β} for Several Airplanes

Roll Control Derivatives, $C_{l_{\delta_a}}$ and $C_{l_{\delta_r}}$

Lateral control (about the X–axis, body or stability) of airplanes can be accomplished with a number of devices:

* ailerons, $C_{l_{\delta_a}}$
* flaperons, $C_{l_{\delta_a}}$
* spoilers, $C_{l_{\delta_s}}$
* differential stabilizer, $C_{l_{i_h}}$
* combination of previous devices
* other devices

Several generic properties of ailerons, spoilers and differential stabilizers will be discussed. A mathematical model used when combinations of these devices are employed is also discussed.

Nearly all airplanes employ some form of directional (yaw) control, usually a rudder. Although undesirable, rudders also tend to produce a rolling moment. This rolling moment must be compensated for by either the pilot or some automatic mechanism. The generic properties of a rudder in generating an undesirable rolling moment are also discussed.

Aileron Rolling Moment Coefficient Derivative, $C_{l_{\delta_a}}$

Figure 3.33 illustrates how ailerons produce a rolling moment. A positive aileron deflection is referred to as one which results in a positive rolling moment about the X–axis. Because ailerons also produce an undesirable yawing moment (See Sub–section 3.1.8), most ailerons are deflected differentially (i.e. one more than the other) to minimize this yawing moment. For that reason an aileron deflection, δ_a , is usually defined as:

$$\delta_a = \frac{1}{2}(\delta_{a_{l.h.s.}} + \delta_{a_{r.h.s.}}) \tag{3.66}$$

The derivative $C_{l_{\delta_a}}$ depends on the following factors:

* aileron chord to wing chord ratio
* wing sweep angle
* Mach number
* aileron inboard and outboard span location
* aileron deflection

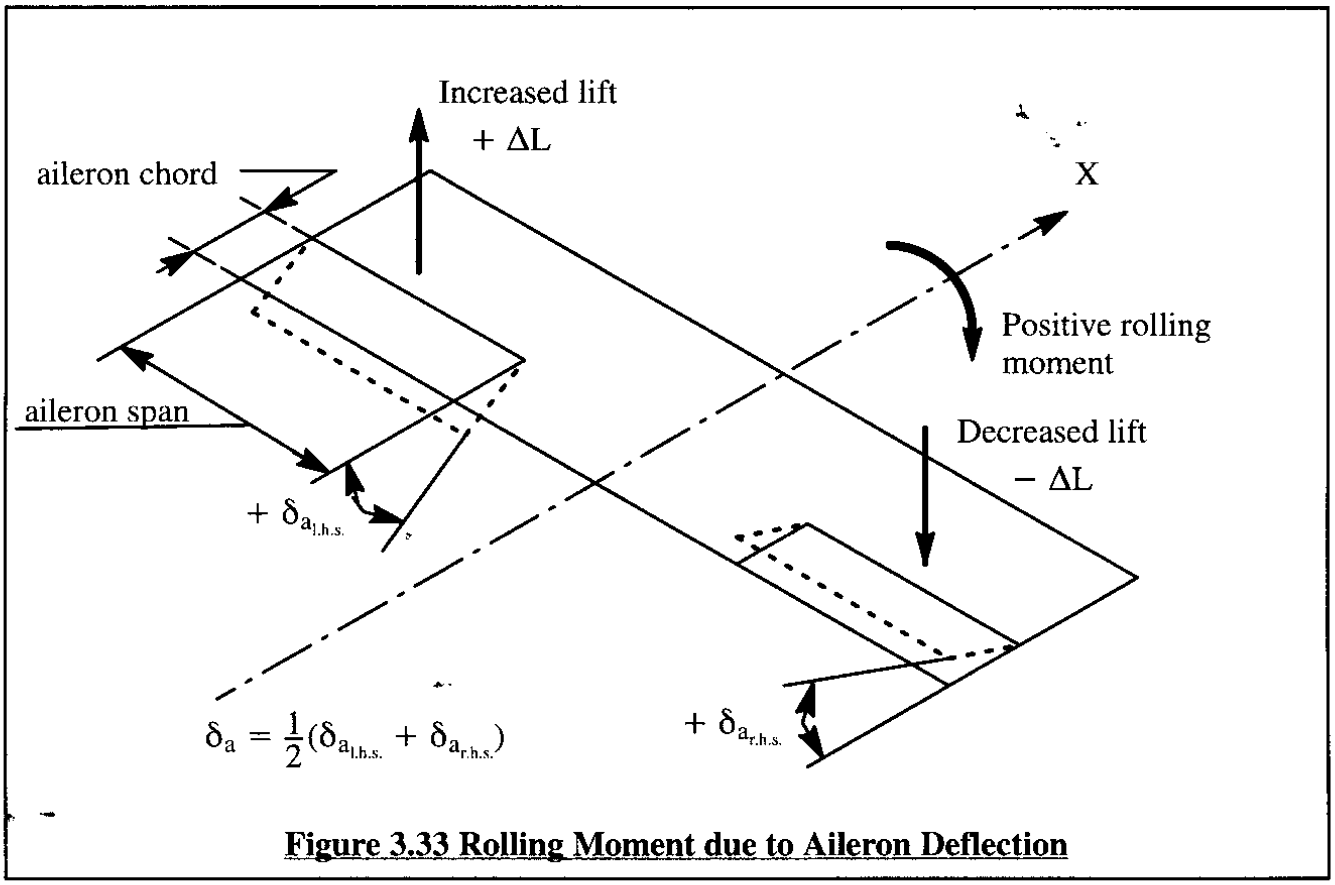

Figure 3.33 Rolling Moment due to Aileron Deflection

When ailerons are deflected more than about 20–25 degrees flow separation tends to occur. The ailerons then loose their effectiveness. Also, close to wing stall, even small downward aileron deflections can produce separation and loss of control effectiveness. In addition, aileron control power is very sensitive to dynamic pressure because of aero–elastic effects. Most high performance airplanes have a so–called aileron reversal speed beyond which the ailerons induce so much elastic wing twist that the sign of the derivative reverses! This effect is discussed in detail in Chapter 7.

At wing sweep angles beyond about 55 degrees, ailerons lose effectiveness because of outboard flow which tends to become parallel to the aileron hinge lines.

In several airplanes, the flaps are moved differentially to act as ailerons. Such devices are referred to as flaperons. They are analyzed as if they are ailerons.

Spoiler Rolling Moment Coefficient Derivative, $C_{l_{\delta_s}}$

Figure 3.34 shows how a spoiler produces a rolling moment. Spoilers when used for roll control are usually deflected on one side only.

The derivative $C_{l_{\delta_s}}$ depends on the following factors:

* spoiler chord to wing chord ratio
* spoiler hingeline location
* wing sweep angle
* spoiler inboard and outboard span location
* spoiler deflection
* Mach number

Maximum spoiler deflections range anywhere from 30–60 degrees.

At wing sweep angles beyond about 55 degrees spoilers loose effectiveness because of outboard flow which tends to become parallel to the spoiler hinge lines.

Differential Stabilizer Rolling Moment Coefficient Derivative, $C_{l_{i_h}}$

Figure 3.35 illustrates how a differentially deflected stabilizer generates a rolling moment.

The derivative $C_{l_{i_h}}$ depends on the following factors:

* stabilizer geometry: aspect ratio, sweep angle and taper ratio
* stabilizer size relative to the wing
* Mach number

Differential stabilizers, because of their relatively small moment arm to the X–axis tend to be used mostly on fighter aircraft: the high wing sweep angle makes ailerons and/or spoilers less effective. In addition, because most fighters have tail–span–to–wing–span ratios close to 1.0 the relative rolling moment arm is still reasonably good. Add the fact that both stabilizer halves on fighters are controlled separately for longitudinal control anyway and the ability for differential deflection (required for roll) comes at little additional weight penalty!

Many airplanes of today employ more than one of these lateral control devices. In airplanes with a mixture of lateral control devices, it is necessary to 'gear' the various lateral control devices together so that they are simultaneously activated when the cockpit controls (lateral stick or left/ right wheel deflection are activated by the pilot.

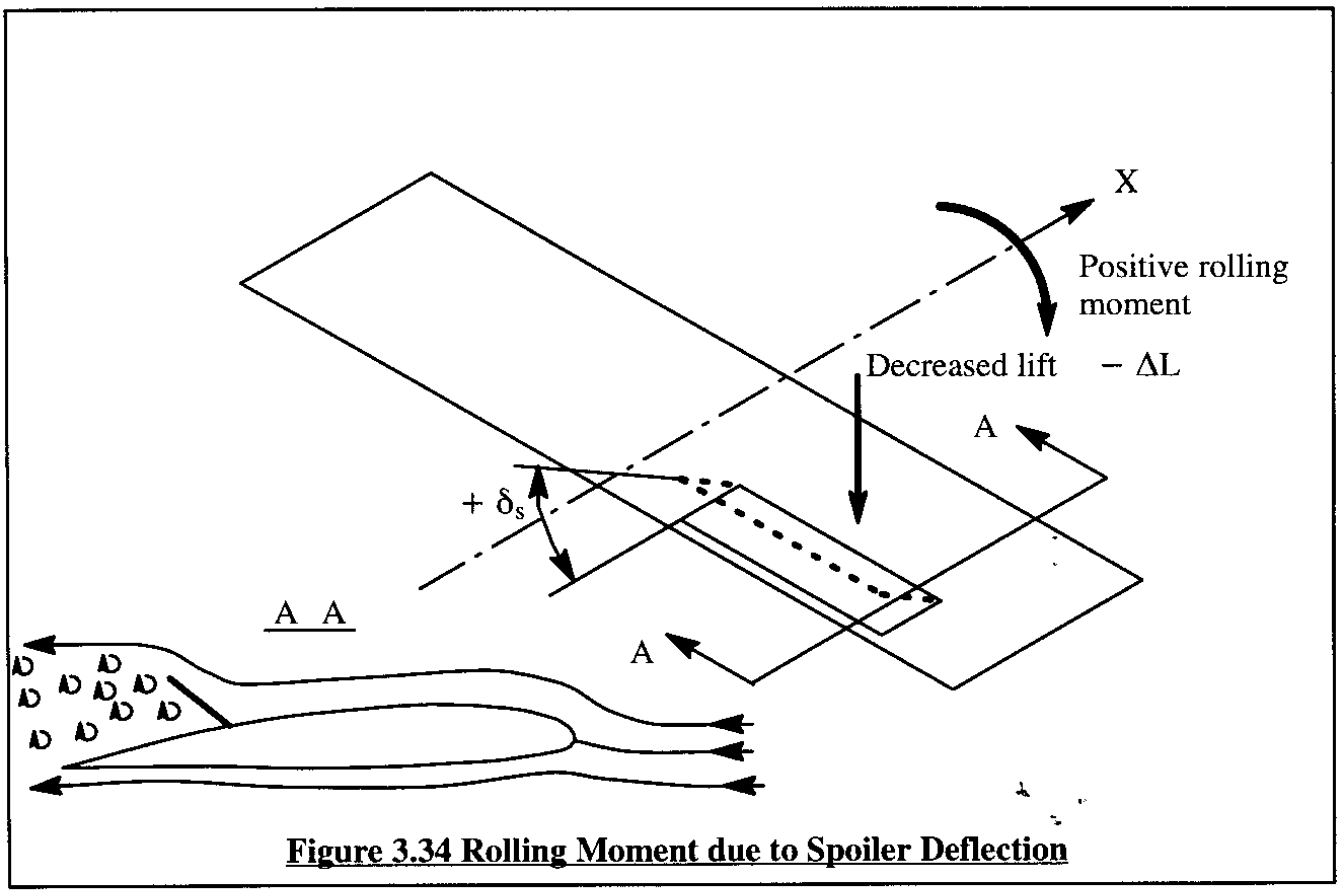

Figure 3.34 Rolling Moment due to Spoiler Deflection

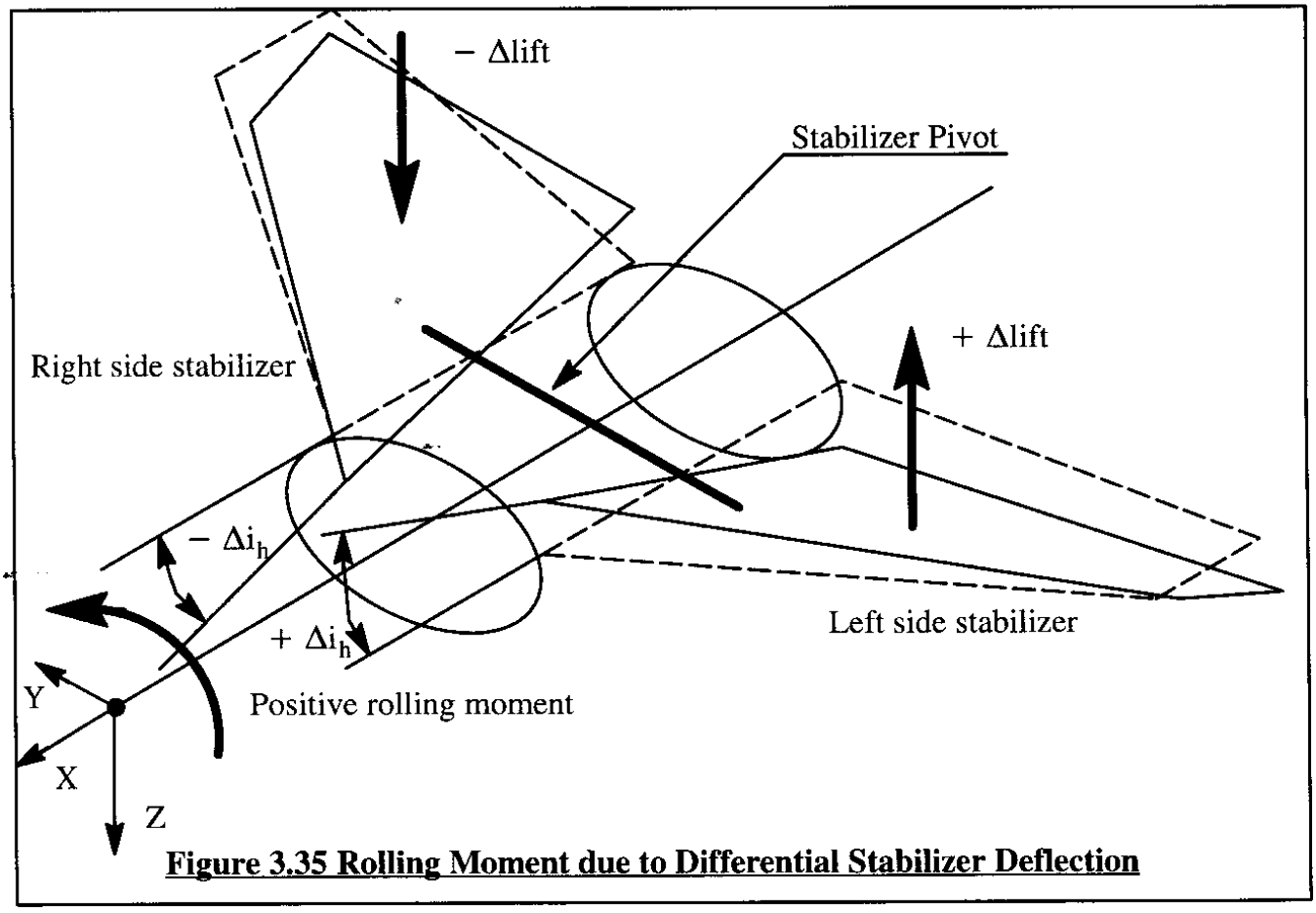

Figure 3.35 Rolling Moment due to Differential Stabilizer Deflection

An example is the Boeing 747 which has three different types of roll control devices: inboard ailerons, outboard ailerons and spoilers: see Figure 3.36.

These three roll control devices are 'geared' to the control wheel in the cockpit. The following equation expresses this gearing:

$$C_{l_{\delta_w}}\delta_w = K_{aw_{outb'd}}C_{l_{\delta_{a_{outb'd}}}}\delta_{a_{outb'd}} + K_{aw_{inb'd}}C_{l_{\delta_{a_{inb'd}}}}\delta_{a_{inb'd}} + K_{sw}C_{l_{\delta_s}}\delta_s \qquad (3.67)$$

where: $C_{l_{\delta_w}} = \partial C_l/\partial\delta_w$ is the rolling moment coefficient derivative due to control wheel deflection, δ_w

$K_{aw_{outb'd}}$ is the outboard–aileron–to–control–wheel gearing ratio. In the 747 this gearing ratio is driven to zero by flap position: when the flaps are retracted, the outboard ailerons remain in place. The other gearing constants are similarly defined.

$C_{l_{\delta_{a_{outb'd}}}} = \partial C_l/\partial\delta_{a_{outb'd}}$ is the outboard aileron control power derivative due to outboard aileron deflection, $\delta_{a_{outb'd}}$. The other control power derivatives are similarly defined.

$\delta_{a_{outb'd}}$ is the outboard aileron deflection. The other control deflections are similarly defined.

Cockpit wheel deflections are limited to about +/– 85 degrees by civil and military regulations. By assuming 85 degrees for the maximum wheel deflection, Eqn (3.67) can be used to determine the numerical magnitude of the roll control power derivative $C_{l_{\delta_w}}$ for airplanes with geared roll control systems. Eqn (3.67) has to be adjusted to the gearing used in any particular airplane.

Figure 3.37 shows examples of the Mach number trend for aileron control power derivatives of several airplanes.

Rolling Moment Coefficient due to Rudder Derivative, $C_{l_{\delta_r}}$

Figure 3.38 shows how a rudder can generate a rolling moment. Note that the rudder deflection is defined as positive when a positive force along the Y–axis is generated. This positive force can be expressed as:

$$F_{A_{y_{v_{rudder}}}} = C_{L_v}\bar{q}_v S_v \qquad (3.68)$$

where:

$$C_{L_v} = C_{L_{\alpha_v}}\alpha_{\delta_r}\delta_r \qquad (3.69)$$

where: $C_{L_{\alpha_v}}$ is the lift–curve slope of the vertical tail

α_{δ_r} is the angle of attack effectiveness of the rudder

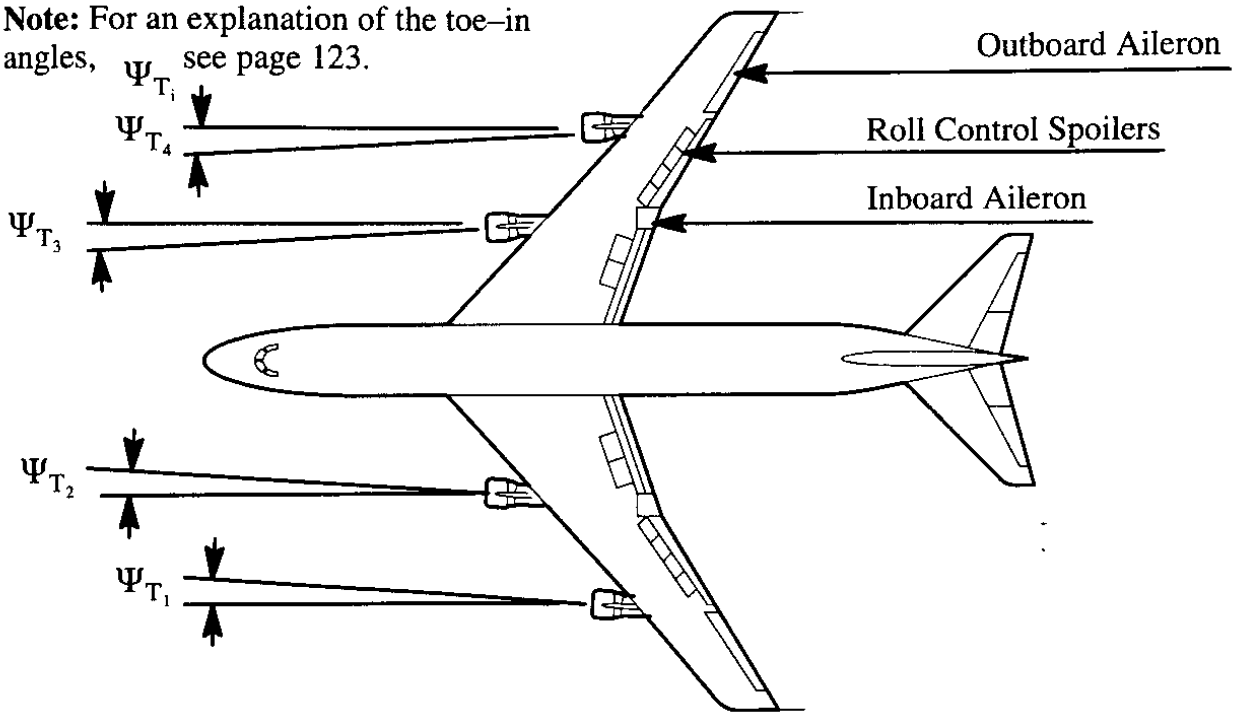

Figure 3.36 Boeing Model 747 with Three Types of Lateral Control

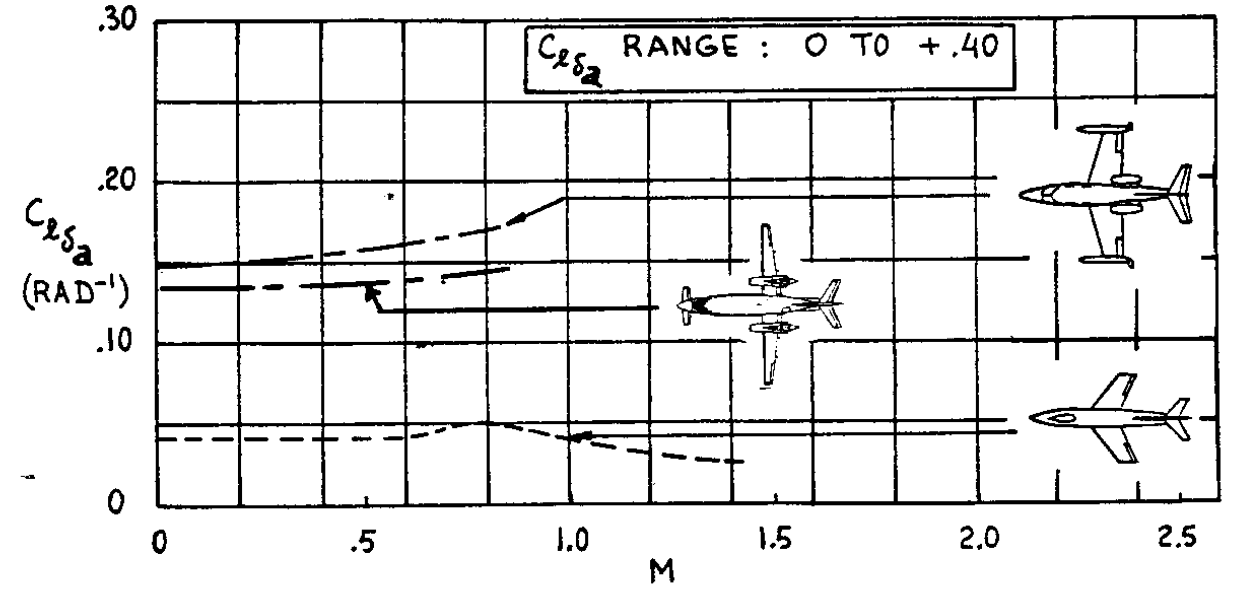

Figure 3.37 Effect of Mach Number on $C_{l_{\delta_a}}$ for Several Airplanes

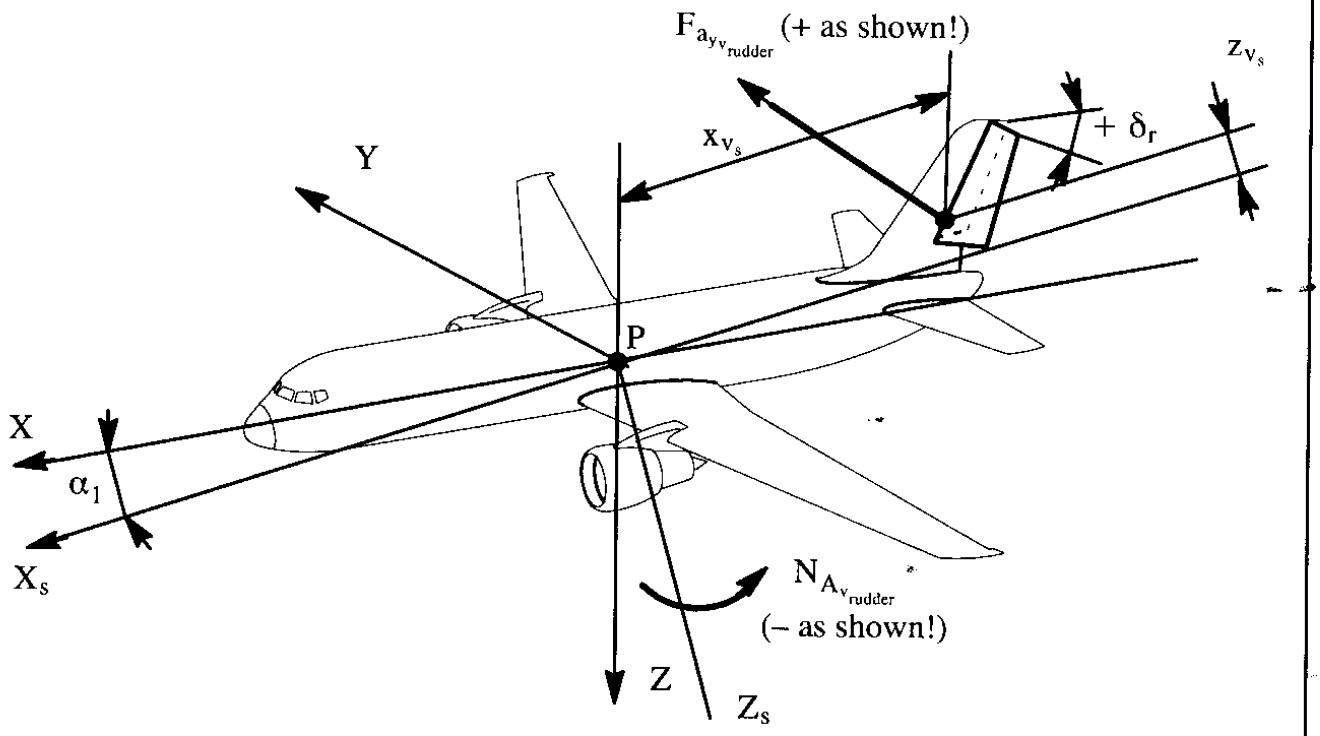

Figure 3.38 Rolling Moment due to Rudder Deflection

The rolling moment due to rudder deflection can be written as:

$$L_{A_{rudder}} = F_{A_{y_{rudder}}} z_{v_s} = C_{l_{\delta_r}} \delta_r \bar{q} S b \tag{3.70}$$

By combining equations (3.68) through (3.70) it is found that:

$$C_{l_{\delta_r}} = C_{L_{\alpha_v}} \alpha_{\delta_r} \bar{q}_v \frac{S_v x_{v_s}}{Sb} \tag{3.71}$$

Note that this derivative is normally positive. However, at angles of attack for which z_{v_s} becomes negative, so does $C_{l_{\delta_r}}$. From a handling qualities viewpoint the derivative $C_{l_{\delta_r}}$ is a problem: particularly positive values of this derivative tend to interfere with a pilot's ability to carry out lateral–directional maneuvers. This is one reason why many airplanes have some type of flight control interconnect between the roll and yaw axis to compensate for the rolling moment due to rudder deflection.

Figure 3.39 shows how the rolling moment due to rudder derivative varies with Mach number for several airplanes.

The steady state model for the airplane aerodynamic rolling moment now is:

$$L_{A_{1_s}} = L_A = (C_{l_\beta}\beta + C_{l_{\delta_a}}\delta_a + C_{l_{\delta_r}}\delta_r) \tag{3.72}$$

For airplanes with a combination of roll control devices it is recommended to replace the term $C_{l_{\delta_a}}\delta_a$ with the term $C_{l_{\delta_w}}\delta_w$ as defined by Eqn (3.67).

Methods for predicting the magnitudes of the derivatives which appear in Eqn (3.72) can be found in Part VI of Reference 3.1.

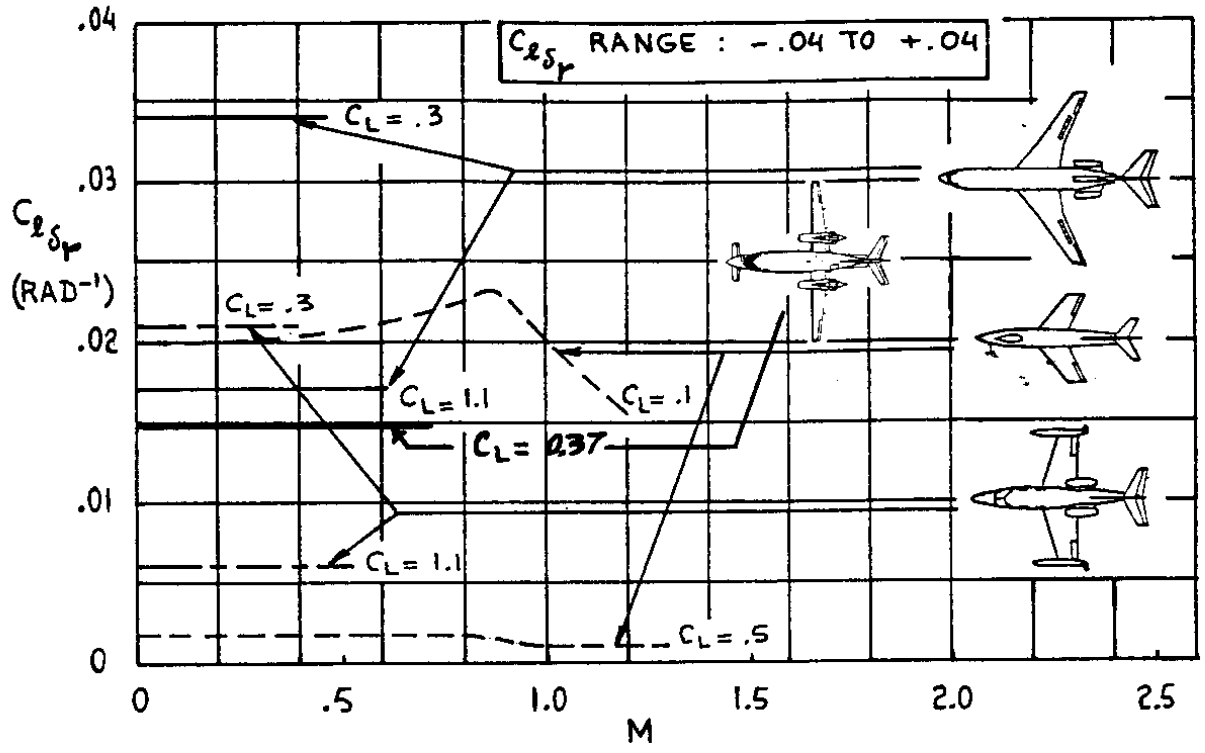

Figure 3.39 Effect of Mach Number on $C_{l_{\delta_r}}$ for Several Airplanes

3.1.9 AIRPLANE AERODYNAMIC SIDE–FORCE

The steady state airplane aerodynamic side–force, F_{A_y}, is non–dimensionalized as:

$$F_{A_y} = C_y \bar{q} S \tag{3.73}$$

where: C_y is the airplane aerodynamic side–force coefficient.

This steady state airplane aerodynamic side–force coefficient depends on the following factors:

* angle of sideslip, β
* deflection of directional control surface(s)
* deflection of lateral control surface
* angle of attack
* Mach number and Reynolds number

For an airplane equipped with ailerons and rudder the side–force coefficient is expressed in first order Taylor series form:

$$C_y = C_{y_o} + C_{y_\beta}\,\beta + C_{y_{\delta_a}}\delta_a + C_{y_{\delta_r}}\delta_r \qquad (3.74)$$

The coefficient and derivatives in Eqn (3.74) must be evaluated at constant Mach number and Reynolds number. Mach number affects primarily the lift curve slope, side–wash and angle of effectiveness terms which affect the coefficient and derivatives in Eqn (3.34). Reynolds number has only a weak effect on the side–force derivatives.

The terms in Eqn (3.74) have the following meanings:

C_{y_0}	is the value of C_y for: $\alpha = \beta = \delta_a = \delta_r = 0$
$C_{y_\beta} = \partial C_y/\partial\beta$	is the change in airplane side–force coefficient due to a change in angle of sideslip (at constant angle of attack)
$C_{y_{\delta_a}} = \partial C_y/\partial\delta_a$	is the change in airplane side–force coefficient due to a change in aileron deflection
$C_{y_{\delta_r}} = \partial C_y/\partial\delta_r$	is the change in airplane side–force coefficient due to a change in rudder deflection

The coefficient C_{y_0} tends to be equal to zero for symmetrical airplanes. The discussion of the coefficient C_{l_0} (page 95) also applies to C_{y_0}.

The derivative C_{y_β} is an important derivative in dutch–roll dynamics (See Chapter 5). It is also important in flight path control when making s–turns without banking at very low height above the ground. The control derivative $C_{y_{\delta_a}}$ is normally negligible. The side force control derivative $C_{y_{\delta_r}}$ is of major importance in determining the yaw control derivative, $C_{n_{\delta_r}}$, as will be seen in Sub–section 3.1.10.

Side–Force Coefficient Due to Sideslip Derivative, C_{y_β}

The side–force due to sideslip may be estimated by summing the effects of various airplane components. For conventional airplanes this yields:

$$C_{y_\beta} = C_{y_{\beta_w}} + C_{y_{\beta_f}} + C_{y_{\beta_v}} \tag{3.75}$$

Wing Contribution, $C_{y_{\beta_w}}$ and Fuselage Contribution, $C_{y_{\beta_f}}$

The wing contribution to C_{y_β} depends primarily on the geometric dihedral angle of the wing. For small geometric dihedral angles the wing contribution is usually negligible.

The fuselage contribution depends strongly on the shape and size of the fuselage in relation to the wing and on the placement of the wing on the fuselage. Methods for estimating the wing/fuselage contributions to C_{y_β} may be found in Part VI of Reference 3.1. For most airplanes these contributions tend to be small.

Vertical Tail Contribution, $C_{y_{\beta_v}}$

The vertical tail contribution to C_{y_β} was explained as part of the discussion of the rolling moment due to sideslip contribution of the vertical tail in Sub-sub-section 3.1.8.1: see Figure 3.31. With the help of Eqn (3.62) it is seen that:

$$F_{A_{y_v}} = C_{y_{\beta_v}}\beta\bar{q}S = -C_{L_{\alpha_v}}\left(1 - \frac{d\sigma}{d\beta}\right)\bar{q}_v S_v \tag{3.76}$$

From this it follows that:

$$C_{y_{\beta_v}} = -C_{L_{\alpha_v}}\left(1 - \frac{d\sigma}{d\beta}\right)\eta_v \frac{S_v}{S} \tag{3.77}$$

Note that the vertical tail contribution depends strongly on the vertical tail size in relation to the wing as well as on the lift-curve slope of the vertical tail. The latter in turn depends mostly on aspect ratio and sweep angle of the vertical tail.

Figure 3.40 shows how C_{y_β} varies with Mach number for several airplanes.

Side Force Control Derivatives, $C_{y_{\delta_a}}$ and $C_{y_{\delta_r}}$

Aileron Side Force Coefficient Derivative, $C_{y_{\delta_a}}$

This derivative is normally negligible. However, in the case of airplanes where the rolling moment controls are in close proximity to a vertical surface (fuselage or vertical tail) a side force which is not negligible may well be generated. Figure 3.41 illustrates an example of how this can occur in the case of a differential stabilizer which is located close to a vertical tail. Whenever this is suspected to be the case windtunnel tests are the only reliable way of obtaining data.

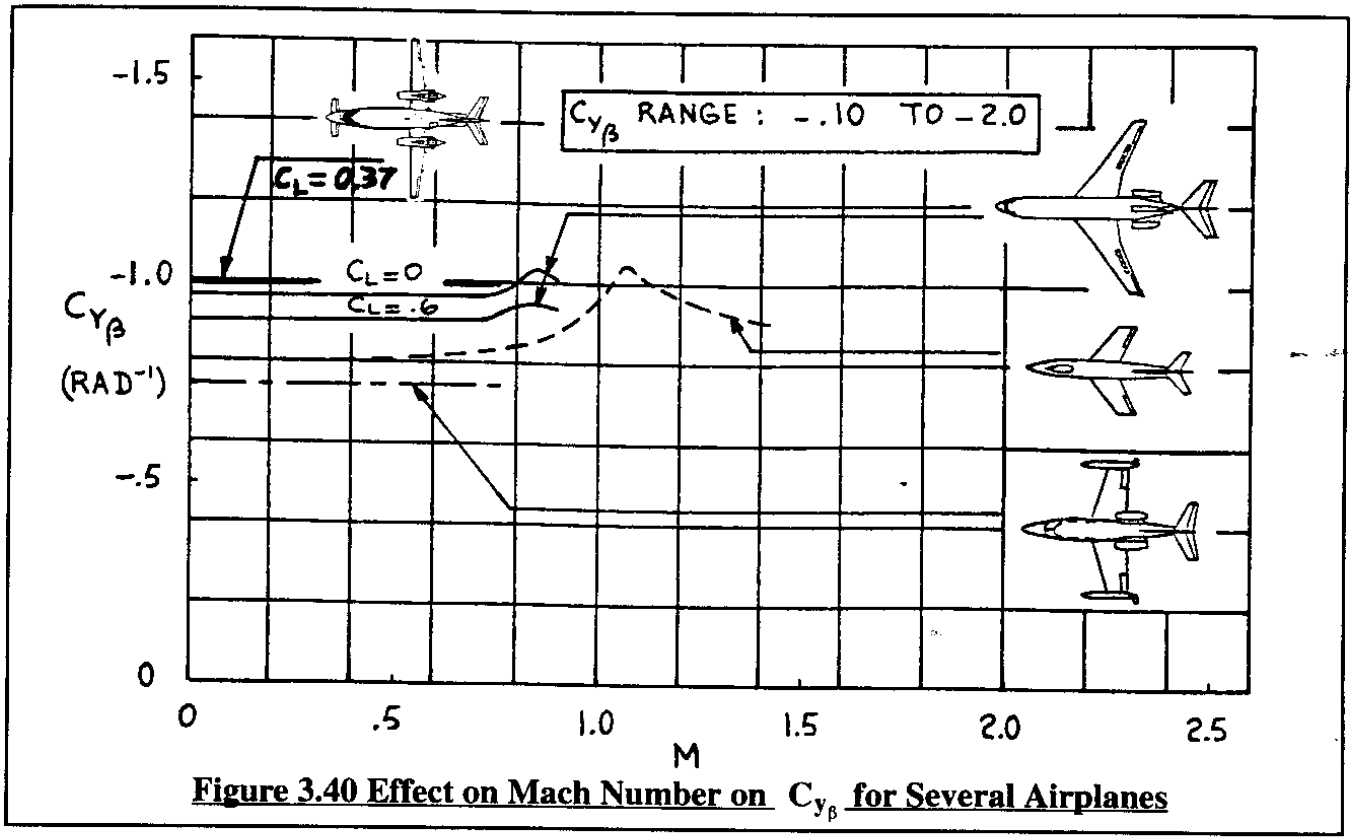

Figure 3.40 Effect on Mach Number on C_{y_β} for Several Airplanes

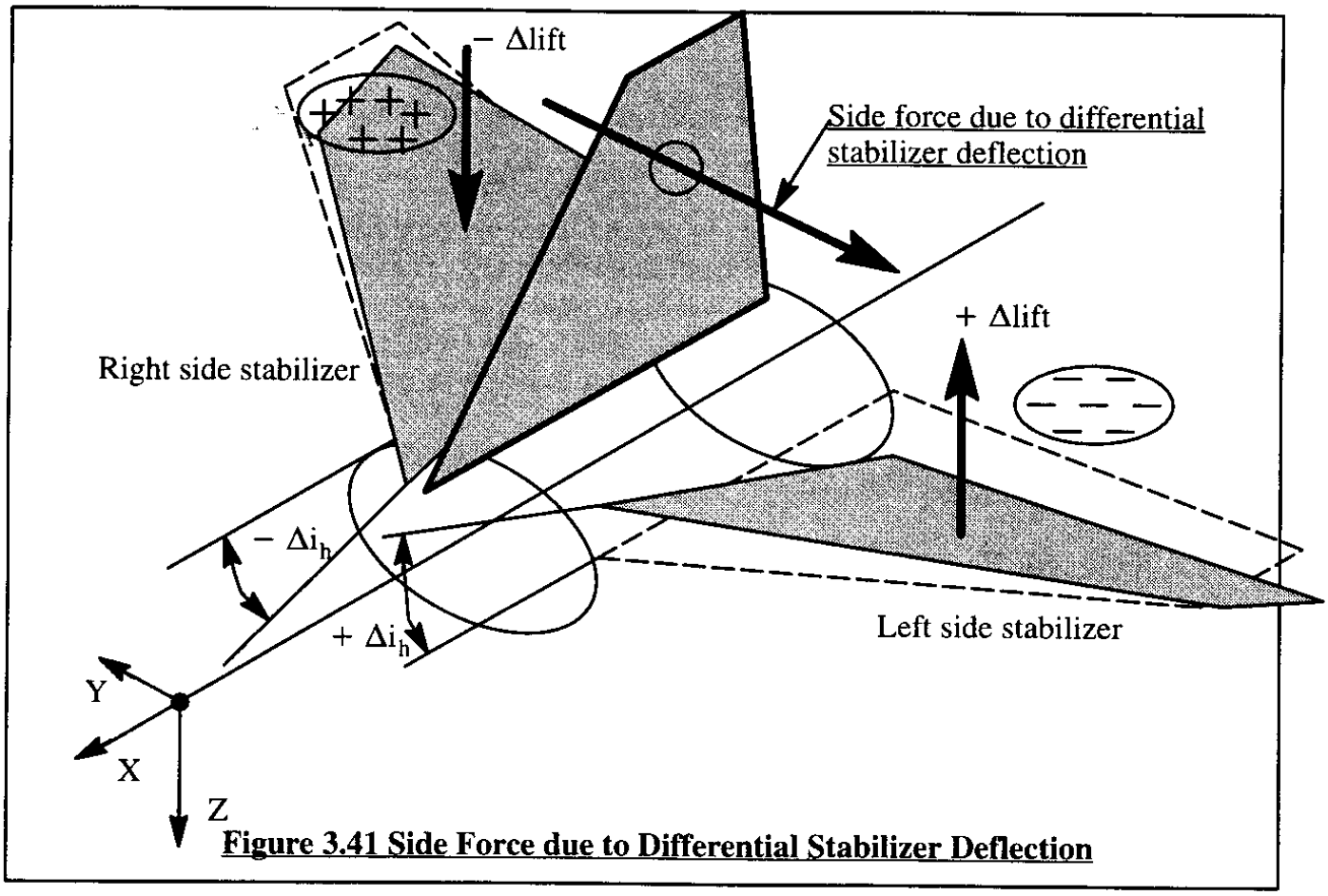

Figure 3.41 Side Force due to Differential Stabilizer Deflection

Rudder Side–Force Coefficient Derivative, $C_{y_{\delta_r}}$

Figure 3.38 shows how a positive rudder deflection yields a positive side–force due to rudder deflection. This side–force is written as:

$$F_{A_{y_{v_{rudder}}}} = C_{y_{\delta_r}} \delta_r \bar{q} S \tag{3.78}$$

Now, by combining Eqns (3.78), (3.68) and (3.69) it is seen that:

$$C_{y_{\delta_r}} = C_{L_{\alpha_v}} \alpha_{\delta_r} \eta_v \frac{S_v}{S} \tag{3.79}$$

Note that the side–force due to rudder derivative depends strongly on the vertical tail size in relation to the wing as well as on the lift–curve slope of the vertical tail. The latter in turn depends mostly on aspect ratio and sweep angle of the vertical tail. Figure 3.42 shows how $C_{y_{\delta_r}}$ varies with Mach number for several airplanes.

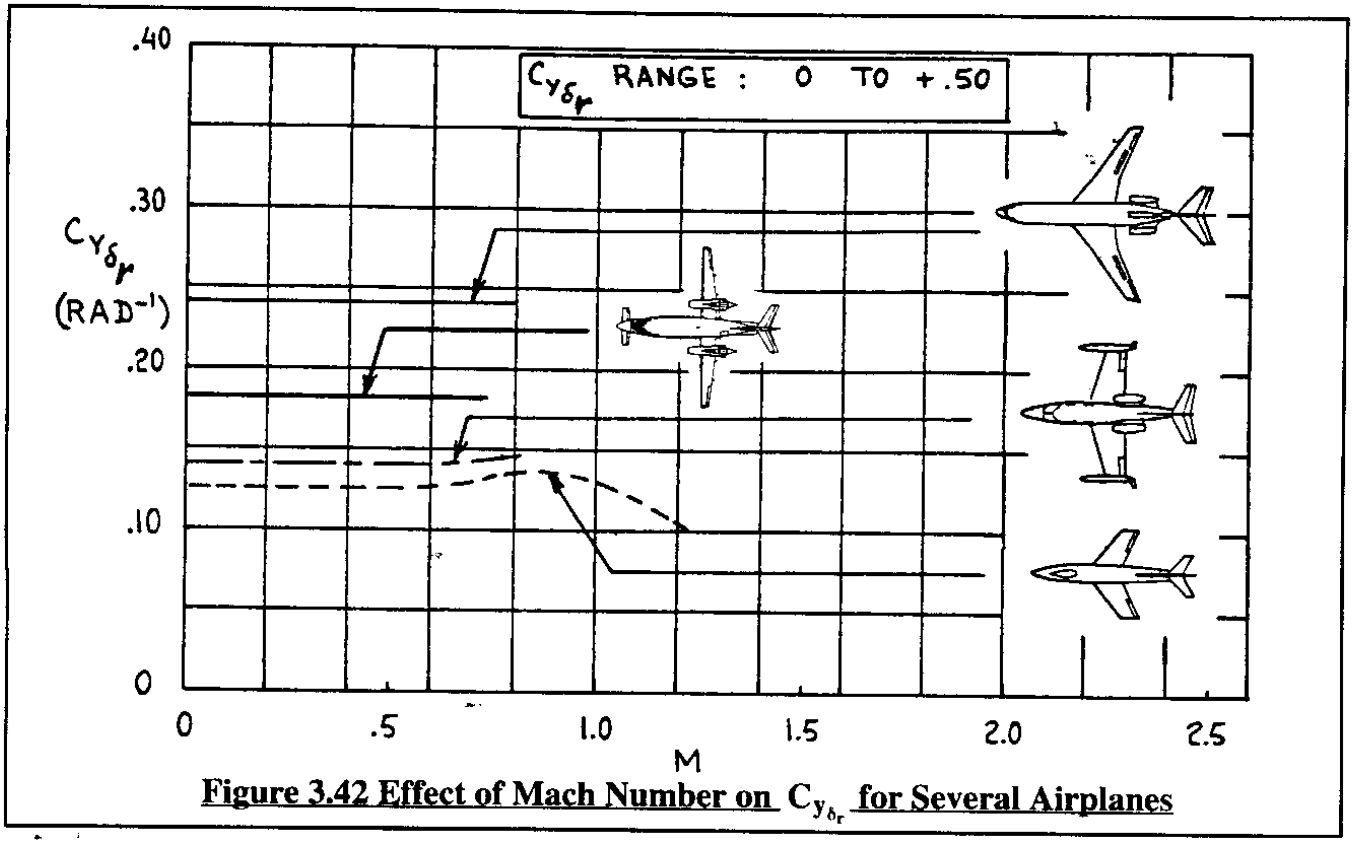

Figure 3.42 Effect of Mach Number on $C_{y_{\delta_r}}$ for Several Airplanes

The steady state model for the airplane aerodynamic side force now is:

$$F_{A_{y_{1_s}}} = F_{A_y} = (C_{y_\beta}\beta + C_{y_{\delta_a}}\delta_a + C_{y_{\delta_r}}\delta_r) \tag{3.80}$$

Methods for predicting the magnitudes of the derivatives which appear in Eqn (3.72) can be found in Part VI of Reference 3.1.

3.1.10 AIRPLANE AERODYNAMIC YAWING MOMENT

The steady state airplane aerodynamic yawing moment, N_A , is non–dimensionalized as:

$$N_A = C_n \bar{q} S b \tag{3.81}$$

where: C_n is the airplane aerodynamic yawing moment coefficient.

The steady state airplane aerodynamic yawing moment coefficient, C_n , depends on the following factors:

* angle of sideslip, β
* angle of attack, α
* Mach number and Reynolds number
* deflection of directional control surface(s)
* deflection of lateral control surface(s)
* moment reference center (usually the c.g.) location

For an airplane equipped with ailerons and rudders, the yawing moment coefficient is expressed in first order Taylor series form:

$$C_n = C_{n_0} + C_{n_\beta}\,\beta + C_{n_{\delta_a}}\delta_a + C_{n_{\delta_r}}\delta_r \tag{3.82}$$

The coefficient and derivatives in Eqn (3.82) are to be evaluated at constant Mach number and Reynolds number. The terms in Eqn (3.82) have the following meanings:

C_{n_0}	is the value of C_n for: $\beta = \delta_a = \delta_r = 0$
$C_{n_\beta} = \partial C_n / \partial \beta$	is the change in airplane yawing moment coefficient due to a change in airplane sideslip angle, β
$C_{n_{\delta_a}} = \partial C_n / \partial \delta_a$	is the change in airplane yawing moment coefficient due to a change in aileron deflection, δ_a
$C_{n_{\delta_r}} = \partial C_n / \partial \delta_r$	is the change in airplane yawing moment coefficient due to a change in rudder deflection, δ_r

The coefficient C_{n_0} tends to be equal to zero for symmetrical airplanes. The discussion of the coefficient C_{l_0} (page 95) also applies to C_{n_0} . The derivative C_{n_β} is an important derivative in dutch roll and spiral dynamics. The derivative C_{n_β} is referred to as the static directional stability derivative. The control derivative $C_{n_{\delta_a}}$ plays a nuisance role. Ideally its value would be zero or perhaps slightly positive. As will be shown, for most ailerons its value is negative. For that reason it is referred to as the adverse aileron–yaw effect. The control derivative $C_{n_{\delta_r}}$ is the rudder control derivative. It is very important in coordinating turns and in helping to overcome asymmetric thrust (or power) situations.

Yawing Moment Coefficient Due to Sideslip Derivative, C_{n_β}

The yawing moment due to sideslip (directional stability) derivative, C_{n_β}, may be estimated by summing the effects of various airplane components. For conventional airplanes this yields:

$$C_{n_\beta} = C_{n_{\beta_w}} + C_{n_{\beta_f}} + C_{n_{\beta_v}} \tag{3.83}$$

Wing Contribution, $C_{n_{\beta_w}}$ and Fuselage Contribution, $C_{n_{\beta_f}}$

The wing contribution to C_{n_β} tends to be negligible, except at high angles of attack.

The fuselage contribution depends strongly on the shape of the fuselage and the amount of projected side area forward and aft of the center of gravity. The so–called Munk effect discussed in Sub–section 2.5.6 also applies to a fuselage in sideslip. For that reason the fuselage contribution to directional stability tends to be strongly negative. Methods for computing the fuselage contribution to C_{n_β} are presented in Part VI of Reference 3.1.

Vertical Tail Contribution, $C_{n_{\beta_v}}$

A physical explanation for the directionally stabilizing effect of a vertical tail may be gleaned from Figure 3.31. The yawing moment due to the vertical tail me be written as:

$$N_v = - F_{A_{y_v}} x_{v_s} = C_{n_{\beta_v}} \beta \bar{q} S b \tag{3.84}$$

where: $F_{A_{y_v}}$ is the side–force due to sideslip as determined from Eqn (3.76).

x_{v_s} is the distance along the stability x–axis from the vertical tail aerodynamic center to the airplane center of gravity.

By combining Eqn (3.76) and Eqn (3.84) it follows that:

$$C_{n_{\beta_v}} = C_{L_{\alpha_v}} (1 - \frac{d\sigma}{d\beta}) \eta_v \frac{S_v \, x_{v_s}}{S b} \tag{3.85}$$

Note that the vertical tail contribution depends strongly on the vertical tail size in relation to the wing as well as on the lift–curve slope of the vertical tail. The latter depends mostly on aspect ratio and sweep angle of the vertical tail. Also, it is seen that the 'moment–arm', x_{v_s}, is important to directional stability.

Figure 3.43 shows how C_{n_β} varies with Mach number for several airplanes.

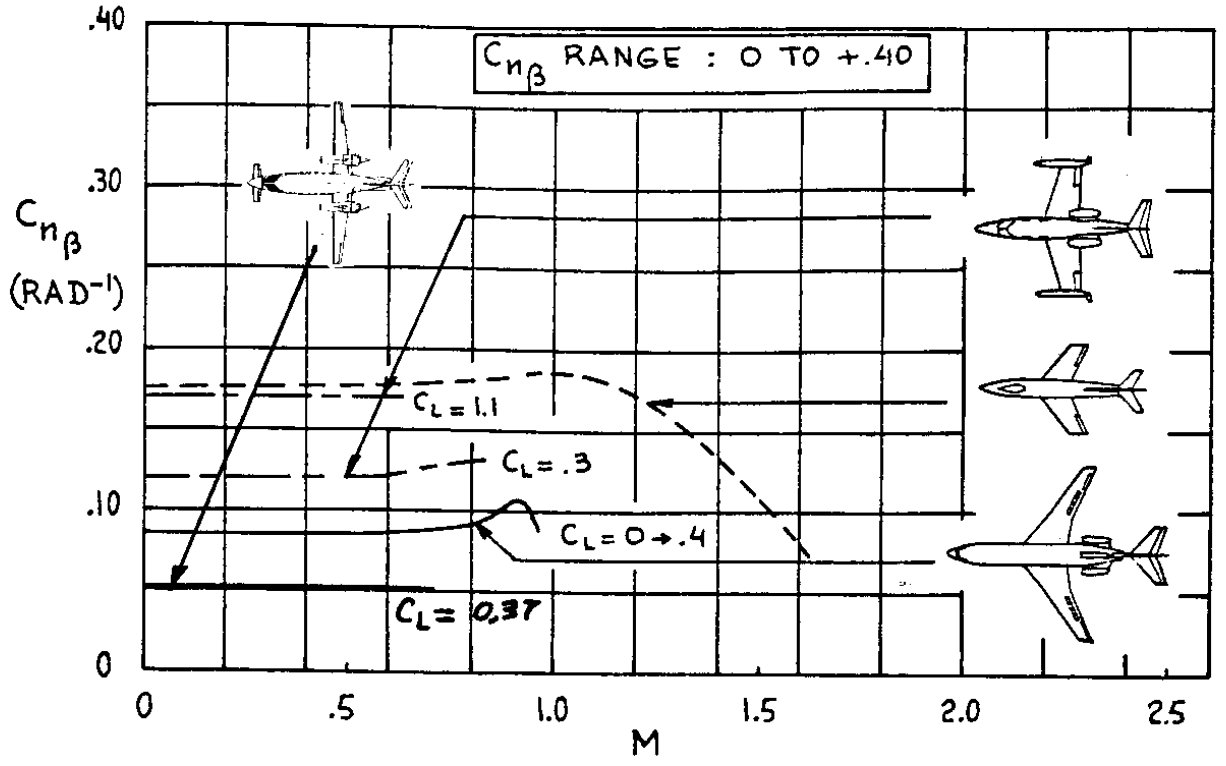

Figure 3.43 Effect of Mach Number on C_{n_β} for Several Airplanes

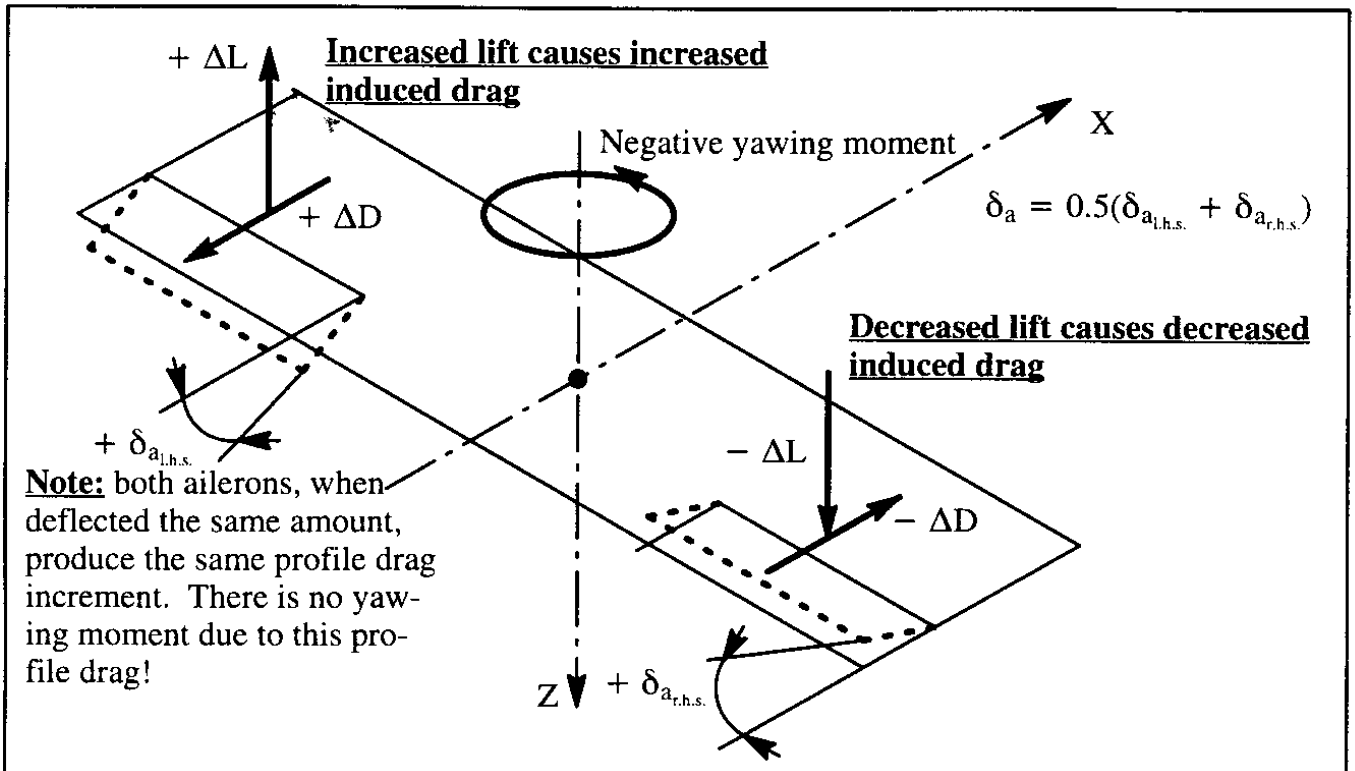

Figure 3.44 Yawing Moment Due to Aileron Deflection

Yawing Moment Control Derivatives, $C_{n_{\delta_a}}$, $C_{n_{\delta_s}}$, $C_{n_{i_h}}$, $C_{n_{\delta_r}}$ and $C_{n_{\delta_{r_{drag}}}}$

Nearly all airplanes employ some form of lateral control as discussed in Sub–section 3.1.8. A problem is, that most roll control devices also introduce a yawing moment. The generic properties of roll control devices which lead to generating yawing moments are now briefly discussed.

Aileron Yawing Moment Coefficient Derivative, $C_{n_{\delta_a}}$

Figure 3.44 shows how conventional ailerons create a negative (called adverse) yawing moment. Note that this yawing moment is caused by the differential induced drag which in turn is caused by the changes in local lift created by the ailerons. The reason the aileron induced yawing moment is called adverse is because it tends to yaw an airplane out of an intended turn.

To eliminate the negative yawing moment due to aileron deflection, either Frise ailerons or differentially deflected (or a combination of both) are used. Figure 3.45 illustrates the effect of Frise ailerons as well as of differentially deflected ailerons. Note, that in both cases a differential profile drag component is produced which is used to off–set the adverse (negative) aileron yaw.

Spoiler Yawing Moment Coefficient Derivative, $C_{n_{\delta_s}}$

Figure 3.34 shows how a spoiler generates a rolling moment. Figure 3.46 shows how a spoiler causes a positive yawing moment. This is referred to as proverse yaw. This is preferred over adverse yaw unless it becomes too proverse!

Methods for computing the yawing moment due to aileron and spoiler control derivatives are found in Part VI of Reference 3.1.

Figure 3.47 shows how $C_{n_{\delta_a}}$ varies with Mach number for several airplanes.

Differential Stabilizer Yawing Moment Coefficient Derivative, $C_{n_{i_h}}$

Figure 3.41 illustrates how a differentially deflected stabilizer generates a side force. Since the center of gravity of the airplane is usually forward of the vertical tail, a yawing moment due to differential stabilizer deflection will also be generated. If this is suspected to be significant, it is advisable to run windtunnel tests to establish the magnitude.

Directional control (about the Z–axis, body or stability) of airplanes can be accomplished with a number of devices:

* rudders ($C_{n_{\delta_r}}$) * drag rudders ($C_{n_{\delta_{r_{drag}}}}$) * other devices

Some of the generic properties of rudders and drag rudders will now be discussed.

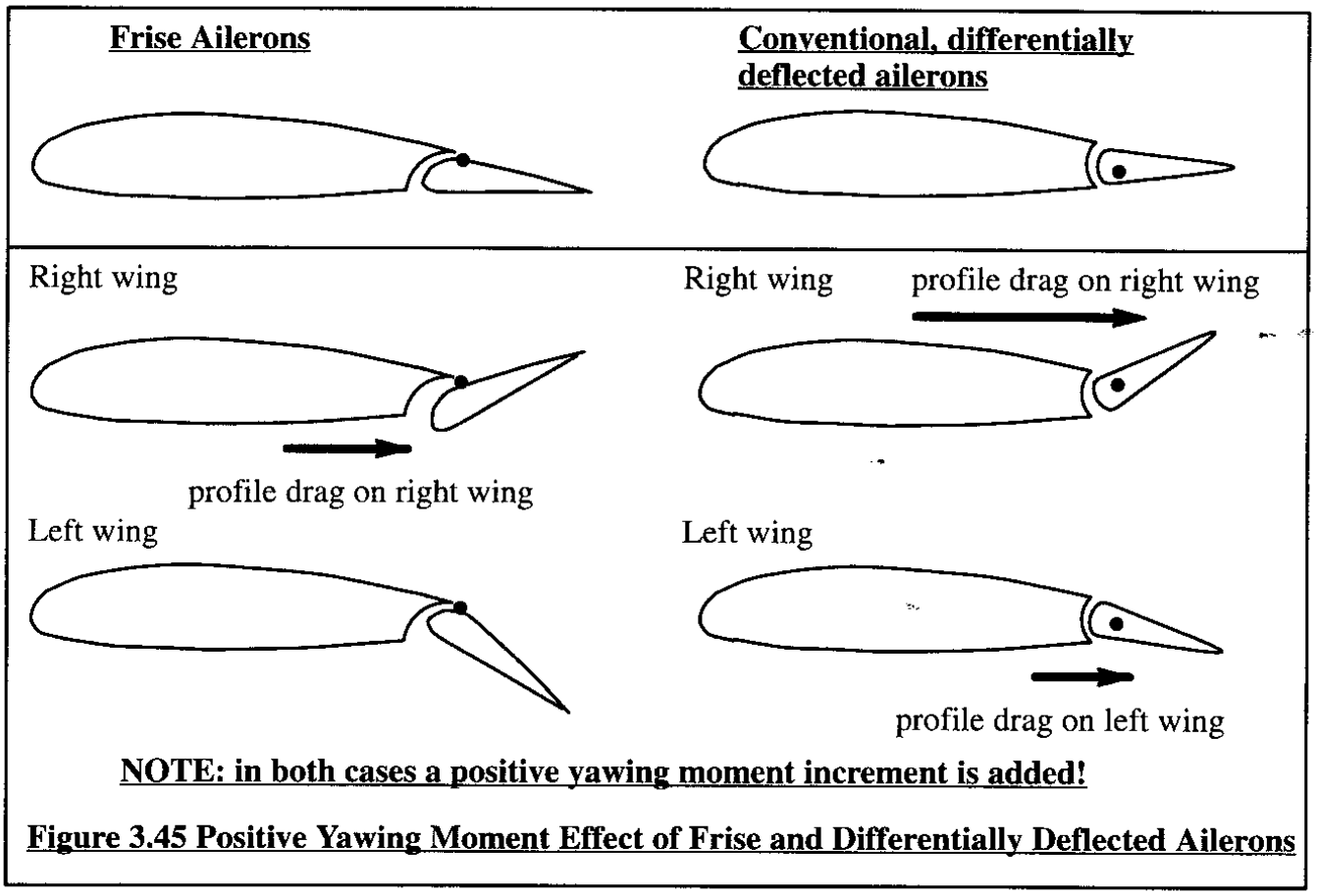

NOTE: in both cases a positive yawing moment increment is added!

Figure 3.45 Positive Yawing Moment Effect of Frise and Differentially Deflected Ailerons

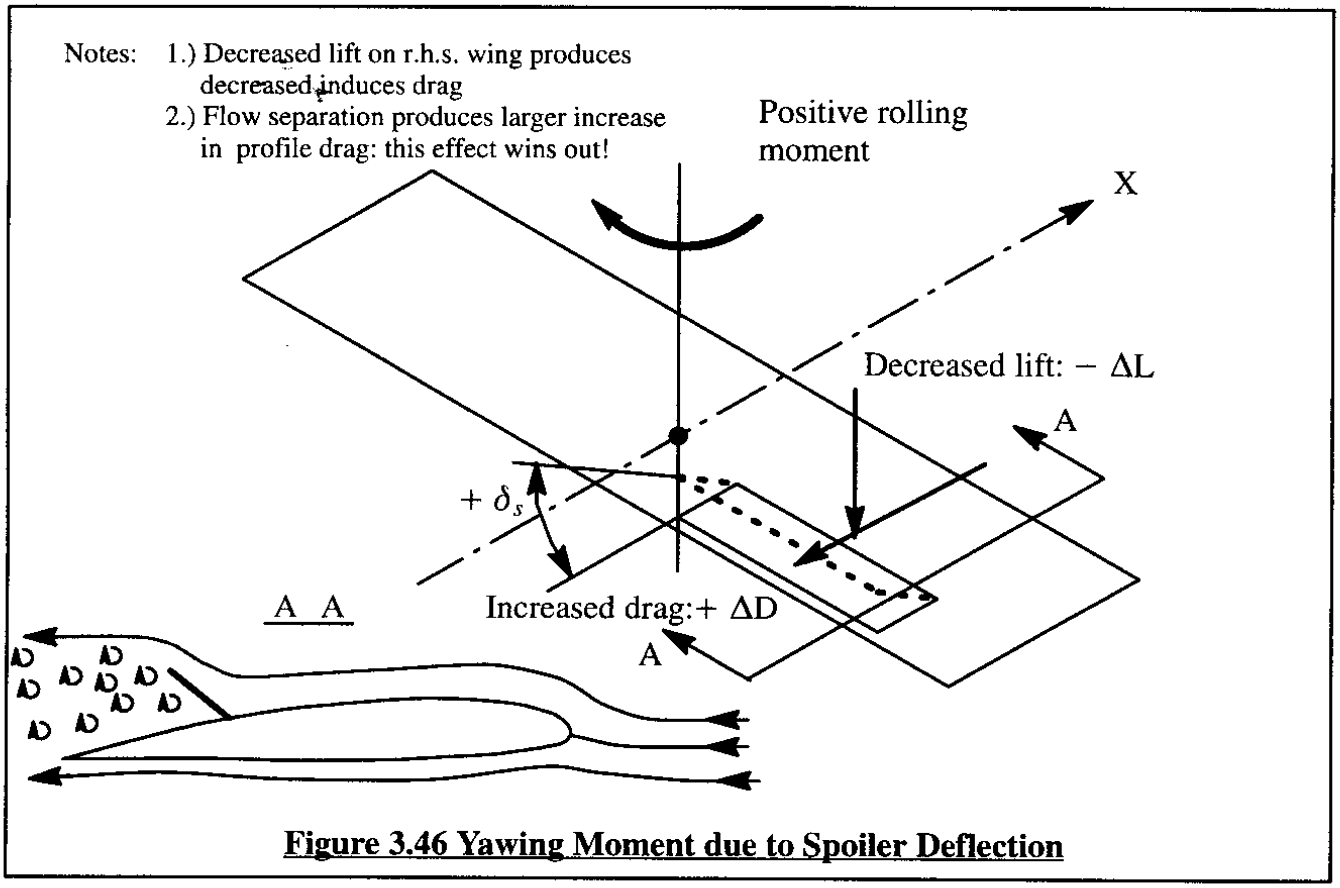

Figure 3.46 Yawing Moment due to Spoiler Deflection

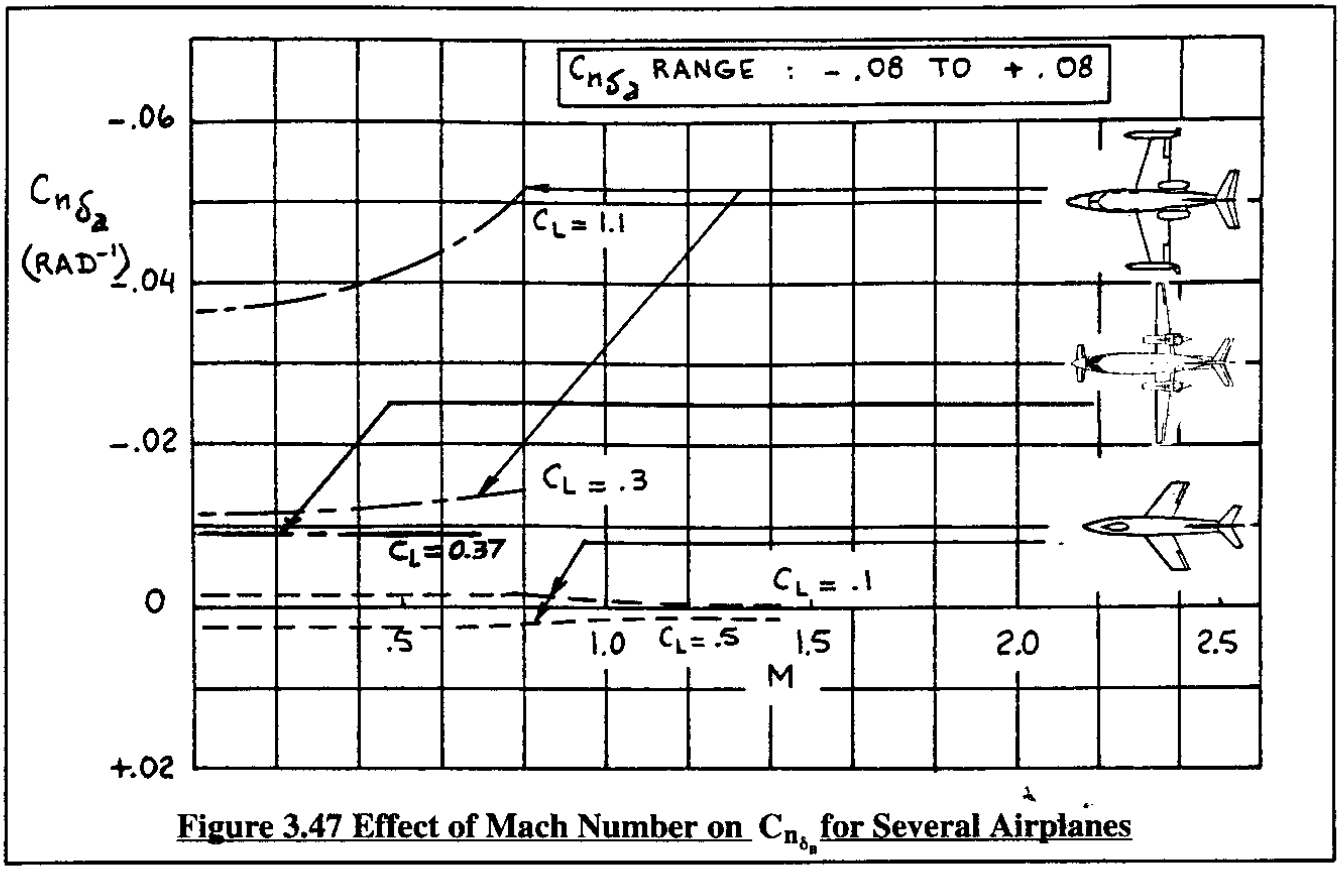

Figure 3.47 Effect of Mach Number on $C_{n_{\delta_a}}$ for Several Airplanes

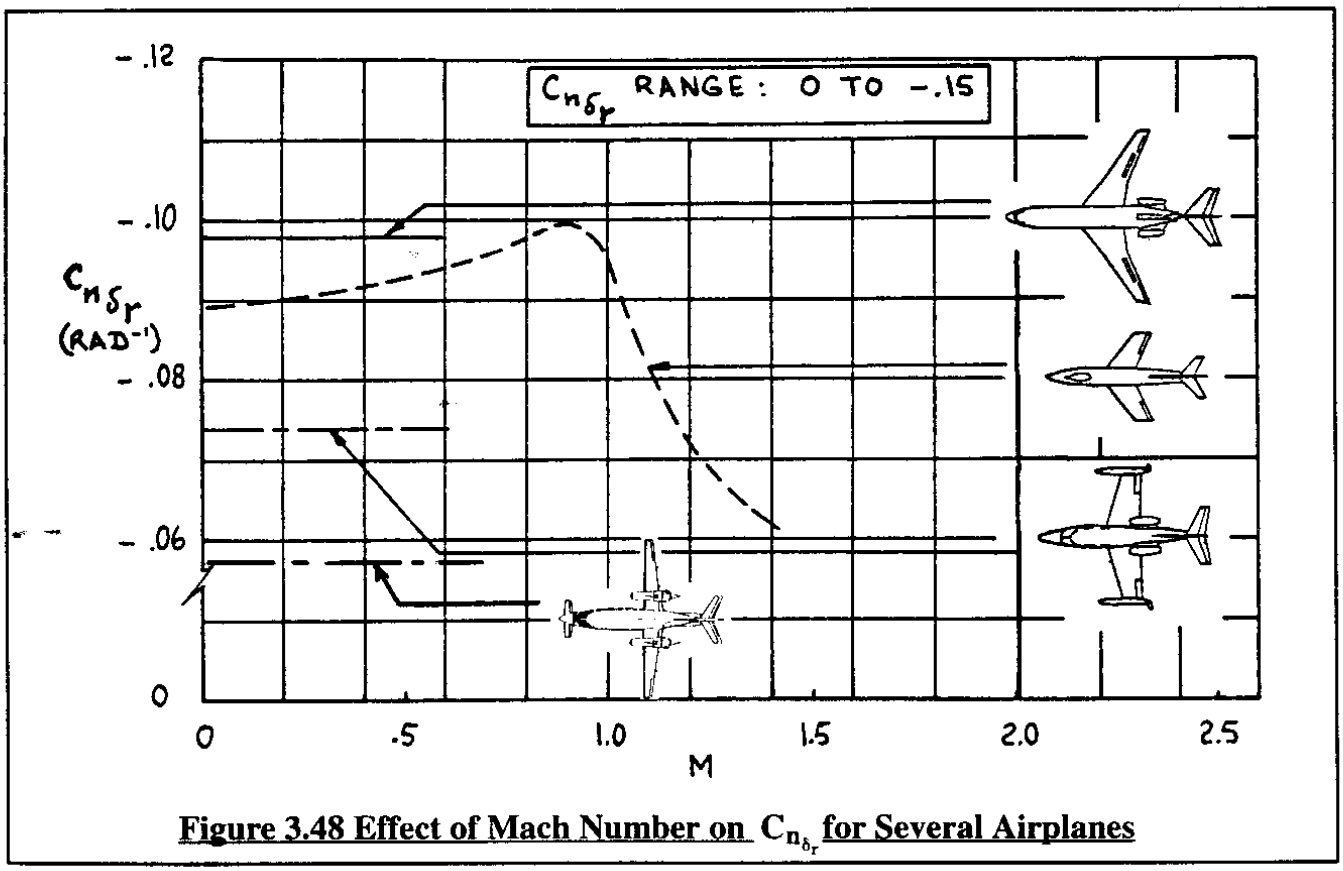

Figure 3.48 Effect of Mach Number on $C_{n_{\delta_r}}$ for Several Airplanes

Rudder Yawing Moment Coefficient Derivative, $C_{n_{\delta_r}}$

Figure 3.38 shows how the side–force due to rudder deflection generates a negative yawing moment:

$$N_{A_{v_{rudder}}} = - F_{a_{y_{v_{rudder}}}} x_{v_s} = C_{n_{\delta_r}} \delta_r \bar{q} S b \tag{3.86}$$

By combining Eqns (3.85), (3.68) and (3.69) it can be shown that:

$$C_{n_{\delta_r}} = - C_{L_{\alpha_v}} \alpha_{\delta_r} \eta_v \frac{S_v x_{v_s}}{S b} \tag{3.87}$$

Note that the directional control derivative, $C_{n_{\delta_r}}$, depends strongly on the vertical tail size in relation to the wing as well as on the lift–curve slope of the vertical tail. The latter in turn depends mostly on aspect ratio and sweep angle of the vertical tail. Also, it is seen that the 'moment–arm', x_{v_s}, is important to directional control power. Finally, the size of the rudder in relationship to the vertical tail size (as determined by S_v) is reflected by the angle–of–attack–effectiveness term α_{δ_r}. The latter term was discussed in Section 2.6.

Figure 3.48 shows how $C_{n_{\delta_r}}$ varies with Mach number for several airplanes.

Drag Rudder Yawing Moment Coefficient Derivative, $C_{n_{\delta_{r_{drag}}}}$

Figure 3.49 shows how a drag rudder generates a yawing moment. The particular drag rudder shown in Figure 3.49 was originally invented by Jack Northrop and is used today in the B–2 stealth bomber. The yawing moment generated by such a drag–rudder can be expressed as:

$$N_{A_{dr}} = \Delta D_{dr}\, y_{dr} = C_{n_{\delta_{r_{drag}}}} \delta_{r_{drag}} \bar{q} S b \tag{3.88}$$

The drag force due to the drag rudder can be modelled as:

$$\Delta D_{dr} = \frac{\partial C_{D_{dr}}}{\partial \delta_{dr}} \delta_{r_{drag}} \bar{q} S \tag{3.89}$$

where: $\delta_{r_{drag}} = 0.5(\delta_{r_{drag_{upper}}} + \delta_{r_{drag_{lower}}})$ is the equivalent drag rudder deflection, positive on the right wing and negative on the left wing.

$\frac{\partial C_{D_{dr}}}{\partial \delta_{r_{drag}}}$ is the incremental drag rudder drag due to drag rudder deflection. In subsonic flight this derivative may be approximated by: $\frac{\partial C_{D_{dr}}}{\partial \delta_{r_{drag}}} = 0.025 \frac{b_{dr}\, c_{dr}}{S}$ 1/deg

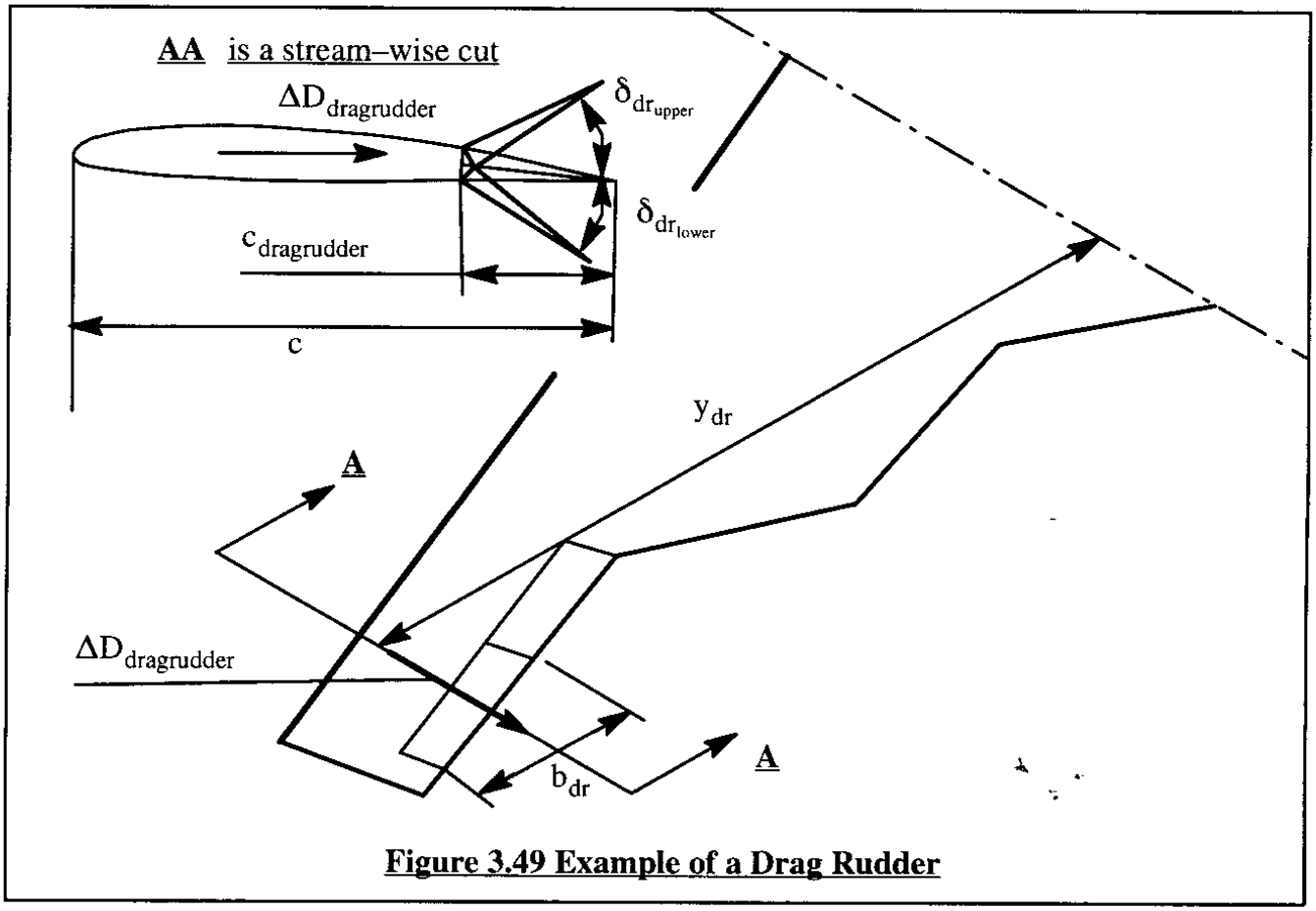

Figure 3.49 Example of a Drag Rudder

where: b_{dr} is the span of the drag rudder and,

c_{dr} is the chord of the drag rudder.

The drag–rudder yawing moment coefficient derivative can now be written as:

$$C_{n_{\delta_{r_{drag}}}} = \frac{0.025 b_{dr} c_{dr} y_{dr}}{Sb} \tag{3.90}$$

In Eqn (3.90) the assumption is made that at 60 degree deflection the drag rudder drag coefficient increment is 0.8 based on its own area. It is also assumed that the drag rudder drag increment varies linearly with drag rudder deflection.

The steady state model for the airplane aerodynamic yawing moment now is:

$$N_{A_{y_{1_s}}} = N_A = (C_{n_\beta}\beta + C_{n_{\delta_a}}\delta_a + C_{n_{\delta_r}}\delta_r) \tag{3.91}$$

Methods for predicting the magnitudes of the derivatives which appear in Eqn (3.72) can be found in Part VI of Reference 3.1.

3.1.11 LATERAL-DIRECTIONAL THRUST FORCES AND MOMENTS

Depending on airplane configuration, failure state of the propulsion system and on the cockpit thrust or power setting(s), there may also be a thrust induced rolling moment, $L_{T_{1_s}}$, a thrust induced side force, $F_{T_{y_{1_s}}}$, and a thrust induced yawing moment, $N_{T_{1_s}}$, acting on the airplane. For these force and moments, the subscripts 1 and s will also be dropped. Furthermore, it will be assumed that the installed values of thrust are known for each engine.

Flight condition and design parameters on which the steady state installed thrust vectors, T_i, depend are defined on page 70.

As mentioned on page 92, whenever airplane components are affected by propeller slipstream and/or by jet exhausts, the aerodynamic, lateral force and moments are all affected. For the lateral directional aerodynamic force and moments corrections for these propulsive installation effects can be made with models as suggested by Eqn (3.43). A more detailed discussion of these effects is beyond the scope of this text.

Figure 3.25 shows how the installed thrust vector for one engine is oriented in the airplane body-fixed axis system. Figure 3.27 shows the orientation and sense of the lateral-directional thrust force and moments. Therefore, the lateral-directional thrust force and moments can be written as:

$$L_{T_{1_s}} = L_T = [\sum_{i=0}^{i=n} T_i(-z_{T_i}\cos\phi_{T_i}\sin\psi_{T_i} - y_{T_i}\sin\phi_{T_i})]\cos\alpha_1 + [\sum_{i=0}^{i=n} T_i(x_{T_i}\cos\phi_{T_i}\sin\psi_{T_i} - y_{T_i}\cos\phi_{T_i}\cos\psi_{T_i})]\sin\alpha_1 \quad (3.92a)$$

$$F_{T_{y_1}} = F_{T_y} = \sum_{i=0}^{i=n} T_i(\cos\phi_{T_i}\sin\psi_{T_i}) \quad (3.92b)$$

$$N_{T_{1_s}} = N_T = [\sum_{i=0}^{i=n} T_i(x_{T_i}\cos\phi_{T_i}\sin\psi_{T_i} - y_{T_i}\cos\phi_{T_i}\cos\psi_{T_i})]\cos\alpha_1 - [\sum_{i=0}^{i=n} T_i(-z_{T_i}\cos\phi_{T_i}\sin\psi_{T_i} - y_{T_i}\sin\phi_{T_i})]\sin\alpha_1 \quad (3.92c)$$

It is to be noted that whenever the engine installation is symmetrical with respect to the airplane XZ-plane AND whenever the thrust output of the engine installation is also symmetrical with respect the airplane XZ-plane, all lateral-directional force and moments are zero!

Assuming that for the case of a symmetrical engine installation, one engine is inoperative (OEI), the lateral force and moments due to the one (asymmetrically) operating engine can be expressed as:

$$L_T = [T_i(z_{T_i}\cos\phi_{T_i}\sin\psi_{T_i} - y_{T_i}\sin\phi_{T_i})]\cos\alpha_1 +$$

$$+ [T_i(x_{T_i} \cos\phi_{T_i} \sin\psi_{T_i} - y_{T_i} \cos\phi_{T_i} \cos\psi_{T_i})] \sin\alpha_1 \tag{3.93a}$$

$$F_{T_y} = T_i(\cos\phi_{T_i} \sin\psi_{T_i}) \tag{3.93b}$$

$$N_T = [T_i(x_{T_i} \cos\phi_{T_i} \sin\psi_{T_i} - y_{T_i} \cos\phi_{T_i} \cos\psi_{T_i})] \cos\alpha_1 +$$

$$- [T_i(z_{T_i} \cos\phi_{T_i} \sin\psi_{T_i} - y_{T_i} \sin\phi_{T_i})] \sin\alpha_1 + \Delta N_{D_i} \tag{3.93c}$$

Whenever an engine or propeller is inoperative, some type of incremental drag arises on that engine. That increase in drag results in an additional drag–induced side force, rolling moment and yawing moment. In many instances only the drag induced yawing moment turns out to be significant from a stability and control viewpoint. That is the reason for the appearance of the ΔN_{D_i} term in Eqn (3.93c). This extra drag due to the inoperative engine must also be accounted for in any climb performance calculations with one (or more) engines inoperative. A method to account for ΔN_{D_i} is presented on page 216.

The lateral thrust–line off–set angle, ψ_{T_i}, and the thrust–line inclination angle ϕ_{T_i}, are small, but not equal to zero in most modern transport airplanes. In such cases these angles are referred to as the engine toe–in angle and toe–up angles respectively. The reason for these angles is to minimize engine nacelle drag in their local flow–field. Figure 3.36 shows the toe–in angles on the Boeing 747. Assuming that the steady state angle of attack and both the toe–in and the toe–up angles are small, equations (3.93) simplify to:

$$L_T \approx T_i(z_{T_i}\psi_{T_i} - y_{T_i}\phi_{T_i}) - T_i y_{T_i}\alpha_1 \tag{3.94a}$$

$$F_{T_y} = T_i\psi_{T_i} \tag{3.94b}$$

$$N_T \approx T_i(x_{T_i}\psi_{T_i} - y_{T_i}) + \Delta N_{D_i} \tag{3.94c}$$

3.1.12 ASSEMBLING THE STEADY STATE LATERAL–DIRECTIONAL FORCES AND MOMENTS

It is now possible to assemble all expressions for the lateral–directional force and moments in matrix format. This is done in Table 3.3: Eqns (3.95a) and (3.95b). Note that the aerodynamic force and moments are treated as linear terms. The thrust terms contain transcendental terms in the steady state angle of attack. Later, in the discussion of the equations of motion in Chapter 4, it will be shown that by introduction of iteration schemes or by using the small angle assumption this problem will fade away.

Table 3.3 Matrix Format for Steady State Lateral–Directional Forces and Moments

$$\begin{Bmatrix} L_{A_{1_s}} \\ F_{A_{y_{1_s}}} \\ N_{A_{1_s}} \end{Bmatrix} = \begin{Bmatrix} L_A \\ F_{A_y} \\ N_A \end{Bmatrix} = \begin{Bmatrix} C_l \bar{q} S b \\ C_y \bar{q} S \\ C_n \bar{q} S b \end{Bmatrix} \quad \textbf{with:}$$

$$\begin{Bmatrix} C_l \\ C_y \\ C_n \end{Bmatrix} = \begin{bmatrix} C_{l_\beta} & C_{l_{\delta_a}} & C_{l_{\delta_r}} \\ (3.52) & (\text{See p.104}) & (\text{See p.106}) \\ C_{y_\beta} & C_{y_{\delta_a}} & C_{y_{\delta_r}} \\ (3.75) & (\text{See p.111}) & (\text{See p.113}) \\ C_{n_\beta} & C_{n_{\delta_a}} & C_{n_{\delta_r}} \\ (3.82) & (\text{See p.117}) & (\text{See p.120}) \end{bmatrix} \begin{Bmatrix} \beta \\ \delta_a \\ \delta_r \end{Bmatrix} \tag{3.95a}$$

$$\begin{Bmatrix} L_T \\ F_{T_y} \\ N_T \end{Bmatrix} = \begin{Bmatrix} \sum_{i=0}^{i=n} T_i (z_{T_i} \psi_{T_i} - y_{T_i} \phi_{T_i}) - T_i y_{T_i} \alpha_1 \\ \sum_{i=0}^{i=n} T_i \psi_{T_i} \\ \sum_{i=0}^{i=n} T_i (x_{T_i} \psi_{T_i} - y_{T_i}) + \Delta N_{D_i} \end{Bmatrix} \tag{3.95b}$$

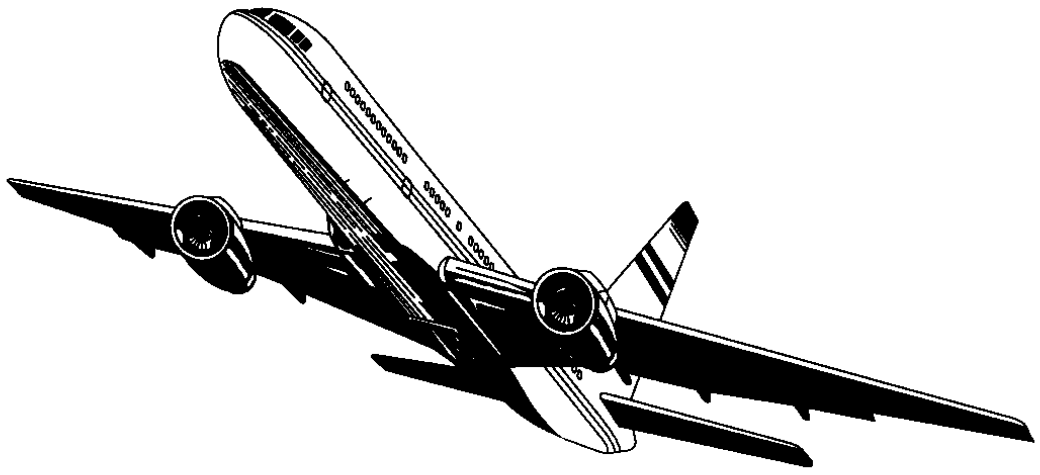

3.2 PERTURBED STATE FORCES AND MOMENTS

Since airplanes differ from one another in configuration, shape and size, it should be expected that it is not feasible to develop a mathematical model for airplane perturbed state force and moments which applies to all airplanes. The approach taken here is to first list the forces and moments to be modeled. Second, those variables of motion which experience shows to have a significant effect on the forces and moments are also listed. For the aerodynamic forces and moments, this is done in the form of a table such as Table 3.4.

The meaning of several perturbed state variables is illustrated in Figure 3.50. This figure should be used in conjunction with Table 3.4. In this table it is assumed that all perturbations are defined relative to a steady state for which: $V_1 = P_1 = R_1 = 0$. If the various thrust vectors which act on the airplane are symmetrical about the XZ–plane, this also means that: $F_{A_{y_{1_s}}} = L_{A_{1_s}} = N_{A_{1_s}} = 0$ is satisfied. Practical experience shows that these are not very restrictive conditions in terms of the validity of the resulting small perturbation equations. In other words, when these conditions are not exactly satisfied, the basic structure of Table 3.4 still applies.

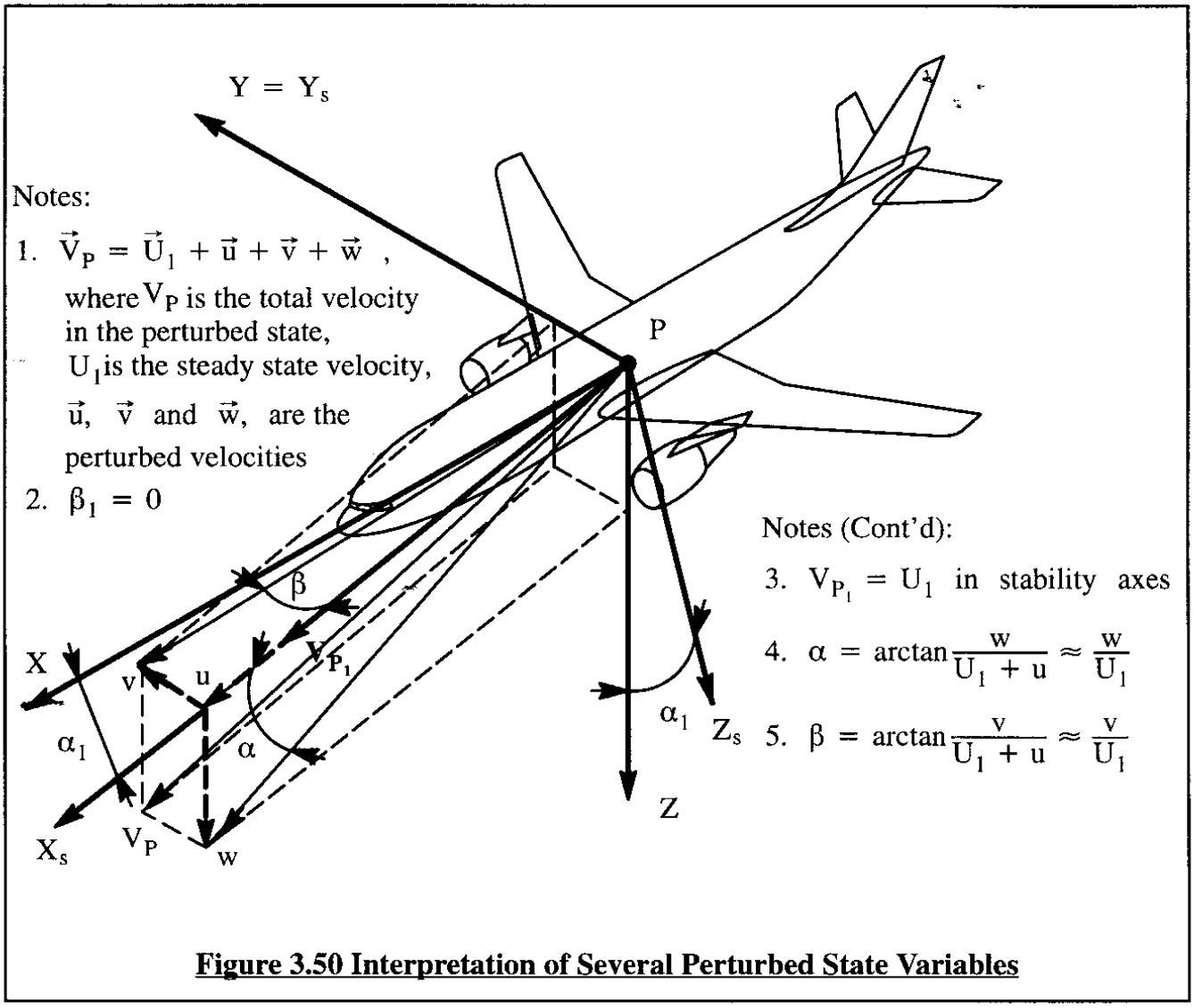

Figure 3.50 Interpretation of Several Perturbed State Variables

Table 3.4 Dependence of Perturbed State Aerodynamic Forces and Moments on Variables

Variable	Direct Variables								Derived Variables				Control Variables			
	u	v	w	p	q	r	$\dot{v}$	$\dot{w}$	$\beta = \frac{v}{U_1}$	$\alpha = \frac{w}{U_1}$	$\dot{\beta} = \frac{\dot{v}}{U_1}$	$\dot{\alpha} = \frac{\dot{w}}{U_1}$	δ_a	δ_e	δ_r	δ_f
f_{A_x}	$\frac{\partial F_{A_x}}{\partial u}$		$\frac{\partial F_{A_x}}{\partial w}$		$\frac{\partial F_{A_x}}{\partial q}$			$\frac{\partial F_{A_x}}{\partial \dot{w}}$		$\frac{\partial F_{A_x}}{\partial \alpha}$		$\frac{\partial F_{A_x}}{\partial \dot{\alpha}}$		$\frac{\partial F_{A_x}}{\partial \delta_e}$		$\frac{\partial F_{A_x}}{\partial \delta_f}$
f_{A_y}		$\frac{\partial F_{A_y}}{\partial v}$		$\frac{\partial F_{A_y}}{\partial p}$		$\frac{\partial F_{A_y}}{\partial r}$	$\frac{\partial F_{A_y}}{\partial \dot{v}}$		$\frac{\partial F_{A_y}}{\partial \beta}$		$\frac{\partial F_{A_y}}{\partial \dot{\beta}}$		$\frac{\partial F_{A_y}}{\partial \delta_a}$		$\frac{\partial F_{A_y}}{\partial \delta_r}$	
f_{A_z}	$\frac{\partial F_{A_z}}{\partial u}$		$\frac{\partial F_{A_z}}{\partial w}$		$\frac{\partial F_{A_z}}{\partial q}$			$\frac{\partial F_{A_z}}{\partial \dot{w}}$		$\frac{\partial F_{A_z}}{\partial \alpha}$		$\frac{\partial F_{A_z}}{\partial \dot{\alpha}}$		$\frac{\partial F_{A_z}}{\partial \delta_e}$		$\frac{\partial F_{A_z}}{\partial \delta_f}$
l_A		$\frac{\partial L_A}{\partial v}$		$\frac{\partial L_A}{\partial p}$		$\frac{\partial L_A}{\partial r}$	$\frac{\partial L_A}{\partial \dot{v}}$		$\frac{\partial L_A}{\partial \beta}$		$\frac{\partial L_A}{\partial \dot{\beta}}$		$\frac{\partial L_A}{\partial \delta_a}$		$\frac{\partial L_A}{\partial \delta_r}$	
m_A	$\frac{\partial M_A}{\partial u}$		$\frac{\partial M_A}{\partial w}$		$\frac{\partial M_A}{\partial q}$			$\frac{\partial M_A}{\partial \dot{w}}$		$\frac{\partial M_A}{\partial \alpha}$		$\frac{\partial M_A}{\partial \dot{\alpha}}$		$\frac{\partial M_A}{\partial \delta_e}$		$\frac{\partial M_A}{\partial \delta_f}$
n_A		$\frac{\partial N_A}{\partial v}$		$\frac{\partial N_A}{\partial p}$		$\frac{\partial N_A}{\partial r}$	$\frac{\partial N_A}{\partial \dot{v}}$		$\frac{\partial N_A}{\partial \beta}$		$\frac{\partial N_A}{\partial \dot{\beta}}$		$\frac{\partial N_A}{\partial \delta_a}$		$\frac{\partial N_A}{\partial \delta_r}$	

Notes: 1. All perturbations are taken relative to a symmetrical steady state: $V_1 = P_1 = R_1 = 0$

2. Blanks in the table indicate that there is no effect, to a first order of approximation

The basic structure of Table 3.4 is based on the following assumptions:

1) blanks in Table 3.4 indicate that a particular perturbed variable has NO effect on a particular perturbed force or moment.

2) partial derivatives in Table 3.4 indicate the slope by which a a particular perturbed force or moment is affected by a particular perturbed variable.

Whether or not these assumptions are satisfied depends largely on the symmetry (or lack thereof) of the airplane configuration being considered. With the exception of airplanes such as shown in Figure 1.3 the assumptions 1) and 2) are generally considered to be reasonable.

Next, an outline of the effect of the perturbed motion variables on the perturbed aerodynamic forces and moments is given.

Effect of a forward speed perturbation, u:

The consequence of a forward speed perturbation is two–fold: the dynamic pressure, $\bar{q} = \frac{1}{2}\rho V_P^2$, and the Mach number, $M = V_P/c$, both change. As a result, the following longitudinal aerodynamic forces and moment will change: F_{A_x}, F_{A_z} and M_A. These changes are expressed with the help of the derivatives: $\frac{\partial F_{A_x}}{\partial u}$, $\frac{\partial F_{A_z}}{\partial u}$ and $\frac{\partial M_A}{\partial u}$ in Table 3.4. Because the steady state lateral–directional force and moments: $F_{A_{y_{1_s}}} = L_{A_{1_s}} = N_{A_{1_s}} = 0$, there will be no changes in F_{A_y}, L_A and N_A due to a forward speed perturbation, u. Therefore, the corresponding rectangles in Table 3.4 have been left blank.

Effect of a lateral speed (or side velocity) perturbation, v:

The effect of a side velocity perturbation, v, can be thought of as a perturbed sideslip angle, $\beta = \frac{v}{U_1}$, as shown in Figure 3.50. The effect of v on dynamic pressure is considered negligible. It was already shown in Section 3.1 that the effect of a change in sideslip angle is to change the lateral–directional force and moments: F_{A_y}, L_A and N_A. These changes are expressed through the derivatives: $\frac{\partial F_{A_y}}{\partial v}$, $\frac{\partial L_A}{\partial v}$ and $\frac{\partial N_A}{\partial v}$ or $\frac{\partial F_{A_y}}{\partial \beta}$, $\frac{\partial L_A}{\partial \beta}$ and $\frac{\partial N_A}{\partial \beta}$ in Table 3.4. As long as the sideslip angle is small, its effect on the longitudinal forces and moment: F_{A_x}, F_{A_z} and M_A is assumed to be negligible. That explains the corresponding blank rectangles in Table 3.4.

Effect of a downward speed (or downward velocity) perturbation, w:

The effect of a downward velocity perturbation, w, can be thought of as a perturbed angle of attack, $\alpha = \frac{w}{U_1}$, as shown in Figure 3.50. The effect of w on dynamic pressure is considered to be negligible. It was already shown in Section 3.1 that the effect of a change in angle of attack is to change the longitudinal forces and moment: F_{A_x}, F_{A_z} and M_A. These changes are ex-

pressed with the aid of the derivatives: $\frac{\partial F_{A_x}}{\partial w}$, $\frac{\partial F_{A_z}}{\partial w}$ and $\frac{\partial M_A}{\partial w}$ or $\frac{\partial F_{A_x}}{\partial \alpha}$, $\frac{\partial F_{A_z}}{\partial \alpha}$ and $\frac{\partial M_A}{\partial \alpha}$ in Table 3.4. As long as the angle of attack is small, its effect on the lateral–directional force and moments: F_{A_y} , L_A and N_A is negligible. That explains the corresponding blank rectangles in Table 3.4.

Effect of a roll rate perturbation, p:

The effect of a small perturbation in roll rate, p, is to cause non–symmetrical changes in local angles of attack over the wing, canard and tail surfaces. It is assumed that these changes take place in an anti–symmetrical manner so that there are negligible effects on the longitudinal aerodynamic forces and moment: F_{A_x} , F_{A_z} and M_A. Strictly speaking, this argument is not valid for a vertical tail. However, in most conventional airplanes the vertical tail effect due to roll rate perturbations is small anyway. The changes in the lateral–directional force and moments: F_{A_y} , L_A and N_A are accounted for through the derivatives: $\frac{\partial F_{A_y}}{\partial p}$, $\frac{\partial L_A}{\partial p}$ and $\frac{\partial N_A}{\partial p}$ as indicated in Table 3.4.

Effect of a pitch rate perturbation, q:

A pitch rate perturbation causes a symmetrical change in angles of attack over the wing, canard, horizontal tail and fuselage. The effect of this is to change the longitudinal aerodynamic forces and moment: F_{A_x} , F_{A_z} and M_A. These changes are expressed with the help of the derivatives: $\frac{\partial F_{A_x}}{\partial q}$, $\frac{\partial F_{A_z}}{\partial q}$ and $\frac{\partial M_A}{\partial q}$, as shown in Table 3.4. The effect of perturbed pitch rate on the lateral–directional force and moments: F_{A_y} , L_A and N_A is assumed to be negligible.

Effect of a yaw rate perturbation, r:

A yaw rate perturbation causes a non–symmetrical change in the local velocities of the wing, canard and horizontal tail. In addition, it causes a non–symmetrical change in local angles of attack over the vertical tail. These changes will generally affect the lateral–directional force and moments: F_{A_y} , L_A and N_A. This is expressed by the derivatives: $\frac{\partial F_{A_y}}{\partial r}$, $\frac{\partial L_A}{\partial r}$ and $\frac{\partial N_A}{\partial r}$ in Table 3.4.

Effect of rate of change of angle of attack, $\dot{\alpha}$

When the angle of attack of an airplane changes with time, the wing produces a vortex field which changes with time. That changing vortex field can have a significant effect on the aerodynamics of the horizontal tail. Such an effect is accounted for by means of so–called $\dot{\alpha}$ derivatives which affect the longitudinal forces and moment: F_{A_x} , F_{A_z} and M_A. The corresponding derivatives: $\frac{\partial F_{A_x}}{\partial \dot{\alpha}}$, $\frac{\partial F_{A_z}}{\partial \dot{\alpha}}$ and $\frac{\partial M_A}{\partial \dot{\alpha}}$ are also shown in Table 3.4. The effect of $\dot{\alpha}$ on the lateral–directional force and moments: F_{A_y} , L_A and N_A is considered negligible.

Effect of rate of change of angle of sideslip, $\dot{\beta}$

When the angle of sideslip of an airplane changes with time, the wing–fuselage combination produces a vortex field which changes with time. That changing vortex field can have a significant effect on the vertical tail. Such an effect is accounted for by means of so–called $\dot{\beta}$ derivatives which affect the lateral–directional force and moments, F_{A_y} , L_A and N_A . The corresponding derivatives: $\frac{\partial F_{A_y}}{\partial \dot{\beta}}$, $\frac{\partial L_A}{\partial \dot{\beta}}$ and $\frac{\partial N_A}{\partial \dot{\beta}}$ are also shown in Table 3.4.

Effect of control surface perturbations, δ_a, δ_e, δ_r and δ_f

It will be assumed that perturbations in longitudinal control surface deflections, such as δ_e and δ_f only affect the longitudinal forces and moment: F_{A_x} , F_{A_z} and M_A through the derivatives: $\frac{\partial F_{A_x}}{\partial \delta_e}$, $\frac{\partial F_{A_z}}{\partial \delta_e}$ and $\frac{\partial M_A}{\partial \delta_e}$ and $\frac{\partial F_{A_x}}{\partial \delta_f}$, $\frac{\partial F_{A_z}}{\partial \delta_f}$ and $\frac{\partial M_A}{\partial \delta_f}$. For other control surfaces, similar derivatives should be substituted.

It will also be assumed that perturbations in lateral–directional control surface deflections, such as δ_a and δ_r only affect the lateral–directional force and moments: F_{A_y} , L_A and N_A. The corresponding derivatives: $\frac{\partial F_{A_y}}{\partial \delta_a}$, $\frac{\partial L_A}{\partial \delta_a}$ and $\frac{\partial N_A}{\partial \delta_a}$ and $\frac{\partial F_{A_y}}{\partial \delta_r}$, $\frac{\partial L_A}{\partial \delta_r}$ and $\frac{\partial N_A}{\partial \delta_r}$ are also shown in Table 3.4.

Whether or not these explanations are applicable depends largely on the symmetry (or lack thereof) of the airplane configuration being considered. With the exception of airplanes such as shown in Figure 1.3 the explanations given before are considered to be reasonable.

Another important assumption which is made at this point is that all perturbed forces and moments are a function of the instantaneous values of the perturbed motion variables only. This assumption is also known as the quasi–steady assumption. It has been pointed out by Etkin in Reference 3.6 that this assumption is not always realistic, depending on the motion frequencies of an airplane. Very roughly, for frequencies above about 10 radians per second the effect of motion frequency on the perturbed forces and moments does become important. In such cases, Etkin and Rodden (References 3.6 and 3.7) have developed alternate formulations for the perturbed forces and moments. Experience has shown that the great majority of rigid airplane stability and control problems can be adequately analyzed with the quasi–steady assumption.

Finally, it will also be assumed that higher order derivatives than the first derivatives accounted for in this text are negligible.

Table 3.5 shows the mathematical model used to represent the perturbed aerodynamic forces and moments, based on these explanations. Where applicable, the derived instead of the direct variables have been used.

Table 3.5 Dimensional Quasi–Steady Model for Perturbed Aerodynamic Forces and Moments

Longitudinal:

$$f_{A_x} = \frac{\partial F_{A_x}}{\partial u}u + \frac{\partial F_{A_x}}{\partial \alpha}\alpha + \frac{\partial F_{A_x}}{\partial \dot{\alpha}}\dot{\alpha} + \frac{\partial F_{A_x}}{\partial q}q + \frac{\partial F_{A_x}}{\partial \delta_e}\delta_e + \frac{\partial F_{A_x}}{\partial \delta_f}\delta_f \qquad (3.96a)$$

$$f_{A_z} = \frac{\partial F_{A_z}}{\partial u}u + \frac{\partial F_{A_z}}{\partial \alpha}\alpha + \frac{\partial F_{A_z}}{\partial \dot{\alpha}}\dot{\alpha} + \frac{\partial F_{A_z}}{\partial q}q + \frac{\partial F_{A_z}}{\partial \delta_e}\delta_e + \frac{\partial F_{A_z}}{\partial \delta_f}\delta_f \qquad (3.96b)$$

$$m_A = \frac{\partial M_A}{\partial u}u + \frac{\partial M_A}{\partial \alpha}\alpha + \frac{\partial M_A}{\partial \dot{\alpha}}\dot{\alpha} + \frac{\partial M_A}{\partial q}q + \frac{\partial M_A}{\partial \delta_e}\delta_e + \frac{\partial M_A}{\partial \delta_f}\delta_f \qquad (3.96c)$$

Lateral–Directional:

$$f_{A_y} = \frac{\partial F_{A_y}}{\partial \beta}\beta + \frac{\partial F_{A_y}}{\partial \dot{\beta}}\dot{\beta} + \frac{\partial F_{A_y}}{\partial p}p + \frac{\partial F_{A_y}}{\partial r}r + \frac{\partial F_{A_y}}{\partial \delta_a}\delta_a + \frac{\partial F_{A_y}}{\partial \delta_r}\delta_r \qquad (3.97a)$$

$$l_A = \frac{\partial L_A}{\partial \beta}\beta + \frac{\partial L_A}{\partial \dot{\beta}}\dot{\beta} + \frac{\partial L_A}{\partial p}p + \frac{\partial L_A}{\partial r}r + \frac{\partial L_A}{\partial \delta_a}\delta_a + \frac{\partial L_A}{\partial \delta_r}\delta_r \qquad (3.97b)$$

$$n_A = \frac{\partial N_A}{\partial \beta}\beta + \frac{\partial N_A}{\partial \dot{\beta}}\dot{\beta} + \frac{\partial N_A}{\partial p}p + \frac{\partial N_A}{\partial r}r + \frac{\partial N_A}{\partial \delta_a}\delta_a + \frac{\partial N_A}{\partial \delta_r}\delta_r \qquad (3.97c)$$

The mathematical model of Table 3.5 has a problem: the variables have physical units ranging from radians to radians/second and ft/sec. For reasons of uniformity it is preferred to make all variables dimensionless. This is achieved as follows:

1) by dividing the speed perturbation u by: U_1

2) by multiplying longitudinal perturbed angular rates by: $\frac{\bar{c}}{2U_1}$

3) by multiplying lateral–directional angular rates by: $\frac{b}{2U_1}$

The effect of this is to alter the model of Table 3.5 to that of Table 3.6. That model will be used in this text.

Table 3.6 Non–Dimensional Quasi–Steady Model for Perturbed Aerodynamic Forces and Moments

Longitudinal:

$$f_{A_x} = \frac{\partial F_{A_x}}{\partial(\frac{u}{U_1})}(\frac{u}{U_1}) + \frac{\partial F_{A_x}}{\partial \alpha}\alpha + \frac{\partial F_{A_x}}{\partial(\frac{\dot{\alpha}\bar{c}}{2U_1})}(\frac{\dot{\alpha}\bar{c}}{2U_1}) + \frac{\partial F_{A_x}}{\partial(\frac{q\bar{c}}{2U_1})}(\frac{q\bar{c}}{2U_1}) + \frac{\partial F_{A_x}}{\partial \delta_e}\delta_e + \frac{\partial F_{A_x}}{\partial \delta_f}\delta_f \quad (3.98a)$$

$$f_{A_z} = \frac{\partial F_{A_z}}{\partial(\frac{u}{U_1})}(\frac{u}{U_1}) + \frac{\partial F_{A_z}}{\partial \alpha}\alpha + \frac{\partial F_{A_z}}{\partial(\frac{\dot{\alpha}\bar{c}}{2U_1})}(\frac{\dot{\alpha}\bar{c}}{2U_1}) + \frac{\partial F_{A_z}}{\partial(\frac{q\bar{c}}{2U_1})}(\frac{q\bar{c}}{2U_1}) + \frac{\partial F_{A_z}}{\partial \delta_e}\delta_e + \frac{\partial F_{A_z}}{\partial \delta_f}\delta_f \quad (3.98b)$$

$$m_A = \frac{\partial M_A}{\partial(\frac{u}{U_1})}(\frac{u}{U_1}) + \frac{\partial M_A}{\partial \alpha}\alpha + \frac{\partial M_A}{\partial(\frac{\dot{\alpha}\bar{c}}{2U_1})}(\frac{\dot{\alpha}\bar{c}}{2U_1}) + \frac{\partial M_A}{\partial(\frac{q\bar{c}}{2U_1})}(\frac{q\bar{c}}{2U_1}) + \frac{\partial M_A}{\partial \delta_e}\delta_e + \frac{\partial M_A}{\partial \delta_f}\delta_f \quad (3.98c)$$

Lateral–Directional:

$$f_{A_y} = \frac{\partial F_{A_y}}{\partial \beta}\beta + \frac{\partial F_{A_y}}{\partial(\frac{\dot{\beta}b}{2U_1})}(\frac{\dot{\beta}b}{2U_1}) + \frac{\partial F_{A_y}}{\partial(\frac{pb}{2U_1})}(\frac{pb}{2U_1}) + \frac{\partial F_{A_y}}{\partial(\frac{rb}{2U_1})}(\frac{rb}{2U_1}) + \frac{\partial F_{A_y}}{\partial \delta_a}\delta_a + \frac{\partial F_{A_y}}{\partial \delta_r}\delta_r \quad (3.99a)$$

$$l_A = \frac{\partial L_A}{\partial \beta}\beta + \frac{\partial L_A}{\partial(\frac{\dot{\beta}b}{2U_1})}(\frac{\dot{\beta}b}{2U_1}) + \frac{\partial L_A}{\partial(\frac{pb}{2U_1})}(\frac{pb}{2U_1}) + \frac{\partial L_A}{\partial(\frac{rb}{2U_1})}(\frac{rb}{2U_1}) + \frac{\partial L_A}{\partial \delta_a}\delta_a + \frac{\partial L_A}{\partial \delta_r}\delta_r \quad (3.99b)$$

$$n_A = \frac{\partial N_A}{\partial \beta}\beta + \frac{\partial N_A}{\partial(\frac{\dot{\beta}b}{2U_1})}(\frac{\dot{\beta}b}{2U_1}) + \frac{\partial N_A}{\partial(\frac{pb}{2U_1})}(\frac{pb}{2U_1}) + \frac{\partial N_A}{\partial(\frac{rb}{2U_1})}(\frac{rb}{2U_1}) + \frac{\partial N_A}{\partial \delta_a}\delta_a + \frac{\partial N_A}{\partial \delta_r}\delta_r \quad (3.99c)$$

Expressions for the partial force and moment derivatives in Table 3.6 will be developed in Sub–sections 3.2.1 through 3.2.13.

3.2.1 PERTURBED STATE, LONGITUDINAL AERODYNAMIC FORCES AND MOMENTS

The perturbed state, longitudinal aerodynamic forces and moments are stated in Table 3.6 Eqns (3.98) and (3.99) in their dimensionless form. It is seen that the partial derivatives of the longitudinal forces and moment with respect to the dimensionless motion and control variables play the key role. The purpose of Sub–sections 3.2.2 through 3.2.13 is to show how these force and moment derivatives may be determined with the help of various stability and control derivatives. The dependence of these stability and control derivatives on airplane configuration design parameters will also be discussed.

3.2.2 AERODYNAMIC FORCE AND MOMENT DERIVATIVES WITH RESPECT TO FORWARD SPEED

According to Table 3.6, the following forces and moment are affected by changes in forward speed, u: F_{A_x} , F_{A_z} and M_A. These forces and moment are non–dimensionalized as follows:

$$F_{A_x} = C_x \bar{q} S \tag{3.100a}$$

$$F_{A_z} = C_z \bar{q} S \tag{3.100b}$$

$$M_A = C_m \bar{q} S \bar{c} \tag{3.100c}$$

The reader is reminded of the fact that F_{A_x} , F_{A_z} and M_A are defined in the stability axis system. Next, the partial differentiations implied by Table 3.6 will be systematically performed for Equations (3.100a) through (3.100c).

Partial Differentiation of Equation (3.100a) with respect to u/U_1

Partial differentiation of Eqn (3.100a) with respect to (u/U_1) , leads to:

$$\frac{\partial F_{A_x}}{\partial(\frac{u}{U_1})} = \frac{\partial C_x}{\partial(\frac{u}{U_1})} \bar{q} S + C_x S \frac{\partial \bar{q}}{\partial(\frac{u}{U_1})} \tag{3.101}$$

At this point it should be recognized that the partial differentiations in Eqn (3.101) carry the following significance:

$$\frac{\partial F_{A_x}}{\partial(\frac{u}{U_1})} \quad \text{implies :} \quad \frac{\partial F_{A_x}}{\partial(\frac{u}{U_1})}\Big|_1$$

In other words, both partial differentiations and the coefficient C_x in Eqn (3.101) must be evaluated in the steady state flight condition for which all perturbed quantities are equal to zero! For the partial differentiation of $\bar{q}$ this has the following consequence:

$$\frac{\partial \bar{q}}{\partial(\frac{u}{U_1})} = U_1 \frac{\partial \bar{q}}{\partial u}\Big|_1 = U_1 \frac{\partial \frac{1}{2}\rho[(U_1 + u)^2 + v^2 + w^2]}{\partial u}\Big|_1 =$$

$$= U_1 \rho (U_1 + u)\Big|_1 = \rho U_1^2 \tag{3.102}$$

Before carrying out the partial differentiation of C_x it is necessary to refer to Figure 3.51 to relate C_x to C_L and C_D. By using the 'small angle' assumption:

$$C_x = -C_D + C_L \alpha \tag{3.103a}$$

Partial differentiation of C_x yields:

$$\frac{\partial C_x}{\partial(\frac{u}{U_1})}\Big|_1 = -\frac{\partial C_D}{\partial(\frac{u}{U_1})}\Big|_1 + \frac{\partial C_L}{\partial(\frac{u}{U_1})}\alpha\Big|_1 = -\frac{\partial C_D}{\partial(\frac{u}{U_1})}\Big|_1 \tag{3.103b}$$

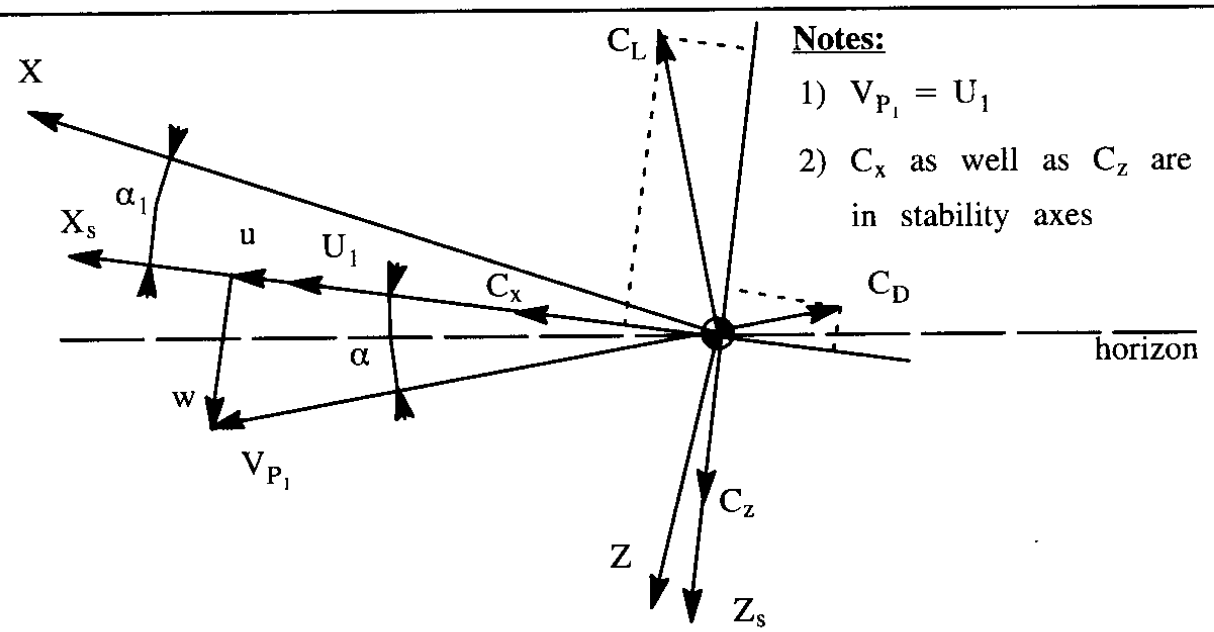

Figure 3.51 Determination of C_x and C_z based on C_L and C_D

From Eqn (3.103a) it follows that in the steady state:

$$C_{x_1} = -C_{D_1} \tag{3.104}$$

The following notation is now introduced:

$$C_{D_u} = \frac{\partial C_D}{\partial(\frac{u}{U_1})}\Big|_1 \tag{3.105}$$

With this notation it is possible to rewrite Eqn (3.101) as:

$$\frac{\partial F_{A_x}}{\partial(\frac{u}{U_1})} = -(C_{D_u} + 2C_{D_1})\bar{q}_1 S \tag{3.106}$$

The derivative C_{D_u} is referred to as the speed–damping derivative. The sign and magnitude of C_{D_u} depends on the steady state Mach number of the airplane. Figure 3.52 shows a typical plot of the steady state drag coefficient versus Mach number (at constant angle of attack!). Since:

$$C_{D_u} = \frac{\partial C_D}{\partial(\frac{u}{U_1})} = \frac{U_1}{a}\frac{\partial C_D}{\partial \frac{u}{a}} = M_1 \frac{\partial C_D}{\partial M} \tag{3.107}$$

The quantity 'a' represents the speed of sound for the steady state flight condition being considered. The numerical magnitude and sign of $\partial C_D/\partial M$ can be determined from a figure like Figure 3.52. Note that $\partial C_D/\partial M$ is generally >0 for M<1 while it is <0 for M>1. Figure 3.53 gives examples of the variation of C_{D_u} with Mach number for several airplanes.

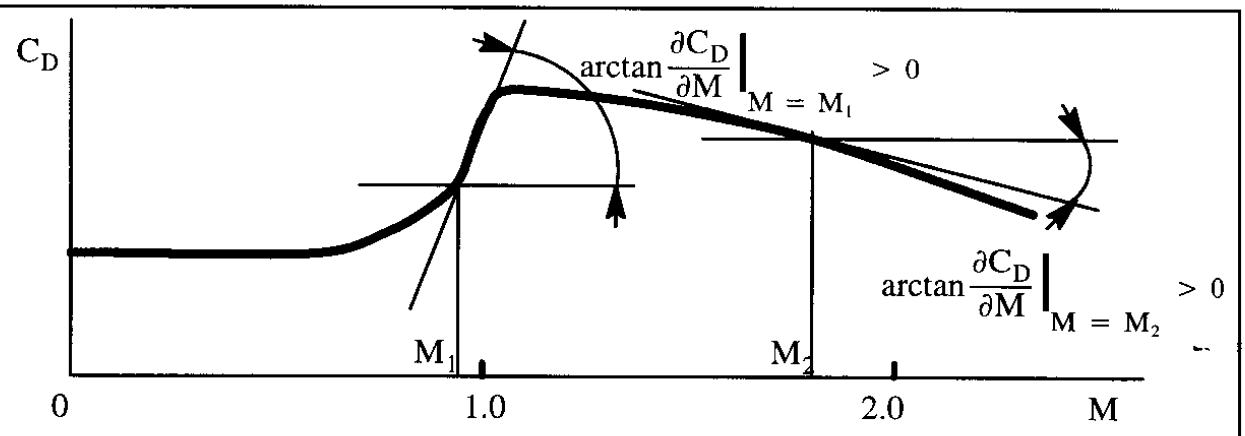

Figure 3.52 Example of Determination of: $\partial C_D/\partial M$

Partial Differentiation of Equation (3.100b) with respect to u/U_1

Partial differentiation of Eqn (3.100b) with respect to (u/U_1) , leads to:

$$\frac{\partial F_{A_z}}{\partial(\frac{u}{U_1})} = \frac{\partial C_z}{\partial(\frac{u}{U_1})}\bar{q}S + C_z S\frac{\partial \bar{q}}{\partial(\frac{u}{U_1})} \tag{3.108}$$

Referring to Figure 3.51 it may be seen that (for small angle α):

$$C_z = -C_L - C_D\alpha \tag{3.109}$$

In the steady state this means:

$$C_{z_1} = -C_{L_1} \tag{3.110}$$

Differentiation of Eqn (3.109) yields:

$$\frac{\partial C_z}{\partial(\frac{u}{U_1})} = -\frac{\partial C_L}{\partial(\frac{u}{U_1})} - \alpha\frac{\partial C_D}{\partial(\frac{u}{U_1})} \tag{3.111}$$

Evaluated at the steady state, this condition produces:

$$C_{z_u} = -C_{L_u} \tag{3.112}$$

Note that:

$$C_{L_u} = \frac{\partial C_L}{\partial(\frac{u}{U_1})}\Big|_1 \tag{3.113}$$

By using Equations (3.112) and (3.110) it follows for Eqn (3.108) that:

$$\frac{\partial F_{A_z}}{\partial(\frac{u}{U_1})} = -(C_{L_u} + 2C_{L_1})\bar{q}_1 S \tag{3.114}$$

The derivative C_{L_u} can be evaluated for high aspect ratio wings as follows. At subsonic speeds, according to the Prandtl–Glauert transformation it is found that:

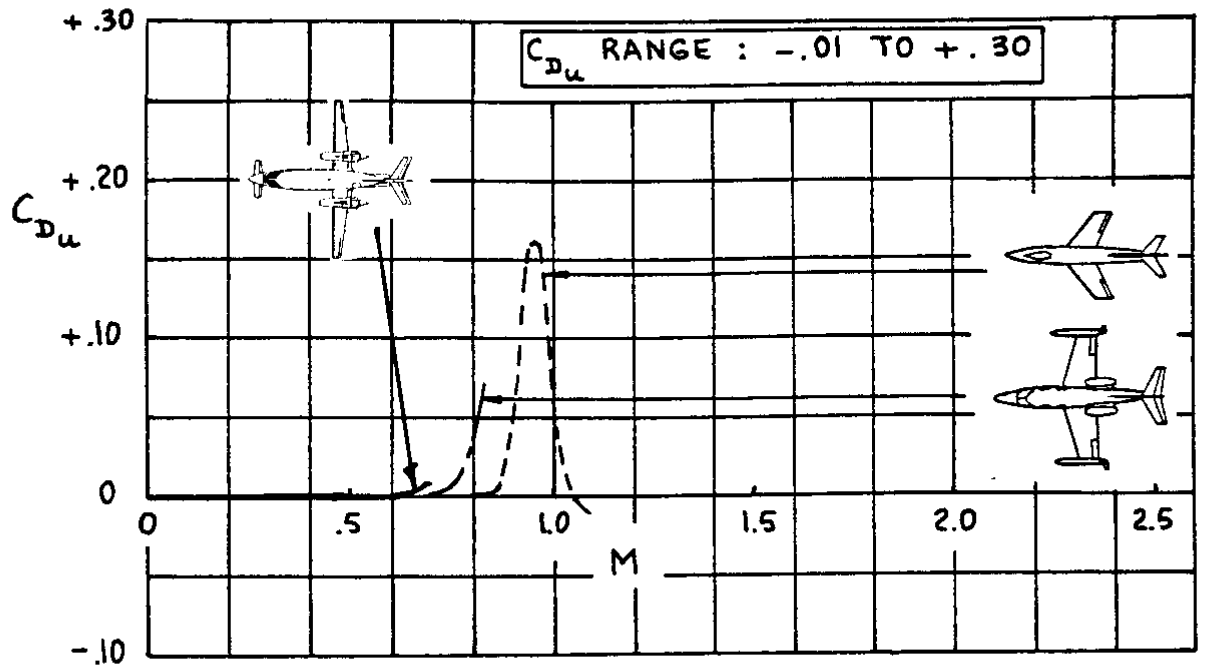

Figure 3.53 Effect of Mach Number on C_{D_u} for Several Airplanes

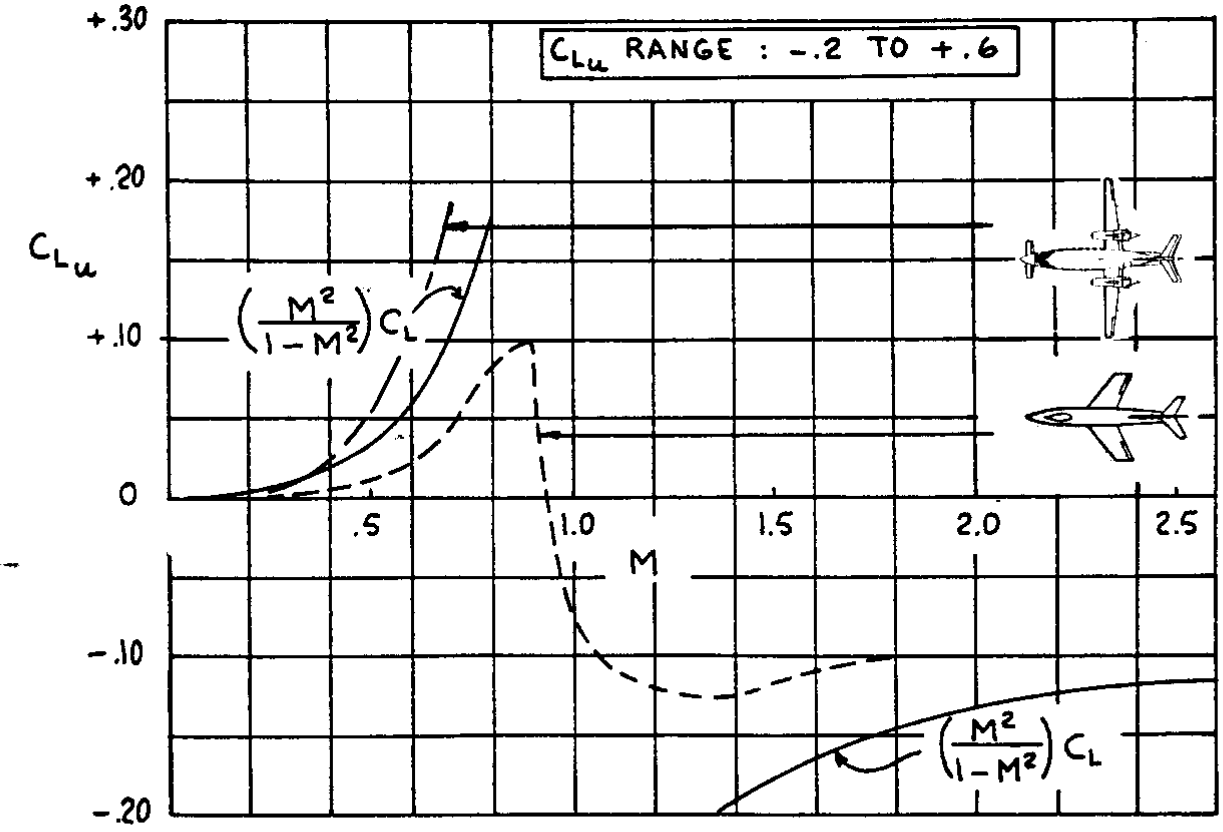

Figure 3.54 Effect of Mach Number on C_{L_u} for Several Airplanes

$$C_L = \frac{C_{L_0} + (C_{L_\alpha}|_{M=0})\alpha}{\sqrt{(1 - M^2)}} \tag{3.115}$$

This expression must now be differentiated with respect to M. For most airplanes, the following first order of approximation is reasonable:

$$\frac{\partial C_{L_0}}{\partial(\frac{u}{U_1})} \approx 0 \tag{3.116}$$

In that case:

$$\frac{\partial C_L}{\partial M} = \frac{M}{(1 - M^2)} C_L \tag{3.117}$$

Recalling Eqn (3.107) it follows that:

$$C_{L_u} = \frac{\partial C_L}{\partial(\frac{u}{U_1})} = \frac{U_1}{a}\frac{\partial C_L}{\partial \frac{u}{a}} = M_1 \frac{\partial C_L}{\partial M} \tag{3.118}$$

Therefore, it follows that:

$$C_{L_u} = \frac{M_1^2}{(1 - M_1^2)} C_L \tag{3.119}$$

Examples of the variation of C_{L_u} with Mach number for several airplanes are presented in Figure 3.54.

Partial Differentiation of Equation (3.100c) with respect to u/U_1

Partial differentiation of Eqn (3.100c) with respect to (u/U_1), leads to:

$$\frac{\partial M_A}{\partial(\frac{u}{U_1})} = \frac{\partial C_m}{\partial(\frac{u}{U_1})}\bar{q}_1 S\bar{c} + C_{m_1} S\bar{c}\rho U_1^2 \tag{3.120}$$

By using the notation:

$$\frac{\partial C_m}{\partial(\frac{u}{U_1})} = C_{m_u} \tag{3.121}$$

it follows that:

$$\frac{\partial M}{\partial(\frac{u}{U_1})} = (C_{m_u} + 2C_{m_1})\bar{q}_1 S\bar{c} \tag{3.122}$$

For gliders, for power–off flight and for power–on flight in airplanes where there is no thrust induced pitching moment about the center of gravity, the condition: $C_{m_1} = 0$ is satisfied in steady state flight. If thrust does contribute to pitching moment, the condition: $C_{m_1} = -C_{m_{T_1}}$ applies

and this term must be accounted for in Eqn (3.122).

For reasons similar to those leading to Eqn (3.118):

$$C_{m_u} = M_1 \frac{\partial C_m}{\partial M} \tag{3.123}$$

The change in pitching moment coefficient due to Mach number is caused by changes in C_{m_0} and by the aft shift in aerodynamic center (and center of pressure) which tend to occur in the high subsonic speed range. If changes in C_{m_0} with Mach number are negligible, it is possible to compute $\partial C_m/\partial M$ from the following equation:

$$\frac{\partial C_m}{\partial M}(\Delta M) = - \Delta \bar{x}_{ac_A} C_{L_1} \tag{3.124}$$

where: $\Delta \bar{x}_{ac_A}$ is the aft shift in airplane aerodynamic center for a change in Mach number, ΔM. In that case, using Eqn (3.123):

$$C_{m_u} = - M_1 C_{L_1} \frac{\partial x_{ac_A}}{\partial M} \tag{3.125}$$

Note that in Eqns (3.124) and (3.125) an aft shift in a.c. is counted as positive! Shifts in a.c. with Mach number can be determined theoretically (See Ref.1, Part VI) or from windtunnel data. It is seen from Eqn (3.125) that in the transonic speed range below M=1, $C_{m_u} < 0$. This implies that for an increase in Mach number, the airplane has a tendency to put the nose down. This phenomenon is referred to as transonic 'tuck'. It can result in unacceptable handling quality behavior. Such behavior can be corrected by careful attention to airfoil design, wing planform design and/or by the introduction of Mach-trim systems.

Figure 3.55 presents examples of the variation of C_{m_u} with Mach number for several example airplanes. Note that the D-558-II 'bucks' the subsonic trend. The reason for this is not known to the author.

3.2.3 AERODYNAMIC FORCE AND MOMENT DERIVATIVES WITH RESPECT TO ANGLE OF ATTACK

According to Table 3.6 the following forces and moment are affected by changes in angle of attack, α: F_{A_x}, F_{A_z} and M_A. These quantities were non-dimensionalized in Eqns (3.100).

Partial Differentiation of Equation (3.100a) with respect to α

Partial differentiation of Eqn (3.100a) with respect to α, leads to:

$$\frac{\partial F_{A_x}}{\partial \alpha} = \frac{\partial C_x}{\partial \alpha} \bar{q} S \tag{3.126}$$

By invoking Eqn (3.103a) it follows that:

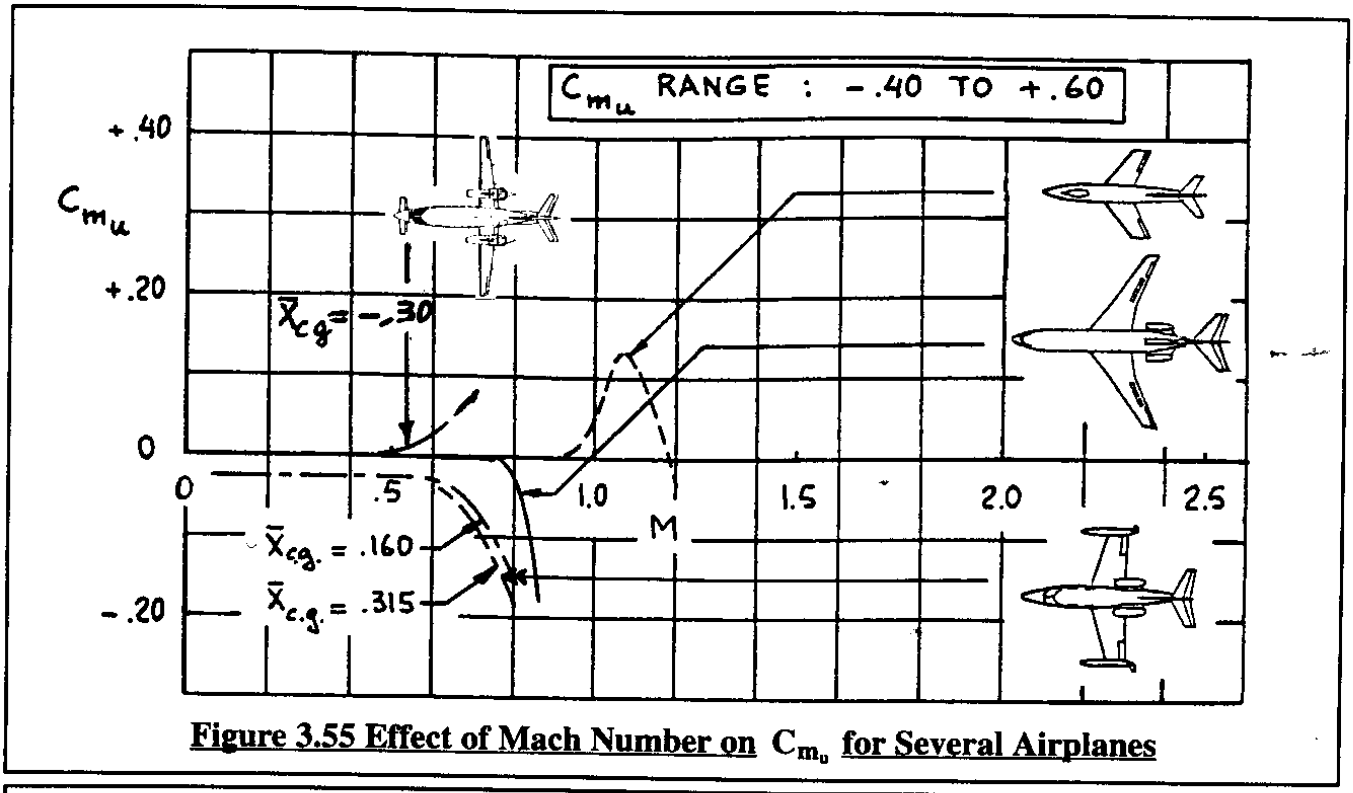

Figure 3.55 Effect of Mach Number on C_{m_u} for Several Airplanes

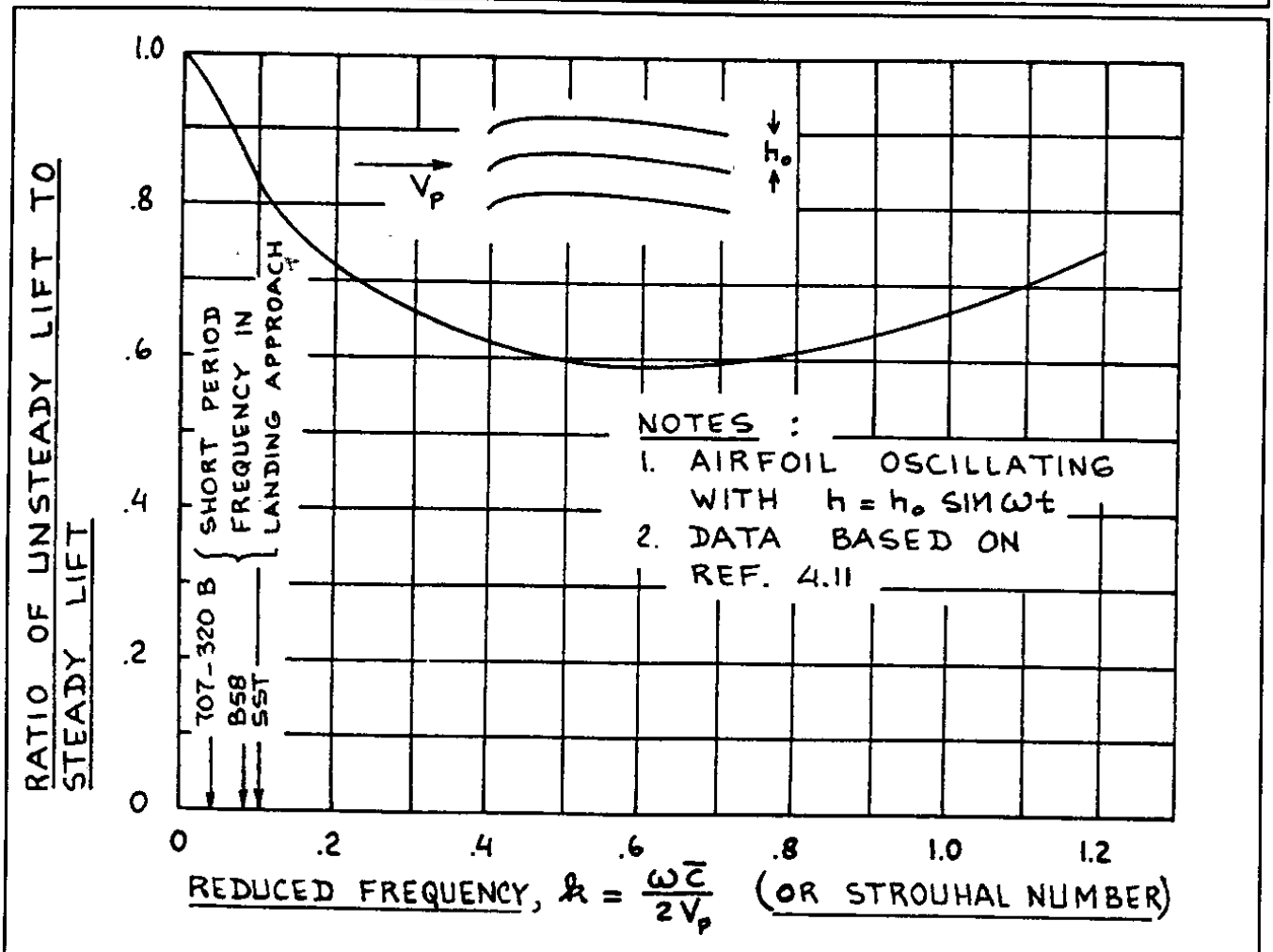

Figure 3.56 Effect of Frequency of Angle of Attack Oscillation Lift

$$C_{x_\alpha} = \frac{\partial C_x}{\partial \alpha} = -\frac{\partial C_D}{\partial \alpha} + \frac{\partial C_L}{\partial \alpha}\alpha + C_L \tag{3.127}$$

After evaluating this result in the steady state flight condition:

$$C_{x_\alpha} = -C_{D_\alpha} + C_{L_1} \tag{3.128}$$

And thus, Eqn (3.126) yields:

$$\frac{\partial F_{A_x}}{\partial \alpha} = (-C_{D_\alpha} + C_{L_1})\bar{q}_1 S \tag{3.129}$$

where the derivative C_{D_α} is obtained from Eqn (3.9).

Partial Differentiation of Equation (3.100b) with respect to α

Partial differentiation of Eqn (3.100b) with respect to α, leads to:

$$\frac{\partial F_{A_z}}{\partial \alpha} = \frac{\partial C_z}{\partial \alpha}\bar{q}S \tag{3.130}$$

From Eqn (3.109) it is found that:

$$C_{z_\alpha} = \frac{\partial C_z}{\partial \alpha} = -\frac{\partial C_L}{\partial \alpha} - \frac{\partial C_D}{\partial \alpha}\alpha - C_D \tag{3.131}$$

After evaluating this result in the steady state flight condition:

$$C_{z_\alpha} = -C_{L_\alpha} - C_{D_1} \tag{3.132}$$

And thus, Eqn (3.130) yields:

$$\frac{\partial F_{A_x}}{\partial \alpha} = -(C_{L_\alpha} + C_{D_1})\bar{q}_1 S \tag{3.133}$$

where the derivative C_{L_α} is obtained from Eqn (3.24).

Partial Differentiation of Equation (3.100c) with respect to α

Partial differentiation of Eqn (3.100c) with respect to α and evaluating the result in the steady state flight condition leads to:

$$\frac{\partial M_A}{\partial \alpha} = \frac{\partial C_m}{\partial \alpha}\bar{q}S\bar{c} = C_{m_\alpha}\bar{q}_1 S\bar{c} \tag{3.134}$$

The derivative C_{m_α} is obtained from Eqn (3.35).

Examples of the variation of C_{D_α}, C_{L_α} and C_{m_α} with Mach number are presented in Figures (3.12), (3.16) and (3.21) respectively.

3.2.4 AERODYNAMIC FORCE AND MOMENT DERIVATIVES WITH RESPECT TO ANGLE OF ATTACK RATE

According to Table 3.6 the following forces and moment are affected by changes in angle of attack rate: F_{A_x} , F_{A_z} and M_A. These quantities were non–dimensionalized in Eqns (3.98). Introduction of angle of attack rate derivatives rests upon the assumption that, as a result of a change in $\dot{\alpha}$ the aerodynamic pressure distribution over the airplane adjusts itself instantaneously to α . This so–called quasi–steady assumption has been shown to be reasonable (Ref. 3.6) as long as the following condition is satisfied:

$$\left[\begin{matrix}\text{reduced}\\ \text{frequency}\end{matrix}\right] = k = \frac{\dot{\alpha}\bar{c}}{2U_1} < 0.04 \tag{3.135}$$

An example of the ratio of unsteady lift to steady lift for a thin airfoil which oscillates up and down in subsonic flow is shown in Figure 3.56. The data in Figure 3.56 suggest that criterion (3.135) is indeed reasonable.

Methods for computing the $\dot{\alpha}$ effect for arbitrary airplane configurations are not yet available. In the mean time the so–called 'lag–of–downwash' method can be used to obtain estimates for the derivatives of F_{A_x}, F_{A_z} and M_A with respect to $\dot{\alpha}$. In this method it is assumed that downwash behind a wing (or other lifting surface) is dependent primarily on the strength of the trailing vortices of the wing in the vicinity of the horizontal tail.

Because vorticity is transported with the flow, a change in downwash at the wing trailing edge (due to a change in angle of attack) will not be felt as a change in downwash at the horizontal tail until a time increment $\Delta t = x_h/U_1$ has elapsed. The quantity x_h is the distance from the 3/4 mgc point on the wing to the aerodynamic center of the horizontal tail.

Depending on overall airplane layout, the following approximation is often satisfied:

$$x_h \approx x_{ac_h} - x_{cg} \tag{3.136}$$

It will be assumed that the downwash at the horizontal tail, ε (t), equals that downwash which corresponds to the wing angle of attack $\alpha(t - \Delta t)$. Therefore, a correction to the horizontal tail angle of attack can be made as follows:

$$\Delta\varepsilon = -\frac{d\varepsilon}{d\alpha}\dot{\alpha}\Delta t = -\frac{d\varepsilon}{d\alpha}\dot{\alpha}\frac{(\bar{x}_{ac_h} - \bar{x}_{cg})}{U_1} \tag{3.137}$$

Next, the partial derivatives of F_{A_x}, F_{A_z} and M_A will be taken one–by one.

Partial Differentiation of Equation (3.100a) with respect to $(\dot{\alpha}\bar{c}/2U_1)$

Partial differentiation of Eqn (3.100a) with respect to $(\dot{\alpha}\bar{c}/2U_1)$ leads to:

$$\frac{\partial F_{A_x}}{\partial(\frac{\dot{\alpha}\bar{c}}{2U_1})} = C_{x_{\dot{\alpha}}}\bar{q}S = -C_{D_{\dot{\alpha}}}\bar{q}S = 0 \tag{3.138}$$

where it is assumed that the effect of downwash lag on drag can be neglected: $C_{D_{\dot{\alpha}}} \approx 0$

Partial Differentiation of Equation (3.100b) with respect to $(\dot{\alpha}\bar{c}/2U_1)$

Partial differentiation of Eqn (3.100b) with respect to $(\dot{\alpha}\bar{c}/2U_1)$, leads to:

$$\frac{\partial F_{A_z}}{\partial(\frac{\dot{\alpha}\bar{c}}{2U_1})} = \frac{\partial C_Z}{\partial(\frac{\dot{\alpha}\bar{c}}{2U_1})}\bar{q}_1 S = C_{Z_{\dot{\alpha}}}\bar{q}_1 S \tag{3.139}$$

Since:

$$C_{Z_{\dot{\alpha}}} = -C_{L_{\dot{\alpha}}} \tag{3.140}$$

The derivative $C_{L_{\dot{\alpha}}}$ is found by observing the fact that $\Delta\varepsilon$ of Eqn (3.137) causes a change in horizontal tail lift coefficient which can be expressed as follows:

$$\Delta C_{L_h} = -C_{L_{\alpha_h}}\Delta\varepsilon = C_{L_{\alpha_h}}\frac{d\varepsilon}{d\alpha}\dot{\alpha}\frac{(x_{ac_h} - x_{cg})}{U_1} \tag{3.141}$$

For the entire airplane this yields:

$$\underset{\text{airplane, caused by } \dot{\alpha}}{\Delta C_L} = C_{L_{\alpha_h}}\frac{d\varepsilon}{d\alpha}\dot{\alpha}\frac{(x_{ac_h} - x_{cg})}{U_1}\eta_h\frac{S_h}{S} \tag{3.142}$$

Partial differentiation w.r.t $(\dot{\alpha}\bar{c}/2U_1)$ and using Eqn (3.140) produces:

$$C_{Z_{\dot{\alpha}}} = -C_{L_{\dot{\alpha}}} = -2C_{L_{\alpha_h}}\frac{d\varepsilon}{d\alpha}\frac{(x_{ac_h} - x_{cg})}{\bar{c}}\eta_h\frac{S_h}{S} \tag{3.143}$$

Introducing the concept of horizontal tail volume coefficient first used in Eqn (3.36):

$$C_{L_{\dot{\alpha}}} = 2C_{L_{\alpha_h}}\eta_h\bar{V}_h\frac{d\varepsilon}{d\alpha} \tag{3.144}$$

Combining Eqn (3.139) with (3.140) and (3.144) results in:

$$\frac{\partial F_{A_z}}{\partial(\frac{\dot{\alpha}\bar{c}}{2U_1})} = -2C_{L_{\alpha_h}}\eta_h\bar{V}_h\frac{d\varepsilon}{d\alpha}\bar{q}_1 S \tag{3.145}$$

Figure 3.57 shows how $C_{L_{\dot{\alpha}}}$ varies with Mach number for several airplanes.

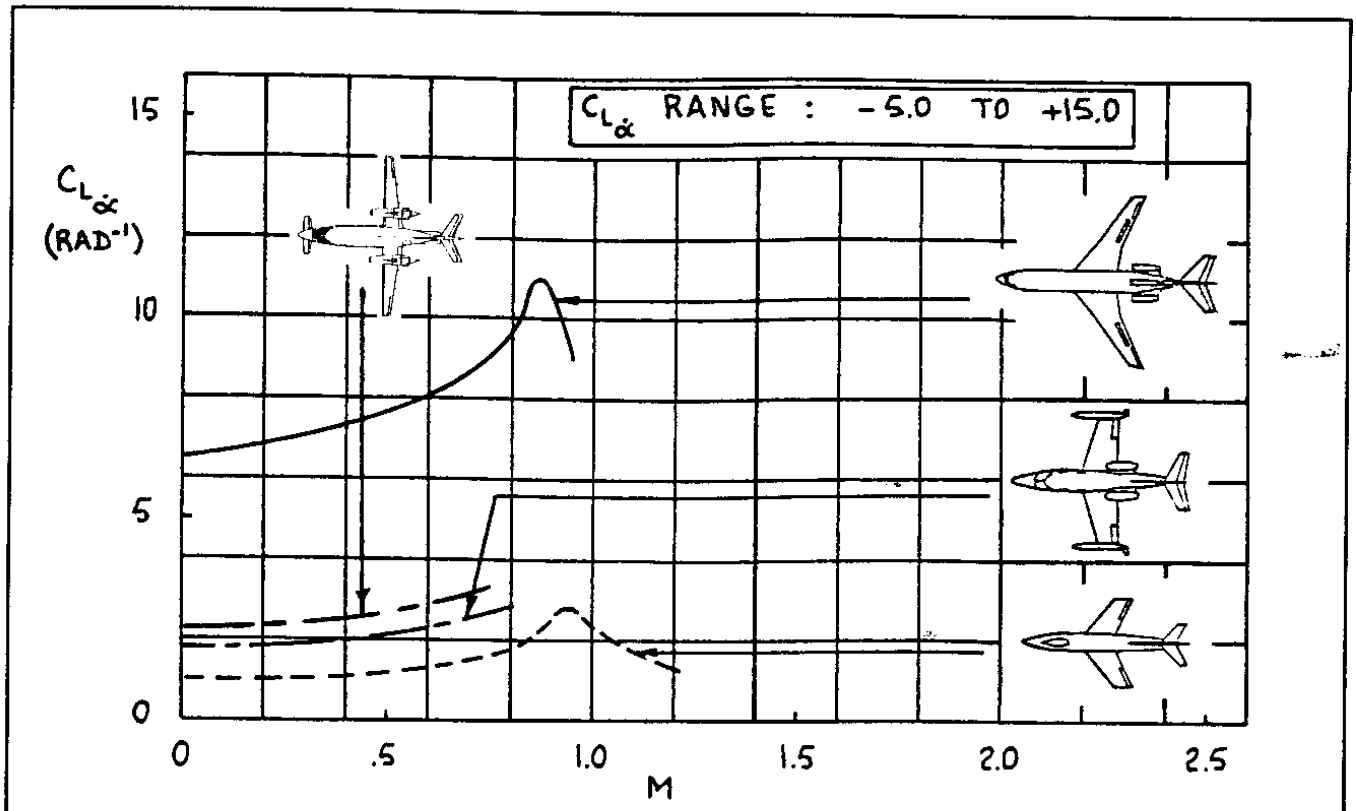

Figure 3.57 Effect of Mach Number on C_{L_α} for Several Airplanes

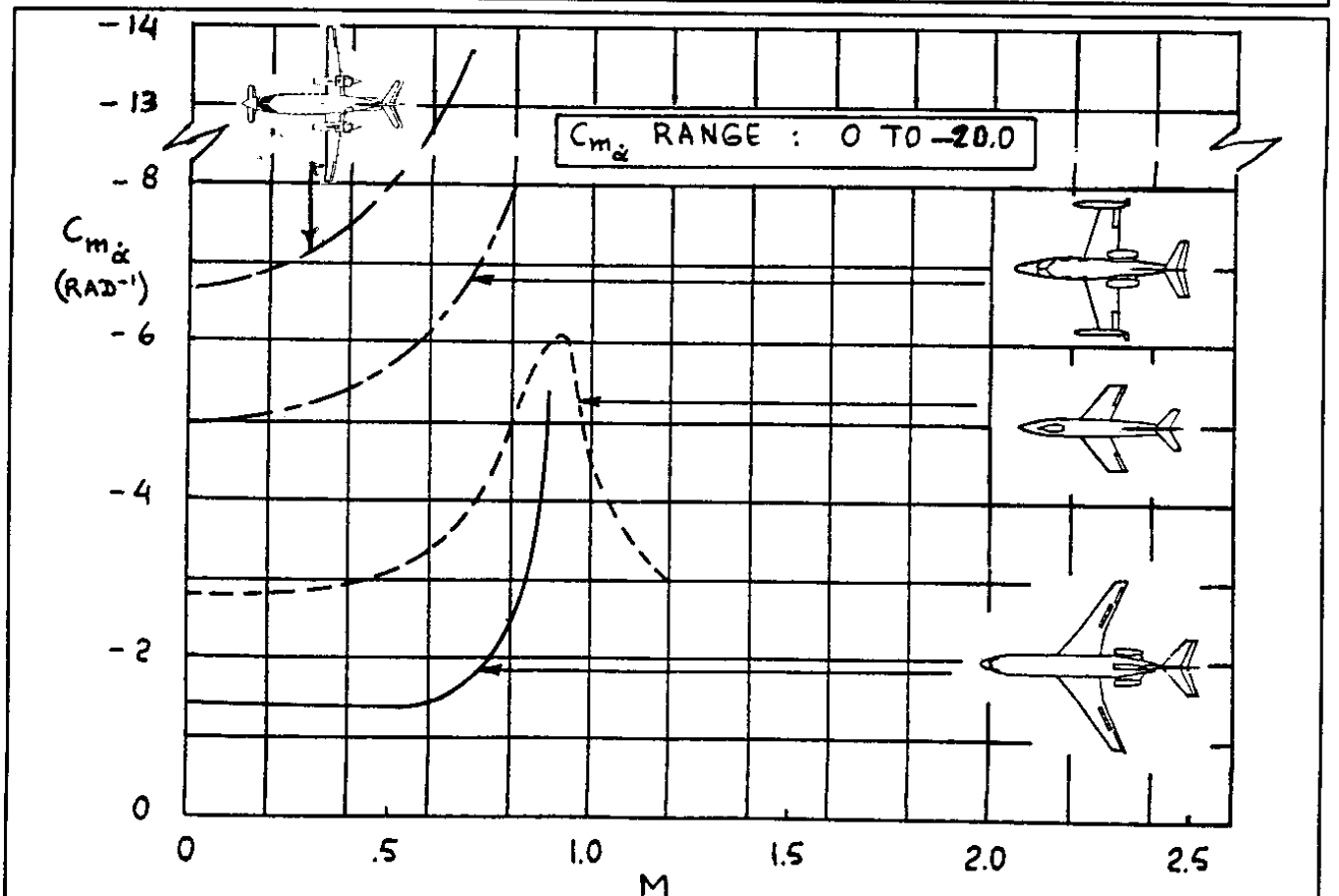

Figure 3.58 Effect of Mach Number on C_{m_α} for Several Airplanes

Partial Differentiation of Equation (3.100c) with respect to $(\alpha\bar{c}/2U_1)$

Partial differentiation of Eqn (3.98c) with respect to $(\alpha\bar{c}/2U_1)$ and evaluation at the steady state leads to:

$$\frac{\partial M_A}{\partial(\frac{\alpha\bar{c}}{2U_1})} = C_{m_\alpha}\bar{q}_1 S\bar{c} \tag{3.146}$$

The derivative C_{m_α} is found from Eqn (3.144) by multiplying by the non-dimensional moment arm of the horizontal tail, $(\bar{x}_{ac_h} - \bar{x}_{cg})$ and accounting for the fact that up-lift on the horizontal tail produces a nose-down pitching moment. This yields:

$$C_{m_\alpha} = -2C_{L_{\alpha_h}}\eta_h\bar{V}_h(\bar{x}_{ac_h} - \bar{x}_{cg})\frac{d\epsilon}{d\alpha} \tag{3.147}$$

Figure 3.58 shows how C_{m_α} varies with Mach number for several airplanes.

3.2.5 AERODYNAMIC FORCE AND MOMENT DERIVATIVES WITH RESPECT TO PITCH RATE

According to Table 3.6 the following forces and moment are affected by changes in pitch rate, q: F_{A_x}, F_{A_z} and M_A. These quantities were non-dimensionalized in Eqns (3.100).

Figure 3.59 shows that the effect of a pitch rate perturbation about the airplane center of gravity is to create 'slewing' velocities at all lifting surfaces. These slewing velocities induce local changes in angle of attack which in turn create lift changes on all lifting surfaces. These lift changes in turn cause increments in induced drag and in pitching moment. It is generally assumed that the pitch rate effect on induced drag is negligible. The effect of pitch rate on lift is not always negligible. The effect of pitch rate on pitching moment is nearly always very important as will be seen in the following derivation for a conventional airplane (wing + tail aft).

Methods for determining pitch rate derivatives for an arbitrary airplane configuration are presented in Part VI of Ref.3.1.

Partial Differentiation of Equation (3.100a) with respect to $(q\bar{c}/2U_1)$

Partial differentiation of Eqn (3.100a) with respect to $(q\bar{c}/2U_1)$, leads to:

$$\frac{\partial F_{A_x}}{\partial(\frac{q\bar{c}}{2U_1})} = C_{x_q}\bar{q}S = -C_{D_q}\bar{q}S = 0 \tag{3.148}$$

where it is assumed that the effect of pitch rate on drag can be neglected: $C_{D_q} \approx 0$.

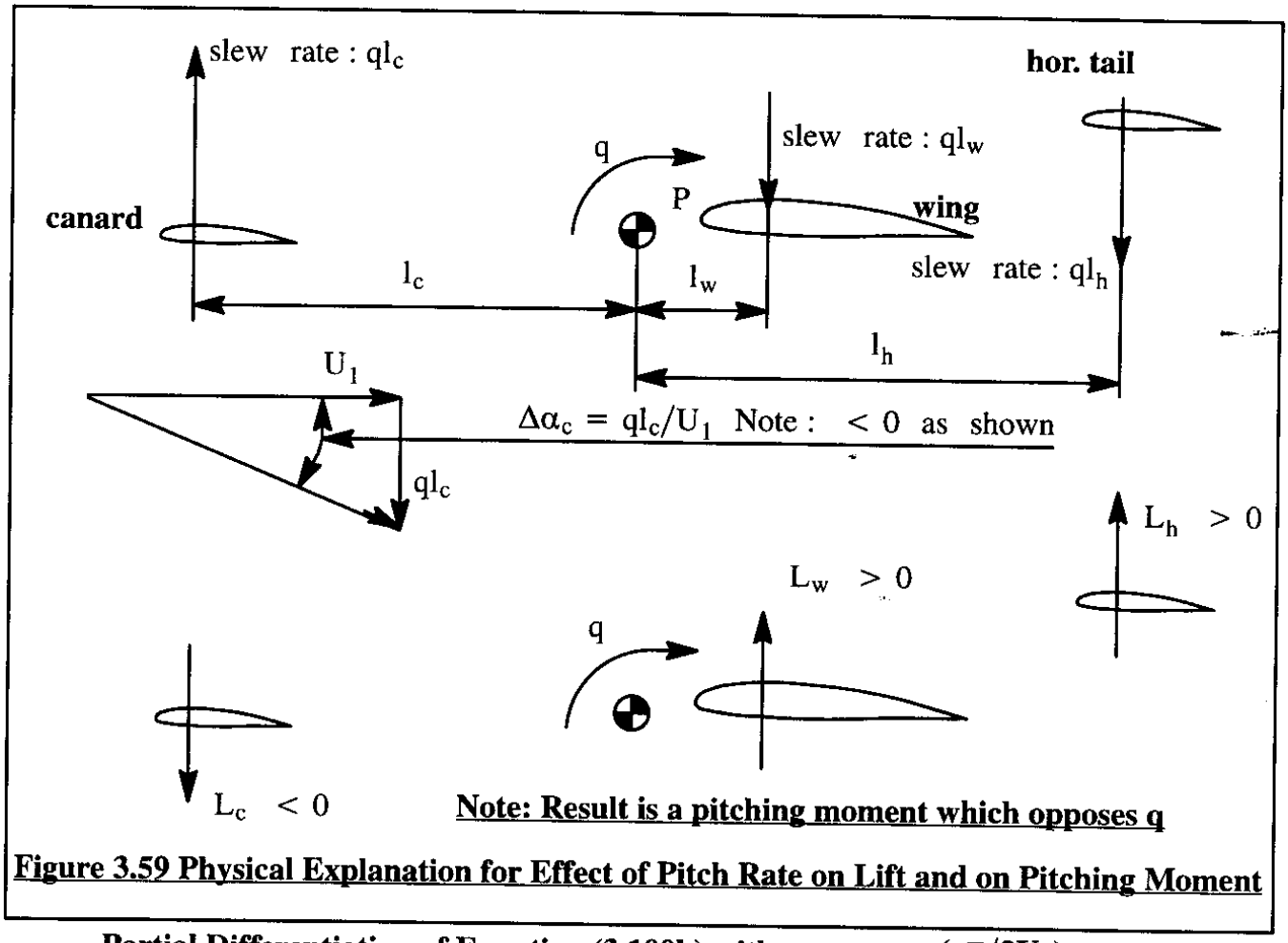

Figure 3.59 Physical Explanation for Effect of Pitch Rate on Lift and on Pitching Moment

Partial Differentiation of Equation (3.100b) with respect to $(q\bar{c}/2U_1)$

Partial differentiation of Eqn (3.100b) with respect to $(q\bar{c}/2U_1)$, leads to:

$$\frac{\partial F_{A_z}}{\partial(\frac{q\bar{c}}{2U_1})} = \frac{\partial C_z}{\partial(\frac{q\bar{c}}{2U_1})}\bar{q}_1 S = C_{z_q}\bar{q}_1 S \tag{3.149}$$

Since:

$$C_{z_q} = -C_{L_q} \tag{3.150}$$

It is seen in Figure 3.59 that pitch rate, q, induces an angle of attack at the canard. Although not shown in Figure 3.59, there is also an induced angle of attack at the horizontal tail:

$$\Delta\alpha_h = \frac{ql_h}{U_1} \tag{3.151}$$

This induced angle of attack at the horizontal tail results in the following induced lift coefficient for the airplane:

$$\left(\Delta C_{L_{\text{airplane, caused by q}}}\right) = C_{L_{\alpha_h}}\frac{ql_h}{U_1}\eta_h\frac{S_h}{S} \tag{3.152}$$

After partial differentiation with respect to $(q\bar{c}/2U_1)$, it follows:

$$C_{L_q} = 2C_{L_{\alpha_h}} \frac{l_h}{\bar{c}} \eta_h \frac{S_h}{S} \tag{3.153}$$

For conventional (i.e. no canard) airplanes, it is found that the center of gravity is located close to the wing aerodynamic center. In that case, there is no canard contribution, the wing contribution is negligible because of its small slew rate BUT, the horizontal tail contribution is important because of its significant moment arm. For such cases it is acceptable to write:

$$l_h = (x_{ac_h} - x_{cg}) \tag{3.154}$$

The consequence of this for conventional airplanes is:

$$\frac{\partial F_{A_z}}{\partial(\frac{q\bar{c}}{2U_1})} = -C_{L_q}\bar{q}_1 S = -2C_{L_{\alpha_h}}\eta_h \overline{V}_h \bar{q}_1 S \tag{3.155}$$

Figure 3.60 shows trends of C_{L_q} with Mach number for several airplanes.

Partial Differentiation of Equation (3.100c) with respect to $(q\bar{c}/2U_1)$

Partial differentiation of Eqn (3.100c) with respect to $(q\bar{c}/2U_1)$ leads to:

$$\frac{\partial M_A}{\partial(\frac{q\bar{c}}{2U_1})} = \frac{\partial C_m}{\partial(\frac{q\bar{c}}{2U_1})}\bar{q}_1 S = C_{m_q}\bar{q}_1 S \tag{3.156}$$

By using reasoning similar to what lead to Eqn (3.147), the reader is asked to show that:

$$C_{m_q} = -2C_{L_{\alpha_h}}\eta_h \overline{V}_h(\bar{x}_{ac_h} - \bar{x}_{cg}) \tag{3.157}$$

Since in many conventional airplanes the wing contribution to C_{m_q} is not entirely negligible, a 'fudge–factor' is often used to produce for the entire airplane (conventional only!):

$$C_{m_q} = -2.2C_{L_{\alpha_h}}\eta_h \overline{V}_h(\bar{x}_{ac_h} - \bar{x}_{cg}) \tag{3.158}$$

It should be observed that the derivative, C_{m_q}, is proportional to the square of the moment arm of the horizontal tail. This is why this derivative is often rather large. The derivative, C_{m_q} is referred to as the pitch–damping derivative. It is very important to the flying qualities of an airplane. Figure 3.61 shows trends of C_{m_q} with Mach number for several airplanes.

3.2.6 AERODYNAMIC FORCE AND MOMENT DERIVATIVES WITH RESPECT TO LONGITUDINAL CONTROL SURFACE AND FLAP DEFLECTIONS

According to Table 3.6 the following forces and moments are affected by changes in control surface and flap deflections, δ_e and δ_f : F_{A_x}, F_{A_z} and M_A. These forces and moment were non–dimensionalized in Eqns (3.100).

Partial differentiation of F_{A_x}, F_{A_z} and M_A with respect to δ_e and δ_f leads to the following expressions:

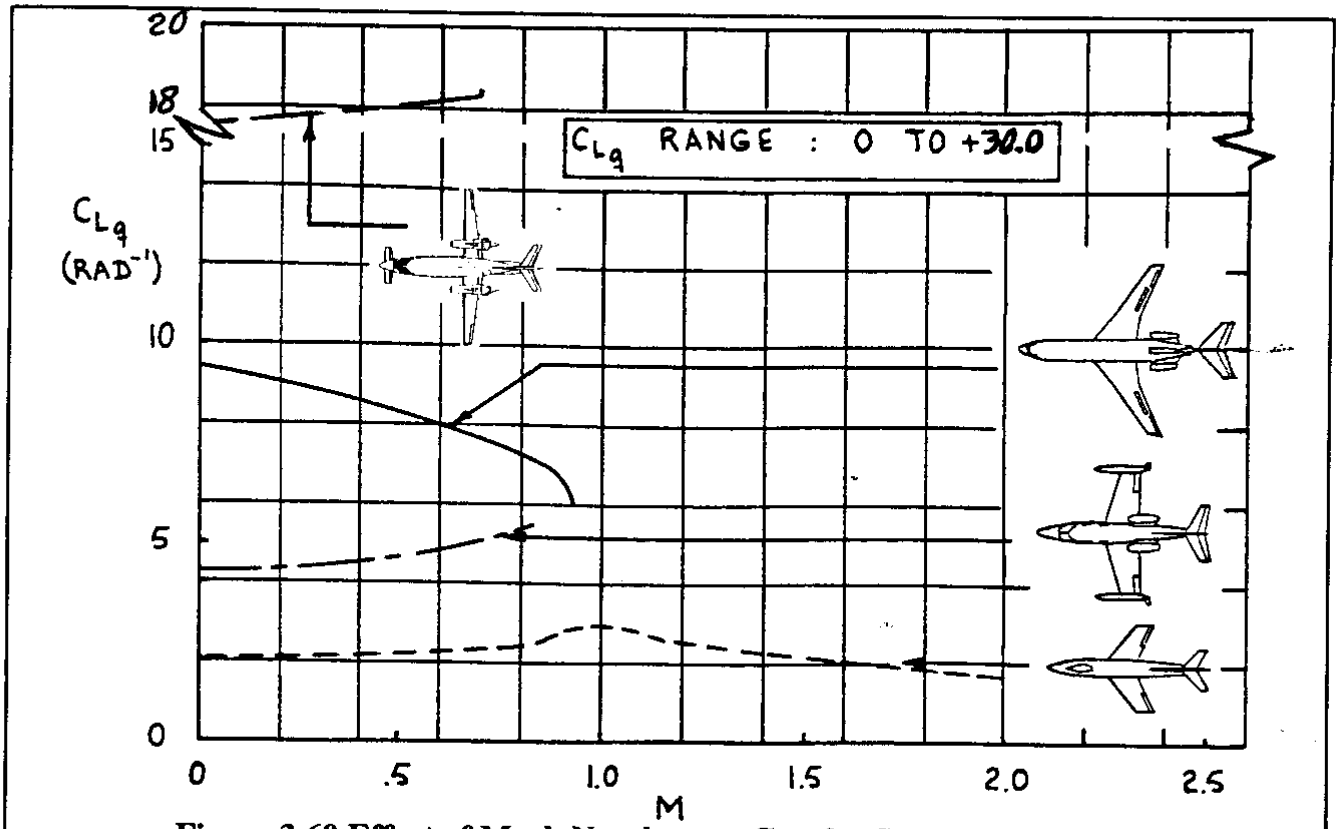

Figure 3.60 Effect of Mach Number on C_{L_q} for Several Airplanes

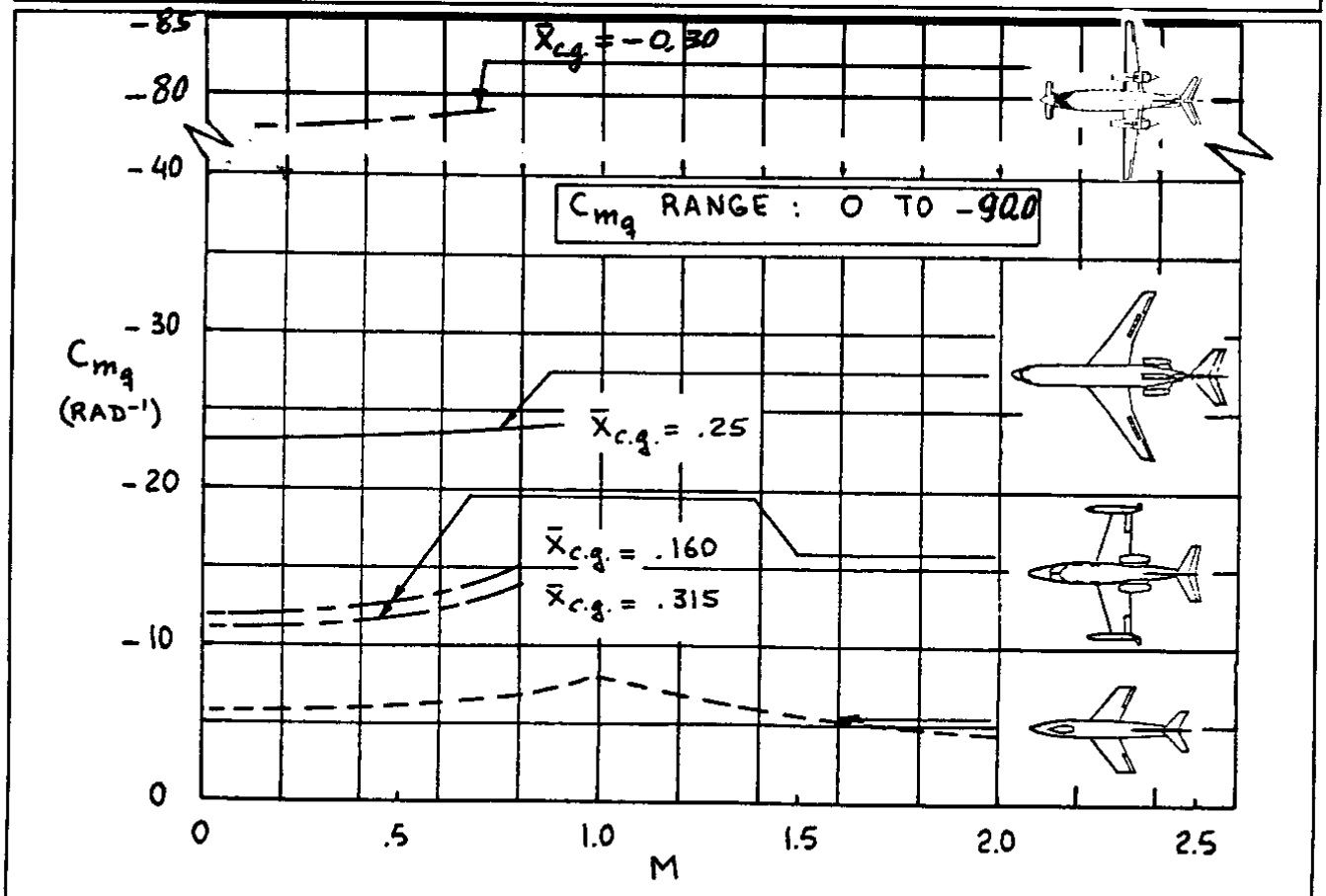

Figure 3.61 Effect of Mach Number on C_{m_q} for Several Airplanes

$$\frac{\partial F_{A_x}}{\partial \delta} = \frac{\partial C_x}{\partial \delta}\bar{q}_1 S = C_{x_\delta}\bar{q}_1 S = -C_{D_\delta}\bar{q}_1 S \tag{3.159}$$

$$\frac{\partial F_{A_z}}{\partial \delta} = \frac{\partial C_z}{\partial \delta}\bar{q}_1 S = C_{z_\delta}\bar{q}_1 S = -C_{L_\delta}\bar{q}_1 S \tag{3.160}$$

$$\frac{\partial M_A}{\partial \delta} = \frac{\partial C_m}{\partial \delta}\bar{q}_1 S\bar{c} = C_{m_\delta}\bar{q}_1 S\bar{c} \tag{3.161}$$

The subscripts used to indicate the control surface type were dropped from Eqns (3.159) through (3.161). Expressions for the elevator and stabilizer control surface derivatives were derived in Sub–sections 3.1.2, 3.1.3 and 3.1.4. For more general control surface derivatives and for flap derivatives the reader may wish to consult Part VI of Ref.3.1.

3.2.7 ASSEMBLING THE PERTURBED LONGITUDINAL AERODYNAMIC FORCES AND MOMENTS

At this point the perturbed, longitudinal aerodynamic forces and moment are assembled in matrix format in Table 3.7.

Table 3.7 Matrix Format for Perturbed State Longitudinal Aerodynamic Forces and Moment

$$\begin{Bmatrix} \frac{f_{A_x}}{\bar{q}_1 S} \\ \frac{f_{A_z}}{\bar{q}_1 S} \\ \frac{m_A}{\bar{q}_1 S\bar{c}} \end{Bmatrix} = \begin{bmatrix} (3.106) & (3.128) & (3.138) & (3.148) & (3.6) \\ -(C_{D_u} + 2C_{L_1}) & (-C_{D_\alpha} + C_{L_1}) & -C_{D_{\dot\alpha}} & -C_{D_q} \approx 0 & -C_{D_{\delta_e}} \\ (3.114) & (3.132) & (3.144) & (3.153) & (3.26) \\ -(C_{L_u} + 2C_{L_1}) & (-C_{L_\alpha} - C_{D_1}) & -C_{L_{\dot\alpha}} & -C_{L_q} & -C_{L_{\delta_e}} \\ (3.122) & (3.134) & (3.147) & (3.158) & (3.37) \\ (C_{m_u} + 2C_{m_1}) & C_{m_\alpha} & C_{m_{\dot\alpha}} & C_{m_q} & C_{m_{\delta_e}} \end{bmatrix} \begin{Bmatrix} \frac{u}{U_1} \\ \alpha \\ \frac{\dot\alpha\bar{c}}{2U_1} \\ \frac{q\bar{c}}{2U_1} \\ \delta_e \end{Bmatrix} \tag{3.162}$$

Notes: 1) Airplanes may have more than one longitudinal control surface. Only the elevator have been included in Eqn (3.162). Additional control surfaces simply expand the size of the matrices.
2) Bracketed numbers refer to equations in the text.
3) All stability derivatives may be computed with the methods of Part VI of Ref.3.1 and/or with the AAA program (Appendix A)

3.2.8 PERTURBED STATE, LATERAL–DIRECTIONAL, AERODYNAMIC FORCES AND MOMENTS

The perturbed state, lateral–directional, aerodynamic forces and moments are defined in Table 3.6 , Eqns (3.99) in their dimensionless form. It is seen that the partial derivatives of the lateral–directional force and moments with respect to dimensionless motion and control variables play the key role. The purpose of Sub–sections 3.2.9 through 3.2.14 is to show how these force and moment derivatives may be determined with the help of various stability and control derivatives.

3.2.9 AERODYNAMIC FORCE AND MOMENT DERIVATIVES WITH RESPECT TO SIDESLIP

According to Table 3.6 the following force and moments are affected by changes in sideslip angle, β: F_{A_y} , L_A and N_A. These force and moments are non–dimensionalized as follows:

$$F_{A_y} = - C_y \bar{q} S \tag{3.163a}$$

$$L_A = - C_l \bar{q} S b \tag{3.163b}$$

$$N_A = - C_n \bar{q} S b \tag{3.163c}$$

The reader is reminded of the fact that F_{A_y} , L_A and N_A are defined in the stability axis system. Next, the partial differentiations implied by Table 3.6 will be systematically performed for Equations (3.163a) through (3.163c). Partial differentiation of Eqns (3.163) with respect to sideslip angle, β, leads to the following expressions:

$$\frac{\partial F_{A_y}}{\partial \beta} = \frac{\partial C_y}{\partial \beta} \bar{q}_1 S = C_{y_\beta} \bar{q}_1 S \tag{3.164}$$

$$\frac{\partial L_A}{\partial \beta} = \frac{\partial C_l}{\partial \beta} \bar{q}_1 S b = C_{l_\beta} \bar{q}_1 S b \tag{3.165}$$

$$\frac{\partial N_A}{\partial \beta} = \frac{\partial C_n}{\partial \beta} \bar{q}_1 S b = C_{n_\beta} \bar{q}_1 S b \tag{3.166}$$

The stability derivatives C_{y_β}, C_{l_β} and C_{n_β} were already discussed in Sub–sections 3.1.9, 3.1.8 and 3.1.10 respectively.

3.2.10 AERODYNAMIC FORCE AND MOMENT DERIVATIVES WITH RESPECT TO SIDESLIP RATE

According to Table 3.6 the following force and moments are affected by changes in sideslip, β: F_{A_y} , L_A and N_A. These force and moments were non–dimensionalized in Eqns (3.163).

Partial differentiation of Eqns (3.163) with respect to sideslip angle, β, leads to the following expressions:

$$\frac{\partial F_{A_y}}{\partial(\frac{\dot{\beta}b}{2U_1})} = \frac{\partial C_y}{\partial(\frac{\dot{\beta}b}{2U_1})}\bar{q}_1 S = C_{y_{\dot{\beta}}}\bar{q}_1 S \tag{3.167}$$

$$\frac{\partial L_A}{\partial(\frac{\dot{\beta}b}{2U_1})} = \frac{\partial C_l}{\partial(\frac{\dot{\beta}b}{2U_1})}\bar{q}_1 Sb = C_{l_{\dot{\beta}}}\bar{q}_1 Sb \tag{3.168}$$

$$\frac{\partial N_A}{\partial(\frac{\dot{\beta}b}{2U_1})} = \frac{\partial C_n}{\partial(\frac{\dot{\beta}b}{2U_1})}\bar{q}_1 Sb = C_{n_{\dot{\beta}}}\bar{q}_1 Sb \tag{3.169}$$

The stability derivatives $C_{y_{\dot{\beta}}}$, $C_{l_{\dot{\beta}}}$ and $C_{n_{\dot{\beta}}}$ are physically analogous to the $\dot{\alpha}$ – derivatives which were discussed in Sub–section 3.2.4. Methods for numerically predicting these $\dot{\beta}$ – derivatives are given in Part VI of Reference 3.1. Except for airplanes in the high subsonic speed range, the $\dot{\beta}$ – derivatives are frequently considered negligible.

3.2.11 AERODYNAMIC FORCE AND MOMENT DERIVATIVES WITH RESPECT TO ROLL RATE

According to Table 3.6 the following force and moments are affected by changes in perturbed roll rate, p: F_{A_y}, L_A and N_A. These force and moments were non–dimensionalized in Eqns (3.163).

Partial differentiation of Eqns (3.163) with respect to roll rate, p, leads to the following expressions:

$$\frac{\partial F_{A_y}}{\partial(\frac{pb}{2U_1})} = \frac{\partial C_y}{\partial(\frac{pb}{2U_1})}\bar{q}_1 S = C_{y_p}\bar{q}_1 S \tag{3.170}$$

$$\frac{\partial L_A}{\partial(\frac{pb}{2U_1})} = \frac{\partial C_l}{\partial(\frac{pb}{2U_1})}\bar{q}_1 Sb = C_{l_p}\bar{q}_1 Sb \tag{3.171}$$

$$\frac{\partial N_A}{\partial(\frac{pb}{2U_1})} = \frac{\partial C_n}{\partial(\frac{pb}{2U_1})}\bar{q}_1 Sb = C_{n_p}\bar{q}_1 Sb \tag{3.172}$$

A physical explanation for how the roll–rate derivatives C_{y_p}, C_{l_p} and C_{n_p} occur is presented in the following.

Side–force coefficient due to roll rate derivative, C_{y_p}

This derivative is usually made up of two components:

$$C_{y_p} = C_{y_{p_{wfh}}} + C_{y_{p_v}} \tag{3.173}$$

The contribution due to the wing–fuselage–horizontal tail, $C_{y_{p_{wfh}}}$, is generally negligible for conventional configurations, particularly when compared to the contribution due to the vertical tail, $C_{y_{p_v}}$. A physical explanation for the aerodynamic mechanism responsible for $C_{y_{p_v}}$ is presented in Figure 3.62. It is seen that due to roll rate p, about the stability X–axis, a force $F_{y_{p_v}}$ is induced on the vertical tail in the negative Y–direction. Note that this force acts at a point, a distance z_{v_s} away from the X–stability axis. That point is assumed to be the vertical tail aerodynamic center due to the additional pressure distribution caused by the roll rate, p. In principle, this distance z_{v_s} is not the same as the distance of the same name–tag in Figure 3.31. However, this difference is usually ignored. Assuming z_{v_s} is known, the local angle of attack due to roll rate induced on the vertical tail is: $\Delta\alpha_v = pz_{v_s}/U_1$. Therefore, the side force on the vertical tail may be modelled as:

$$F_{y_{p_v}} = C_{L_{\alpha_v}}\left(\frac{pz_{v_s}}{U_1}\right)\bar{q}_v S_v \tag{3.174}$$

The side–force due to roll rate on the entire airplane can be written as:

$$F_{y_p} = C_y \bar{q} S = -C_{L_{\alpha_v}}\left(\frac{pz_{v_s}}{U_1}\right)\bar{q}_v S_v \tag{3.175}$$

From this, by partial differentiation w.r.t. $\frac{pb}{2U_1}$ it follows that:

$$C_{y_p} \approx C_{y_{p_v}} = -2C_{L_{\alpha_v}}\left(\frac{z_{v_s}}{b}\right)\eta_v\left(\frac{S_v}{S}\right) \tag{3.176}$$

Although Eqn (3.176) suggests that the sign of C_{y_p} is generally negative, it is evident from Figure 3.62 that the sign of the moment arm, z_{v_s} can reverse at high angles of attack. Figure 3.63 shows examples of the variation of C_{y_p} with Mach number for several airplanes.

The derivative C_{y_p} is normally not a very important derivative in terms of its effect on airplane dynamic stability. However, in the synthesis of turn–coordination modes in auto–pilots, this derivative should not be neglected.

Rolling moment coefficient due to roll rate derivative, C_{l_p}

This derivative is usually made up of three components:

$$C_{l_p} = C_{l_{p_{wf}}} + C_{l_{p_h}} + C_{l_{p_v}} \tag{3.177}$$

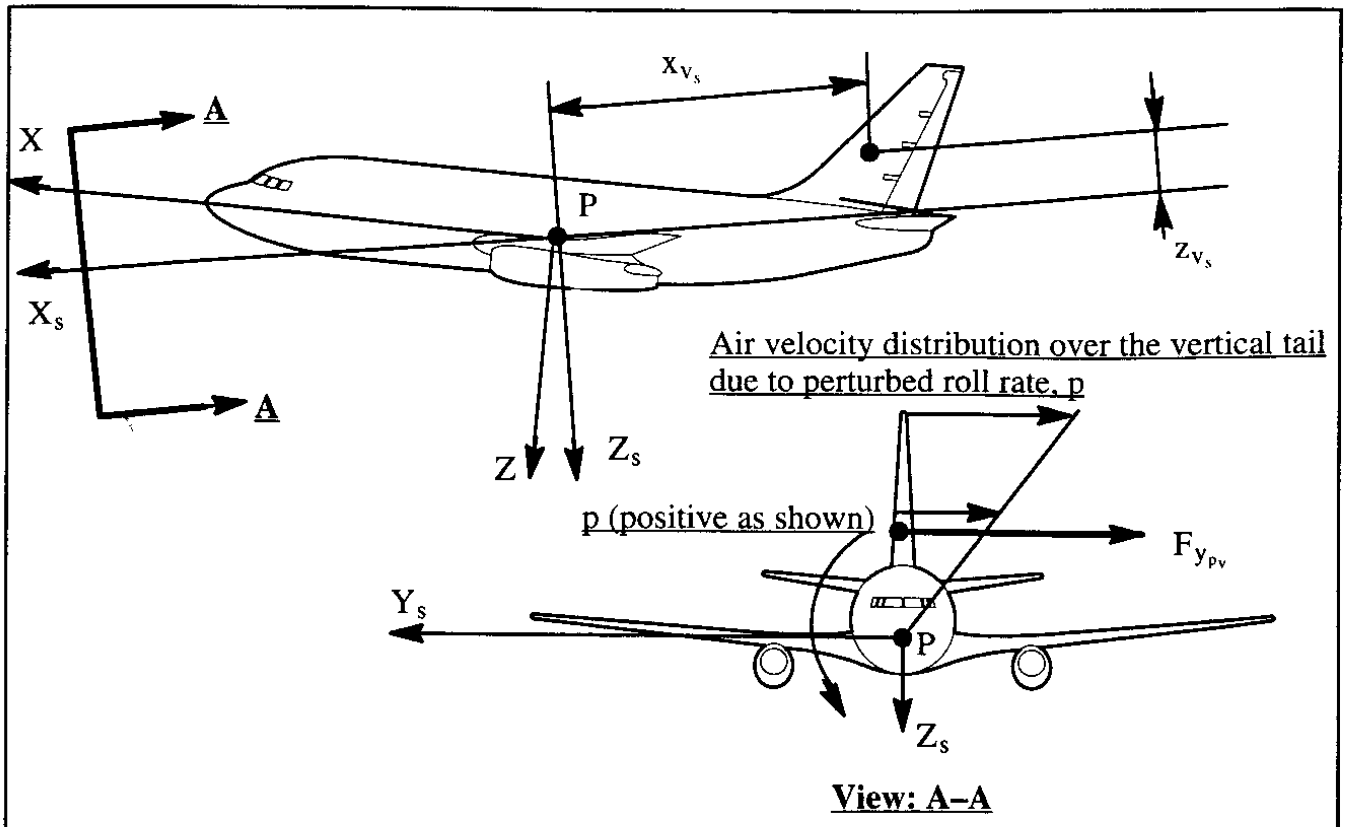

Figure 3.62 Physical Explanation for Side Force due to Roll Rate

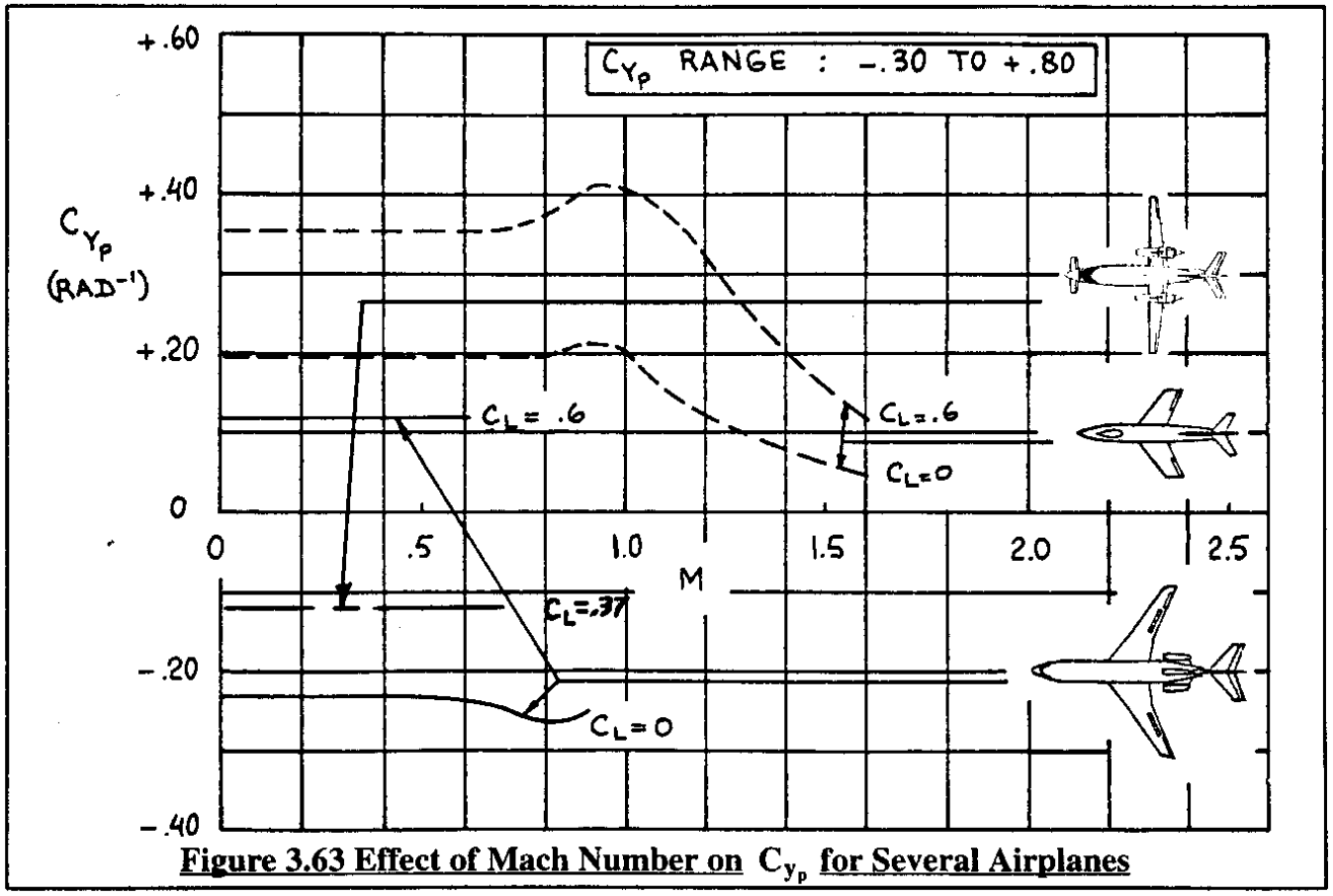

Figure 3.63 Effect of Mach Number on C_{y_p} for Several Airplanes

A physical explanation for the principal aerodynamic mechanism which is responsible for $C_{l_{p_{wf}}}$ and $C_{l_{p_h}}$ is provided in Figure 3.64. It is seen that, as long as the flow remains attached, the effect of perturbed roll rate, p, is to create an asymmetrical lift distribution which opposes the roll rate. That is why the derivative C_{l_p} is referred to as the roll–damping derivative.

The roll damping derivative, C_{l_p}, plays a very important role in determining the handling qualities of an airplane, as will be seen in Chapter 5.

Methods for computing the $C_{l_{p_{wf}}}$ and $C_{l_{p_h}}$ contributions to C_{l_p} are given in Part VI of Reference 3.1. From these methods it is clear that aspect ratio and sweep angle of the wing and the horizontal tail are the dominating factors which determine roll damping. From these methods it is also clear that unless the ratio of fuselage–width–to–wing–span is larger than about 0.3 the following approximation applies:

$$C_{l_{p_w}} \approx C_{l_{p_{wf}}} \tag{3.178}$$

To estimate the effect of the horizontal tail, it is treated as if it is a wing. The resulting value of the horizontal tail damping derivative, based on the geometry of the horizontal tail is referred to as $\overline{C}_{l_{p_h}}$. The value of $C_{l_{p_h}}$ based on airplane geometry is then obtained from:

$$C_{l_{p_h}} = \overline{C}_{l_{p_h}} \frac{S_h b_h^2}{S b^2} \tag{3.179}$$

An expression for $C_{l_{p_v}}$ can be found with the help of Eqn (3.176). The reader is asked to show that:

$$C_{l_{p_v}} = -2C_{L_{\alpha_v}} \left(\frac{z_{v_s}}{b}\right)^2 \eta_v \left(\frac{S_v}{S}\right) \tag{3.180}$$

Figure 3.65 shows examples of how C_{l_p} varies with Mach number for several airplanes.

Yawing moment coefficient due to roll rate derivative, C_{n_p}

This derivative is normally made up of two components:

$$C_{n_p} = C_{n_{p_{wf}}} + C_{n_{p_v}} \tag{3.181}$$

The horizontal tail contribution tends to be insignificant for conventional airplanes with tails which are small compared to the wing. The wing–fuselage contribution is normally dominated by the wing and is caused by three mechanisms:

1) wing drag increase 2) wing lift vector tilting 3) wing tip suction

A physical explanation for these three effects follows.

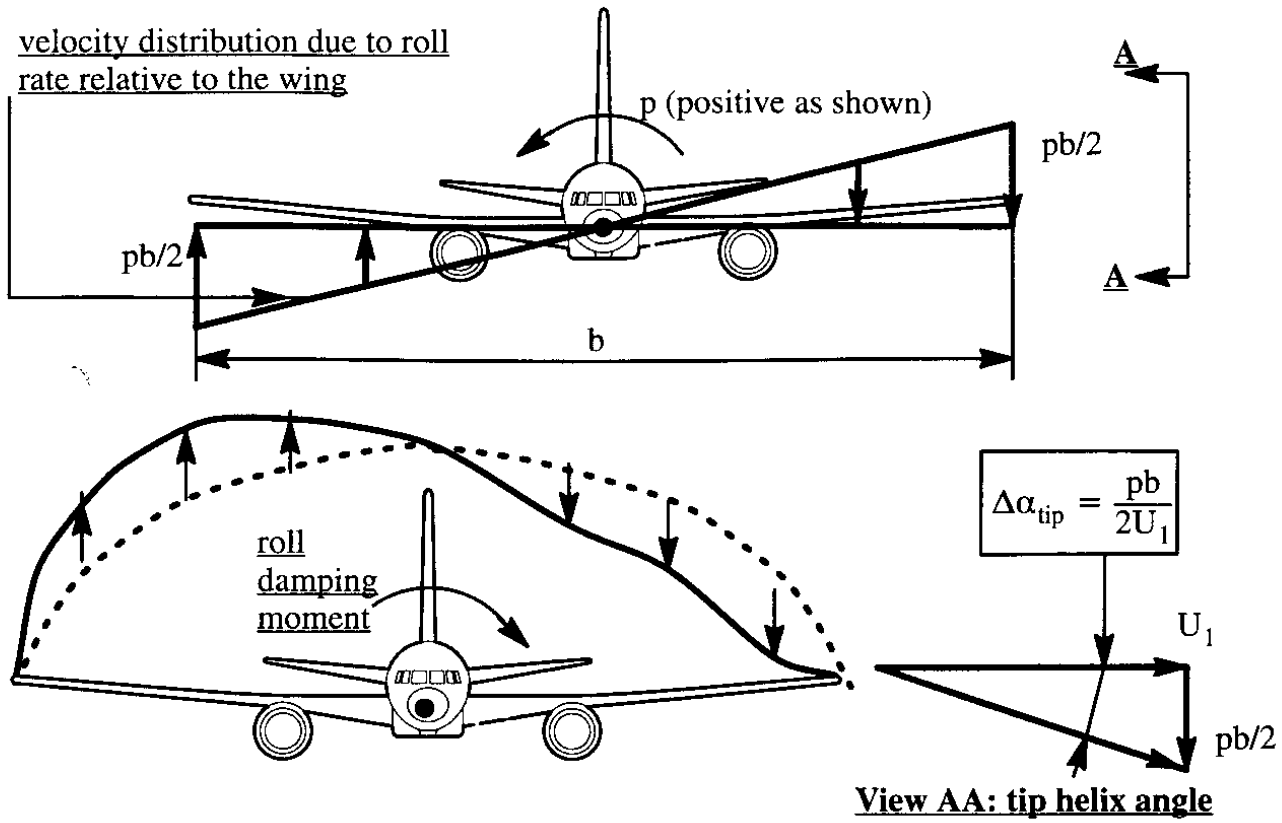

Figure 3.64 Physical Explanation for Rolling Moment due to Roll Rate

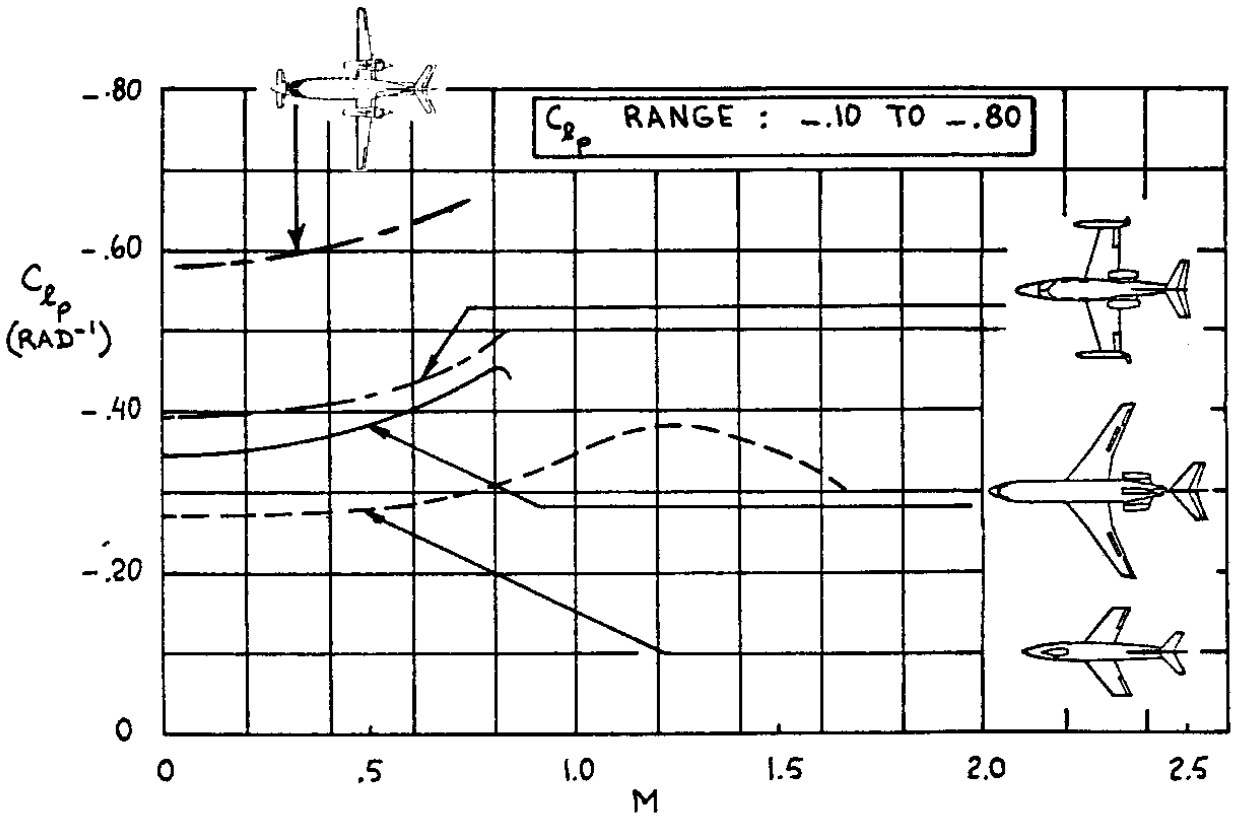

Figure 3.65 Effect of Mach Number on C_{l_p} for Several Airplanes

1) wing drag increase

Figure 3.66 shows that as a result of the rolling motion of the wing the local angles of attack over the wing span are altered. For a positive roll rate (right wing down) the right wing experiences an increase in local angle of attack while the left wing experiences a similar decrease in local angle of attack. Figure 3.66 illustrates this for spanwise stations +y and –y. These angle of attack changes are seen to produce changes in local lift and drag. It is seen that the effect of the increase in drag at spanwise stations +/– y is to generate a positive increment in the yawing moment due to roll rate.

2) wing lift vector tilting

It is seen from Figure 3.66 that the changes in lift produced by roll rate at spanwise stations +/– y result in a 'tilting' of the total local lift vectors in such a way as to produce a negative yawing moment due to roll rate.

3) wing tip suction

The wing tip suction effect is illustrated in Figure 3.67. It is seen that if a wing is carrying no net lift, there is no net side force due to roll rate. However, as soon as a wing carries a certain amount of lift, the addition of a positive roll rate causes a net positive side force due to the effect of wing–tip suction. Clearly the magnitude of this tip suction effect is a function of the wing geometry. Low aspect ratio wings with relatively large tip thickness tend to develop fairly significant net suction forces due to roll rate. It all depends on where the center of this tip suction force is located relative to the airplane center of gravity as to how much yawing moment due to roll rate this effect will produce. The insert in Figure 3.67 shows that if the airplane c.g. is forward of this tip suction center, a negative yawing moment contribution due to roll rate is produced.

The vertical tail contribution to C_{n_p} is referred to as $C_{n_{p_v}}$. Its effect is most easily seen by referring back to Figure 3.62. The side force on the vertical tail is seen to produce a yawing moment which tends to be positive at low to moderate angles of attack. The vertical tail contribution can be estimated through the use of Eqn (3.180) to produce:

$$C_{n_{p_v}} = 2C_{L_{\alpha_v}}\left(\frac{z_{v_s}}{b}\right)\left(\frac{x_{v_s}}{b}\right)\eta_v\left(\frac{S_v}{S}\right) \tag{3.182}$$

Methods for estimating all contributions to C_{n_p} are given in Part VI of Reference 3.1. It turns out that the correct prediction of even the sign of this contribution is difficult. It will be shown in Chapter 5 that the effect of the derivative C_{n_p} on airplane dynamic stability is frequently rather weak. If such is the case, it may not matter whether or not the sign of C_{n_p} is properly predicted. In cases where the airplane is shown to be sensitive to sign and magnitude of C_{n_p}, it is usually necessary to run 'roll–rate–model–tests' in the windtunnel.

Figure 3.68 shows examples of how C_{n_p} varies with Mach number for several airplanes.

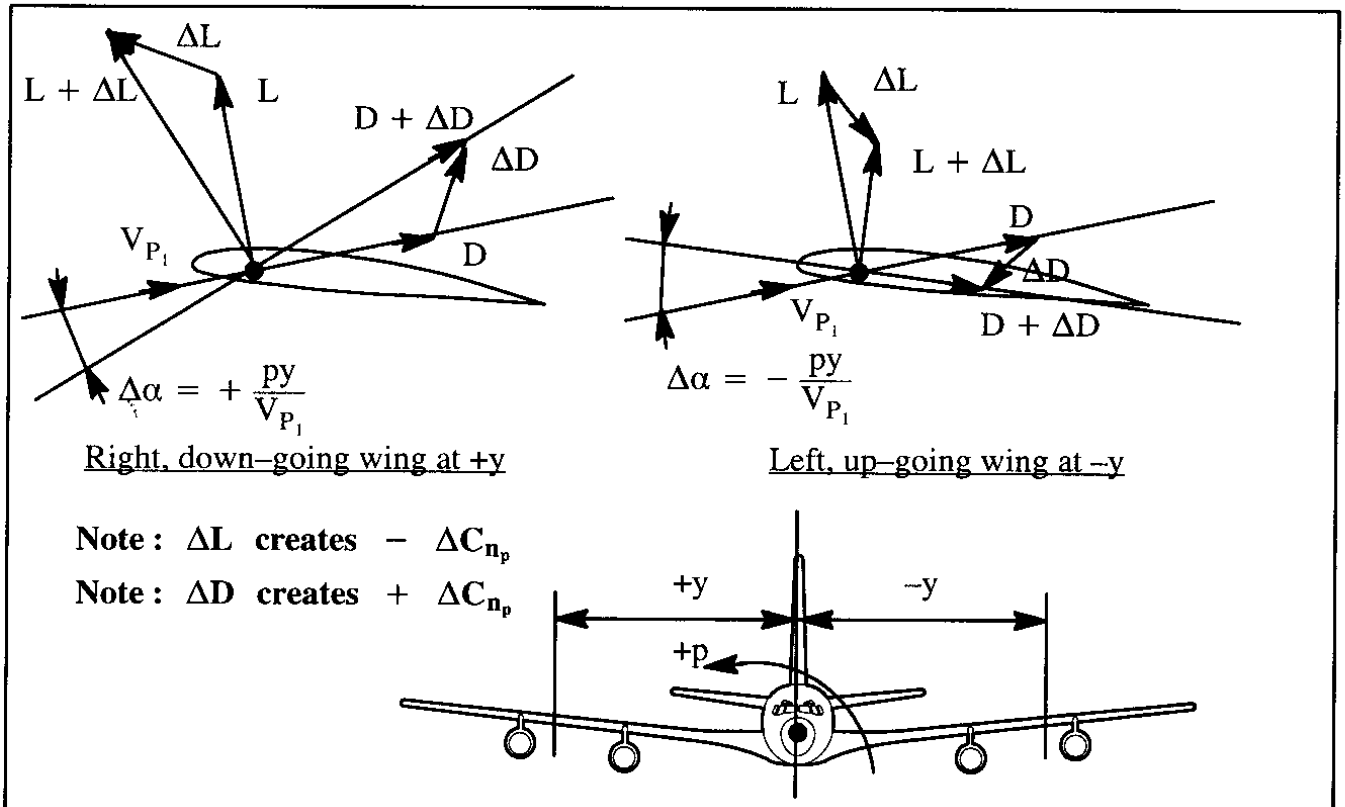

Figure 3.66 Explanation of Lift and Drag Vector Tilting on $C_{n_{p_{wf}}}$

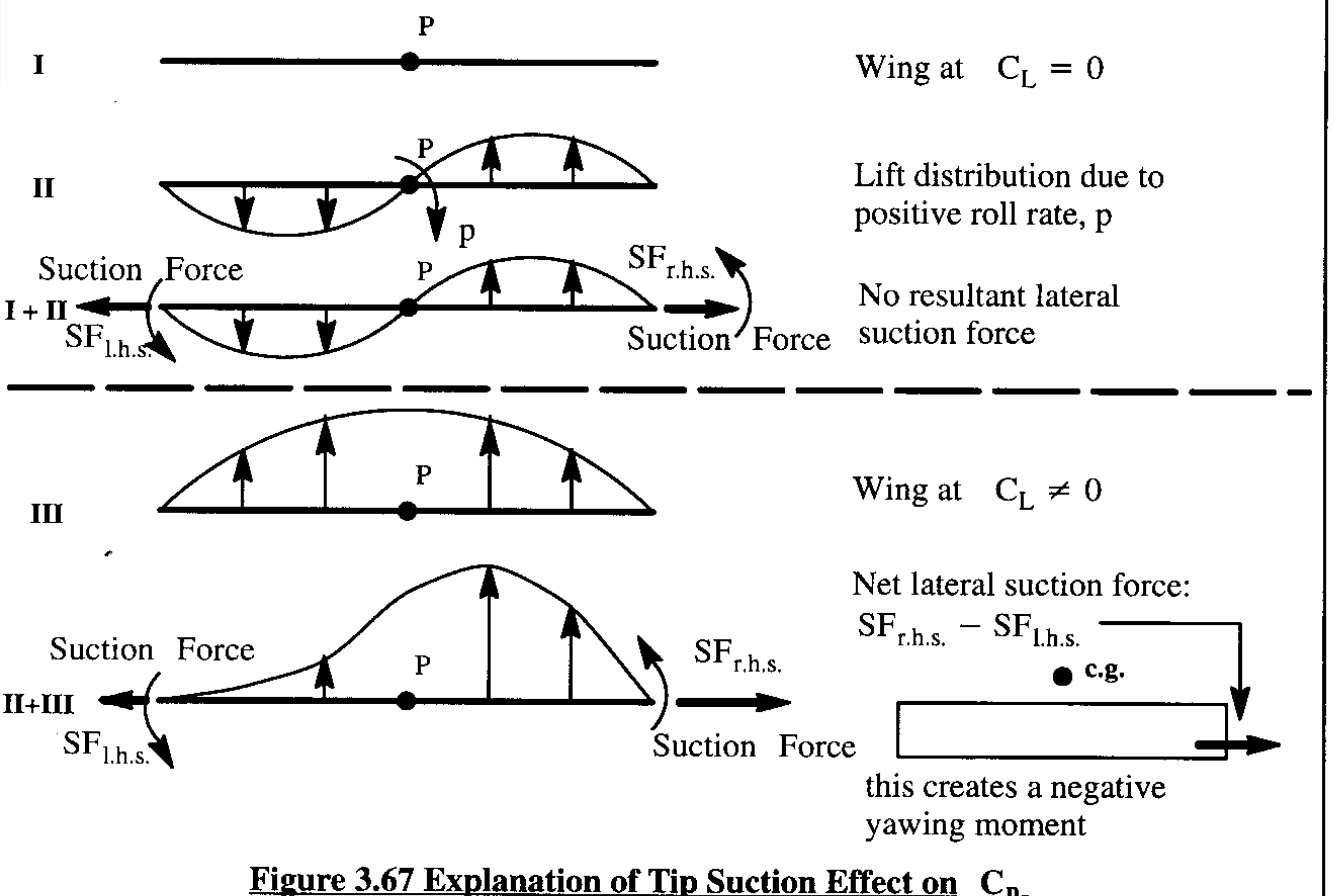

Figure 3.67 Explanation of Tip Suction Effect on $C_{n_{p_{wf}}}$

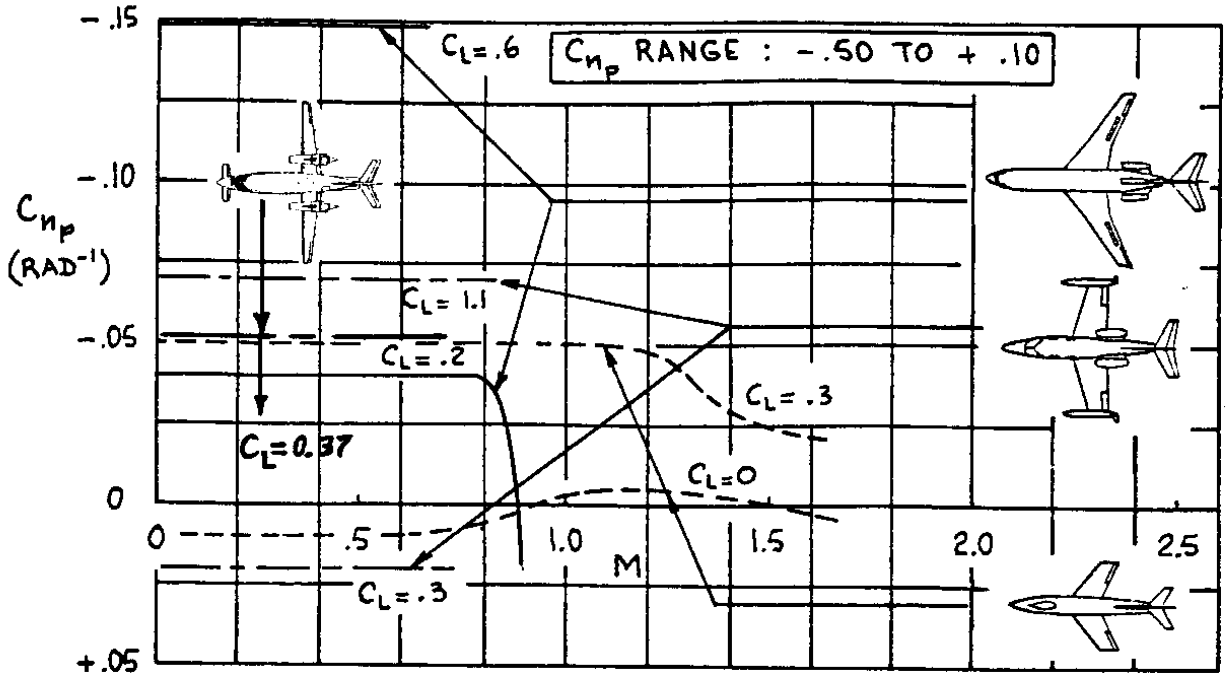

Figure 3.68 Effect of Mach Number on C_{n_p} for Several Airplanes

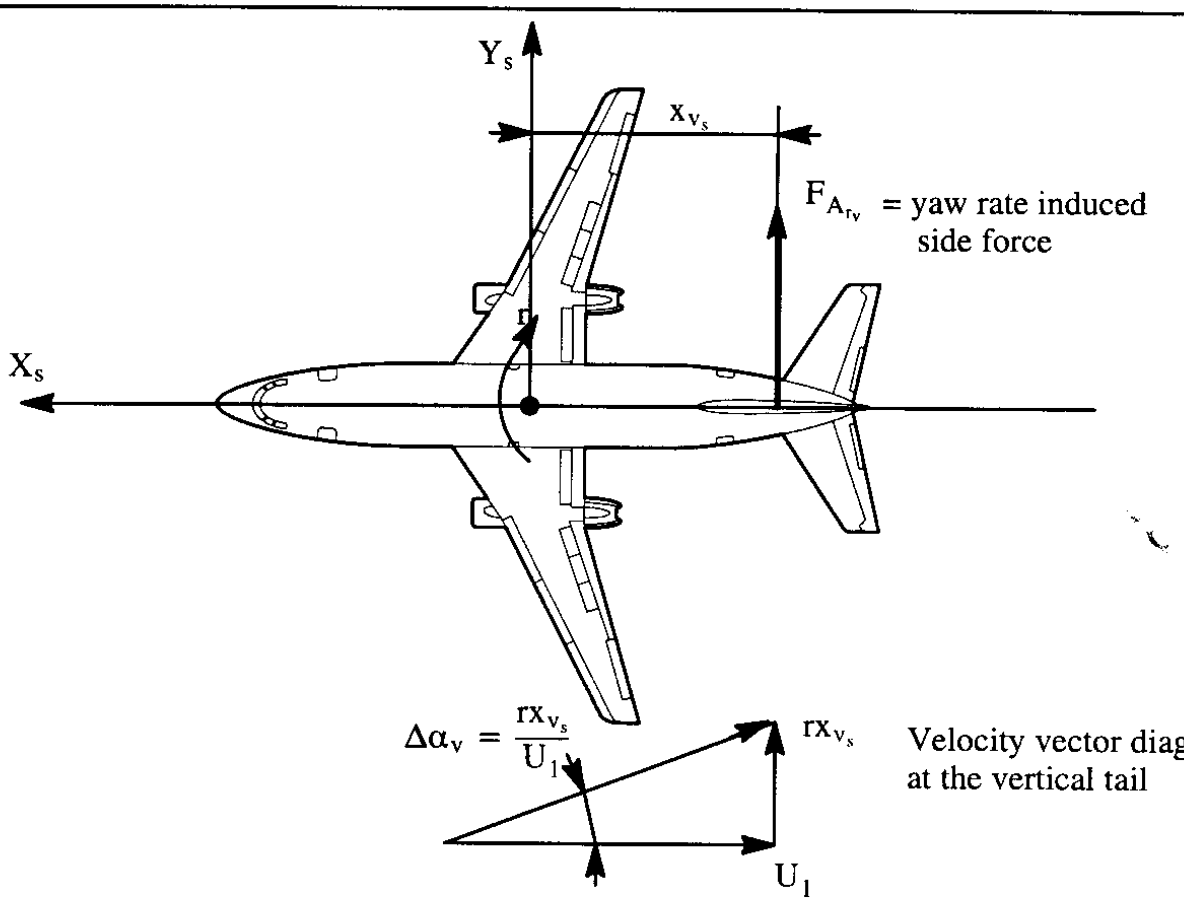

Figure 3.69 Explanation of Side Force due to Yaw Rate

3.2.12 AERODYNAMIC FORCE AND MOMENT DERIVATIVES WITH RESPECT TO YAW RATE

According to Table 3.6 the following force and moments are affected by changes in perturbed yaw rate, r: F_{A_y} , L_A and N_A . These force and moments were non-dimensionalized in Eqns (3.163). Partial differentiation of Eqns (3.163) with respect to yaw rate, r, leads to the following expressions:

$$\frac{\partial F_{A_y}}{\partial(\frac{rb}{2U_1})} = \frac{\partial C_y}{\partial(\frac{rb}{2U_1})}\bar{q}_1 S = C_{y_r}\bar{q}_1 S \tag{3.183}$$

$$\frac{\partial L_A}{\partial(\frac{rb}{2U_1})} = \frac{\partial C_l}{\partial(\frac{rb}{2U_1})}\bar{q}_1 Sb = C_{l_r}\bar{q}_1 Sb \tag{3.184}$$

$$\frac{\partial N_A}{\partial(\frac{rb}{2U_1})} = \frac{\partial C_n}{\partial(\frac{rb}{2U_1})}\bar{q}_1 Sb = C_{n_r}\bar{q}_1 Sb \tag{3.185}$$

A physical explanation for how the yaw-rate derivatives C_{y_r} , C_{l_r} and C_{n_r} occur is presented in the following.

Side-force coefficient due to yaw rate derivative, C_{y_r}

This derivative is usually made up of two components:

$$C_{y_r} = C_{y_{r_{wfh}}} + C_{y_{r_v}} \tag{3.186}$$

The contribution due to the wing-fuselage-horizontal tail, $C_{y_{r_{wfh}}}$, is generally negligible for conventional configurations, particularly when compared to the contribution due to the vertical tail, $C_{y_{r_v}}$. A physical explanation for the aerodynamic mechanism responsible for $C_{y_{r_v}}$ is presented in Figure 3.69. It is seen that the effect of yaw rate is to induce an angle of attack at the vertical tail which gives rise to the following side force:

$$F_{A_{y_v}} = C_{L_{\alpha_v}}(\frac{rx_{v_s}}{U_1})\bar{q}_v S_v \tag{3.187}$$

In this expression, the side-wash due to yaw rate has been neglected. In terms of total airplane side force it is also possible to write:

$$F_{A_{y_v}} = C_{y_v}\bar{q}S \tag{3.188}$$

By differentiating the coefficient C_{y_v} with respect to $rb/2U_1$ it is possible to show:

$$C_{y_r} \approx C_{y_{r_v}} = C_{L_{\alpha_v}}(\frac{2x_{v_s}}{b})\eta_v(\frac{S_v}{S}) \tag{3.189}$$

Examples of the trend of C_{y_r} with Mach number are given in Figure 3.70.

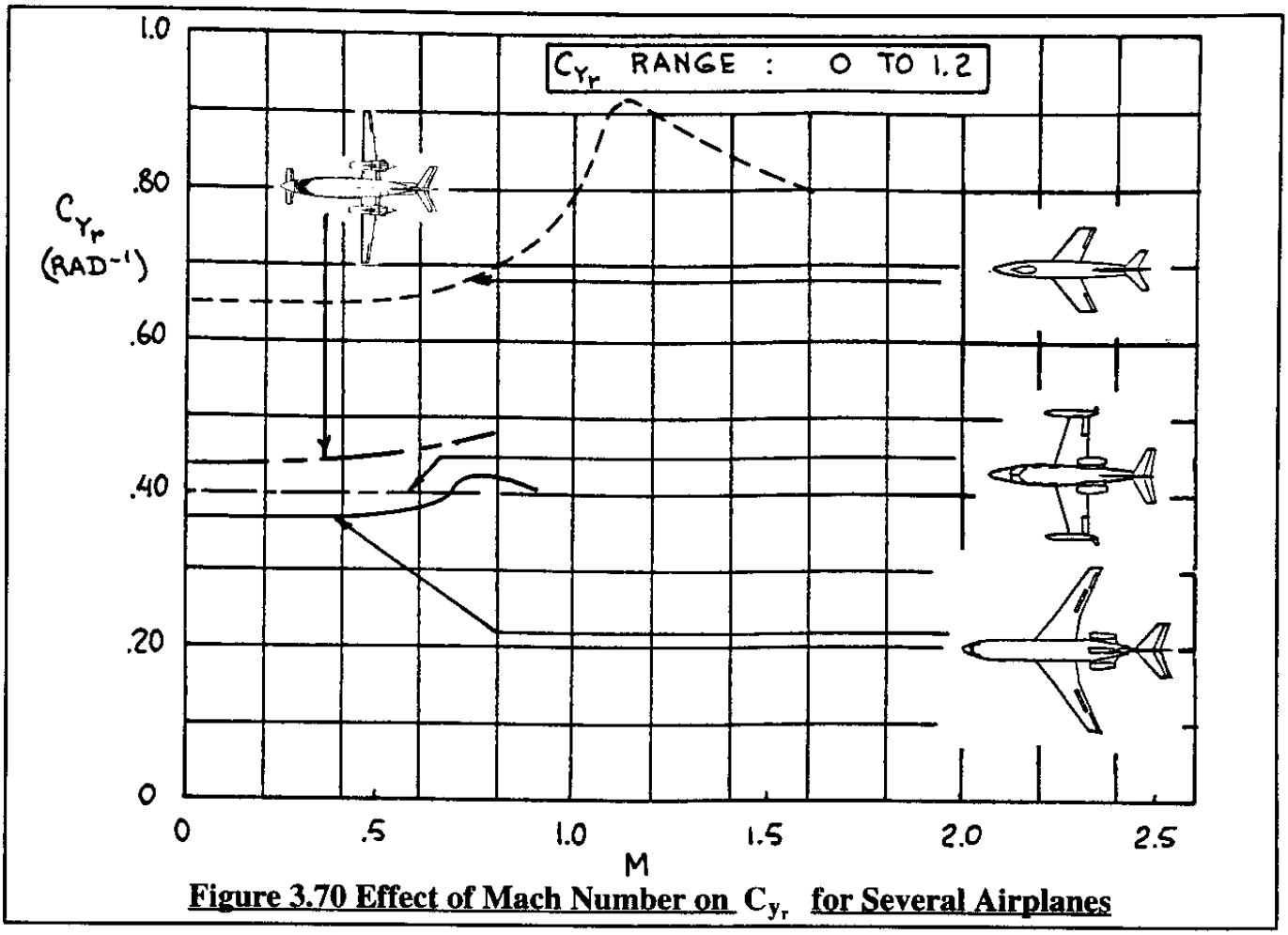

Figure 3.70 Effect of Mach Number on C_{y_r} for Several Airplanes

Rolling moment coefficient due to yaw rate derivative, C_{l_r}

This derivative is generally made up of the following contributions:

$$C_{l_r} = C_{l_{r_{wf}}} + C_{l_{r_h}} + C_{l_{r_v}} \tag{3.190}$$

The contribution of the horizontal tail is frequently neglected. Figure 3.71 contains the physical explanation for the occurrence of the wing–fuselage contribution, $C_{l_{r_{wf}}}$, and the vertical tail contribution, $C_{l_{r_v}}$. Methods for estimating the numerical magnitude of $C_{l_{r_{wf}}}$ are presented in Part VI of Reference 3.1. The reader is asked to show that the vertical tail contribution can be expressed as:

$$C_{l_{r_v}} = C_{L_{\alpha_v}}\left(\frac{2x_{v_s}z_{v_s}}{b^2}\right)\eta_v\frac{S_v}{S} \tag{3.191}$$

Observe that, depending on the magnitude of the airplane steady state angle of attack, α_1, the sign of $C_{l_{r_v}}$ can be either positive or negative. The wing–fuselage contribution, $C_{l_{r_{wf}}}$, is always

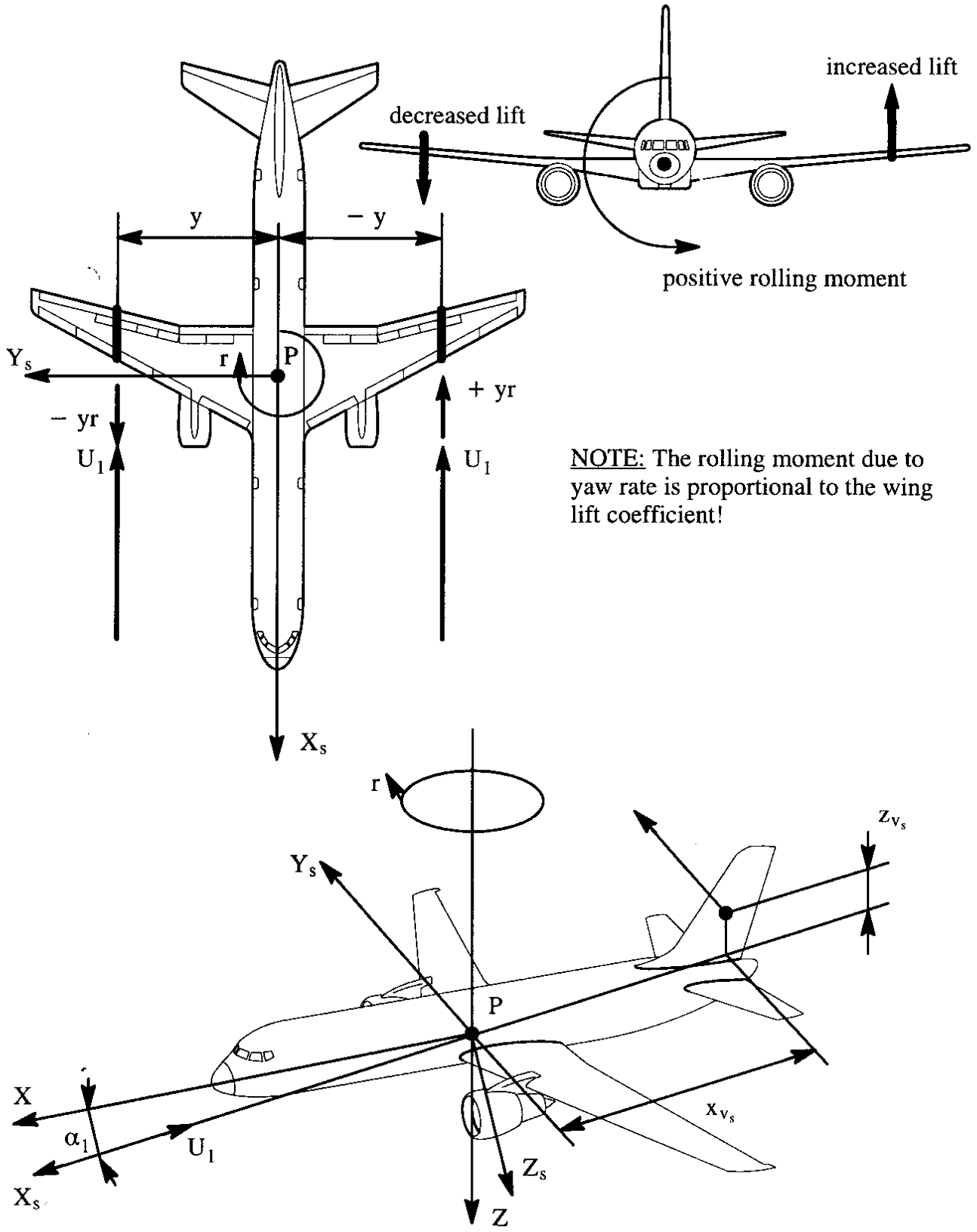

Figure 3.71 Physical Explanation for the Wing–Fuselage and Vertical Tail Contributions to Rolling moment due to Yaw Rate

positive for attached flow situations and normally outweighs the magnitude of the vertical tail contribution. This makes the derivative C_{l_r} usually positive. Figure 3.72 presents examples of how C_{l_r} varies with Mach number for several airplanes.

Yawing moment coefficient due to yaw rate derivative, C_{n_r}

This derivative is generally made up of the following contributions:

$$C_{n_r} = C_{n_{r_{wf}}} + C_{n_{r_v}} \tag{3.192}$$

For most airplanes, the contribution of the horizontal tail to the derivative C_{n_r} is quite negligible. The wing–fuselage contribution, $C_{n_{r_{wf}}}$, is dominated by the change in induced drag as a result of the differential velocity distribution induced by yaw rate. This may be seen from Figure 3.71. Methods for computing the wing–fuselage contribution may be found in Part VI of Reference 3.1.

Figure 3.71 also illustrates how the vertical tail contributes to C_{n_r}. It turns out, that for most airplanes this contribution is very important, mostly because of the fact that it is proportional to the square of the moment arm of the vertical tail. The reader is asked to show that:

$$C_{n_{r_v}} = -C_{L_{\alpha_v}}\left(\frac{2x_{v_s}^2}{b^2}\right)\eta_v\frac{S_v}{S} \tag{3.193}$$

The yaw damping derivative, C_{n_r} has an important effect on airplane flying qualities. Figure 3.73 shows examples of how C_{n_r} varies with Mach number for several airplanes.

3.2.13 AERODYNAMIC FORCE AND MOMENT DERIVATIVES WITH RESPECT TO LATERAL–DIRECTIONAL CONTROL SURFACE DEFLECTIONS

According to Table 3.6 the following force and moments are affected by changes in aileron and rudder deflections: F_{A_y}, L_A and N_A. These force and moments were non–dimensionalized in Eqns (3.163). Partial differentiation of Eqns (3.163) with respect to any lateral–directional control surface deflection, δ, leads to the following expressions:

$$\frac{\partial F_{A_y}}{\partial \delta} = \frac{\partial C_y}{\partial \delta}\bar{q}_1 S = C_{y_\delta}\bar{q}_1 S \tag{3.194}$$

$$\frac{\partial L_A}{\partial \delta} = \frac{\partial C_l}{\partial \delta}\bar{q}_1 Sb = C_{l_\delta}\bar{q}_1 Sb \tag{3.195}$$

$$\frac{\partial N_A}{\partial \delta} = \frac{\partial C_n}{\partial \delta}\bar{q}_1 Sb = C_{n_\delta}\bar{q}_1 Sb \tag{3.196}$$

The subscripts used to indicate which particular control surface type is used were dropped from Equations (3.194) – (3.196). A discussion of the various lateral–directional control surface derivatives is presented in Sub–sections 3.1.8 through 3.1.10.

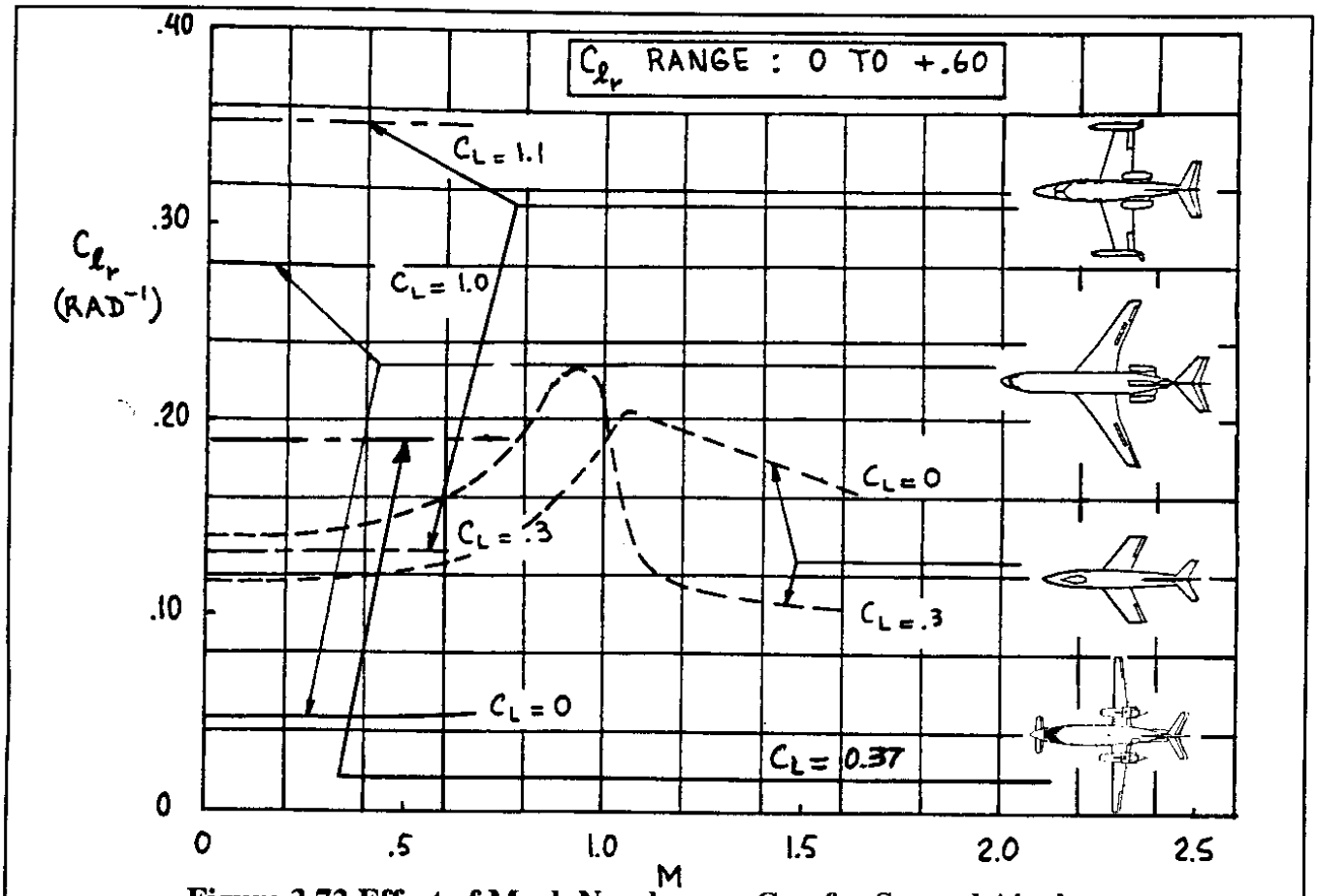

Figure 3.72 Effect of Mach Number on C_{l_r} for Several Airplanes

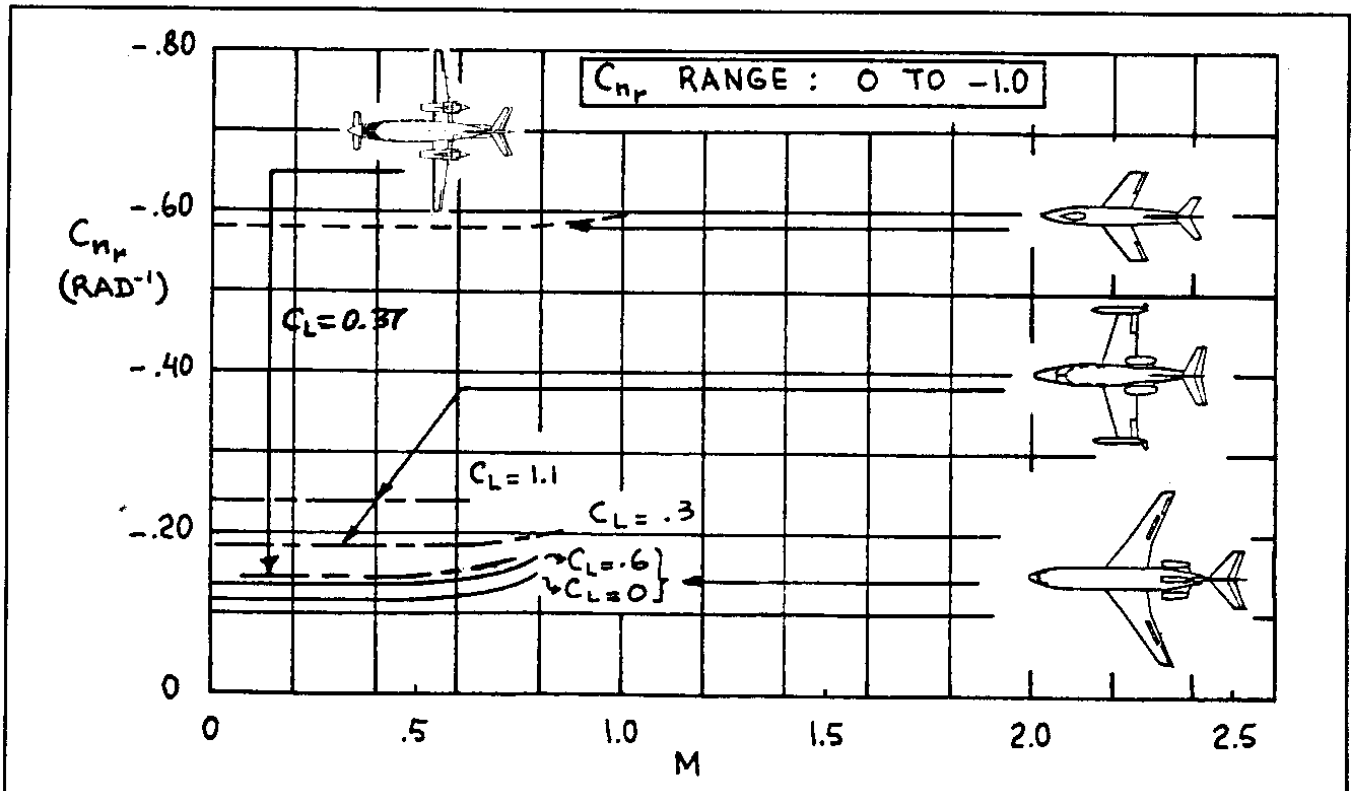

Figure 3.73 Effect of Mach Number on C_{n_r} for Several Airplanes

3.2.14 ASSEMBLING THE PERTURBED LATERAL–DIRECTIONAL AERODYNAMIC FORCES AND MOMENTS

At this point the perturbed, lateral–directional aerodynamic force and moments are assembled in matrix format in Table 3.8. This is the format used in the discussion of the perturbed equations of motion in Chapter 5.

Table 3.8 Matrix Format for Perturbed State Lateral–Directional Aerodynamic Force and Moments

$$\begin{Bmatrix} \frac{f_{A_y}}{\bar{q}_1 S} \\ \frac{l_A}{\bar{q}_1 Sb} \\ \frac{n_A}{\bar{q}_1 Sb} \end{Bmatrix} = \begin{bmatrix} (3.75) & (3.167) & (3.173) & (3.186) & (3.1.8) & (3.1.8) \\ C_{y_\beta} & C_{y_{\dot\beta}} & C_{y_p} & C_{y_r} & C_{y_{\delta_a}} & C_{y_{\delta_r}} \\ (3.52) & (3.168) & (3.177) & (3.190) & (3.1.8) & (3.1.8) \\ C_{l_\beta} & C_{l_{\dot\beta}} & C_{l_p} & C_{l_r} & C_{l_{\delta_a}} & C_{l_{\delta_r}} \\ (3.84) & (3.169) & (3.181) & (3.192) & (3.1.8) & (3.1.8) \\ C_{n_\beta} & C_{n_{\dot\beta}} & C_{n_p} & C_{n_r} & C_{n_{\delta_a}} & C_{n_{\delta_r}} \end{bmatrix} \begin{Bmatrix} \beta \\ \frac{\dot\beta b}{2U_1} \\ \frac{pb}{2U_1} \\ \frac{rb}{2U_1} \\ \delta_a \\ \delta_r \end{Bmatrix} \tag{3.197}$$

Notes: 1) Airplanes may have more than one lateral–directional control surface.
Only the aileron and rudder have been included in Eqn (3.197).
For additional control surfaces simply expand the size of the matrices.
2) Bracketed numbers refer to equations and/or sections in the text.
3) All stability derivatives may be computed with the methods of Part VI of Ref. 3.1 and/or with the AAA program (Appendix A)

3.2.15 PERTURBED STATE LONGITUDINAL AND LATERAL–DIRECTIONAL THRUST FORCES AND MOMENTS

It is possible to make a case for the existence of perturbed thrust forces and moments as functions of all perturbed motion variables: u, v, w, p, q and r. As it turns out, for most airplanes only the variables u, v and w have significant effects on the perturbed thrust forces and moments. The reader is cautioned however, not to take this for granted for all future configurations!

The consequence of assuming that only the perturbed motion variables u, v and w have significant effects on the perturbed thrust forces and moments is the mathematical model given in Equations (3.198) through (3.203):

$$f_{T_x} = \frac{\partial F_{T_x}}{\partial(\frac{u}{U_1})}(\frac{u}{U_1}) + \frac{\partial F_{T_x}}{\partial \alpha}\alpha \tag{3.198}$$

$$f_{T_z} = \frac{\partial F_{T_z}}{\partial(\frac{u}{U_1})}(\frac{u}{U_1}) + \frac{\partial F_{T_z}}{\partial \alpha}\alpha \tag{3.199}$$

$$m_T = \frac{\partial M_T}{\partial(\frac{u}{U_1})}(\frac{u}{U_1}) + \frac{\partial M_T}{\partial \alpha}\alpha \tag{3.200}$$

$$f_{T_y} = \frac{\partial F_{T_y}}{\partial \beta} \tag{3.201}$$

$$l_T = \frac{\partial L_T}{\partial \beta} \tag{3.202}$$

$$n_T = \frac{\partial N_T}{\partial \beta} \tag{3.203}$$

Detailed expressions for the perturbed thrust force and moment derivatives are developed in Sub–sections 3.2.16 through 3.2.18.

3.2.16 THRUST FORCE AND MOMENT DERIVATIVES WITH RESPECT TO FORWARD SPEED

Based on Sub–section 3.2.2 the perturbed longitudinal, thrust forces and moment are non–dimensionalized as follows:

$$F_{T_x} = C_{T_x}\bar{q}S \tag{3.204a}$$

$$F_{T_z} = C_{T_z}\bar{q}S \tag{3.204b}$$

$$M_T = C_{m_T}\bar{q}S\bar{c} \tag{3.204c}$$

The reader is reminded of the fact that F_{T_x} , F_{T_z} and M_T are defined in the stability axis system. Next, the partial differentiations implied by Equations (3.198) – (3.200) will be systematically performed for Equations (3.204a) – (3.204c).

Partial Differentiation of Equation (3.204a) with Respect to u/U_1

Partial differentiation of Equation (3.204a) with respect to u/U_1, leads to:

$$\frac{\partial F_{T_x}}{\partial(\frac{u}{U_1})} = \frac{\partial C_{T_x}}{\partial(\frac{u}{U_1})}\bar{q}S + C_{T_x}S\frac{\partial \bar{q}}{\partial(\frac{u}{U_1})} \tag{3.205}$$

Evaluation at the steady state, recalling Eqn (3.102) and using the following notation: $C_{T_{x_u}} = \frac{\partial C_{T_x}}{\partial(\frac{u}{U_1})}$, it can be shown that:

$$\frac{\partial F_{T_x}}{\partial(\frac{u}{U_1})} = C_{T_{x_u}} \bar{q}_1 S + 2C_{T_{x_1}} \bar{q}_1 S \tag{3.206}$$

The steady state thrust coefficient, $C_{T_{x_1}}$ is normally equal to the steady state drag coefficient because T=D in level steady state flight. The derivative $C_{T_{x_u}}$ depends on the characteristics of the propulsion system. Five cases will be considered:

Case 1: Gliders or power–off flight

Case 2: Airplanes equipped with rockets

Case 3: Airplanes equipped with pure jets and fan jets

Case 4: Airplanes equipped with variable pitch propellers

Case 5: Airplanes equipped with fixed pitch propellers

Case 1: Gliders or power–off flight

Since there is no thrust in this case: $C_{T_{x_u}} = C_{T_{x_1}} = 0$, so that:

$$\frac{\partial F_{T_x}}{\partial(\frac{u}{U_1})} = 0 \tag{3.207}$$

Case 2: Airplanes equipped with rockets

The installed thrust output of a rocket engine does **not** (to a first order approximation) depend on the flight speed: $C_{T_{x_u}} = 0$. Therefore:

$$\frac{\partial F_{T_x}}{\partial(\frac{u}{U_1})} = 2C_{T_{x_1}} \bar{q}_1 S \tag{3.208}$$

Case 3: Airplanes equipped with pure jets and fan jets

In this case it is necessary to establish the variation of installed thrust with Mach number, with altitude and with fuel flow (or throttle position). Methods for determining installed thrust from engine manufacturer's thrust data are found in Part VI of Reference 3.1.

Figure 3.74 shows an example of estimated installed thrust data for a small, single engine fan–jet trainer. The slope $\partial F_{T_x}/\partial M$ may be measured directly from graphs such as presented in Figure 3.74. Having done so, the following is obtained:

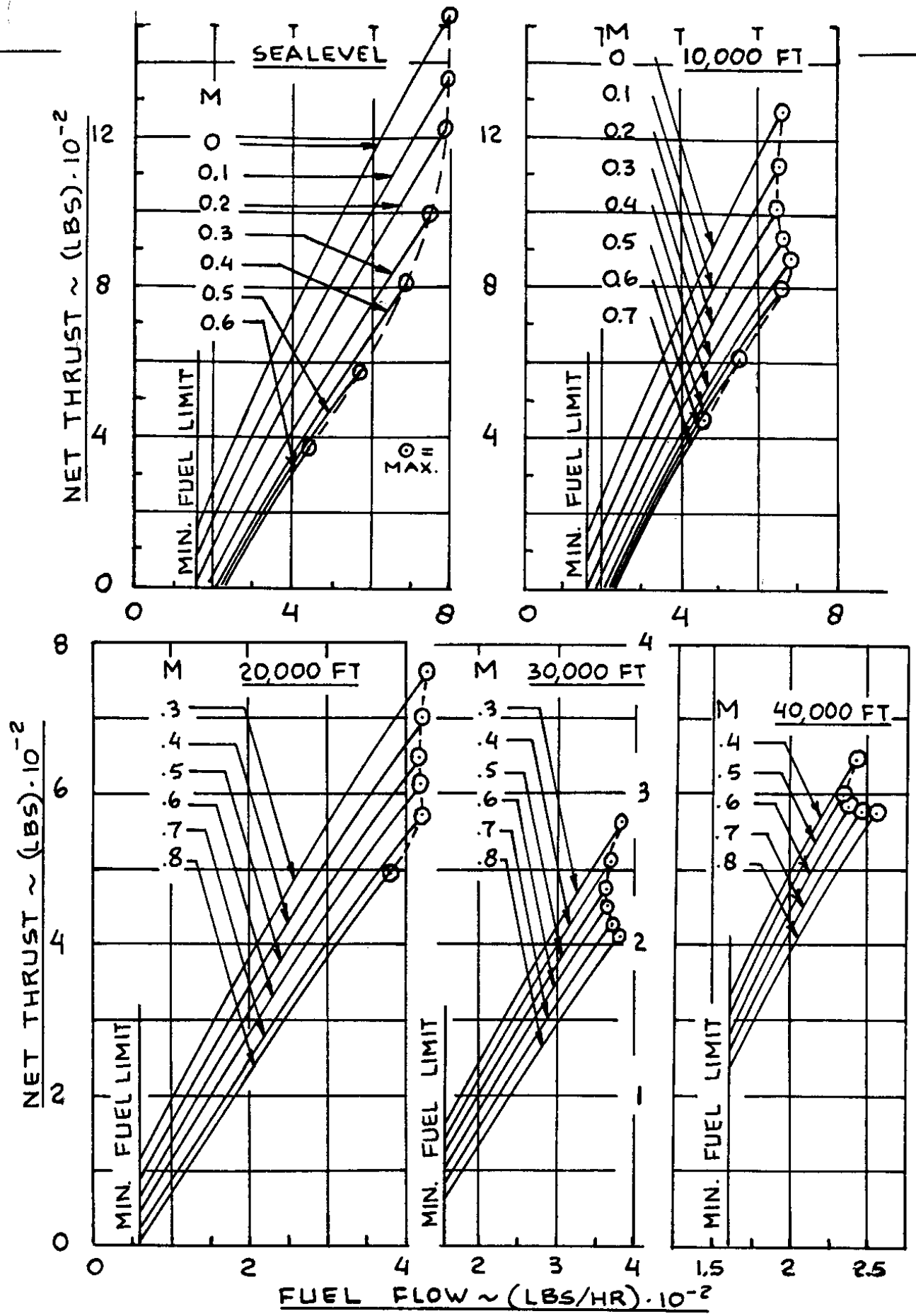

Figure 3.74 Example of Installed Thrust Versus Altitude, Mach Number and Fuel Flow

$$C_{T_{x_u}} = \frac{M_1}{\bar{q}_1 S}\frac{\partial F_{T_x}}{\partial M} - 2C_{T_{x_1}} \tag{3.209}$$

With Eqn (3.206) it is now found that:

$$\frac{\partial F_{T_x}}{\partial(\frac{u}{U_1})} = M_1 \frac{\partial F_{T_x}}{\partial M} \tag{3.210}$$

Case 4: Airplanes equipped with variable pitch propellers

It will be assumed that the thrust inclination angle, ϕ_T, is negligible, so that the thrust axis is aligned with the X–axis. It will also be assumed that for a variable pitch (= constant speed) propeller, the thrust–horsepower output is essentially constant with small changes in forward speed. Thus:

$$T(U_1 + u) \approx F_{T_x}(U_1 + u) \approx \text{constant} \tag{3.211}$$

Partial differentiation with respect to u/U_1 and evaluating the result at the steady state flight condition (u=0) yields:

$$\frac{\partial F_{T_x}}{\partial(\frac{u}{U_1})} = -F_{T_{x_1}} = -C_{T_{x_1}}\bar{q}_1 S \tag{3.212}$$

Comparison with Eqn (3.206) shows that in this case:

$$C_{T_{x_u}} = -3C_{T_{x_1}} \tag{3.213}$$

Case 5: Airplanes equipped with fixed pitch propellers

In general, only low cost, low performance airplanes are equipped with fixed pitch propellers. The following assumptions will be made:

1) In the steady state flight condition, the propeller is operating at a known rpm, n_{prpm} This is expressed as $n_{prps} = n_{rpm}/60$ rps (rotations per second).

2) A propeller performance diagram is available from which the variation of propeller efficiency, η_p, for a given propeller advance ratio, $J = U_1/(n_{prps}D_p)$, is known at constant propeller blade angle. Examples of such propeller performance diagrams are found in Reference 3.9 (pages 298–329).

3) The engine is operating at a constant brake–horsepower level, BHP, as set by the throttle.

Assuming that the airplane has n_p propellers, the following relation holds for the total installed thrust output for this case:

$$F_{T_x} = \frac{n_p 550 \eta_p BHP}{U_1} \tag{3.214}$$

Partial differentiation with respect to u/U_1 now yields after evaluating the result at the steady state flight condition:

$$\frac{\partial F_{T_x}}{\partial(\frac{u}{U_1})} = n_p[\frac{-550\eta_p(BHP)}{U_1} + 550(BHP)\frac{\partial \eta_p}{\partial u}] \tag{3.215}$$

The derivative $\partial\eta_p/\partial u$ can be expressed as follows,:

$$\frac{\partial \eta_p}{\partial u} = (\frac{\partial \eta_p}{\partial J})(\frac{\partial J}{\partial u}) \tag{3.216}$$

where: the propeller advance ratio, $J = U_1/(n_{prps}D_p)$, so that $\partial J/\partial u = 1/n_{prps}D_p$. Therefore it is found that:

$$\frac{\partial F_{T_x}}{\partial(\frac{u}{U_1})} = n_p[\frac{-550\eta_{p_1}(BHP)}{U_1} + \frac{550(BHP)}{n_{prps}D_p}\frac{\partial \eta_p}{\partial J}] \tag{3.217}$$

This can be rewritten as follows:

$$\frac{\partial F_{T_x}}{\partial(\frac{u}{U_1})} = -C_{T_{x_1}}\bar{q}_1 S + \frac{T_1 U_1}{\eta_{p_1} n_{prps} D_p}\frac{\partial \eta_p}{\partial J} \tag{3.218}$$

The derivative $\partial\eta_p/\partial J$ can be obtained from the propeller performance diagram mentioned before under 2). Comparison with Eqn (3.206) shows that:

$$C_{T_{x_u}} = -3C_{T_{x_1}} + \frac{C_{T_{x_1}} U_1}{\eta_{p_1} n_{prps} D_p}\frac{\partial \eta_p}{\partial J} \tag{3.219}$$

Partial Differentiation of Equation (3.204b) with Respect to u/U_1

Partial differentiation of Equation (3.204a) with respect to u/U_1 leads to:

$$\frac{\partial F_{T_z}}{\partial(\frac{u}{U_1})} = C_{T_{z_u}}\bar{q}_1 S + 2C_{T_{z_1}}\bar{q}_1 S \tag{3.220}$$

The derivative $C_{T_{z_u}}$ and the coefficient $C_{T_{z_1}}$ are negligible for most conventional airplane configurations. It should be kept in mind that for airplanes with vectorable thrust this is definitely not the case! For conventional airplanes it will be assumed that:

$$\frac{\partial F_{T_z}}{\partial(\frac{u}{U_1})} = 0 \tag{3.221}$$

Partial Differentiation of Equation (3.204c) with Respect to u/U_1

Partial differentiation of Eqn (3.204c) with respect to u/U_1 yields:

$$\frac{\partial M_T}{\partial(\frac{u}{U_1})} = C_{m_{T_u}}\bar{q}_1 S\bar{c} + 2C_{m_{T_1}}\bar{q}_1 S\bar{c} \tag{3.222}$$

For conventional propulsive arrangements the derivative $C_{m_{T_u}}$ is obtained from the derivative $C_{T_{x_u}}$ by multiplying with the non-dimensional moment arm of the thrust-line relative to the center of gravity, $d_T/\bar{c}$:

$$C_{m_{T_u}} = - C_{T_{x_u}} \frac{d_T}{\bar{c}} \tag{3.223}$$

where: d_T is defined in Figure 3.26. Note that d_T is counted as positive if the thrust-line is above the center of gravity.

The value of the steady state thrust-pitching moment coefficient, $C_{m_{T_1}}$, depends on the airplane trim state. For pitching moment equilibrium in the steady state flight condition, the following condition should be met:

$$C_{m_{T_1}} + C_{m_1} = 0 \tag{3.224}$$

Since the aerodynamic and the thrust pitching moment coefficients apparently cancel each other in steady state flight, the total variation of airplane pitching moment with perturbed speed, u, is given by:

$$\frac{\partial(M_A + M_T)}{\partial \frac{u}{U_1}} = (C_{m_u} + C_{m_{T_u}})\bar{q}_1 S\bar{c} \tag{3.225}$$

The numerical magnitude of $C_{m_{T_u}}$ is negligible for those airplane configurations where the thrust-line passes close by the center of gravity.

3.2.17 THRUST FORCE AND MOMENT DERIVATIVES WITH RESPECT TO ANGLE OF ATTACK

The perturbed longitudinal, thrust forces and moment are non-dimensionalized as shown in Equations (3.204). In the following, these expressions will be partially differentiated with respect to the perturbed airplane angle of attack, α.

Partial Differentiation of Equation (3.204a) with Respect to α

Partial differentiation of Equation (3.204a) with respect to α leads to:

$$\frac{\partial F_{T_x}}{\partial \alpha} = C_{T_{x_\alpha}} \bar{q}_1 S \tag{3.226}$$

For the normal range of angles of attack and for most conventional airplanes the derivative $C_{T_{x_\alpha}}$ is negligible:

$$C_{T_{x_\alpha}} \approx 0 \tag{3.227}$$

Partial Differentiation of Equation (3.204b) with Respect to α

Partial differentiation of Equation (3.204b) with respect to α leads to:

$$\frac{\partial F_{T_z}}{\partial \alpha} = C_{T_{z_\alpha}} \bar{q}_1 S \tag{3.228}$$

The physical cause of the derivative $C_{T_{z_\alpha}}$ is the so–called propeller and/or inlet normal force which occur as a result of perturbations in angle of attack. The physical reason for such normal forces is the change in flow momentum in a direction perpendicular to the spin axis of the propeller or turbine. The corresponding flow geometry of these effects is illustrated in Figure 3.75. The magnitudes of these normal forces are normally sufficiently small that they can be be neglected when compared to changes in aerodynamic lift due to angle of attack perturbations. Therefore:

$$C_{T_{z_\alpha}} \approx 0 \tag{3.229}$$

Partial Differentiation of Equation (3.204c) with Respect to α

Despite the assumption which leads to Eqn (3.229), the pitching moment contribution due to this derivative may not be negligible at all! Partial differentiation of Equation (3.204c) with respect to α leads to:

$$\frac{\partial M_T}{\partial \alpha} = C_{m_{T_\alpha}} \bar{q}_1 S \bar{c} \tag{3.230}$$

In the following, expressions will be derived from which $C_{m_{T_\alpha}}$ may be estimated. This will be done for two cases:

- Case 1) Propeller driven airplanes
  Case 2) Jet driven airplanes

Case 1) Propeller Driven Airplanes

Figure 3.75 shows the propeller normal force, N_p, as well as the moment arm of this force about the center of gravity. The propeller normal force, N_p, may be expressed as:

$$N_p = C_{N_p} \bar{q} S_p \tag{3.231}$$

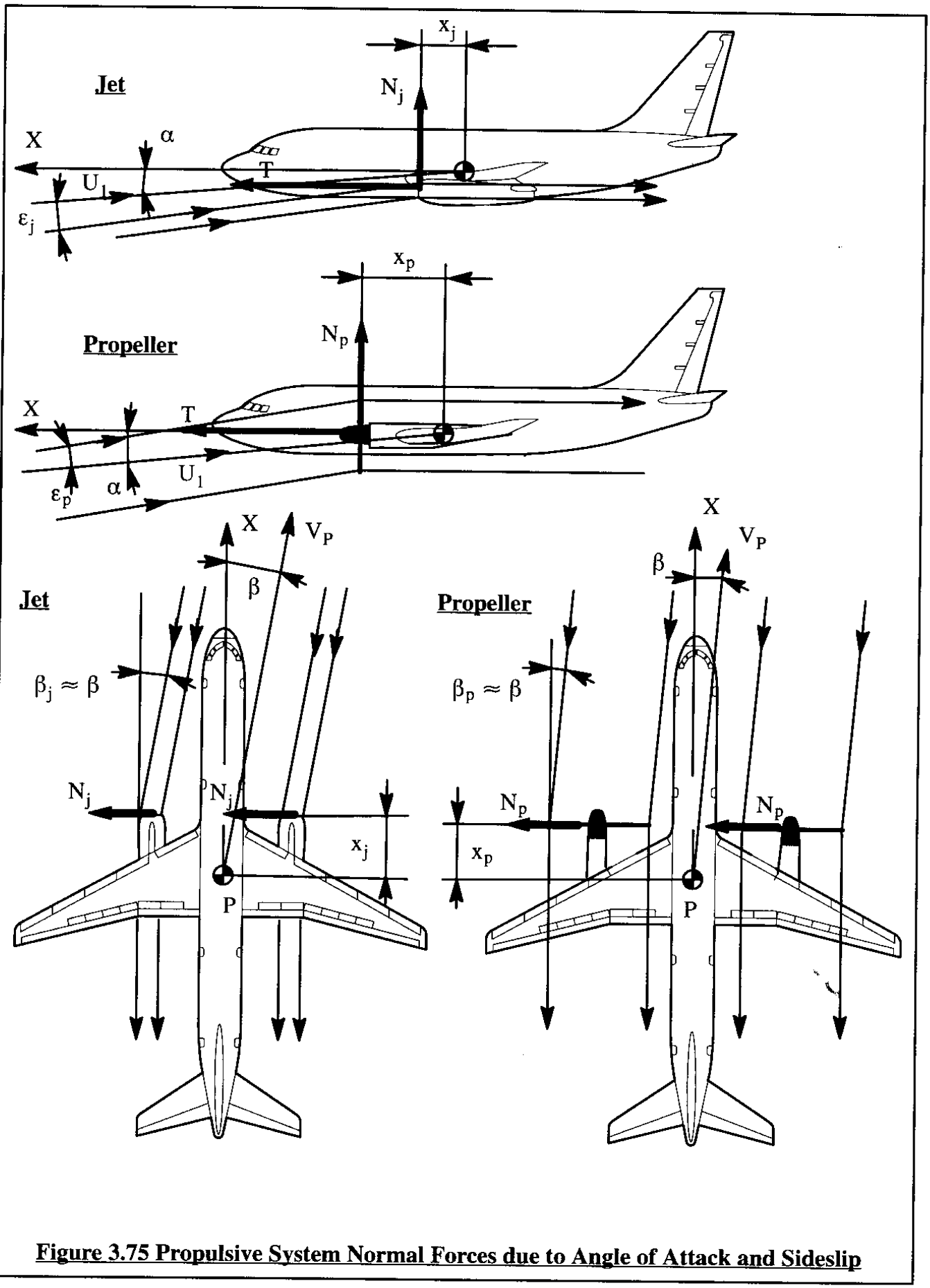

Figure 3.75 Propulsive System Normal Forces due to Angle of Attack and Sideslip

The pitching moment coefficient due to the propeller normal force can be written as:

$$C_{m_{T_{N_p}}} = n_p C_{N_p} \frac{x_p S_p}{\bar{c} S} \tag{3.232}$$

where: n_p is the number of propellers

x_p is the moment arm of the propeller disk

$S_p = \frac{\pi}{4} D_p^{\,2}$ is the propeller disk area

D_p is the propeller diameter

For tractor propellers, the propeller plane is usually in the wing up–wash field. Therefore, the propeller normal force coefficient, C_{N_p}, is proportional to the propeller angle of attack, α_p (this is the angle between the propeller spin axis and the free stream velocity vector in the steady state). Differentiating Eqn (3.232) with respect to α_p yields:

$$C_{m_{T_\alpha}} = n_p \frac{x_p S_p}{\bar{c} S} \frac{\partial C_{N_p}}{\partial \alpha_p} \frac{\partial \alpha_p}{\partial \alpha} \tag{3.233}$$

Since:

$$\alpha_p = \alpha + \varepsilon_p + \begin{matrix}\text{some constant} \\ \text{incidence } \measuredangle\end{matrix} \tag{3.234}$$

where: ε_p is the wing induced up–wash at the propeller

it follows that:

$$\frac{\partial \alpha_p}{\partial \alpha} = 1 + \frac{\partial \varepsilon_p}{\partial \alpha} \tag{3.235}$$

Therefore:

$$C_{m_{T_\alpha}} = n_p \frac{x_p S_p}{\bar{c} S} \frac{\partial C_{N_p}}{\partial \alpha_p} \left(1 + \frac{\partial \varepsilon_p}{\partial \alpha}\right) \tag{3.236}$$

Methods for determining $\partial C_{N_p}/\partial \alpha$ and the up–wash gradient, $\partial \varepsilon_p/\partial \alpha$, may be found in References 3.4, 3.5 and 3.10. The reader should keep in mind that the propeller flow downstream of the propeller plane may in turn affect the downwash at the horizontal tail. Reference 3.4 contains an approach for computing these effects.

Case 2) Jet Driven Airplanes

Figure 3.75 also shows the jet engine normal force, N_j, and the moment arm of the jet engine nacelle inlet about the center of gravity. The jet engine normal force, N_j, may be expressed as:

$$N_j = \dot{m}' V_i \sin\left(\alpha + \varepsilon_j + \begin{matrix}\text{someconstant} \\ \text{incidence } \measuredangle\end{matrix}\right) \tag{3.237}$$

where: $\dot{m}'$ is the mass flow rate through the engine

V_i is the inlet flow velocity

ε_j is the wing induced up–wash at the inlet

The inlet flow velocity, V_i , may be determined from:

$$V_i = \frac{\dot{m}'}{A_i \ \varrho_i} \tag{3.238}$$

where: A_i is the inlet cross sectional area

ϱ_i is the inlet air density

The pitching moment contribution due the normal forces from n_j jet engines is:

$$C_{m_{T_N}} = n_j \frac{(\dot{m}')^2 x_j}{A_i \ \varrho_i \ \bar{q}_1 S\bar{c}} (\alpha + \varepsilon_j + \begin{matrix}\text{some constant} \\ \text{incidence}\end{matrix} \ \measuredangle) \tag{3.239}$$

where: n_j is the number jet engines

x_j is the moment arm of the engine inlet

Upon differentiation with respect to α, it follows that:

$$C_{m_{T_\alpha}} = n_j \frac{(\dot{m}')^2 x_j}{A_i \ \varrho_i \ \bar{q}_1 S\bar{c}} (1 + \frac{\partial \varepsilon_j}{\partial \alpha}) \tag{3.240}$$

Methods for determining the up–wash gradient $\partial \varepsilon_j / \partial \alpha$ may be found in Part VI of Ref. 3.1.

The reader should observe that the derivative, $C_{m_{T_\alpha}}$ {of Eqn (3.236) or (3.240)} when added to the derivative, C_{m_α} {of Eqn (3.35)} yields the so–called power–on value of the static longitudinal stability derivative. It is suggested that the reader use the procedure of page 89 to redefine the aerodynamic center of an airplane with power on.

Note that Eqn (3.240) yields a positive (unstable) contribution to longitudinal stability. The reader should observe that a tractor installation tends to reduce overall airplane longitudinal stability whereas a pusher installation tends to enhance longitudinal stability.

3.2.18 THRUST FORCE AND MOMENT DERIVATIVES WITH RESPECT TO ANGLE OF SIDESLIP

Based on Sub–section 3.2.9 the perturbed longitudinal, thrust forces and moment are non–dimensionalized as follows:

$$F_{T_y} = C_{T_y} \bar{q} S \tag{3.241a}$$

$$L_T = C_{l_T}\bar{q}Sb \tag{3.241b}$$

$$N_T = C_{n_T}\bar{q}Sb \tag{3.241c}$$

The physical cause of the derivatives in Eqns (3.241) is the so–called propeller and/or inlet normal force which occur as a result of perturbations in angle of sideslip. The physical reason for such normal forces is the change in flow momentum in a direction perpendicular to the spin axis of the propeller or turbine. The corresponding flow geometry of these effects is shown in Figure 3.75. The magnitudes of these normal forces are normally sufficiently small that they can be be neglected when compared to changes in aerodynamic side–force due to angle of sideslip perturbations.

The reader is reminded of the fact that F_{T_y} , L_T and N_T are defined in the stability axis system. Next, the partial differentiations implied by Equations (3.164) – (3.166) will be systematically performed for Equations (3.241a) – (3.241c).

Partial Differentiation of Equation (3.241a) with Respect to β

Partial differentiation of Equation (3.241a) with respect to β leads to:

$$\frac{\partial F_{T_y}}{\partial \beta} = C_{T_{y_\beta}}\bar{q}_1 S \tag{3.242}$$

For the normal range of angles of attack and for most conventional airplanes the derivative $C_{T_{y_\beta}}$ is negligible:

$$C_{T_{y_\beta}} \approx 0 \tag{3.243}$$

Partial Differentiation of Equation (3.241b) with Respect to β

Partial differentiation of Equation (3.241b) with respect to β leads to:

$$\frac{\partial L_T}{\partial \beta} = C_{l_{T_\beta}}\bar{q}_1 Sb \tag{3.244}$$

For the normal range of angles of attack and for most conventional airplanes the derivative $C_{l_{T_\beta}}$ is negligible:

$$C_{l_{T_\beta}} \approx 0 \tag{3.245}$$

Partial Differentiation of Equation (3.241c) with Respect to β

Partial differentiation of Equation (3.241c) with respect to β leads to:

$$\frac{\partial N_T}{\partial \beta} = C_{n_{T_\beta}} \bar{q}_1 Sb \tag{3.246}$$

The reader is asked to show that, by analogy to the development in Sub-section 3.2.17 for the pitching moment, it follows that the derivative $C_{n_{T_\beta}}$ may be written as:

$$C_{n_{T_\beta}} = -\, n_j \frac{(\dot{m}')^2 x_j}{A_i\ \rho_i\ \bar{q}_1 Sb} \tag{3.247}$$

Note the minus sign in Eqn (3.247). The reader should observe, that a tractor installation tends to reduce overall airplane directional stability whereas a pusher installation tends to enhance directional stability.

3.2.19 ASSEMBLING THE PERTURBED STATE LONGITUDINAL AND LATERAL-DIRECTIONAL THRUST FORCES AND MOMENTS

At this point the perturbed, longitudinal and lateral-directional thrust forces and moments are assembled in matrix format in Table 3.9.

Table 3.9 Matrix Format for Perturbed State Longitudinal and Lateral-Directional Thrust Forces and Moments

$$\begin{Bmatrix} \frac{f_{T_x}}{\bar{q}_1 S} \\ \frac{f_{T_z}}{\bar{q}_1 S} \\ \frac{m_T}{\bar{q}_1 S\bar{c}} \end{Bmatrix} = \begin{bmatrix} (3.206) & (3.227) \\ (C_{T_{x_u}} + 2C_{T_{x_1}}) & 0 \\ (3.221) & (3.229) \\ 0 & 0 \\ (3.225) & (3.230) \\ (C_{m_{T_u}} + 2C_{m_{T_1}}) & C_{m_{T_\alpha}} \end{bmatrix} \begin{Bmatrix} \frac{u}{U_1} \\ \alpha \end{Bmatrix} \tag{3.248}$$

$$\begin{Bmatrix} \frac{f_{T_y}}{\bar{q}_1 S} \\ \frac{l_T}{\bar{q}_1 Sb} \\ \frac{n_T}{\bar{q}_1 Sb} \end{Bmatrix} = \begin{Bmatrix} (3.243) \\ 0 \\ (3.245) \\ 0 \\ (3.247) \\ C_{n_{T_\beta}} \end{Bmatrix} \beta \tag{3.249}$$

Note: bracketed numbers refer to equations in the text

3.3 OVERVIEW OF USUAL SIGNS FOR AERODYNAMIC COEFFICIENTS AND DERIVATIVES

To enable the reader to quickly review the various sign conventions and 'usual' signs which occur for the many aerodynamic coefficients and derivatives, Figures 3.76 through 3.79 are included in this Section.

These figures also allow the reader to review the pertinent perturbations which are associated with various aerodynamic derivatives. It is hoped that these figures will be useful when reviewing the material presented in Sections 3.1 and 3.2.

3.4 SUMMARY FOR CHAPTER 3

To solve the airplane equations of motion developed in Chapter 1, it is necessary to have available a set of mathematical models which relate the aerodynamic and thrust forces and moments to the appropriate motion and control surface variables. The purpose of this Chapter was to develop and discuss these models.

The equations of motion in Chapter 1 are divided into two sets: equations for steady state and equations for perturbed state flight respectively. Similarly, the mathematical models for aerodynamic and thrust forces and moments are also divided into steady state models (Section 3.1) and perturbed state models (Section 3.2).

In estimating the magnitudes of the various coefficients and derivatives, it is important to account for the effect of major airplane components, such as: wing/fuselage, vertical tail, horizontal tail, canard, nacelles etc. In all cases, physical explanations and derivations were presented to provide the reader with an appreciation for the relative contributions of these components. To acquaint the reader with typical numerical magnitudes for these coefficients and derivatives, numerical examples for the most important stability and control derivatives are given for four different airplanes.

Finally, the propulsive installation of an airplane can have significant effects on several coefficients and derivatives. The most important of these effects were also discussed.

Appendix B contains a listing of stability and control derivatives for several flight conditions and for a range of different airplanes.

A question which always arises is: how important is any given stability and control derivative to the in–flight behavior of a given airplane? That question is addressed in Chapter 5. It is shown in Chapter 5, that by carrying out a so–called derivative sensitivity analysis, it is possible to determine the importance of any derivative and inertial parameter.

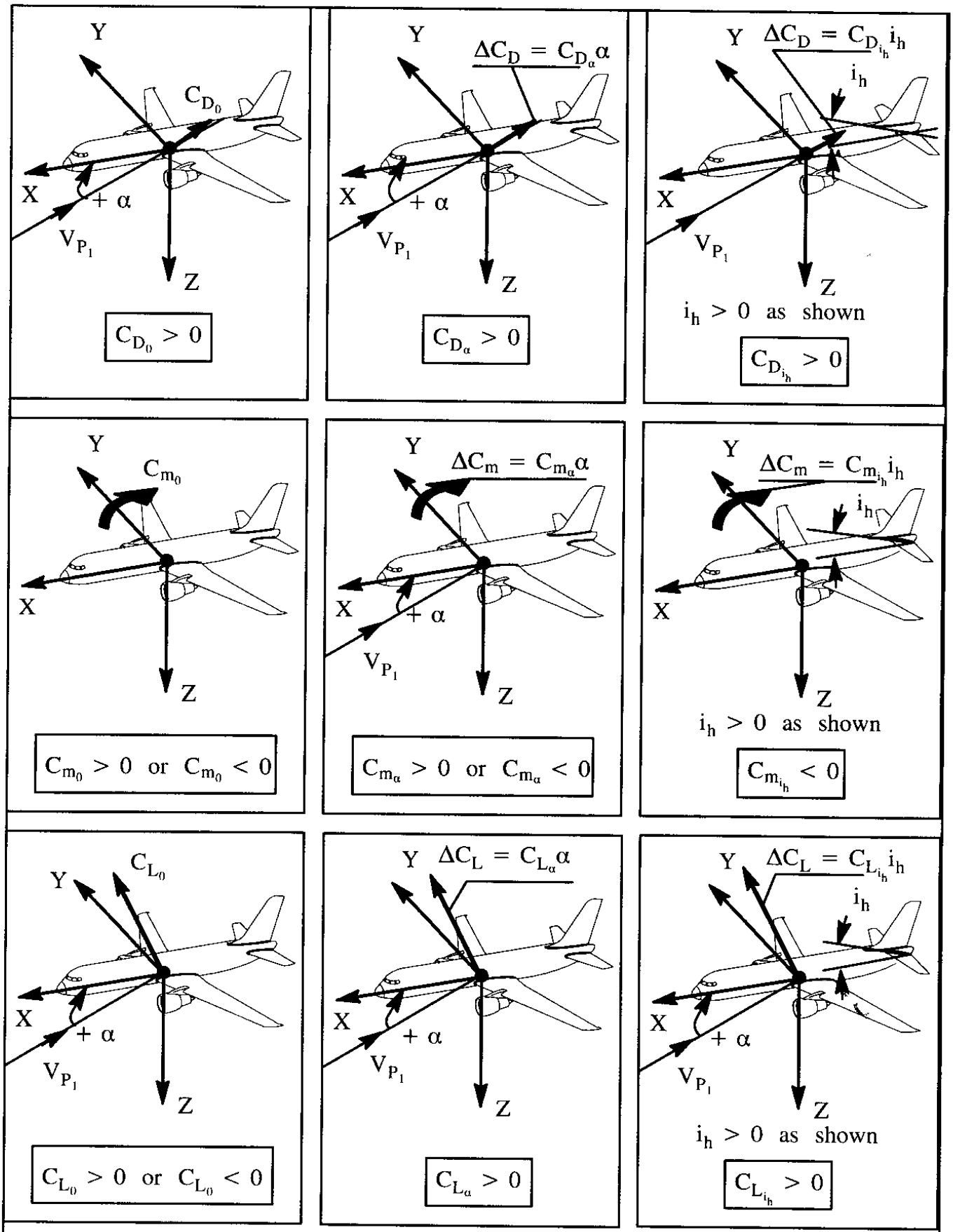

Figure 3.76 Review of Signs of Steady State Longitudinal Force and Moment Derivatives

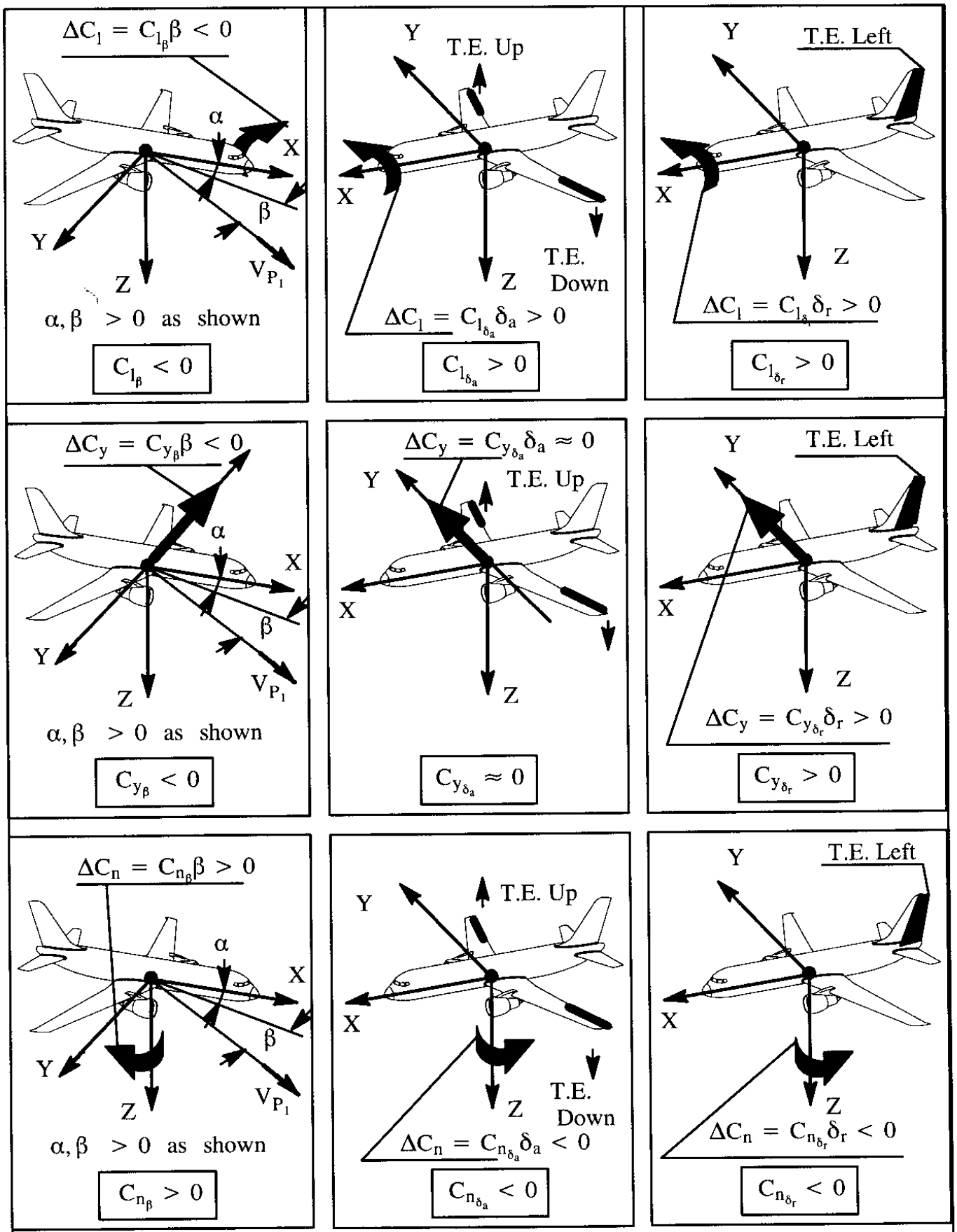

Figure 3.77 Review of Signs of Steady State Lateral–Directional Force and Moment Derivatives

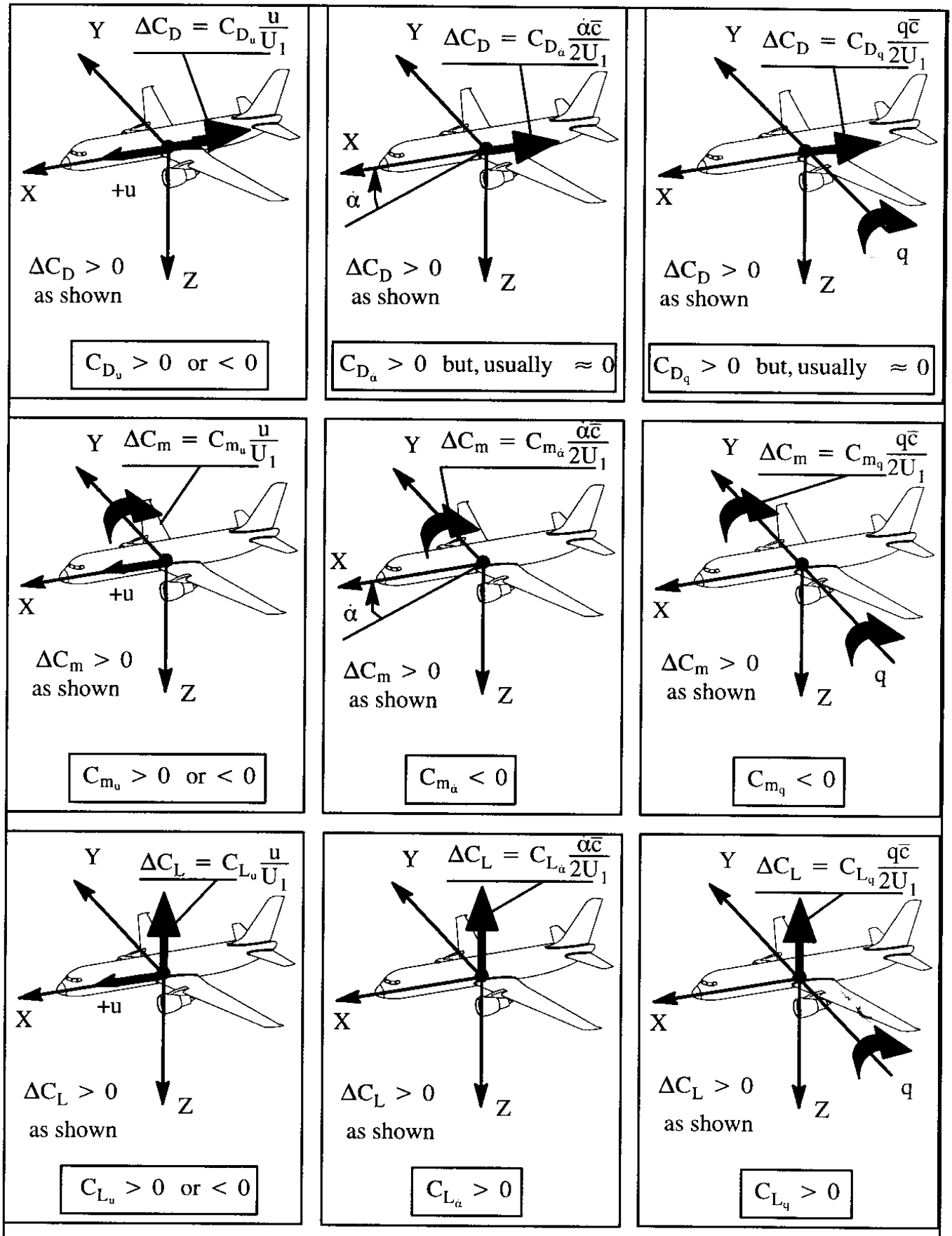

Figure 3.78 Review of Signs of Perturbed State, Longitudinal Speed and Rate Derivatives

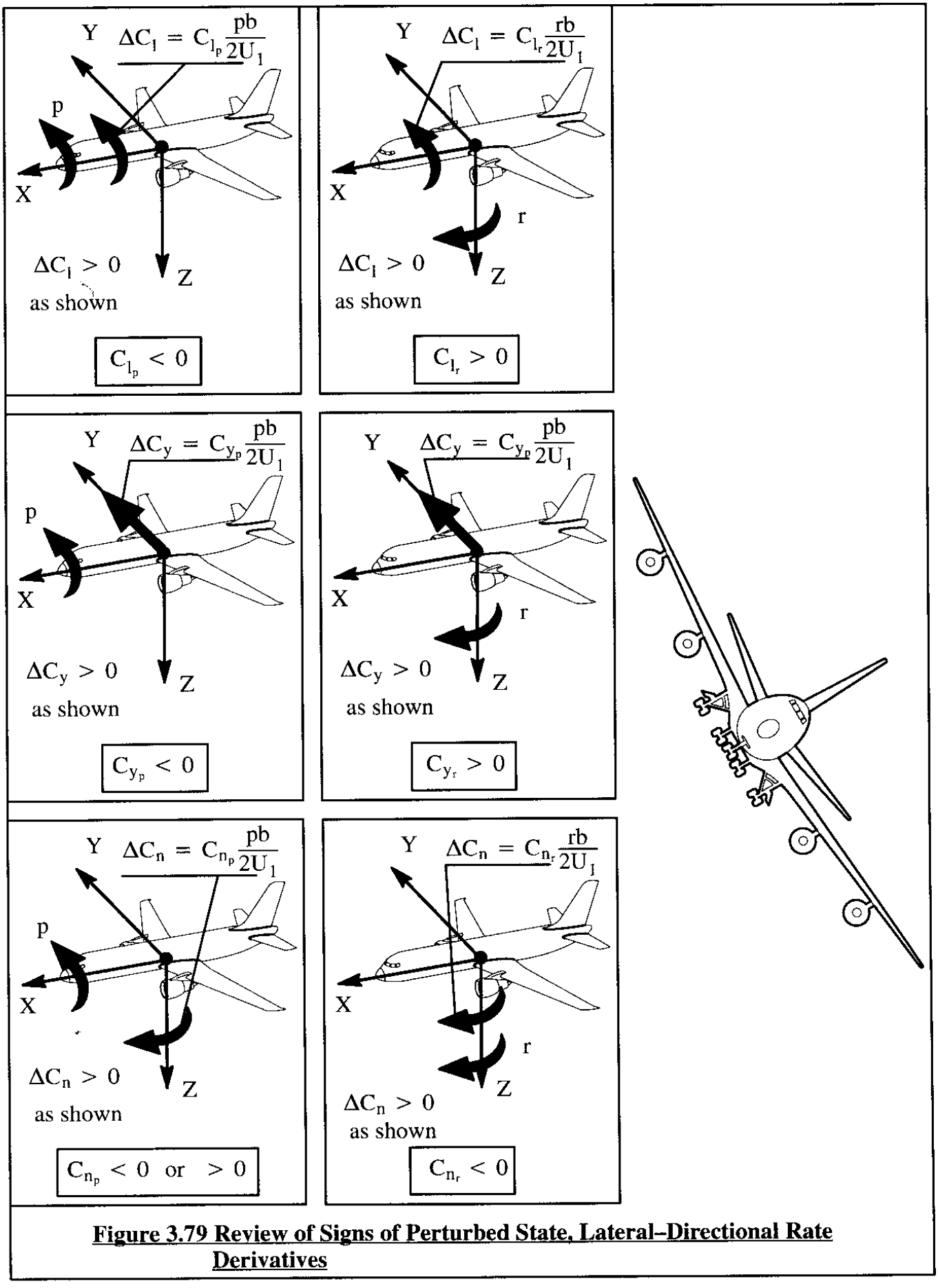

Figure 3.79 Review of Signs of Perturbed State, Lateral–Directional Rate Derivatives

3.5 PROBLEMS FOR CHAPTER 3

3.1 Re–derive Eqns (3.24), (3.25) and (3.26) for a canard (like the Beechcraft Starship) and for a three–surface airplane (like the Piaggio P–180). Assume that the canard airplane has a trailing edge control surface on the canard (called a canard–vator). Data on both airplanes may be found in Jane's All the World's Aircraft of the 1991–1994 period.

3.2 Re–derive Eqns (3.35), (3.36) and (3.37) for a canard (like the Beechcraft Starship) and for a three–surface airplane (like the Piaggio P–180). Assume that the canard airplane has a trailing edge control surface on the canard (called a canard–vator).

3.3 An airplane has a wing and a horizontal tail with identical planform and airfoil geometry (i.e. aspect ratio, sweep angle, camber, thickness ratio and taper ratio). Assume that the tail size is 1/4 that of the wing. Assuming that the wing has 3 degrees of geometric dihedral angle, how much anhedral angle must the tail have for the airplane to have zero dihedral effect?

3.4 Complete the following table.

Parameter to be increased	Quantity Affected	Fill in: Increase, decrease or no change. Also: indicate the sense of the change (i.e. + or –)
S_v	C_{n_β}	Example: Increases positively.
x_{v_s}	C_{n_β}	??
x_{v_s}	$C_{n_{\delta_r}}$	??
$C_{L_{\alpha_h}}$	$C_{m_{i_h}}$	??
wing camber	C_{m_0}	??
S_h	x_{ac_A}	??
$\bar{x}_{cg}$	C_{m_α}	??
S_v	C_{l_β}	??
$\bar{V}_h$	C_{m_q}	??
S_v	C_{n_r}	??
x_{v_s}	C_{n_r}	??

3.5 Explain why a conventional wing–fuselage combination with a vertical canard mounted at the nose of the fuselage is always directionally unstable.

Note: The following problems require the availability of either Parts V and VI of Reference 3.1 or of the AAA program described in Appendix A.

3.6 Find a three–view for the Fokker F–100 jet transport (see Jane's All the World's Aircraft of the 1991–1994 period). Calculate all stability derivatives in Eqn (3.46a). Do this for the following flight conditions:

* high altitude cruise at design cruise weight
* takeoff at sea–level and at maximum takeoff weight
* landing approach and at design landing weight

Perform sanity checks on your answers by comparing with suitable graphs in this chapter.

3.7 Find a three–view for the Fokker F–100 jet transport (see Jane's All the World's Aircraft of the 1991–1994 period). Calculate all stability derivatives in Eqn (3.95a). Do this for the following flight conditions:

* high altitude cruise at design cruise weight
* takeoff at sea–level and at maximum takeoff weight
* landing approach and at design landing weight

Perform sanity checks on your answers by comparing with suitable graphs in this chapter.

3.8 Find a three–view for the Boeing 777 jet transport (see Jane's All the World's Aircraft of the 1993+ period). Calculate all stability derivatives in Eqn (3.162). Do this for the following flight conditions:

* high altitude cruise at design cruise weight
* takeoff at sea–level and at maximum takeoff weight
* landing approach and at design landing weight

Perform sanity checks on your answers by comparing with suitable graphs in this chapter.

3.9 Find a three–view for the Boeing 777 jet transport (see Jane's All the World's Aircraft of the 1993+ period). Calculate all stability derivatives in Eqn (3.197). Do this for the following flight conditions:

* high altitude cruise at design cruise weight
* takeoff at sea–level and at maximum takeoff weight
* landing approach and at design landing weight

Perform sanity checks on your answers by comparing with suitable graphs in this chapter.

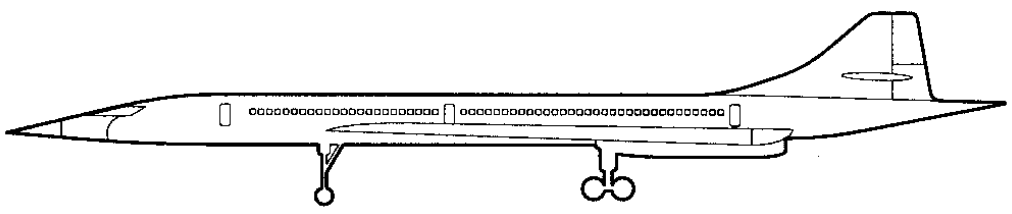

3.6 REFERENCES FOR CHAPTER 3

3.1 Roskam, J.; Airplane Design, Parts I through VIII; Design, Analysis and Research Corporation, 120 East Ninth Street, Suite 2, Lawrence, Kansas, 66044, USA; 1990.

3.2 Mattingly, J.D.; Heiser, W.H. and Daley, D.H.; Aircraft Engine Design; AIAA Education Series, 1987.

3.3 Kerrebrock, J.L.; Aircraft Engines and Gas Turbines; MIT Press, Cambridge, MA, 1977.

3.4 Wolowics, C.H. and Yancey, R.B.; Longitudinal Aerodynamic Characteristics of Light, Twin-engine Propeller Driven Airplanes; NASA TN D-6800; 1972.

3.5 Perkins, C.D. and Hage, R.E.; Airplane Performance, Stability and Control; J. Wiley & Sons; 1949.

3.6 Etkin, B.; Dynamics of Flight; J. Wiley & Sons; 1959.

3.7 Rodden, W.P. and Giesing, W.P.; Application of Oscillatory Aerodynamic Theory for Estimation of Dynamic Stability Derivatives; Journal of Aircraft, Vol. 7, No. 3, May-June 1970, pp 272-275.

3.8 Fung, Y.C.; An Introduction to the Theory of Aeroelasticity; J. Wiley & Sons;1955.

3.9 Lan, C.E. and Roskam, J.; Airplane Aerodynamics and Performance; Design, Analysis and Research Corporation, 120 East Ninth Street, Suite 2, Lawrence, Kansas, 66044, USA; 1997.

3.10 Ribner, H.S.; Notes on the Propeller and Slipstream in Relation to Stability; NACA WR L-25, 1944 (Formerly NACA ARR L4I12a).